Master's thesis

NTNU
Norwegian University of Science and Technology
Faculty of Natural Sciences
Department of Biology

Johan Edvard Iversen

Use of Wastewater from Recirculating Aquaculture System (RAS) for Cultivation of Microbial Biofilm Communities

Master's thesis in Biotechnology (MBIOT5)
Supervisor: Kjell Inge Reitan
Co-supervisor: Kari Attramadal and Deni Ribicic
August 2023

NTNU
Norwegian University of
Science and Technology

Johan Edvard Iversen

Use of Wastewater from Recirculating Aquaculture System (RAS) for Cultivation of Microbial Biofilm Communities

Master's thesis in Biotechnology (MBIOT5)
Supervisor: Kjell Inge Reitan
Co-supervisor: Kari Attramadal and Deni Ribicic
August 2023

Norwegian University of Science and Technology
Faculty of Natural Sciences
Department of Biology

NTNU
Norwegian University of
Science and Technology

Acknowledgements

This master thesis was written as part of the Wasteless project at the faculty of natural sciences, department of Biology, at the Norwegian university of science and technology (NTNU). The wasteless project is an industry research project owned by Nofitech AS, led by SINTEF Ocean AS, and including the partners NTNU and Hardingsmolt AS. The project is founded by the Norwegian research council and the industry partners Nofitech AS and Hardingsmolt AS.

Firstly, I would like to thank my supervisor Kjell Inge Reitan, as well as my co-supervisors Kari Johanne Kihle Attramadal and Deni Ribicic for guidance through the thesis. Kjell Inge and the co-supervisors have believed in this project and been a valuable support for me in my work. They have shared their knowledge and experience, which has been highly appreciated. In addition to my supervisors, I would like to thank the rest of the team of the Wasteless project for all the good discussions and valuable inputs they have contributed with. A special thanks to Hubert Bonnefond, microalgae expert- and CEO of the DareWin project at Inria, who has been a guiding star throughout this master's thesis. Finally, I would like to thank Marianne Aas at Sintef Ocean AS and Dag Altin at NTNU for helping me out in the lab.

Secondly, I would like to thank the team at the RAS facility Hardingsmolt AS for the collaboration, and the good work they did with operating the pilot reactors. The team at Hardingsmolt also supported the master's thesis with RAS water for the experiments. I am grateful for the collaboration.

At last, I would like to thank my family and my friends for being supportive and believing in me. They have encouraged me during this process, helping me to stay focused and motivated. A special thanks to Lise, Simen, Hanne, Liva, and Tørris, you are awesome. My study mates have made these five years on NTNU memorable and unforgettable. I am undoubtedly grateful for the time we have had together.

Abstract

The increasing demand for sustainable food can partly be solved by the production of aquatic species in recirculating aquaculture systems (RAS). In the Norwegian aquaculture industry, Atlantic salmon (*Salmo salar*) is often hatched and grown in freshwater RAS until the fish develops into smolt, by which the smolt is transferred to net pens in the sea. Lately, a popular strategy is to keep the smolt in RAS with brackish water for an increased period, allowing the fish to grow bigger before it is transferred to sea. This cuts production time in the sea, thereby reducing problems related to sea lice. In RAS, the cultivation water is always treated to remove organic matter, ammonia, and carbon dioxide. Oxygen is added to the cultivation water prior to the rearing units. This allows an increased recirculation of the rearing water; however, some of the water needs to be exchanged daily to cope with the accumulation of nitrate. Nitrogen (N) is fixed industrially from the atmosphere into fertilizer, which is particularly energy demanding and carbon dioxide intensive. Similarly, phosphate (P) is introduced to the RAS with the fish feed, which is a limited resource obtained by mining. It is estimated that the phosphorus mines will be exhausted within the next 50–100 years, which highlights the importance of scavenging valuable nutrients such as N and P from the RAS water.

This master's thesis is part of the Wasteless project, a collaboration between the Norwegian university of science and technology (NTNU), Nofitech AS, Sintef Ocean AS, and Hardingsmolt AS. The aim of the project is to cultivate a microbial biofilm community containing microalgae with the RAS water as cultivation medium, and in that way bioremediate carbon, N, and P from the RAS water. The nutrients can be recovered into microbial biomass which can be harvested and potentially used as an ingredient in fish feed or for other purposes. In this master's thesis, four lab scale experiments and one pilot demonstration at the RAS facility Hardingsmolt AS were performed to cultivate microbial biofilm with RAS water as cultivation medium. The master's thesis investigated different selection parameters: Light, silica, nutrients, and harvest rate, to see whether they influenced the productivity and species composition of the microbial biofilm. The prokaryote and eukaryote components of the biofilm were investigated through 16- and 18S ribosomal RNA amplicon sequencing. The prokaryote part of the biofilm was analyzed through identification of the hypervariable region (V) 3 and 4 in DNBSEQ sequencing, whereas the eukaryote part of the biofilm was analyzed through investigation of the V7 in DNBSEQ sequencing, and the whole ribosomal DNA operon (V1-9) with Oxford nanopore technologies sequencing.

The major findings were that the productivity of the microbial communities was influenced by the selection parameters tested; however, that the species composition was not. The results showed that light was necessary to cultivate a microbial biofilm containing microalgae. The productivity was significantly increased when silica was added, as well as when the nutrient load of the RAS water was high. It was demonstrated that the biofilm should be harvested every 12^{th} day to obtain the highest productivity and biomass yield. The characterization of the prokaryote part of the community showed that the biofilms, the initial RAS water, and the nitrifying biofilter were dominated by heterotrophic bacteria. The most abundant taxa were *Alphaproteobacteria*, followed by *Gammaproteobacteria* and *Flavobacteriia*. The eukaryote part of the biofilms contained a variety of species; however, two diatom microalgae species were highly dominating: *Phaeodactylum tricornutum* and *Nitzschia sp.* Diatoms can produce a repertoire of fatty acids, among others the valuable fatty acids eicosapentaenoic acid (EPA) and docosahexaenoic acid (DHA), which highlights the potential of the microbial biomass as a sustainable ingredient in fish feed.

Sammendrag

Den økende etterspørselen etter bærekraftig mat kan delvis løses ved produksjon av akvatiske arter i resirkulerende akvakultursystemer (RAS). I norsk havbruksnæring blir atlantisk laks (*Salmo salar*) ofte klekket og kultivert i ferskvann på land, inntil laksen utvikler seg til smolt, hvorved den overføres til merder i sjø. I det siste har en populær strategi vært å holde smolten i lengre perioder på land, i RAS med brakkvann, slik at fisken er større før den overføres til sjø. Dette korter ned produksjonstiden i sjø, noe som redusere problemer tilknyttet lakselus. I RAS blir oppdrettsvannet alltid behandlet for å fjerne organisk materiale, ammoniakk og karbondioksid. I tillegg blir kultiveringsvannet tilført oksygen før det går tilbake til fisken. Dette tillater en økt resirkulering av RAS vannet. Likevel må noe av oppdrettsvannet byttes ut på en daglig basis for å fortynne konsentrasjonen av nitrat, som ellers akkumuleres til høye nivåer. Nitrogen (N) fikseres industrielt fra atmosfæren til gjødsel, noe som er spesielt energi krevende og karbon dioksid intensivt. På lik linje blir fosfor (P) introdusert til RAS gjennom fiske fôret. P er en begrenset ressurs som oppnås gjennom gruvedrift. Det er estimert at fosfor-gruvene vil være tome i løpet av de neste 50-100 årene, noe som kaster lys på viktigheten av å gjenvinne viktige næringsstoffer som N og P fra RAS vannet.

Denne masteroppgaven er en del av Wasteless-prosjektet, et samarbeid mellom Norges teknisk-naturvitenskapelige universitet (NTNU), Nofietech AS, Sintef Ocean AS, og Hardningsmolt AS. Målet med prosjektet er å dyrke biofilm bestående av bakterier og mikroalger på RAS-vann, og på den måten rense ut karbon, nitrogen og fosfat fra RAS-vannet. Næringsstoffene kan tas opp og bindes i mikrobiell biomasse, og på den måten gjenvinnes ved at biomassen høstes. Denne masteroppgaven består av fire eksperimenter i laboratorieskala, samt en pilotdemonstrasjon ved RAS-anlegget Hardingsmolt AS, hvor mikrobiell biofilm ble dyrket med RAS-vann som dyrkingsmedium. Masteroppgaven undersøkte ulike seleksjons parametere for mikrobiell seleksjon: Lys, silikat, næringsstoffer og høstingsfrekvens, med hensikt å undersøke om disse parameterne påvirket produktivitet og artssammensetning av biofilmen. De prokaryote og eukaryote delene av biofilmen ble undersøkt gjennom sekvensering av 16- og 18S ribosomalt RNA amplikon sekvensering. Den prokaryote delen ble analysert ved identifisering av hypervariabel region (V) 3 og 4 i DNBSEQ-sekvensering, mens den eukaryote delen av biofilmen ble analysert ved identifisering av V7 i DNBSEQ-sekvensering, og hele det ribosomale DNA operonet (V1-9) i Oxford nanopore technology sekvensering.

Hovedfunnene i denne masteroppgaven var at den mikrobielle produktiviteten ble påvirket av seleksjonsparameterne som ble testet, men at artssammensetningen ikke ble spesielt påvirket. Resultatene viste at lys var nødvendig for å dyrke en biofilm bestående av bakterier og mikroalger. Produktiviteten ble økt betydelig når silikat ble tilsatt kultiveringsmediet, samt når næringsinnholdet i RAS-vannet var høyt. Det ble vist at biofilmen burde høstes hver tolvte dag for å oppnå høyest mulig produktivitet og biomasseutbytte. Karakteriseringen av den prokaryote delen av samfunnet viste at biofilmen, startvannet og det nitrifiserende biofilteret var dominert av heterotrofe bakterier. De mest tallrike artene var fra av klassen *Alfaproteobakterier*, etterfulgt av *Gammaproteobakterier* og *Flavobakterier*. Den eukaryote delen av biofilmen inneholdt et mangfold av arter, hvor mikroalgedelen av samfunnet besto hovedsakelig av to typer kiselalger: *Phaeodactylum tricornutum* og *Nitzschia sp.* Kiselalger kan produsere mange typer fettstyrer, blant annet de essensielle fettsyrene eikosapentaensyre (EPA) og dokosaheksaensyre (DHA), noe som fremhever potensialet for bruk av den mikrobielle biomassen som en bærekraftig ingrediens i fiskefôr.

Table of Contents

List of Abbreviations

ASV	Amplicon sequence variants
Anammox	Anaerobic ammonium oxidation
ANOVA	Analysis of variance
AOA	Ammonia oxidizing archaea
AOB	Ammonia oxidizing bacteria
AO	Ammonia oxidation
BGI	Beijing Genomics Institute
C	Carbon
CC	Carrying capacity
Comammox	Complete oxidation of ammonia to nitrate
DNA	Deoxyribonucleic acid
DMSP	Dimethylsulfoniopropionate
DIC	Dissolved inorganic carbon
DIN	Dissolved inorganic nitrogen
DHA	Docosahexaenoic acid
EPA	Eicosapentaenoic acid
FCR	Feed conversion ratio
V	Hypervariable region
HRT	Hydraulic retention time
LSU	Large ribosomal subunit
NO	Nitrite oxidation
NOB	Nitrite oxidizing bacteria
N	Nitrogen
Nofitech	Norwegian fishfarming technologies AS
NS	Norwegian standards
NTNU	Norwegian University of Science and Technology
ONT	Oxford Nanopore Technologies
P	Phosphorus
PAR	Photosynthetic active radiation
PUFA	Poly unsaturated fatty acids
PCR	Polymerase chain reaction
PCoA	Principal coordinate analysis
QIIME2	Quantitative Insight Into Microbial Ecology 2
RAS	Recirculating aquaculture system
RNA	Ribonucleic acid
rDNA	Ribosomal DNA
rRNA	Ribosomal RNA
SSU	Small ribosomal subunit
SRT	Solids retention time
SDG	Sustainable Development Goal
USA	The United States of America
TAN	Total ammonia nitrogen
TSS	Total suspended solids
TAG	Tri-acyl glycerol
UN	United Nations

1. Introduction

1.1 Circular production in Atlantic salmon land-based aquaculture

The United Nations (UN) has estimated the world population to reach 8.5 billion people by 2030, 9.7 billion by 2050 and to exceed 11 billion in 2100 (United Nations, 2015, van Hoof et al., 2019, Ytrestøyl et al., 2015). In 2015, the UN projected that nearly 690 million people, accounting 8.9% of earth's population, are suffering from hunger (United Nations, 2022a). Following the same pattern, the number of people living in hunger is projected to reach 840 million by 2030, demonstrating the big challenges that have to be overcome to be able to realize UN Sustainable Development Goal (SDG) 2: Zero hunger (United Nations, 2022a). If hunger and malnutrition are to be combated, more sustainable food needs to be produced from the oceans (van Hoof et al., 2019). European union (EU) agendas, such as EU Blue Growth strategy, The Food 2030 agenda, and Food from our Oceans vision, truly reflects the importance and aim of utilizing the marine environments for sustainable food production (van Hoof et al., 2019).

One of the fish species that is important for aquaculture is Atlantic salmon (*Salmo salar*). Compared to animals farmed on land e.g., cattle and pigs, which have a fairly high feed conversion ratio (FCR) of 8.49 and 4.91, respectively (Peters et al., 2014), Atlantic salmon has a FCR of 1.1 (Elvy et al., 2022, Mowi, 2019). Because of the high food utilization ratio, Atlantic salmon is a good production alternative for sustainable food production. The annual production of Atlantic salmon exceeds 2 million metric tons of fish, with Norway as the top producer (Love et al., 2020, Cadillo-Benalcazar et al., 2020). In 2019, Norway alone produced 1.3 million tons of Atlantic salmon (Statistisk sentralbyrå, 2020).

Atlantic salmon is an anadromous species. During the first period of life Atlantic salmon are hatched and farmed in freshwater, as alevins, fry and parr, respectively. Thereafter, as the fish develop into smolt (~0.1 kg), they are traditionally transferred to sea water. The fish can be kept on land as post-smolts (~0.15 – 0.6 kg), super-smolts (~1.0 kg), or even till market size (4.5-5 kg), or the fish can be transferred to sea for grow out (≥4.5 kg) (Love et al., 2020, Fossmark et al., 2021).

Today, the most recognized technology for land-based fish-farming is recirculating aquaculture systems (RAS). RAS reduces water usage and cuts cost related to heating and pumping of water (Martins et al., 2010). Due to water recirculation, water treatment is needed to maintain good rearing conditions for the fish. Among other things, this always includes removal of particles, ammonium (NH_4^+), and carbon dioxide (CO_2), as well as re-oxygenation of the rearing water (Fjellheim et al., 2016, Ahmed and Turchini, 2021). It was demonstrated in a pilot RAS that high degree of water recirculation (~99% per. day) is possible (Yogev et al., 2017); however, some of the water needs to be exchanged to dilute- and remove compounds that otherwise build up to toxic concentrations for the fish (Fjellheim et al., 2016). This includes for instance nitrate (NO_3^-) and heavy metals (Fjellheim et al., 2016, von Ahnen et al., 2021). To reduce the water consumption, additional water treatment can be included (e.g., denitrification and membrane filtration).

In RAS, nitrate is generated from the biological conversion of ammonium (nitrification), which is excreted into the rearing water by fish and bacterial metabolism (Fjellheim et al., 2016, Kolarevic et al., 2012). Nitrate is either consumed by denitrifying bacteria, which is released into the air, or diluted from the system by addition of an appropriate amount of new make-up water to maintain the desired levels of nitrate for the fish. Release of N and P into the recipient water bodies can lead to eutrophication, which can end in algal blooms

and fish deaths (Yuan et al., 2018, Yogev et al., 2020). In either case, N is lost to the environment as nitric gas (N_2) or dissolved inorganic nitrogen (DIN), respectively (Deng et al., 2020, Gao et al., 2020). Nitrate is an important element and is an essential part of fertilizers (Wang et al., 2019b, Cherkasov et al., 2015). Nitrogen (N) is fixed industrially from the atmosphere to fertilizer, which is particularly energy demanding and carbon dioxide intensive (Adams et al., 2018, Cherkasov et al., 2015, Erisman et al., 2011). Phosphate is introduced to RAS with the fish feed (Aas et al., 2019, Yogev et al., 2020). Phosphorus (P) is a limited resource, which is obtained by mining (Yogev et al., 2020). It is estimated that the phosphorus mines will be exhausted within the next 50–100 years (Yogev et al., 2020, Yuan et al., 2018). In addition, mining and processing of phosphate rock is associated with high energy requirements, using >20.5 kilowatt hours per ton of ore (DOE, 2002). Nitrogen and phosphorus are essential elements in all living cells, contributing as building blocks in cell membranes, pigments, amino acids, and enzymes (Da Costa and Ito, 2003, Blanco and Blanco, 2017, Yogev et al., 2020). Having that in mind, the usefulness of scavenging and utilizing N and P from wastewater treatments, such as RAS, is emphasized.

Even though Atlantic salmon is a good feed utilizer, large amounts of feed is used in intensive farming. Today, there is not enough sustainable resources coming from the sea to formulate fish feed (Gong et al., 2019, Aas et al., 2019). Consequently, large amounts of plant-based ingredients such as soy protein concentrate are used (Ytrestøyl et al., 2015, Aas et al., 2019, Krogdahl et al., 2020, Kononova et al., 2019). The increased use of plant-based ingredients has negative effects on both climate change and fish flesh composition (Gong et al., 2019, Sprague et al., 2016, Agovino et al., 2019). One negative effect is linked to the deforestation of rainforest, which is associated with some of the terrestrial production of plant based proteins (Silva and Lima, 2018, Atlas, 2020). The transportation of plant-based ingredients also releases a lot of climate gases. In addition, some question the use of terrestrial land for production of animal feed, rather than using the area directly for human food production (Froehlich et al., 2018). The increased amount of plant ingredients in the feed has shown negative effects on the fatty acid profile of the fish, reducing the level of the essential fatty acids eicosapentaenoic acid (EPA) and docosahexaenoic acid (DHA) in the fish flesh (Sprague et al., 2016, Gong et al., 2019). This demonstrates the need for sustainable feed ingredients with high protein content and a proper fatty acid profile.

Microalgae can be cultivated in wastewater, from which they can assimilate N and P, as well as consuming CO_2 as their source of carbon (Christenson and Sims, 2011, Guzzon et al., 2008, Kesaano and Sims, 2014, Zhuang et al., 2018). Some microalgae have high growth rates (Patel et al., 2021b, Krzemińska et al., 2014) and contain high levels of fat and proteins (Sørensen et al., 2016, Patel et al., 2022), including the coveted, essential fatty acids EPA and DHA (Gong et al., 2019, Sørensen et al., 2016). Some species of microalgae can grow as biofilm, which makes them more readily harvested (Liu et al., 2013, Christenson and Sims, 2011). The harvested biomass has potential to be used as an ingredient in feed (Patel et al., 2021a, Christenson and Sims, 2011, Gong et al., 2019), pharmaceuticals (Hong et al., 2019), fertilizers (Christenson and Sims, 2011, Yogev et al., 2020, Liu et al., 2020), and as a component in biogas production (Patel et al., 2021a, Christenson and Sims, 2011, Kesaano and Sims, 2014, Krzemińska et al., 2014, Patel et al., 2020). With microbial cultivation strategies, valuable nutrients such as N and P can be efficiently incorporated into algal biofilm (Patel et al., 2020, Kesaano and Sims, 2014), which can be harvested and potentially used for other purposes.

1.2 The RAS system at Hardingsmolt AS

The RAS at Hardingsmolt AS was delivered by Norwegian Fishfarming Technologies AS (Nofitech AS). The RAS consists of four octagonal rearing tanks, coupled to two separate water treatment circuits. The water treatment (*Figure 1*) include mechanical filtration of particles (Hex drum filter, 10-500 µm), biological filtration of ammonium (moving bed biofilter, nitrification), removal of carbon dioxide and total gas supersaturation (vacuum trickle filter degasser), re-oxygenation of rearing water (oxygen cones), and fine particle removal on a side stream (Ratz protein skimmer, <30 µm). In addition to the water treatment, some of the rearing water is exchanged with new intake water (~20 m^3 h^{-1}). The water parameters within RAS, such as temperature and salinity, are maintained near constant, and monitored.

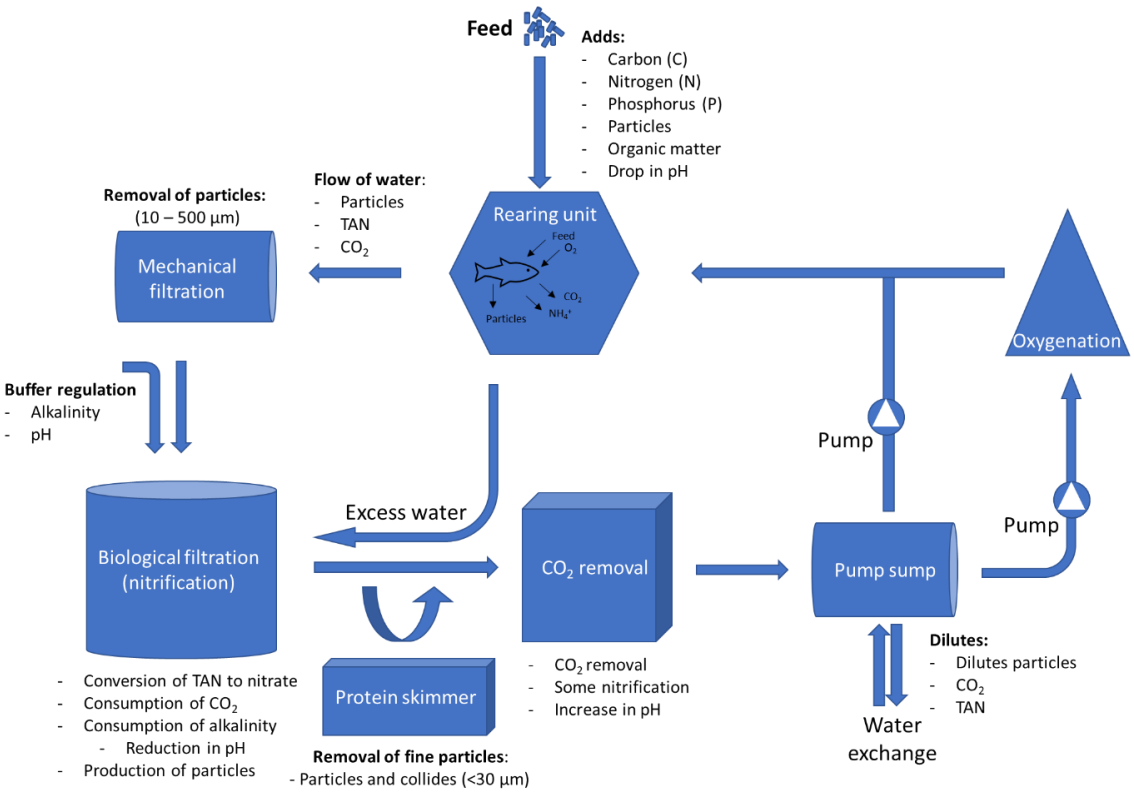

Figure 1: A simplified illustration of the RAS at Hardingsmolt AS, the commercial site at which the pilot reactors were operated. The illustration shows the input of feed to the raring unit and the subsequent nutrient flux through the system. The RAS technology was delivered by Nofitech AS. The illustration shows the rearing tank and the water treatment loop: Mechanical filtration of particles (Hex drum filter, 10-500 µm), biological removal of ammonium (moving bead biofilter, nitrification), CO_2 removal (vacuum trickle filter degasser), and oxygenation (oxygen cones) of the process water. In addition, a side stream of the water is treated in a protein skimmer (Ratz protein skimmer) for removal of smaller particles and colloides. The pump sump is illustrated, in which water is stored before it is pumped back into the rearing unit or leaves through the overflowing outlet from the RAS.

1.3 Which bacteria and archaea are dominating in RAS, and what do they do?

RAS is a dynamic system where different elements such as water, fish, air, and feed is introduced to the system (*Figure 1*). In addition, rearing equipment is used, as well as the daily interaction between staff and RAS contributes to the microbial diversity of RAS (Blancheton et al., 2013, Attramadal et al., 2012, Dahle et al., 2022). Studies show that different microorganisms inhabit different habitats in RAS, such as the biofilter, the rearing

water, fish skin, and fish gut (Schreier et al., 2010, Dehler et al., 2017, Bugten et al., 2022, Dahle et al., 2022). Which microorganisms inhibit which habitat depends on the specific properties of the microorganism to occupy a niche, as well as available resources, competition with other microorganisms, and the microbial carrying capacity (CC). It is practical to divide the microorganisms that inhabit RAS in two major groups according to their source of energy; heterotrophic- and autotrophic microorganisms (Blancheton et al., 2013). Bacteria and archaea influence the fish in RAS through effects on the physicochemical environment as well as through direct interactions with the fish.

In the rearing water, compounds are produced from fish- and microbial metabolism. Ammonia (NH_3) is the major excretion product from the nitrogen metabolism of teleost fish species and is also released from the microbial breakdown of urine, feed, and faeces (Fjellheim et al., 2016, Kolarevic et al., 2012, Suhr et al., 2013). Depending on temperature, salinity, and pH, ammonia exists in two forms in water (*Figure 2*): the neutral, toxic ammonia (NH_3) and the less toxic, ionized ammonium (NH_4^+). Together, the sum of the nitrogen molecule of the neutral and ionized form is annotated as total ammonia nitrogen (TAN). A common operational limit for production of Atlantic salmon production is 2 mg L^{-1} TAN (Fjellheim et al., 2016, Fossmark et al., 2021).

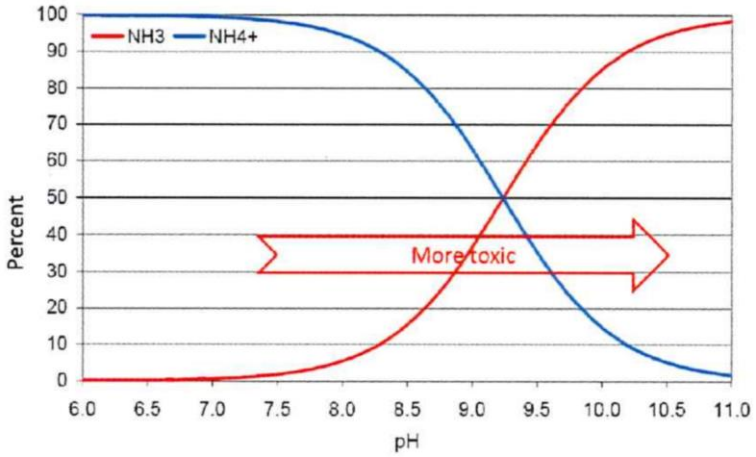

Figure 2: The effect of pH on TAN and its respective forms: Ammonia (NH_3) and ammonium (NH_4^+). The figure is collected from (Fjellheim et al., 2016).

Ammonia is highly toxic to Atlantic salmon, with negative effects for as low as 2 µg L^{-1} (Fjellheim et al., 2016). In RAS, ammonia is converted to the less toxic nitrite (NO_2^-, with common operational limit <0.5 mg L^{-1}) (Fjellheim et al., 2016) and further to nitrate (NO_3^-) in the aerobic nitrifying biofilter. Atlantic salmon can tolerate high levels of nitrate (<100 mg L^{-1}) without suffering negative effects (Davidson et al., 2017, Freitag et al., 2015). It is known that anaerobic ammonium oxidation (Anammox) and complete oxidation of ammonia to nitrate (Comammox) contributes to the conversion of ammonia to nitrate (*Appendix A, Table A. 1*) (Qi et al., 2022); however, the dominating process in RAS is nitrification. Nitrification is carried out by chemolithoautotrophic nitrifiers settling in biofilms together with heterotrophs (Blancheton et al., 2013, He et al., 2018, Hüpeden et al., 2020).

Nitrification is a two-step processes, carried out by two separate groups of microorganisms. The first step is the conversion of ammonia to nitrite, which is carried out by ammonia oxidizing bacteria (AOB) and ammonia oxidizing archaea (AOA) (Bollmann et al., 2011, He et al., 2018). These species are typically named nitroso-, and common species are presented in *Table 1*. Ammonium oxidation (AO) require and consume oxygen. The

ammonium is used as an electron donor and the oxygen is used as an electron acceptor. Protons ($2H^+$) are produced in the process. The second step of nitrification is the conversion of nitrite to nitrate. This step of the process is caried out by nitrite oxidizing bacteria (NOB) (Wentzel et al., 2003), by which the specific species are typically annotated nitro- (*Table 1*). In nitrite oxidation (NO), nitrite is used as an electron donor, being oxidized to nitrate with oxygen as the final electron acceptor (Wentzel et al., 2003).

In some RAS the hydraulic retention time (HRT) is increased to introduce more new water to dilute nitrate to an acceptable level in the system. The dissolved nitrogenous waste is then released from the system through the outlet waste stream. In other systems, nitrate removal is accomplished by the anaerobic conversion of nitrate to nitrogen gas (N_2), a process called denitrification (*Table 1*) (van Rijn et al., 2006, Lekang, 2020). Denitrification is carried out by facultative anaerobic microorganisms, oxidizing nitrate to elemental nitrogen (N_2) in the absence of oxygen, which is aerated out of the system (van Rijn et al., 2006). There are also other pathways linked to nitrate removal (*Appendix A, Table A. 1*); however, denitrification is the preferred choice in RAS having technology for treatment of nitrate.

In addition to being a source of ammonia, uneaten feed and faeces contain organic matter which is consumed by heterotrophic microorganisms. Heterotrophs respire oxygen, using organic matter as their electron donor and oxygen (if available) as their electron acceptor (*Table 1*). Even though the diversity among heterotrophs is large, RAS communities are often dominated by A*lphaproteobacteria* and *Gammaproteobacteria* (Blancheton et al., 2013, Tal et al., 2003, Wietz et al., 2009).

Table 1: The most important microbial processes taking place in RAS biofilters, with respective reaction-equation, and typical microbes responsible for the process. The table was modified from (Schreier et al., 2010, Blancheton et al., 2013, Tal et al., 2003, Wietz et al., 2009).

Process	Reaction equation	Microorganisms
Nitrification		*-Nitrosomonas sp.*
		-Nitrosomonas cryotolerans
Ammonium oxidation (AO)	$NH_4^+ + 1.5O_2$	*-Nitrosomonas europaea*
	$\rightarrow NO_2^- + 2H^+ + H_2O$	*-Nitrosomonas cinnybus/nitrosa*
		-Nitrosococcus mobilis
Nitrite oxidation (NO)	$NO_2^- + H_2O$	*-Nitrospira marina*
	$\rightarrow NO_3^- + 2H^+ + 2e^-$	*-Nitrospira moscoviensis*
Heterotrophic respiration	$CH_2O + O_2 \rightarrow CO_2 + H_2O$	*-Alphaproteobacteria*
		-Gammaproteobacteria
Denitrification		*-Thiomicrosporia denitrificans*
Heterotrophic	$5CH_3COO^- + 8NO_3^- + 3H^+$	*-Pseudomonas stutzeri*
	$\rightarrow 10HCO_3^- + 4N_2(g) + 4H_2O$	*-Pseudomonas sp.*
		-Paracoccus denitrificans

There are three major ways of removing DIN from RAS. Two of them have already been described; increasing the HRT of the system and utilizing denitrification to convert DIN into nitrogen gas. These two alternatives do not allow reuse of nutrients. As tremendous energy is put into fixing atmospheric nitrogen into ammonia in fertilizers, it is a big waste to release the nutrient back into the atmosphere as nitrogen gas- or to the recipient water bodies as nitrate. The third option is to cultivate plants or microalgae on the nitrogen rich RAS water, allowing bioremediation of both nitrogen and phosphorus. Microalgae and plants assimilate DIN and P into biomass, which can be harvested and used for other purposes. As microalgae tolerate saline water, they are the preferred choice when saline RAS water is used as the cultivation medium. With respect to the UN SDG 12: Responsible consumption and production, the third option of removing DIN from RAS is a more sustainable alternative (United Nations, 2022b).

1.4 Microalgae and parameters affecting their growth

Cultivation of microalgae is a promising tool for efficient treatment of RAS wastewater, allowing removal of excessive nutrients as well as binding them into algal biomass (Liu et al., 2020). Microalgae are categorized as photosynthetic, unicellular, aquatic micro-organisms residing in both fresh- and marine waters (Liu et al., 2020, Ruane et al., 2010). They can assimilate both ammonium, nitrite, and nitrate from the surrounding environment, exemplified with the assimilation of nitrate, which can be accomplished through assimilatory nitrate reduction. In the cells, nitrate is reduced to nitrite and further to ammonia before it is incorporated in amino acids and used for synthesis of proteins. As their source of carbon, microalgae consume dissolved inorganic carbon (DIC), either as carbon dioxide (aq) or bicarbonate (HCO_3^-), or they can use atmospheric carbon dioxide or bacterial degraded organic carbon (Christenson and Sims, 2011, Kesaano and Sims, 2014).

The bioavailability of DIC in the water is influenced by the pH of the system (Kumar Singh et al., 2022, Moheimani, 2013). There is an equilibrium between carbon dioxide, carbonic acid (H_2CO_3), bicarbonate (HCO_3^-), and carbonate (CO_3^{2-}), which is referred to as the carbonate system (*Equation I*). The equilibrium is highly affected by the pH, which directly effects in what form the DIC is more abundant in the medium. As microalgae consume DIC, the equilibrium is pushed towards carbon dioxide, which reduce the number of free protons (H^+) in the medium. Consequently, the pH of the system increases, which shifts the equilibrium towards carbonate. This might potentially create a carbon limitation for the microalgae. However, processes in RAS, like respiration and nitrification, works the other way, producing carbon dioxide and consuming bicarbonate. Linking these counterparts may reduce the need for extra buffering of the RAS water to sustain a neutral pH.

Equation I: The carbonate system: Carbon dioxide (CO_2), carbonic acid (H_2CO_3), bicarbonate (HCO_3^-), and carbonate (CO_3^{2-}) (Stips et al., 2016, Turley et al., 2004).

$$CO_2 + H_2O \Leftrightarrow H_2CO_3 \Leftrightarrow H^+ + HCO_3^- \Leftrightarrow H^+ + CO_3^{2-} \quad (I)$$

Due to feeding, respiration, and fish metabolism, RAS water has potential as a medium for microalgae cultivation. The key elements for microalgae cultivation is carbon, nitrogen, phosphorus, and silica (in the case of diatoms) (Kesaano and Sims, 2014). For microalgae cultivation, the nutrient ratios of C:N:P is often used as an indicator of the growth opportunities of the system, using the Redfield ratio (106:16:1, molar basis) as a standard for balanced growth (Redfield, 1963). The ratios are used to predict possible limitations in the system and can be used to alter the conditions to minimize these. In addition, several micronutrients (calcium, magnesium, potassium, iron, manganese, sulfur, zinc, copper, and cobalt) are required in trace amounts. The concentration of silica in RAS is dependent

on the water source and dilution ratio between sea- and freshwater. In seawater, a typical concentration is between ~1-20 mg L^{-1} (Zhang et al., 2019, Haidari et al., 2022). Silica is essential for most diatoms, being an requirement for cell wall biosynthesis (Kumar Singh et al., 2022). In general, pH and light energy are important factors impacting the growth of microalgae (Kumar Singh et al., 2022). Cell processes like cell membrane fluidity, membrane transport, cell cycle regulation, and protein folding are pH dependent (Kumar Singh et al., 2022, Orij et al., 2011). The optimal pH for microalgae is species dependent; however, the range is often found within the interval of 6-9 for species coming from the sea (Brindhadevi et al., 2021, Moheimani, 2013).

Light is the source of energy in the photosynthesis and is therefore an essential factor for microalgae growth. Even though microalgae can alter their photosynthetic apparatus to adapt to the intensity of the light inflicted upon them, algal growth inhibition may occur when the light intensity is too high (photoinhibition) or too low (photo limitation) (Kesaano and Sims, 2014). Photoinhibition occurs when the light intensity is above the treshhold of the microalgae, creating disruption of chloroplast lamellae and inactivation of CO_2-fixing enzymes (Brindhadevi et al., 2021, Juneja et al., 2013, Wahidin et al., 2013). Optimal light intensity- and light wavelength is species specific; however, (Hill et al., 2009) and (Liu et al., 2013) described light saturation at 100 and 150 µmol photon $m^{-2}\,s^{-1}$, respectively. On the other hand, (Hill and Fanta, 2008) considered growth below 88 µmol photon $m^{-2}\,s^{-1}$ as light limited. Research shows that microalgae can be cultivated above or below their optimal range, which can modify the biochemistry of the microalgae, resulting in increased levels of tri-acyl glycerol (TAG) or poly-unsaturated fatty acid (PUFA) content (Brindhadevi et al., 2021). High light intensities can boost lipid content, increasing it to more than 60% of the dried biomass (Ruane et al., 2010). (Zhuang et al., 2018) found that proteins, lipids, and polysaccharides can constitute more than 95% of the dried biomass of microalgal cells, highlighting the potential as a sustainable ingredient in fish feed.

1.5 Attached growth and microbial biofilm

In wastewater treatment, microalgae cultivation has been used as a tool for bioremediation for several years (Liu et al., 2020). Historically, large scale cultivation of microalgae has been done in suspended cultures in high-rate algal ponds or raceways (Liu et al., 2020). Several microalgae species exhibit a rapid growth rate, have high productivity, and efficient removal of N and P (Ruane et al., 2010, Kesaano and Sims, 2014, Liu et al., 2020). In contrast to suspended growth systems, attached growth systems consume less water and space (Zhuang et al., 2018), and are useful tools to optimize light distribution. An attached growth system for wastewater treatment is achieved by providing a favorable surface for microbial attachment, as well as proper conditions to metabolize the pollutant of concern (Kesaano and Sims, 2014).

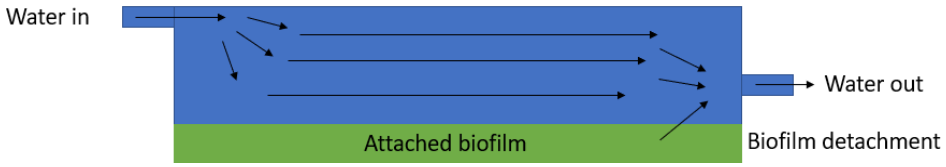

Figure 3: The relationship between solids retention time (SRT) and hydraulic retention time (HRT) is illustrated in an attached growth system (here, a horizontal system). The attached nature of the biofilm (green) allows the SRT to be low, resulting in less loss of biofilm. The HRT can be kept high (illustrated as three black arrows), treating a large amount of water.

Compared to suspended systems, attached growth systems has a higher potential of wastewater treatment, has good productivity (Zhuang et al., 2018), and is more robust against shock loading (Kumar et al., 2011, Blancheton et al., 2013). An attached biofilm is more readily harvested. By scraping the attached biofilm, the harvest can be easy and cost-efficient, possibly reducing the energy requirement related to dewatering with 99.7% (Ozkan et al., 2012, Zhuang et al., 2018). When microalgae are grown in attached growth systems, the microalgae are less prone to wash out (Kumar et al., 2011, Blancheton et al., 2013). The attached nature of the biofilm allows the microalgae to remain in the system, thereby increasing the solids retention time (SRT). Consequently, attached growth systems offers the ability of increasing the SRT above that of the HRT (Liu et al., 2020, Zhuang et al., 2018), giving the opportunity of keeping a high SRT while the HRT is kept low. Utilizing this, attached growth systems can have robust water cleaning, despite fluctuations in the water flow (Zhuang et al., 2018, Liu et al., 2020).

One way of growing microalgae in an attached growth system is the horizontal flat plate system for attached growth. In such system, a solid surface is provided for the microalgae, which is fully or partly submerged in the cultivation medium. The plates are horizontally placed, with light coming from above (*Figure 3*).

A disadvantage with horizontal systems for attached cultivation of microalgae is the reduced cultivation opportunities of a horizontal construction, limiting the growth to only one layer (if natural light is used), as well as on only one side of the cultivation plate. An alternative strategy is to grow attached microalgae in a vertical cultivation system (*Figure 4*), and in that way reduce the construction area needed. By utilizing three dimensions, as well as two cultivation sides, several racks of vertically placed systems can be stacked together, and in that way increase the biomass production per square meter of land area used. By applying artificial light to promote microalgae growth, light limitations can be overcome.

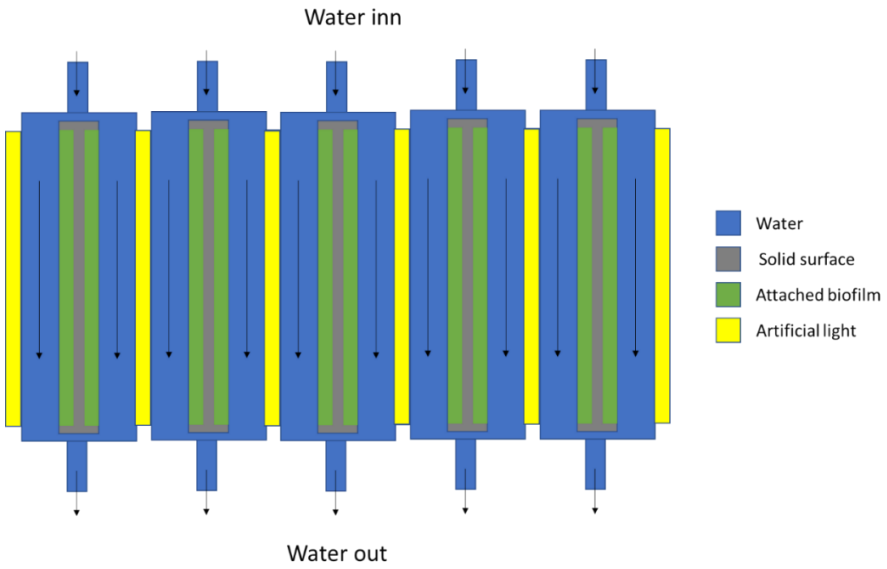

Figure 4: A hypothetical system for cultivation of photoautotrophic biofilm in a vertical attached cultivation system. The illustration shows 5 vertical cultivation systems for photoautotrophic microalgae growth. The water (blue) is flowing from a higher to a lower level, annotated by the black arrows. The water flows by the attached biofilm (green), which bioremediate N, P, and C from the RAS wastewater as it goes by. The attached biofilm is growing on a solid surface (gray). Artificial light (yellow) is added to support the photoautotrophic growth.

1.6 Methods for studying microbial communities

Microorganisms usually live in complex microbial communities, often containing numerous different species interacting with each other and their surroundings (Madigan, 2019, Pham and Kim, 2012, Berdy et al., 2017). Microbiologists have tried to investigate these communities by cultivation- and isolation techniques, isolating single strains from the mixture (Hahn et al., 2019). As only ~2 percent of microorganisms can be grown in the lab (Wade, 2002), this technique is insufficient to use on complex microbial communities. This is illustrated by the observations done by (Lebedeva et al., 2008), who used 12 years of work to successfully isolate a strain of *Nitrospira* (*Candidatus Nitrospira bockiana*). Because of this, other methods for studying complex microbial communities were desired.

From the establishment in 1977, Sanger sequencing was the only method for deoxyribonucleic acid (DNA) sequencing for more than 20 years (Barba et al., 2014). The first-generation sequencing platform was limited to only one DNA strain at the time (Sanger et al., 1977), which was both expensive and time consuming. Even though automated large-scale systems for Sanger sequencing were developed, the need for better sequencing platforms was desired. As a result, second-generation sequencing platforms were developed in the onset of the 21st century, initiated by Roche and Solexa (van Dijk et al., 2014). The second-generation sequencing platforms were based on sequencing by synthesis technology, which offered both efficient sequencing and low costs (Schuster, 2008, Barba et al., 2014). These sequencing platforms can sequence millions of DNA fragments simultaneously, distinguishing different reads based on already prepared libraries (Clark et al., 2019, Mardis, 2008, Ansorge, 2009, Reis-Filho, 2009).

As a subsidiary of the Beijing Genomics Institute (BGI) group, MGI Tech launched a series of second-generation sequencing machines, which are based on DNA nanoball technology (Kumar et al., 2019). The sequencing follows a *de novo* sequencing by synthesis approach, where fluorescent labeled nucleotides are used to reveal the nucleotide sequence of the DNA molecules synthesized. One of those machines are the DNBSEQ platform, which allows sequencing with reduced costs and read length of approximately 300 base pairs (Kumar et al., 2019).

A limitation with the Second-generation sequencing platforms is the relatively short read length, forcing the researchers to choose a subset of the studied genes to sequence (typically 16–33% of the total length). In microbial community analysis, more species can have the same amplified region, which can result in reduced resolution and depth of the investigation (Fuks et al., 2018). Together with PacBio, Oxford nanopore sequencing are third generation sequencing platforms (Clark et al., 2019), which are based on single molecule real time sequencing. Adapted and commercialized by Oxford Nanopore Technologies (ONT), nanopore sequencing offer the power to sequence longer stretches of DNA, allowing better phylogenetic and taxonomic resolution, as well as allowing the high throughput seen in the second-generation sequencing technologies.

ONT is based on a nanopore detector composed of a membrane with a channel (~1 nm in diameter) separating two aqueous compartments. Due to the negative nature of DNA, the DNA molecule passively diffuses through the channel based on the electrical flow of ions. The nanopore channel is so small it only permits one nucleotide (ssDNA) to pass at the time. As the DNA molecule diffuses from the negative to the positive compartment, a detector records the change of current in the pore. Each base has its own electrical pattern, revealing the composition of bases in the DNA molecule (Clark et al., 2019).

Compared to DNBSEQ sequencing, a limitation with Oxford nanopore sequencing is the relatively high error rate. However, it is advantageous above DNBSEQ because of its high speed and its ability to handle long DNA-molecules (Clark et al., 2019).

An environmental sample can contain a plethora of prokaryote and eukaryote species, as well as archaea and viruses. For instance, a sample collected from the sea could contain several strains of bacteria, microalgae, protozoan, ciliates, fungus, amoeba, and nematodes. There are different molecular approaches that can be utilized for species identification in such samples. In amplicon sequencing, selected regions of the genome are amplified by polymerase chain reaction (PCR) to generate defined regions that can be used to sequence and differentiate species from each other.

For this purpose, highly conserved regions, such as the ribosomal ribonucleic acid (RNA) (rRNA) genes encoding the 16- and 18S rRNA, as well as the 28S ribosomal subunits, are often used (Lundberg et al., 2013). The amplified regions contain conserved and variable regions. Conserved regions are sequences of DNA that are conserved between species of interest. This can for instance be sequences involved in translation, where the conserved gene has an essential structural function in the ribosome protein. An example is the universally conserved sites G530, A1492, and A1493 in 16S rRNA sequences, which have a crucial role in binding tRNA to the A site of the ribosome (Wang and Qian, 2013). In contrast, variable regions are sequences of DNA that vary between different organisms. This can be differences in proteins and single nucleotide polymorphisms (Fuks et al., 2018). The conserved regions are used to make primers for PCR that are compatible with DNA molecules coming from all the different species. After sequencing the DNA molecules, the variable regions are used to separate the different species from each other.

Common marker genes used for species separation are the small ribosomal DNA (rDNA) regions 16- and 18S, for prokaryotes and eukaryotes, respectively (Langille et al., 2013, Karst et al., 2018). The 16- and 18S rDNA contain several highly conserved regions accompanied by a variety of variable regions (Fuks et al., 2018). Both genes are composed of nine hypervariable regions (V) V1 to V9. Generally, prokaryote species are often identified by amplification of 16S, by 341F and 805R primer spanning at V3 and V4 region, while eukaryotes can be targeted by a variety of primers at V7 for the corresponding 18S marker gene (Fuks et al., 2018, Hadziavdic et al., 2014).

1.7 The wasteless project

The release of N and P from RAS into recipient waterbodies exhibit a threat to the environment and is a meaningless loss of valuable nutrients. Instead, these nutrients could be incorporated into microbial biomass, which could be harvested and used for other purposes. This master thesis is founded on the Wasteless project, a cooperation between Norwegian university of science and technology (NTNU), Sintef Ocean AS, Nofitech AS, and Hardingsmolt AS, and is funded by the Norwegian Research Council and the industry partners of the project.

The objective of the project is to reduce the discharge of N and P from RAS into recipient water bodies, and to move the dissolved nutrients of the RAS water into biomass that can contribute to a more sustainable feed production. The project aims to use a photoautotrophic biofilter to cultivate a microbial biofilm community consisting of bacteria and microalgae already present in the RAS water. By using different selection parameters, the species composition of the biofilm can possibly be altered to contain more favorable species, thereby potentially increasing the content of protein and fat in the biomass. Characterization of the microbial community is therefore important to understand what

individuals are present under which conditions. As the biofilm grows, nutrients are moved from the RAS water into microbial biomass. By harvesting the biofilm, nutrients can be recovered in a form that can be useful in feed production or fertilizer. By implementing a photoautotrophic biofilter in RAS, the water use and treatment components of the RAS facility can possibly be reduced, as well as the nutrient discharge from the RAS.

1.8 Aims

The main goal of this master's thesis was to cultivate a microbial biofilm consisting of a consortium of microorganisms already present in the RAS water, with the RAS water as cultivation medium. The following subgoals were defined, each with specific experiments shown in brackets:

1. How three different light intensities influenced the growth and composition of the microbial biofilm (experiment 1).
2. How the addition of silica influenced the productivity and the microbial species composition of the biofilm (experiment 2).
3. How the nutrient load, as well as the addition of certain micronutrients influenced the productivity, the biomass yield, and the species composition of the biofilm (experiment 3).
4. How three different harvest rates influenced the productivity and the species composition in a developed biofilm system (experiment 4).
5. Compare the biomass yield and the species composition obtained in two pilot reactors operated at the RAS facility Hardingsmolt AS, with those obtained in the lab experiments at NTNU Sealab.

To solve the aims of this master's theses, it was desired to start with small, controlled, bench experiments in batch. In this way, the growth and species composition could easily be monitored and sampled. To see whether light, addition of silica, the nutrient load, and the addition of micronutrients influenced the microbial growth and species composition of the biofilm, cell cultivation flasks were used as cultivation compartments. These were suited due to their manageable size, the ability to visually inspect the growth, as well as the capability of controlling the environment. Later, as details about the RAS water became clear, the intensity and size of the experiments were increased. As a result, flow through photoautotrophic reactors were used to mimic a real RAS, as well as two pilot reactors operated at the RAS facility Hardingsmolt AS. The development of the microbial communities was investigated genetically by targeting the genomic 16- and 18S rRNA marker genes in DNBSEQ and Oxford nanopore sequencing, for the prokaryote and eukaryote parts the community of the biofilm, respectively.

2. Materials and methods

2.1 RAS water coming from Hardingsmolt AS

All experiments were performed with RAS water collected in periods where the RAS was stocked with fish. The experiments were conducted with batches of RAS water. For each batch, the RAS water was collected just after particle filtration (drum filter) into 50 or 1000 L plastic containers. The containers were transported from the RAS facility to the lab by truck. The duration of the transport varied between 1 and 2 days; however, the cans were stored 2-10 days outside the RAS facility before they were picked up- and transported to the lab. In the lab, the containers were stored in the dark, at 6°C. The concentration of nitrite-N, nitrate-N, and phosphate-P were analyzed in the lab (*Dissolved inorganic N and P in the RAS water*).

2.2 Design of the cultivation experiments

This master' thesis consisted of four separate experiments executed at the lab at NTNU Sealab, as well as two pilot reactors operated at the RAS facility Hardingsmolt AS (*Table 2*). All experiments gave valuable information on mixed community photoautotrophic biofilm cultivation on RAS water. The first experiment was planned as a planktonic experiment to test light. As the growth turned out to be benthic, the method used to measure growth was not suitable. In the second experiment, silica was added to test whether the concentration in the RAS water was sufficient for optimal growth of the benthic community, among others consisting of diatoms. Similarly, the third experiment tested the nutrient load of the RAS water, as well as addition of certain micronutrients. This was done to investigate whether the RAS water contained enough nutrients for microbial growth. In the last lab-experiment, flow through systems were built, where three different harvesting rates were tested to see what was more beneficial in relation to biomass yield and species composition of the biofilm.

Table 2: The number and design of the experiments conducted in this thesis, as well as the different variables studied- and analysis executed.

Number	Experiment	Variables studied		Analyses		
		Light intensities	Other	Biomass	SGR	Microbial community
1	Effect of light	High, Medium, Low				X
2	Effect of silica	High	± Silica	X	X	X
3	Effect of nutrients	High	Added nutrients	X	X	X
4	Effect of harvest rate	High	Harvest rates	X	X	X
5	Pilot demonstration	High	Horizontal, Vertical	X		X

*SGR = specific growth rate.

In addition, two photoautotrophic attached growth pilot reactors for biofilm production were operated at the smolt facility Hardingsmolt AS for approximately three months. This was done to proof the concept, that it was possible to obtain biomass on site, and to investigate the species composition of the biofilm at site.

At the facility, the temperature of the rearing water was maintained at ~13°C. As it was desired to keep the conditions like the RAS, all the experiments were conducted at 13°C to mimic the real-life environment of the RAS.

2.2.1 Effect of light

For each condition (high, medium and no light: ~240, ~160, <20 µE m^{-2} s^{-1}, respectively) quadruplicate cell cultivation flasks (0.850 L) were used. The light intensity was measured with a light meter (WALZ, ULM-500, WALZ GmbH, Germany). The flasks were oriented vertically in respect to the light source to give maximum light penetration into the flasks. Each flask was equipped with two tubes: One for aeration (compressed atmospheric air, ~3 bubbles per second) and one for sampling (*Figure 5*). The air was filtered (0.22 µm, hydrophobic filter) to avoid contamination into the flasks. To minimize the risk of contamination, all equipment were autoclaved, or acid washed before use. All 12 cell cultivation flasks were incubated with RAS water: 0.765 L autoclaved RAS water (9/10 of the total volume) and 0.085 L non-autoclaved RAS water (1/10 of the total volume). The dilution was done to make sure that plenty of nutrients were available for the microorganisms.

During the experimental period (16 days), measurements of the temperature and the microbial growth was conducted. Samples for genetic community analysis were obtained at day 0, 13, and 16 (*Microbial consortia analysis*). At harvest, separate syringes were used to avoid cross contamination. The cell cultivation flasks were shaken (2-3 times) before samples were collected. The first 2 mL were always discarded to remove any leftover sample in the sapling tube from the day before. The microbial growth was monitored with use of a spectrophotometer (OD_{460} and OD_{750}) (UviLine 9100, SI Analytics, Germany).

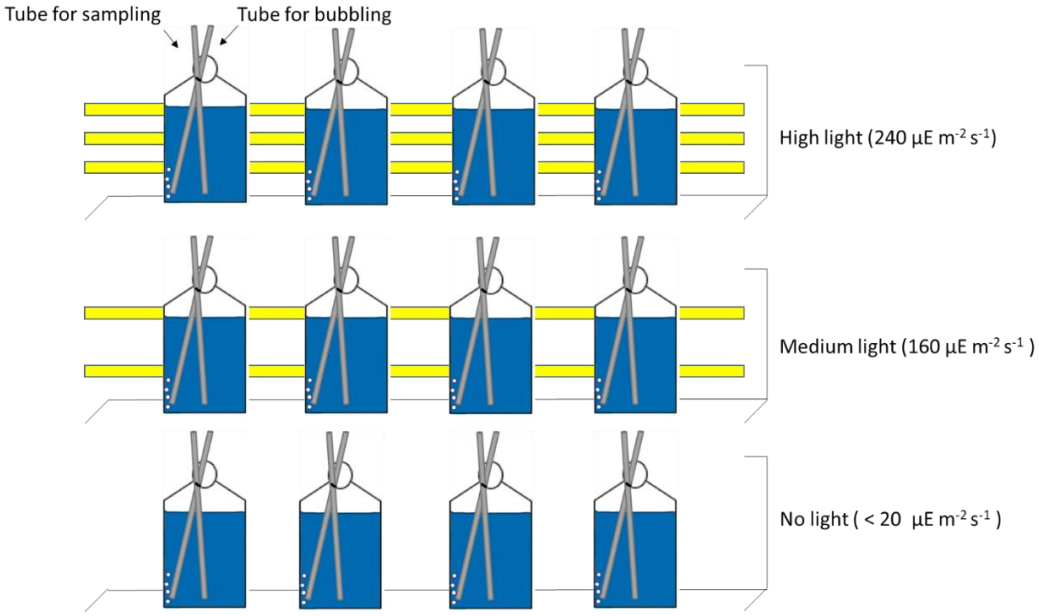

Figure 5: The experimental setup of the experiment testing light intensity. The illustration shows three growth conditions (High (240), Medium (160), and No (<20) light (µE $m^{-2}s^{-1}$)), with respective quadruplicates. In each flask two tubes are exemplified as grey straws to illustrate the tubes for sampling and bubbling, respectively.

2.2.2 Effect of silica

A total of 60 (0.019 L, 0.0025 m^2) and 16 (0.060 L, 0.0075 m^2) cell cultivation flasks were used. The experiment was conducted to investigate whether biofilm development was limited by silica. For the treatment: Silica, silica ((Na_2SiO_3 – 5(H_20)), 1 µL mL^{-1}) was added to the cell cultivation flasks (30 small and 8 big) in respect to the silicate solution (*Table 3*). The control: No silica, contained only RAS water. The cell cultivation flasks were inoculated with a combination of autoclaved RAS water and experimental water coming from the previous experiment. This was done to make sure that the start water contained benthic diatoms.

At day 15, Conway medium (1 µL mL^{-1}) (*Table 3*) was added to all cell cultivation flasks to overcome issues concerning nutrient limitations. The cell cultivation flasks were incubated at constant light (203 - 333 µE $m^{-2}s^{-1}$) throughout the experimental period (37 days). The light source was a light bench. The light intensity was measured with a light meter (WALZ, ULM-500). To minimize the effect of varying light intensity below the light bench, the cell cultivation flasks were distributed randomly (*Appendix D, Figure D. 2*).

During the experimental period (T0-T37) the biomass concentration (g m^{-2}) was estimated based on either microscope analysis (T0-T27) (*Microscopic method to follow biofilm growth*) or by weighting of the dried biomass (T30-T37) (*Dry weight*). Triplicates from both conditions were used to represent the biofilm development during the experimental period. Duplicate samples were harvested for genomic community analysis at day 0, 31 and 36 (*Microbial consortia analysis*).

Table 3: The chemical composition of the Conway medium and the silicate solution used in the experiment testing addition of silica. The table shoes the content of each stock solution, together with the respective concentration. The table was modified from (Andersen, 2005)

Conway Medium		**Silicate solution**
Nitrate	$NaNO_3$ (100.0 g L^{-1})	Na_2SiO_3 – $5H_2O$ (22.5 g L^{-1})
Phosphate	NaH_2PO_4 (17.4 g L^{-1})	
Trace metals	Na-EDTA (30 g L^{-1})	
	$FeCl_3$ - $6H_2O$ (1.3 g L^{-1})	
	$MnCl_2$ - $4H_2O$ (0.36 g L^{-1})	
	$ZnCl_2$ (0.0211 g L^{-1})	
	$CoCl_2$ - $6H_2O$ (0.0200 g L^{-1})	
	$CuSO_4$ - $5H_2O$ (0.0200 g L^{-1})	
	$(NH_4)_6Mo_7O_{24}$ - $4H_2O$ (0.0900 g L^{-1})	
	H_3BO_3 (30.0 g L^{-1})	
Vitamins	Thiamin HCl (0.10 g L^{-1})	
	Cyanocobalamin (B12) (0.005 g L^{-1})	

2.2.3 Effect of nutrients

The experiment was executed in two parts to investigate the growth potential of the RAS water coming from Hardingsmolt AS. The first part tested high and low nutrient load, to see if the nutrient load influenced the biomass yield and the productivity of the biofilm. The second part tested addition of certain micronutrients, to see if the concentration of that particular nutrient was low in the RAS water.

In both parts, the cell cultivation flasks were incubated at constant light (203 – 333 µE m^{-2} s^{-1}). The light intensity was measured with a light meter (WALZ, ULM-500). The light source was a light bench. Due to varying light intensity beneath the bench, the cell cultivation flasks were placed randomly to adjust for this error.

The first part of the experiment lasted 18 days and tested high and low nutrient load. The treatment: High nutrient load (High N), contained thirty small (0.019 L, 0.0025 m^2) and four big (0.060 L, 0.0075 m2) cell cultivation flasks, which were inoculated with a combination of autoclaved RAS water (9/10) and non-autoclaved RAS water (1/10).

The control: Low nutrient load (Low N), contained thirty small and four big cell cultivation flasks, which were inoculated with a combination of RAS water (1/10) and nutrient poor autoclaved RAS water (9/10) collected when the fish in the RAS were not fed (starvation).

In addition, 6 small cell cultivation flasks were inoculated with non-autoclaved RAS water (10/10) to see if the dilution influenced the development of biofilm.

The second part of the experiment was an extension of the first part. The second part included all the cell cultivation flasks coming from the previous part (high- and low nutrient load), as well as the six flasks containing only RAS water. From the previous High_N condition, triplicate cell cultivation flasks were inoculated with different nutrient (*Appendix, Table C. 1*). The condition "Only RAS" and the control (Low_N) were the same flasks as the ones used in the first part of the experiment.

During the experimental period (T0-T48) the biomass concentration (g m^{-2}) was estimated based on microscope analysis (T0-T18) (*Microscopic method to follow biofilm growth*) or dry weight (T20 and T48) (*Dry weight*). Triplicate samples from both conditions were used to represent the development of biofilm throughout the experimental period. At the last day of the experiment (T48), all cell cultivation flasks were harvested. For the cell cultivation flasks with an addition of nutrient (19 mL), the harvested samples were made homogeneous before they were split in two. One part (13 mL) was used to measure dry weight (g m^{-2}), whereas the rest of the sample (6 mL) where used to analyze the microbial community. All the small cell cultivation flasks of the control: Low_N (19 mL) were used to measure dry weight (g m^{-2}). The big cell cultivation flasks (60 mL) were harvested for genomic community analysis (*Microbial consortia analysis*).

2.2.4 Effect of harvest rate

For each condition: Harvest every 4th day, harvest every 8th day, and harvest every 12th day, quadruplicate flow through systems (0.34x 0.25x 0.16 m) were used with corresponding growth plates (0.26x 0.19x 0.005 m) for attached biofilm growth. The growth plates were covered with texture to support algal attachment and growth. The 12 cultivation systems (*Figure 6*) (hereby called the reactors) were supplied with 1.25 L of unfiltered RAS water. All the reactors were inoculated (10 mL) with biomass coming from the RAS facility Hardingsmolt AS (1.0 g biomass 0.250 L^{-1} RAS water).
The first 8 days of the experiment, the reactors were acclimated and incubated with RAS water in batch. Thereafter, a continuous flow of RAS water (0.10 L h^{-1} = 2.5 L day^{-1}) was started. Each of the reactors had their own separate water supply. At day 16 of the incubation and acclimation period, the waterflow was increased (0.146 L h^{-1} = 3.5 L day^{-1}). At day 18, all the growth plates were harvested to promote an equal start point for the experiment (T_0). The following 36 days, the reactors were harvested according to the harvesting interval of their specific condition: Every 4th-, 8th-, or 12th day.
The light intensity was maintained at 230 – 288 µE $m^{-2}s^{-1}$, measured with a light meter (WALZ, ULM-500). The light source was a light bench.

At harvest, water was removed from the reactors and the growth plates were put in a ~30 degrees angel to allow the water to come off without inflicting mechanical stress on the biofilm (~5 minutes). The growth plates were then transferred to aluminum foil to dry for ~5 more minutes. The biofilm was scraped off (Cocraft, Trowel) the growth plates, and collected directly into weighted 50 mL falcon tubes. A small fraction (~0.5 mL) of the sample was transferred into weighted 2 mL Eppendorf tubes for subsequent genetic community analysis (*Microbial consortia analysis*); however, most of the harvested biomass was dried- and weighted to estimate the biomass concentration (g m^{-2}) (*Dry weight*).

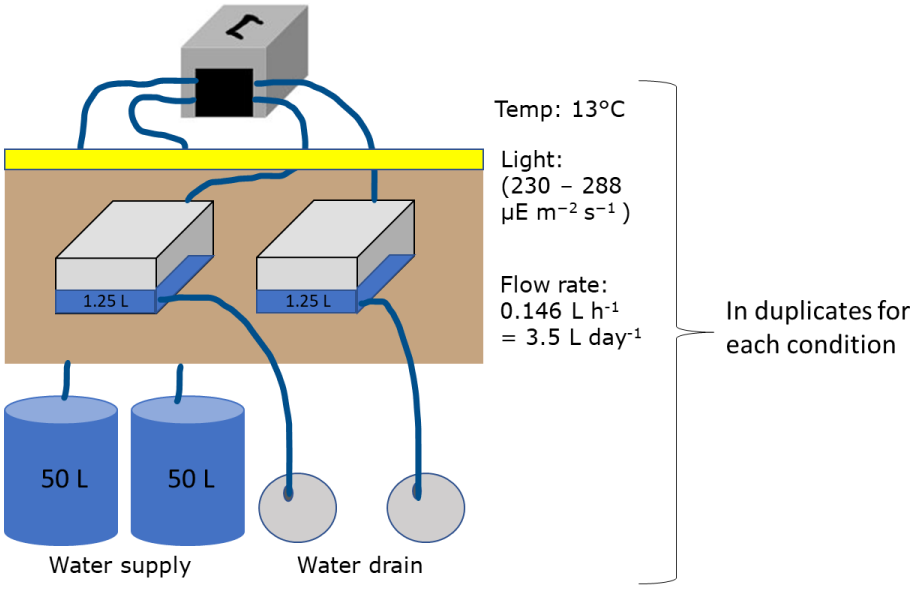

Figure 6: The experimental setup of the experiment testing harvest rate, showing one set of reactors, which were in duplicates. For each condition: Harvest every 4th day, harvest every 8th day, and harvest every 12th day. The water supply is illustrated as blue cylinders containing 50L of RAS water. The reactors are illustrated as gray boxes containing 1.25 L of RAS water (blue). From each of the blue cylinders, a continuous flow (3.5 L day^{-1}) of new RAS waters was introduced to the reactors through hoses (blue straws), connecting the water supply to the respective reactor through a peristaltic pump (grey and black cube). The reactors were placed on a bench (brown), with the light source (230-288 µE m^{-2} s^{-1}) above (yellow). From each reactor, a water outlet (blue hose) allowed the water to be removed from the reactors, released into the water drain (grey).

2.2.5 Pilot demonstration at Hardingsmolt AS

Two photoautotrophic bioreactors (from now on called the reactors) for attached cultivation of microalgae were tested as pilot reactors at the RAS facility Hardingsmolt AS. The reactors were operated for ~3 months. The designs of the reactors are confidential; however, one had vertically oriented attached growth plates and the other had horizontally oriented growth plates. The growth plates were made from polycarbonate, covered with fabric. The water was coming from above, trickling onto the growth plates. The reactors were coupled to a continuous stream of RAS water (~13°C), collected just after the mechanical particle removal (drum filtration) in the water treatment loop (*Figure 1*). Light was provided to select for microalgae growth (DEL Light, 24 W, 4500 K). The last three days of operation, the reactors were harvested every day. At harvest, the biomass was scraped off the plates with a scraping tool (Cocraft, Trowel). The biomass was collected directly into 50 mL falcon tubes and stored at -18°C, before they were transported to the lab and stored at -80°C. Samples were used to calculate biomass yield (g m^{-2}) (*Dry weight*), as well as to investigate the microbial community (*Microbial consortia analysis*).

2.3 Analyses

2.3.1 Dissolved inorganic N and P in the RAS water

For each batch of RAS water, the water was mixed well before samples (4, 2, 2, and 3 replicates, for the experiments testing light intensity, addition of silica, addition of nutrients, and harvest rates, respectively) were collected for water analysis, and stored at -20°C. The day before the RAS water was analyzed, the collected samples were thawed in a fridge overnight. All the samples were filtered (25 mm, 0.45 µm), before they were analyzed in an autoanalyzer (Flow Solution IV System, O.I. Analytical Flow Solution IV System, O.I. Analytical, USA). Nitrate, nitrite, and phosphate were analyzed fluorometrically according to Norwegian standards (NS): NS 4745 (1991), NS 4744 (1975) and NS 4724 (1984), for determination of N-NO_3^-, N-NO_2^-, and P-PO_4^{3-}, respectively. The analyses were carried out at Trondhjem Biological station, NTNU.

2.3.2 Harvest of biofilm

A. Wet weight and volume

The wet weight of the biomass was measured by weighting the harvested biomass after it was collected into weighted 50 mL falcon tubes. The volume of the harvested biomass was obtained by using the graduation lines at the falcon tubes. Tubes were stored at -80°C.

B. Thickness of biofilm

The thickness of the biofilm was calculated based on the volume (mL) of biofilm harvested from the cultivation plates (m^3), with respect to the size of the growth plates (0.19 x 0.26 m; m^2). The thickness was calculated according to *Equation II*.

Equation II: Calculation of the biofilm thickness. Biofilm was scraped and collected directly into 50 mL falcon tubes, where the amount (mL) of biomass was measured based on the graduation lines on the tubes. Then, the measured volume was rearranged into cubic meters (m^3) before the thickness of the biofilm was calculated in respect to the size of the growth plate. The equation is based on the formula for a rectangular parallelepiped (LxWxH).

$$1\ mL = 0.001\ L = 0.001\ dm^3 = 0.000001\ m^3$$

$$\text{Thickness of biofilm (m)} = \frac{\text{Amount of biomass (m3)}}{(0.19\ \text{m x}\ 0.26\ \text{m})} \quad \text{(II)}$$

C. Dry weight

Weighted falcon tubes containing biomass were stored at -80°C. The samples were put directly from the freezer into the freeze drier (FreeZone® Benchtop freeze Dryers, 70080**** 8L -50°C Series, Labconco, USA) and freeze dried for 48 hours. Thereafter, the dry weight was weighted. The amount of dried biomass (g) was then normalized to the size of the cultivation area (m^2), generating the biomass yield (g m^{-2}).

D. Microscopic method to follow biofilm growth

The development of biofilm was also monitored with microscope data (average %area). Pictures were taken with an inverse microscope (Nikon eclipse TE2000-S, Nikon Corporation, Japan) on 100x (testing addition of silica) and 200x (testing addition of nutrients) magnification, at eleven specific coordinates in the cell cultivation flasks. The microscope was operated with Nikon software (NIS-Elements F, Nikon Corporation, Japan), with specific settings according to *Table 4*. The pictures were analyzed with the photo management program ImageJ (ImageJ 1.53e, National Institutes of Health, USA), according to Macro 1 and Macro 2 for the two experiments, respectively (*Appendix E, Macro E. 1* and *Macro E. 2*).

The data was investigated with different statistical approaches (Box plot, QQ-Plot, Shapiro test, Residuals VS Fitted plot, and a Normality test) to get an indication of outliers. The statistical approach pointed out specific values, which were manually inspected before decided on, whether to remove them from the dataset or not. *Figure 7* shows four photos (A, B, C, D), where two of the photos (A and B) produced false values. The statistical approach considered these datapoints as outliers, which was confirmed manually. *Figure 7* also shows two pictures (C and D) which were interpreted properly by ImageJ. After outliers had been removed, a correlation between average %area and average dry weight (g m^{-2}) was made (*Figure 8*). The best fitted line was drawn, producing a correlation coefficient between the two designations ($y = 0.219x + 26.417$), which was used to extrapolate values of %area into dry weight (g m^{-2}).

Table 4: The settings used with Nikon software to take microscope pictures with Nikon microscope.

Setting	Specifics
Mode	Normal
Resolution	
Fast (focus)	1280x960
Quality (capture)	2560x1920
Exposure	
Mode	Auto exposure
AE compensation	+0.6 EV
Exposure	4 ms
Gain	1.40x
Color	
Contrast	Dynamic
	Auto white

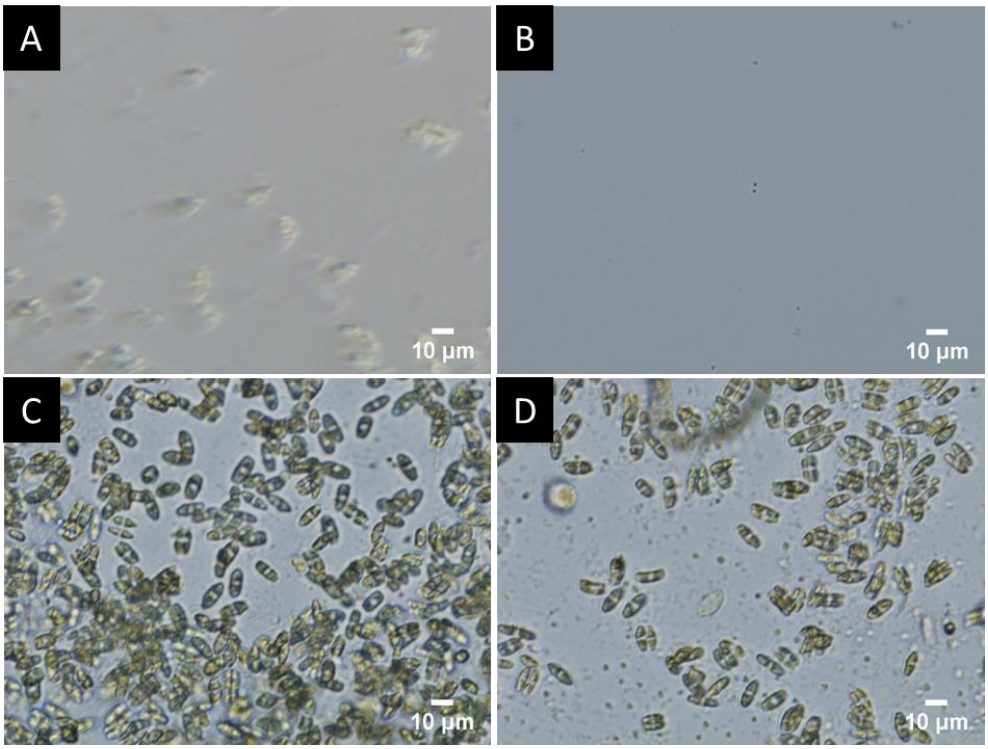

Figure 7: Microscope pictures (A, B, C, and D) taken in an inverse microscope at 200x magnification. Photo A and B are photos of bad quality and no growth, respectively. They were interpreted as photos with high percentage coverage (99.7%) in the ImageJ analysis. Picture C and D illustrates pictures of good quality, which the program managed to interpret correctly.

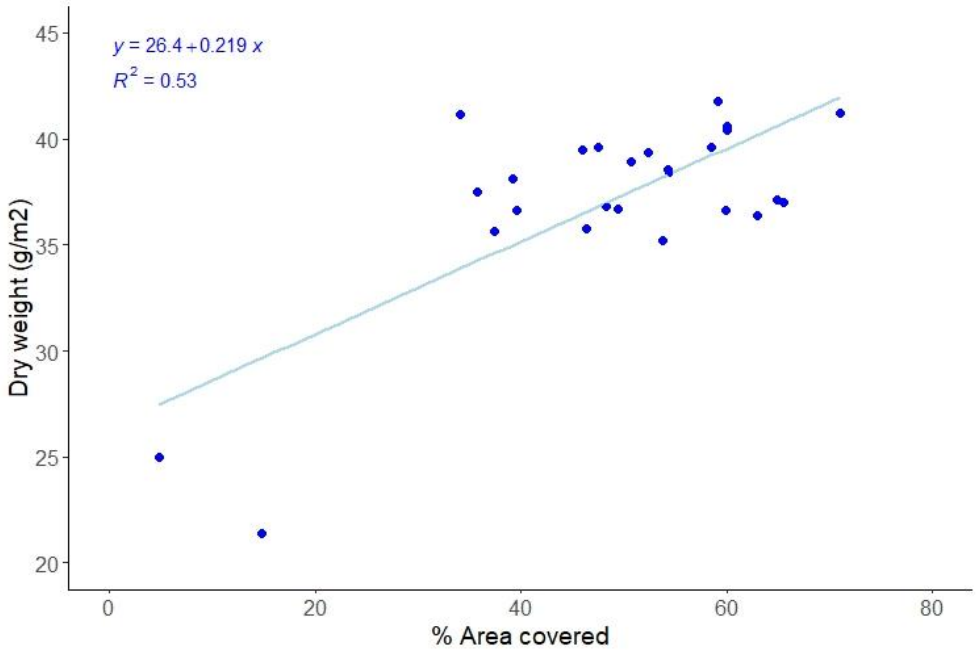

Figure 8: A scatterplot showing data from both designations (%area and g m^{-2}) of the samples obtained at the same experimental day. The best fitted line (y = 0.219x + 26.417) shows the correlation between the two designations, offering a way to extrapolate values of one designation into the other. The P-value of the slope was 0.000023 and the R^2 was 0.53.

E. Productivity

The productivity (g m^{-2} day^{-1}) and the maximum productivity for the different experiments were estimated based on the biomass yield (g m^{-2}). The productivity and the maximum productivity describe the biomass yield per day during the experimental period and during the period with the highest growth, respectively. Both the productivity and the maximum productivity were calculated with *Equation III.*

Equation III: The formula used to determine the productivity and the maximum productivity for the different experiments. g2 and g1 represents the biomass concentration at the final (t2) and initial (t1) time of the growth, respectively. Both the productivity and the maximum productivity were normalized to square meters (m^2), with respect to the size of the different cultivation surfaces used.

$$\text{Productivity } \left(\frac{g}{day} * \frac{1}{m2}\right) = \frac{g2 - g1}{(t2 - t1)} x \frac{1}{m2)} \quad \text{(III)}$$

F. Growth rate

The growth rate (μ) is the increase per day during the exponential phase of the microbial growth. The growth rate was determined based on the logarithm of the dry weight (g m^{-2}) for the samples during this period. The growth rate was calculated based on *Equation IV.*

Equation IV: The calculation used to estimate the specific growth rate (μ). g2 and g1 represents the biomass yield at the final (t2) and initial (t1) time of the exponential phase of the growth period, respectively (Kumar Singh et al., 2022).

$$\text{Specific growth rate } (\mu) = \left(\frac{\ln(g2) - \ln(g1)}{t2 - t1}\right) \quad \text{(IV)}$$

2.4 Microbial consortia analysis

2.4.1 Sample preparation and DNA extraction

Samples were either filtered (Durapore, PVDF membrane filters (0.22 μm) or Whatman Glass microfiber filters (GF/F, 0.22 μm)), directly frozen biomass, or biofilter carriers. For the filtered samples, the amount of filtrated water (mL) was measured. After filtration, the filters were snap frozen in liquid nitrogen and stored in a fridge (-80°C).

The unfiltered biomass was collected directly into 2 mL Eppendorf tubes and frozen (-80°C). All the samples coming from Hardingsmolt AS, biomass and biofilter carriers, were collected into 2 mL Eppendorf tubes and 50 mL centrifuge tubes, respectively. These were first frozen and stored at the facility (-18°C), before they were transported to the lab and stored there (-80°C).

Before extraction, the samples were defrosted and prepared. Both filters and biofilter carriers were cut into small pieces and put into separate bead-beating tubes (grain size = 0.80 and 0.60 μm, Zymo Research, The United States of America (USA)). The samples containing directly frozen biomass were transferred into bead-beating tubes and weighted. For each sample, sterile equipment was used (washed or autoclaved). After sample preparation, the extraction was executed as described in the user manual of the DNA extraction kit, soil samples (*Appendix J*) (ZymoBIOMICS™ DNA Miniprep Kit, Zymo Research, USA).

2.4.2 DNA quality control

Nanodrop spectrophotometer (NanoDrop, ND-1000, Thermo Fisher Scientific, USA) was operated with respective software (ND-1000 V3.8.1, Thermo Fisher Scientific, USA) and used to measure the DNA concentration (ng μL^{-1}) of the samples, as well as the ratio between the wavelength: 260/280nm and 260/230nm. Hydrochloric acid (HCl) (2.0 µL, [0.5M]) were pipetted onto the pedestal of the Nanodrop apparatus (~1 minute) to clean the apparatus before use. The droplet was removed with a fine paper wipe. Thereafter, MilliQ water (2.0 µL) were put on the pedestal (~1 minute) to remove any remaining HCl. The droplet was wiped off. Again, MilliQ water (2.0 µL) was added to the pedestal and the apparatus was initiated. After initiation, the pedestal was wiped, and DNA/RNA free water (2.0 µL) was added to the pedestal as a blank. After the blank was measured, the droplet was wiped off. The samples were loaded onto the pedestal one at a time (2.0 µL) and measured. When all samples had been measured, HCl (2.0 µL) was added to the pedestal to clean it (~1 minute). The droplet was wiped off and MilliQ water (2.0 µL) was added. After ~1 minute, the droplet was wiped off, and the apparatus was turn off.

Because NanoDrop has less sensitivity compared to Qubit, the DNA concentration (ng μL^{-1}) of the samples were also measured with Qubit (Qubit© 3.0 Fluorometer, Thermo Fisher Scientific, USA). Qubit Fluorometers utilize a fluorescent dye, that specifically binds to the DNA. Qubit allows for an increased sensitivity and a more reliable measurement. Based on the results of the NanoDrop, the amount of DNA (1-20µL) used for Qubit was decided on. For each sample, the DNA was mixed with the appropriate volume of Qubit working solution to a final volume of 200 µL. The further procedure was done according to the user manual (Qubit™ 1X dsDNA HS Assay kits)(Thermo Fisher Scientific, 2020).

2.4.3 Preparing samples for DNBSEQ at BGI Genomics

Samples (25.0 µL) were pipetted onto a 96-well plate and sealed with aluminum foil. The samples, with respective information on DNA concentration (ng μL^{-1}), the 260/280 nm ratio, and the 260/230 nm ratios, were sent to BGI Genomics for DNBSEQ sequencing of the prokaryotic 16S rDNA- and the eukaryotic 18S rDNA marker genes. For the prokaryote part of the community, amplicons of the V3-V4 region of the 16S ribosomal rRNA gene were amplified with PCR (338F: 5'-ACTCCTACGGGAGGCAGCAG-3', 806R: 5'-GGACTACHVGGGTWTCTAAT-3'), and later sequenced with DNBSEQ. For the eukaryote part of the community, amplicons of the V7 region of the corresponding 18S rRNA gene was amplified with PCR (960F: 5’-GGCTTAATTTGACTCAACRCG-3’, NSR1438: 5’-GGGCATCACAGACCTGTTAT-3’), and later sequenced.

At BGI, 30 ng of qualified DNA template was used for PCR with 16- and 18S rRNA fusion primers for prokaryotes and eukaryotes, respectively. After amplification of the desired amplicons, all the PCR-products were purified by Agencourt AMPure XP beads, dissolved in elution buffer, and eventually labeled to finish the library construction. Library size and concentration was detected by Agilent 2100 Bioanalyzer. Qualified libraries were sequenced in the DNBSEQ platform according to their insert size. After sequencing, the raw data was filtered to obtain high-quality clean data. This was determined based on overlapping regions in the clean reads. Thereafter, the filtered high quality clean data was merged to tags. This procedure, as well as the data filtering and tags connection is described in *Appendix K*.

2.4.4 Library preparation and Nanopore sequencing

The library preparation was done according to the Oxford nanopore PCR Barcoding Kit protocol (Oxford Nanopore Technologies, 2019). The protocol was modified in the way that amplicons were made beforehand. The protocol therefore starts at the End-prep step in the protocol. The PCR Barcoding Kit (SQK-PBK004) was used in the library preparations, and flow cell priming was done according to the Flow cell priming kit (EXP-FLP002). The eukaryote part of the microbial community of the samples were target (3NDf_18S - 21R_28S). The eukaryote genomic DNA operon was flanked by the forward and reverse primers: 5'-GGCAAGTCTGGTGCCAG and 5'-GACGAGGCATTTGGCTACCTT, respectively. The length of the targeted amplicon were species dependent; however, the length was expected to be within the length of 4000-6000 bp. Based on the DNA concentration (ng μL^{-1}), appropriate volumes of DNA were transferred to separate PCR tubes (DNA LoBind tube, Eppendorf, Germany) and diluted with nuclease free water to reach a final concentration of DNA [30 ng μL^{-1}] and volume (10.5 µL) in the tubes. Forward (1 µL, [50 nM]) and reverse (1 µL, [50 nM]) primers were added to the LoBind tubes, together with the mastermix (12.5 µL, LongAmp Hot Start Taq 2X Master Mix, New England Biolabs, USA). All reagents were stored on ice during the procedure. PCR was executed in a thermocycler (Bio-Rad, iCycler, Bio-Rad Laboratories, USA), according to *Table 5*.

After length and quality had been validated, the samples were prepared for nanopore sequencing (End-Prep, PCR adapters ligation- and amplification, Rapid adapter ligation, and Priming- and loading the SpotOn flow cell), according to the protocol (Appendix J) (Oxford Nanopore Technologies, 2019). One exception to the protocol was made; rather than applying 50 µL samples, 25 µL samples were used in the initial step (End-Prep). Therefore, half of the volume of the reagents used in this step (End prep procedure) were used. The prepared library was loaded on a flow cell (Spot-ON Flow Cell, R9.4 Version, Oxford Nanopore Technologies, United Kingdom), and sequenced with use of ONT MinION sequencer (MinION Mk1B, Oxford Nanopore Technologies, United Kingdom). Sequencing was initiated through MinKnow software (MinKnow, Version 20.10, Oxford Nanopore Technologies, United Kingdom), with option selected for basecalling, quality filtering (Q score > 7), and demultiplexing. Based on the Barcoding kit, up to 12 uniquely marked samples could be loaded onto the flow cell. In total, 3 sequencing runs were performed on three different flow cells. Overall, 21 samples were sequenced.

The PCR products were validated by electrophoresis (Agilent, TapeStation 4150, Agilent Technologies, USA), and the data was analyzed in appropriate software (Agilent TapeStation Controller Software 4.1.1, Agilent Technologies, USA) (*Appendix G*). Tapestation electrophoresis was done according to the protocol for dsDNA molecules in the range of 200 to >60000 basepairs (Agilent Technologies, 2015). After length and quality had been validated, the samples were prepared for nanopore sequencing (End-Prep, PCR adapters ligation- and amplification, Rapid adapter ligation, and Priming- and loading the SpotOn flow cell), according to the protocol (*Appendix J*) (Oxford Nanopore Technologies, 2019). One exception to the protocol was made; rather than applying 50 µL samples, 25 µL samples were used in the initial step (End-Prep). Therefore, half of the volume of the reagents used in this step (End prep procedure) were used.

The prepared library was loaded on a flow cell (Spot-ON Flow Cell, R9.4 Version, Oxford Nanopore Technologies, United Kingdom), and sequenced with use of ONT MinION sequencer (MinION Mk1B, Oxford Nanopore Technologies, United Kingdom). Sequencing was initiated through MinKnow software (MinKnow, Version 20.10, Oxford Nanopore Technologies, United Kingdom), with option selected for basecalling, quality filtering (Q score > 7), and demultiplexing. Based on the Barcoding kit, up to 12 uniquely marked samples could be loaded onto the flow cell. In total, 3 sequencing runs were performed on three different flow cells. Overall, 21 samples were sequenced.

Table 5: The settings used for PCR in the thermocycler to amplify the specific DNA amplicons used for characterization of the eukaryotic 18s rDNA.

Cycle step	Temperature	Time	No. of cycles
Initial denaturation	94	1 min	1
Denaturation	94	30 secs	
Annealing	61	30 secs	30
Extension	65	3 min 45 secs	
Final extension	65	5 min	1
Hold	4	inf.	

2.4.5 Bioinformatics and the community analysis

A. DNBSEQ sequencing

The sequences delivered by BGI Genomics were DNBSEQ reads, and the data were composed of demultiplexed paired-end sequences with quality (fastq). Obtained sequencies were treated using Quantitative Insight Into Microbial Ecology 2 (QIIME2) pipeline (Qiime-2023.2) (Bolyen et al., 2019). Initially, forward and reverse read for each sample were loaded in appropriate QIIME2 artifact. Subsequently, quality control (based on Phred value > 20), denoising, and Amplicon Sequence Variants (ASV) calling was conducted using DADA2 algorithm (Callahan et al., 2016). DADA2 was used subsequently to merge complementary ASV for the forward and reverse reads. Additionally, a table containing ASVs and counts was generated for each sample. Furthermore, chimera sequences were screened and filtered based on DADA2 de novo approach. Next, representative sequences were aligned using MAFFT (de novo multiple sequence aligner) (Katoh et al., 2009), before masked and phylogenetic tree was generated using FastTree (Price et al., 2009). Finally, taxonomic assignment was set to each of the representative sequences. This was conducted with use of the Silva Classifier (Silva, v.138) (Yilmaz et al., 2013), specifically pretrained for the primer-set region used to amplify sequenced amplicons. Then, taxonomy was added to a biom file (the recognized standard for the Earth Microbiome Project) and imported into RStudio for subsequent diversity analysis.

B. Oxford nanopore sequencing

The demultiplexed sequences generated with Oxford nanopore sequencing were treated with Minimap2 (Li, 2021). Primary sequence alignment was identified, while one or more secondary alignments were discarded. Moreover, alignments were filtered based on minimum query coverage (30%) and maximum divergence (70%) against the small ribosomal subunit (ssu) or the large ribosomal subunit (lsu) of the Silva database (Silva, v.138) (Yilmaz et al., 2013). Finally, a table reporting how many reads aligned to each sequence in the database was generated.

C. Diversity analysis

For the investigation of the prokaryote part of the community, non-bacterial sequences (e.g., chloroplast and mitochondria), sequences that were less then ~5% abundant, as well as species that were undefined at the Kingdom level, were removed from the further analysis. For the investigation of the eukaryote part of the community, ONT sequences that were less then ~5% abundant were assigned as "Other", as well as undefined sequences were assigned as "Unassigned".

For the diversity analysis, the samples had to contain a similar sampling depth before further analysis could be carried out. Sampling depth refers to the number of sequencing-reads obtained during sequencing for the different samples. Among the samples investigated, an equal sampling depth is important to correctly compute the diversity matrices and to carry out the statistical analysis. The sampling depth was chosen in such a manner to allow most of the samples to be retained in the further analysis.

When an equal sampling depth had been set, an Alpha rarefaction plot was created to see whether the sequencing effort was good at the selected sampling depth. Based on the steepness/flatness of the Alpha rarefaction plot, it was possible to tell whether the sequencing effort was sufficient to recapture most of the community members of the samples. The Shannon diversity index (Shannon, 1948) and Chao index (Chao, 1984) were used to investigate the microbial diversity and richness, respectively. The assumptions (testing outliers, normality, and homogeneity) were tested to decide what statistical tests could be used to check the significance of the investigation.

Unweighted UniFrac measurements and Bray-Curtis dissimilarity analysis were used to examine the differences across treatments (beta diversity). Unweighted UniFrac measurements were used to investigate the species diversity between treatments (Lozupone and Knight, 2005), which is based on the concept of UniFrac. UniFrac quantifies the fraction of branch length on a phylogenetic tree that is unique to either of the compared samples. Unweighted UniFrac measurements are used to calculate dissimilarities between communities by counting the number of branches that are unique for each community, regardless of the length of the branches. The measurement does not consider the abundance and relative abundance of taxa, but rather focuses solely on the presence or absence of specific linages. Similarly, Bray-Curtis dissimilarity was used to compare differences between samples based on the number of amplicon sequence variants (ASVs) in a sample (Bray and Curtis, 1957). The Bray-Curtis dissimilarity analysis considers both the presence and abundance of different taxa for the communities compared to each other. The results of the unweighted UniFrac measurements and the Bray-Curtis dissimilarity analysis were combined and presented in principal coordinate analysis (PCoA) plots (Krzanowski and Krzanowski, 2000). At the end, the relative abundance (% of total sequences) of the different taxa were plotted in a bar chart for each condition, with respective taxonomic classification.

The sequences obtained by DNBSEQ sequencing were used for all above, whereas sequences obtained by ONT sequencing was only used for taxonomic classification (bar chart with relative abundance).

2.5 Statistical analysis

Statistical analyses were carried out using the R program, version 2022.02.0+443 for Windows (Team, 2022). Plots were made in ggplot2 (Wickham, 2016). The experiments testing light intensity and harvest rate were done in quadruplicates, whereas the experiments testing addition of silica and addition of nutrients were executed in triplicates. For each experiment, mean ± standard deviations were calculated and reported. To calculate growth rate, log transformed data were used.

For each experiment, the data representing the microbial growth was investigated with different approaches to check both normality and variance. For each dataset, a QQ-Plot was used to investigate whether the data had extremes at the edges. Similarly, a histogram was used to see if the data was normally distributed, or if it was shifted to either side. Subsequent Shapiro Wilk test was used to decide if the data was normally distributed or not. Thereafter, Levene's test was used to check the homogeneity of the variance of the

data. A Residuals VS Fitted plot was used to investigate the linearity of the data. The assumptions of analysis of variance (ANOVA) were tested (outliers, normality, and homogeneity) for both the data on microbial growth and for the genetic investigation. This was used to decide which statistical methods could be used to examine the significance of the data.

If the data failed on any of the assumptions, non-parametric statistical approaches were used for the statistical investigation of the data. Kruskal Wallis test, the equivalent to the parametric one-way ANOVA was used to test whether at least one of the conditions stochastically dominated over the other. Kruskal-Wallis test compares the medians of the conditions tested, determining whether the medians of the tested groups are different or not. The hypothesis of the test is that the population medians are equal (H0), or that population medians are not equal (H1). If the experiment contained more than two variables, a Pairwise Wilcoxon (Wilcoxon signed-rank test) and/or Dunn's test (Dunn's Multiple Comparison Test) Post Hoc honesty tests were used to investigate whether one- or more of the conditions were significantly different from the others. Both the Pairwise Wilcoxon test and the Dunn's test were performed with a multiple testing correction, implying p-value adjustment in respect to Benjamini-Hochberg and Bonferroni, for the growth potential and the genetic analysis, respectively.

If the data satisfied the assumptions, a parametric ANOVA test was used to investigate whether at least one of the conditions stochastically dominated over the other. If the experiment contained more than two variables, Tukey's honest significance test with a multiple testing correction, implying p-value adjustment in respect to Bonferroni was used.

For the genetic analysis, the Shannon diversity index and the Chao1 index were used to calculate the differences between distances for the samples. The composition differences (Bray-Curtis distances) of ASVs for the different conditions were plotted in PCoA plots, and the Pairwise Adonis test was used to test the significance of the distances.

Statistical values of $p < 0.05$ were considered significant, rejecting the null hypothesis between groups (Kumar Singh et al., 2022).

2.6 Cooperation with another student

The four experiments conducted in this master's thesis, as well as the pilot demonstration at Hardingsmolt AS were carried out together with another master student: Lise Rønning, who investigated the biochemical composition of the developing biofilm. During the experiments, planning, construction, maintenance, and sampling were done together. Lise was responsible for the water analysis, whereas I was responsible for the data handling and the statistical investigation. However, all the downstream experimental work and the later data management was done individually.

3. Results

3.1 Effect of light intensity

3.1.1 Nutrient content of the RAS water

The analyzed concentration of dissolved inorganic N and P in the batch of RAS water is presented in *Table 6*. The salinity was 12.8 PPT. The batch of RAS water had a balanced N:P ratio of 13:1.

Table 6: Parameters of the RAS water used in the experiment testing light intensity.

Water parameter	**mg L^{-1}**
Nitrite ($N\text{-}NO_2^-$)	0.23 ± 0.01
Nitrate ($N\text{-}NO_3^-$)	36.0 ± 2.5
Phosphate ($P\text{-}PO_4^{3-}$)	2.7 ± 0.2

3.1.2 Microbial growth

In the conditions testing medium and high light, a benthic biofilm of microalgae established. No growth was observed in the condition testing no light. The method used to monitor the microbial growth (spectrophotometer) was not suitable; however, visual inspections suggested that the biofilm was thicker when more light was applied.

3.1.3 Microbial community analysis

A. Microscope pictures

Microscope pictures (*Figure 9*) revealed that the benthic community contained diatom microalgae species. Two different diatoms were observed; however, one seemed to be more dominating.

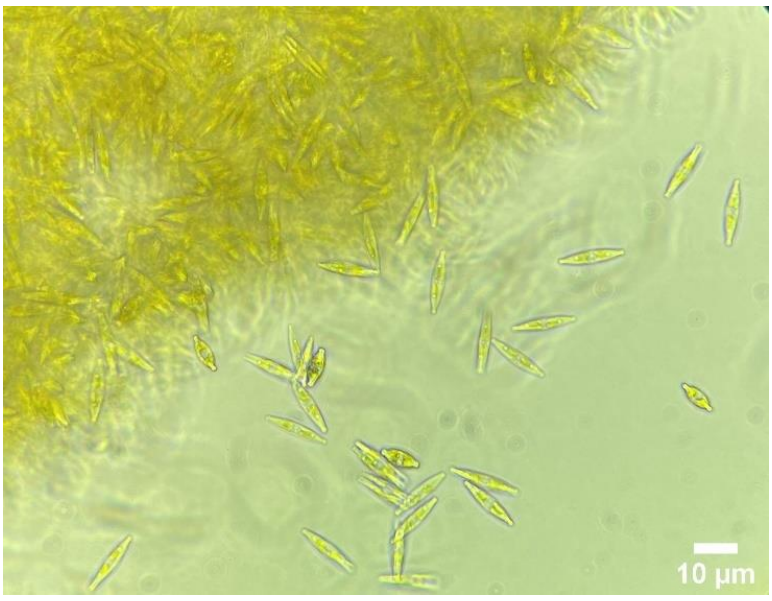

Figure 9: A microscope picture taken in a light microscope at 400x magnification. The picture was taken at the end of the experimental period (T16), for the condition having medium light intensity (160 µE m^{-2} s^{-1}). Two types of diatom microalgae species were observed. This was confirmed by microalgae expert- and CEO of the DareWin project at Inria, Hubert Bonnefond (Bonnefond, 2022).

B. Prokaryote part of the community

Table 7: Taxa (Class/Order/Family/Genus) of the three most abundant prokaryote species for the different conditions (high, medium, and no light), as well as from the start water.

Condition	Taxa (Class/Order/Family/Genus)	Abundance (%)
High light	*Alphaproteobacteria /Parvibaculales/uncultured/uncultured*	11.9
	Alphaproteobacteria /Parvibaculales/uncultured/uncultured	10.8
	Gammaproteobacteria/Alteromonadales/Alteromonadaceae/Glaciecola	8.5
Medium light	*Alphaproteobacteria/Rhodobacterales/Rhodobacteraceae/Marivita*	13.2
	Pseudomonas/Pseudomonadales/Pseudomonadaceae/Pseudomonas	11.8
	Flavobacteriia/Flavobacteriales/Crocinitomicaceae/Crocinitomix	11.0
No light	*Flavobacteriia/Flavobacteriales/Flavobacteriaceae/Unassigned*	25.5
	Gammaproteobacteria/Oceanospirillales/Alcanivoracaceae1/Alcanivorax	22.1
	*F*lavobacteriia*/Flavobacteriales/Flavobacteriaceae/Unassigned*	20.0
Start water	*Gammaproteobacteria/Xanthomonadales/Unassigned/Unassigned*	37.6
	Gammaproteobacteria/Xanthomonadales/Unassigned/Unassigned	36.3
	Alphaproteobacteria/Rhodobacterales/Rhodobacteraceae/Unassigned	6.7

The genetic analysis showed that the most abundant prokaryote contributors (*Table 7*) of the microbial communities were species of the taxonomic Class *Alphaproteobacteria*, *Gammaproteobacteria*, *Pseudomonas*, and *Flavobacteriia*. On the Genus level, *Glaciecola, Marivita*, *Pseudomonas, Crocinitomix,* and *Alcanivorax* were abundant. The results shows that there was no significant difference between the conditions. The composition differences (Bray-Curtis distances) of ASVs for the different conditions are presented in a PCoA plot (*Appendix H, Figure H. 3*). The relative abundance of prokaryote species for the different conditions are presented in a bar chart (*Appendix H, Figure H. 4*).

C. Eukaryote part of the community

The most abundant eukaryote species (*Figure 10* and *Appendix H*, *Figure H. 6*) of the microbial community was similar between the two conditions having light (high and medium); however, the abundancy varied between them. Taxonomic classification of the communities for the conditions testing high and medium light showed that two diatom microalgae species were dominating: Nitzschia (*Nitzschia sp. ChengR-2013*) (relative abundance = 62%, and 75%, respectively), followed by Phaeodactylum (*Phaeodactylum tricornutum CCAP 1055/1*) (relative abundance = 16% and 3%, respectively). This was underlined by the investigation of the diatom community (*Figure 11*). In addition, both conditions contained fungi (*Mortierellomycotina incertae sedis*) (relative abundance = 9%, and 5%, respectively), eukaryote decomposers (*Thraustochytrids sp.*) (relative abundance = 15% and 8%, respectively), and microalgae parasites (*Aphelidium desmodesmi*).

When no light was added, the relative abundance of diatom microalgae species was low (relative abundance < 2%). Instead, the community was dominated by Choanoflagellates (*Craspedida codonosigidae*) (relative abundance = 47%), fungi (*Mortierellomycotina incertae sedis*) (relative abundance = 15%), and ciliates (*Cinetochilum ovale*) (relative abundance = 21%).

The start water was abundant in metazoan (Unassigned) (relative abundance = 71%) and fungi (*Mortierellomycotina incertae sedis*) (relative abundance = 10%).

There was a significant difference between the condition having high light, compared to no light (p = 0.02). The PCoA plot (*Figure H. 5*) shows the composition differences (Bray-Curtis distances) of ASVs for the different conditions.

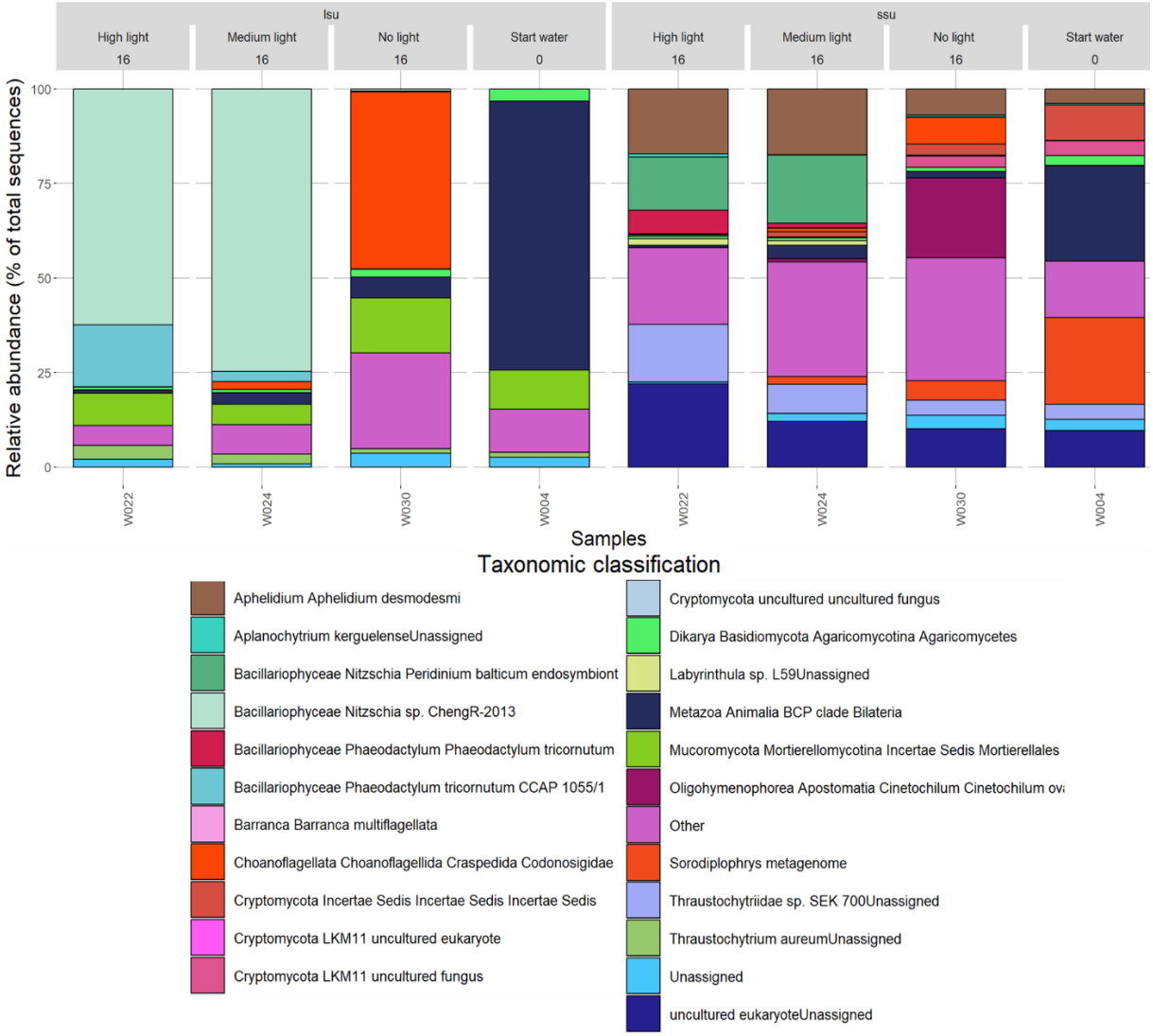

Figure 10: The relative abundance (%of total sequences) of eukaryote species in the community coming from the different conditions, as well as the start water, in the experiment testing addition of light. The specific light condition (high-, medium-, and no- light) is indicated, as well as what time (0 or 16) the samples were collected. The taxonomic classification is presented on the bottom, with respective color coding.

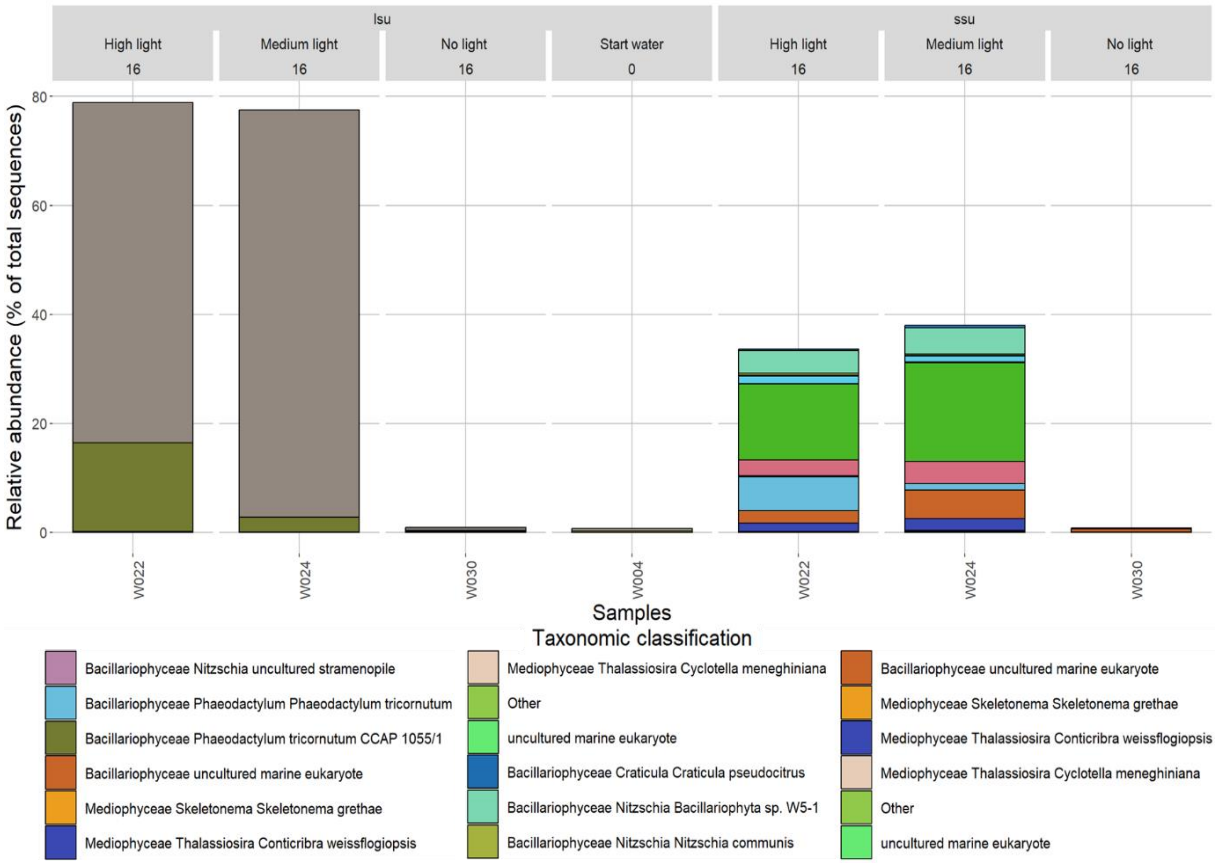

Figure 11: The relative abundance (%of total sequences) of diatom microalgae species in the eukaryote community of the experiment testing addition of light. The specific light condition (high-, medium-, and no- light) is indicated, as well as what time (0 or 16) the samples were collected. The taxonomic classification is presented on the bottom, with respective color coding.

3.2 Effect of addition of silica

3.2.1 Nutrient content of the RAS water

The analyzed concentration of dissolved inorganic N and P in the batch of RAS water are presented in *Table 8*.

Table 8: The water parameters of the RAS water used in the experiment testing addition of silica.

Water parameter	**mg L^{-1}**
Nitrite ($N\text{-}NO_2^-$)	0.1 ± 0.003
Nitrate ($N\text{-}NO_3^-$)	4.9 ± 0.1
Phosphate ($P\text{-}PO_4^{3-}$)	0.8 ± 0.1

3.2.2 Biomass, productivity, and growth rate

The first 28 days of the experiment (*Figure 12*), extrapolated data was used. Kruskal-Wallis test revealed that the addition of silica had a significant (p = 0.00035) effect on the biomass yield during this period (T0-T28). Compared to the control (n=3), the treatment (n=3) obtained a higher productivity, maximal productivity, and growth rate before Conway medium was added (*Table 9*).

At the end of the experiment (T30-T37) (*Figure 12*), dry weight measurements (g m^{-2}) were used. Kruskal-Wallis test did not find a significant difference (p = 0.6) in biomass yield between treatment and control. During this period, the productivity and growth rate (*Table 9)* showed that the control had a higher productivity compared to the treatment; however, the growth rate was lower.

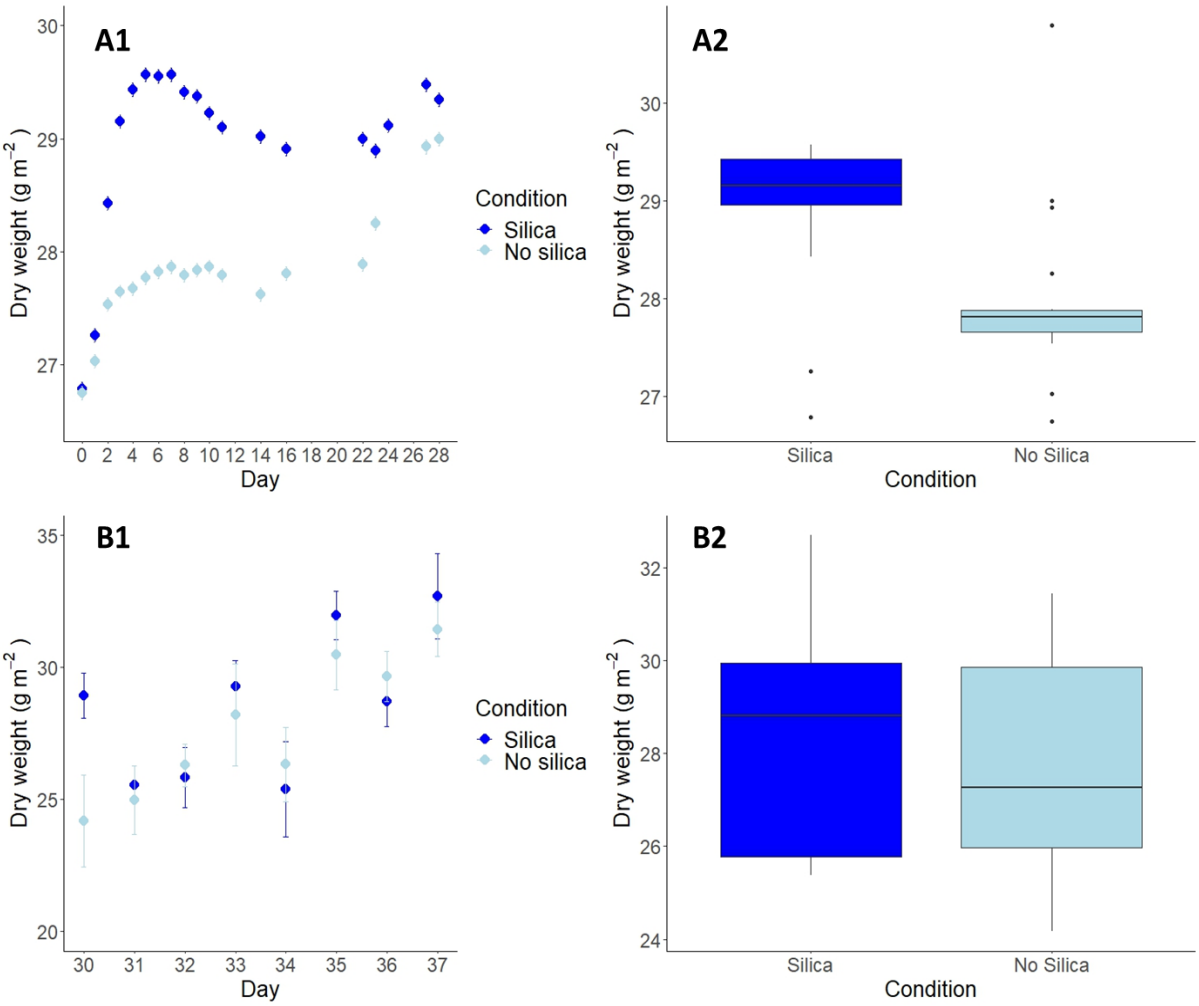

Figure 12: To the left, two scatterplots (A1 and B1) showing the effect of silica on the biomass yield during the experimental period. The respective standard errors are indicated as error bars. To the right, two box plots (A2 and B2) showing the distribution of datapoints during the experimental period.

Table 9: The productivity, the maximum productivity, and the growth rate for the treatment: Addition of silica, and the control: No addition of silica, before and after Conway medium was added. Significance is annotated as p-values (***p < 0.001, **p < 0.01, *p < 0.05, p > 0.049).

Condition	Productivity ($g\ m^{-2}\ day^{-1}$)	Maximal productivity ($g\ m^{-2}\ day^{-1}$)	Growth rate (Day^{-1})
Before Conway			
Silica (T0-T15)	0.09 ± 0.05	0.60 ± 0.08**	0.029 ± 0.003*
No silica (T0-T15)	0.04 ± 0.02*	0.20 ± 0.04**	0.002 ± 0.0002***
After Conway			
Silica (T15-T28)	0.05 ± 0.02	-	0.005 ± 0.0007
No silica (T15-T28)	0.12 ± 0.11	-	0.05 ± 0.02
Silica (T30-T37)	0.70 ± 0.39	-	0.07 ± 0.03
No silica (T30-T37)	1.01 ± 0.16***	-	0.05 ± 0.01*

3.2.3 Microbial community analysis

A. Microscope pictures

Microscope pictures (*Figure 13* and *Figure 14*) show that both treatment and control contained diatom microalgae species. During the experimental period, a new sigmoidal microalgae species occurred.

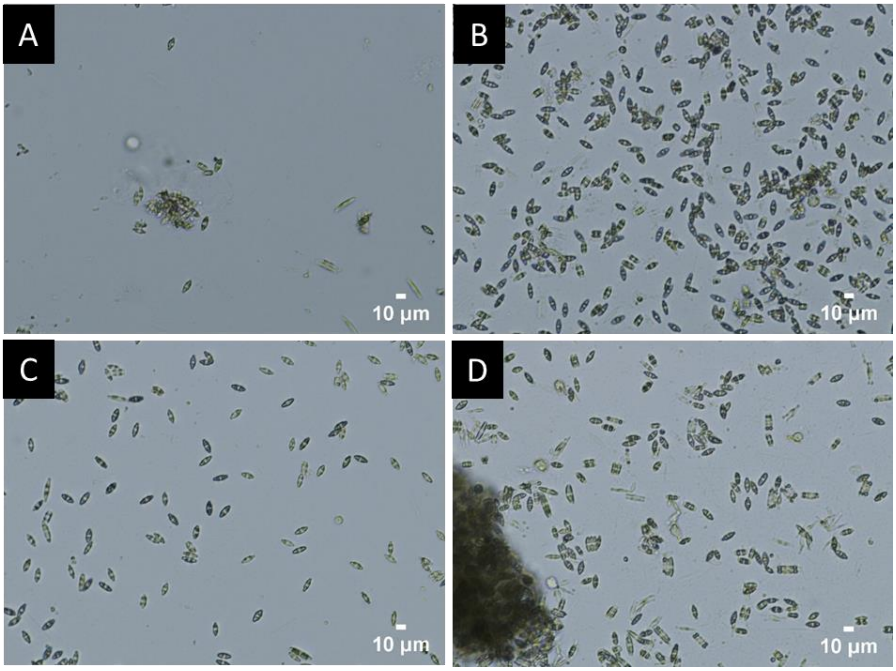

Figure 13: Microscope pictures (A, B, C, D) taken at 100x magnification in an inverse microscope. At the top, from left to right, pictures (A, B) of the treatment: Addition of silica, at day 0 (T0) and 11 (T11), respectively. At the bottom, from left to right, pictures (C, D) of the control: No addition of silica, at day 0 (T0) and 11 (T11), respectively.

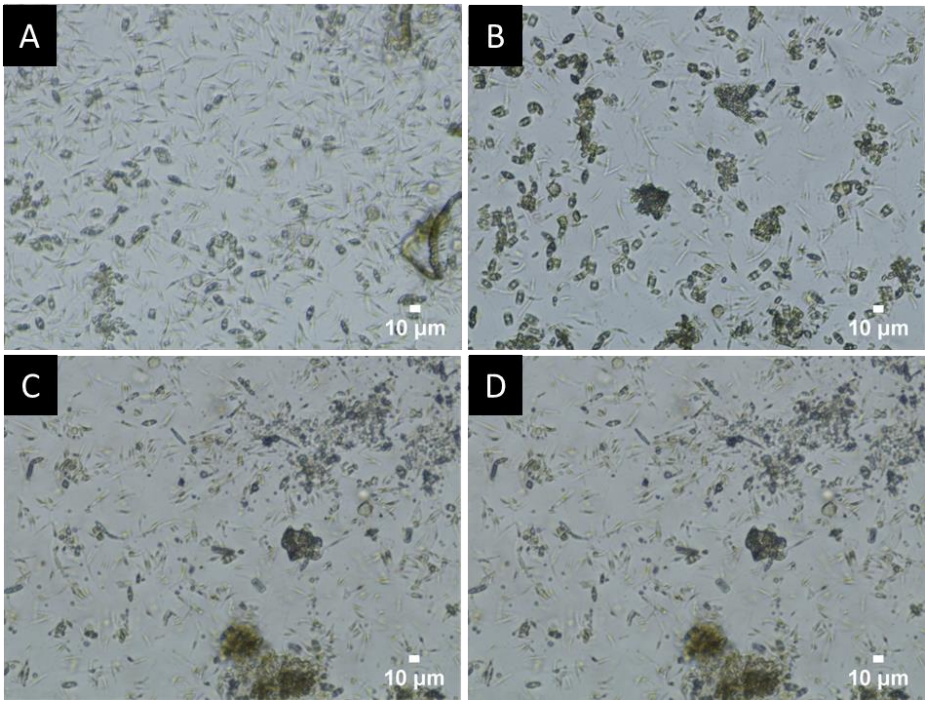

Figure 14: Microscope pictures (A, B, C, D) taken at 100x magnification in an inverse microscope at day 28 (T28). At the top, from left to tight, pictures (A, B) of the treatment: Addition of silica. At the bottom, pictures (C, D) of the control: No addition of silica.

B. Prokaryote part of the community

The genetic analysis showed that the most abundant prokaryote contributors (*Table 10*) of the microbial communities were mainly species coming from the taxonomic Class *Alphaproteobacteria*, *Gammaproteobacteria*, and *Flavobacteriia*. On the Genus level, *Marivita*, *Glaciecola, Maribacter,* and *Shewanella* were the most abundant.

The results showed that there was no significant difference between the samples. The composition differences (Bray-Curtis distances) of ASVs for the different conditions are presented in a PCoA plot (*Appendix H, Figure H. 7)*. The relative abundance of prokaryote species for the different conditions are presented in a bar chart (*Appendix H, Figure H. 8*).

Table 10: Taxa (Class/Order/Family/Genus) of the three most abundant prokaryote species for the treatment (addition of silica), the control (no addition of silica), and the start water.

Condition	Taxa (Class/Order/Family/Genus)	Abundance (%)
Treatment	*Alphaproteobacteria/Rhodobacterales/Rhodobacteraceae/Marivita*	24.8
	Gammaproteobacteria/Alteromonadales/Alteromonadaceae/ Glaciecola	20.1
	Alphaproteobacteria/Rhodobacterales/Rhodobacteraceae/Marivita	17.2
Control	*Alphaproteobacteria/Rhodobacterales/Rhodobacteraceae/Marivita*	28.8
	Alphaproteobacteria/Rhodobacterales/Rhodobacteraceae/Marivita	27.9
	Flavobacteriia/Flavobacteriales/Flavobacteriaceae/Maribacter	18.8
Start water	*Flavobacteriia/Flavobacteriales/Flavobacteriaceae/Unassigned*	14.6
	Flavobacteriia/Flavobacteriales/Flavobacteriaceae/Unassigned	12.2
	Gammaproteobacteria/Alteromonadales/Shewanellaceae/ Shewanella	6.8

C. Eukaryote part of the community

The most abundant eukaryote species (*Figure 15* and *Appendix H*, *Figure H. 10*) was similar between treatment and control; however, the relative abundancy varied. The taxonomic classification showed that both were highly dominated by the diatom Phaeodactylum (*Phaeodactylum tricornutum CCAP 1055/1*) (relative abundancy = 82% and 77%, respectively). These findings were highlighted by solely looking at the diatom communities (*Figure 16*). Both were also dominated by fungi (*Mortierellomycotina incertae sedis)* (relative abundancy = 14% and 10%, respectively), microalgae parasites (*Aphelidium desmodesmi*), and protists (*Aplanochytrium kerguelense*).

The start water was abundant in other eukaryote species rather than diatoms (relative abundance < 1%). Instead, the start water contained two types of fungi: *Mortierellomycotina incertae sedis* (relative abundancy = 31%) and *Cryptomycota incertae sedis* (relative abundance = 24%), as well as metazoans (Unassigned) (relative abundance = 16%). No significant difference was found between the conditions ($p > 0.1$). The composition differences (Bray-Curtis distances) of ASVs for the different conditions are presented in a PCoA plot.

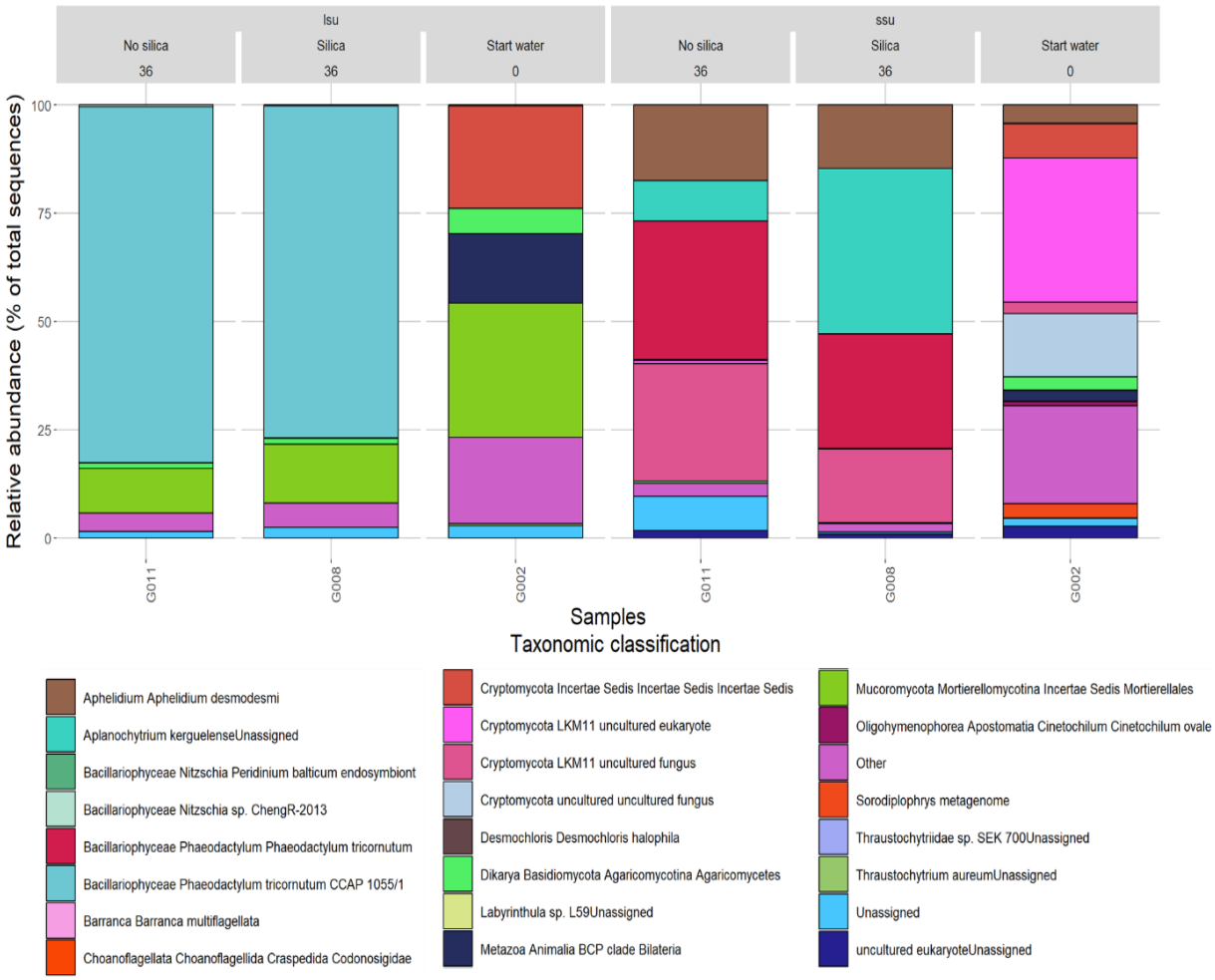

Figure 15: The relative abundance (%of total sequences) of eukaryote species in the community of the experiment testing addition of silica. The sequences were obtained by ONT sequencing. The treatment: Addition of silica, the control: No addition of silica, as well as the start water are shown. The timepoint for when the samples were collected (0 or 36) are shown. The taxonomic classification is presented on the bottom, with respective color coding.

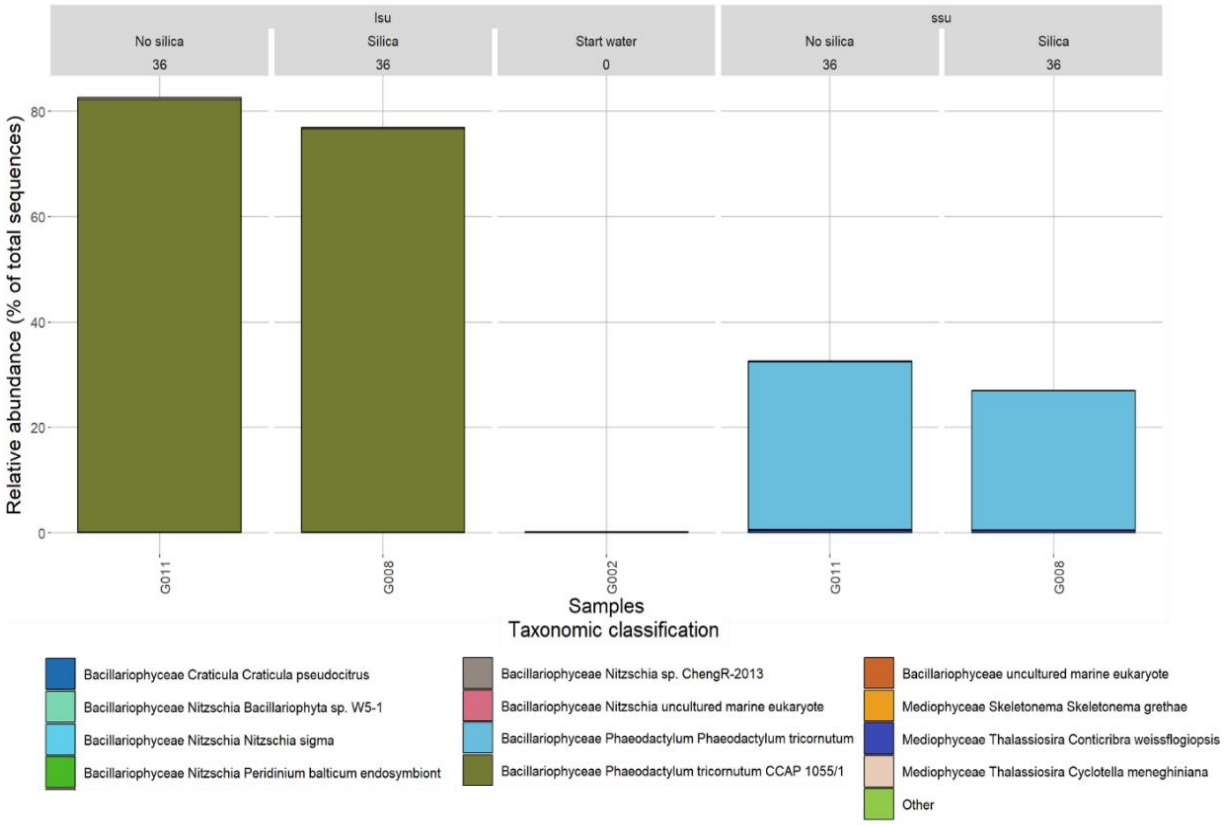

Figure 16: The relative abundance (%of total sequences) of diatom microalgae species in the eukaryote community of the experiment testing addition of silica. The sequences were obtained by ONT sequencing. The treatment: Addition of silica, the control: No addition of silica, as well as the start water are shown. The timepoint for when the samples were collected (0 or 36) are shown. The taxonomic classification is presented on the bottom, with respective color coding.

3.3 Effect of nutrient additions

3.3.1 Nutrient content of the RAS water

The analyzed concentration of dissolved inorganic N and P in the batch of RAS water are presented in *Table 11*. The salinity was 11.2 PPT.

Table 11: The water parameters of the RAS water coming from Hardingsmolt AS, used in the experiment testing addition of nutrients.

Water parameter	**mg L^{-1}**
Nitrite ($N\text{-}NO_2^-$)	0.1 ± 0.001
Nitrate ($N\text{-}NO_3^-$)	32.6 ± 1.6
Phosphate ($P\text{-}PO_4^{3-}$)	2.0 ± 0.4

3.3.2 Biomass, productivity, and growth rate

The first part of the experiment tested high and low nutrient load (n=3). The second part of the experiment tested different nutrient additions (n=3, except Only_RAS (n=6) and low nutrient load (n=30)).

A. High and low nutrient load

In the first part of the experiment (T0-T18) (*Figure 17*), Kruskal-Wallis test revealed that the treatment: High nutrient load, had a significant (p = 0.004) effect on the biomass yield (g m^{-2}). The productivity and growth rate (*Table 12*) showed that the treatment obtained a significantly higher productivity and maximum productivity compared to the control.

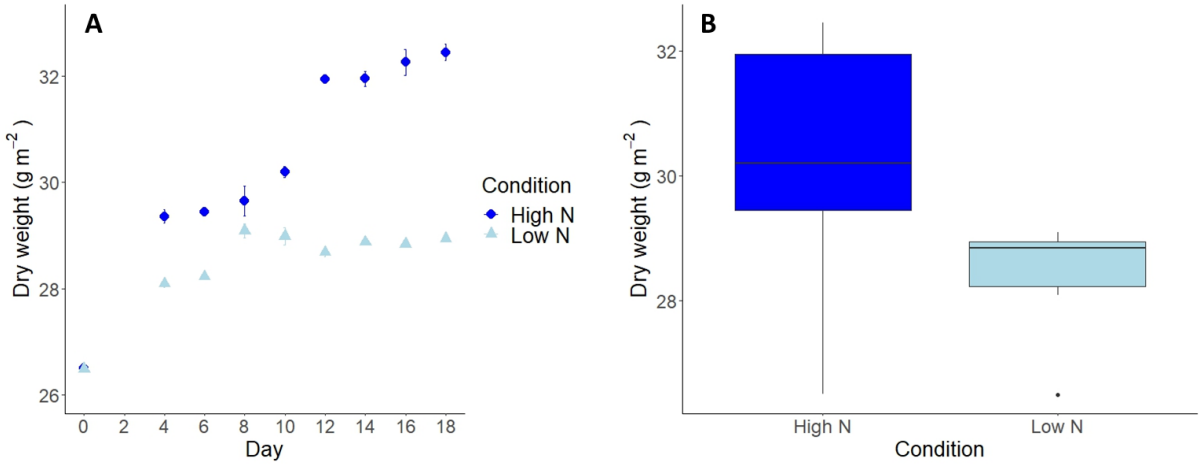

Figure 17: To the left, a scatterplot (A) showing the effect of the treatment: High nutrient load (High N) (n=3), and the control: Low nutrient load (Low N) (n=3), on the biomass yield (g m^{-2}) during the experimental period of 18 days. Respective standard errors were indicated as error bars. To the right, a box plot (B) showing the distribution of datapoints.

Table 12: The productivity, maximum productivity, and the growth rate for the treatment: High nutrient load, and the control: Low nutrient load. The respective standard error is indicated. The significant of the calculated values are annotated as p-values (***p < 0.001, **p < 0.01, *p < 0.05, p > 0.049).

Condition	Productivity (g m^{-2} day^{-1})	Maximum productivity (g m^{-2} day^{-1})	Growth rate (Day^{-1})
High nutrient load	0.317 ± 0.036***	-//-	0.005 ± 0.0012
Low nutrient load	0.108 ± 0.033*	0.259 ± 0.045*	0.11 0.003

B. Addition of nutrients

In the second part of the experiment, different nutrient additions were tested (*Table C. 1*). Kruskal-Wallis test revealed that it was a significant (p = 0.000003) difference in biomass yield (g m^{-2}) between treatments (*Figure 18*). Pairwise Wilcoxon test found a significant effect for all treatments (p = 0.03) compared to the control: Low nutrient load (Low_N). However, no significant difference was observed among the different treatments (p = 0.3 – 1) when compared to each other.

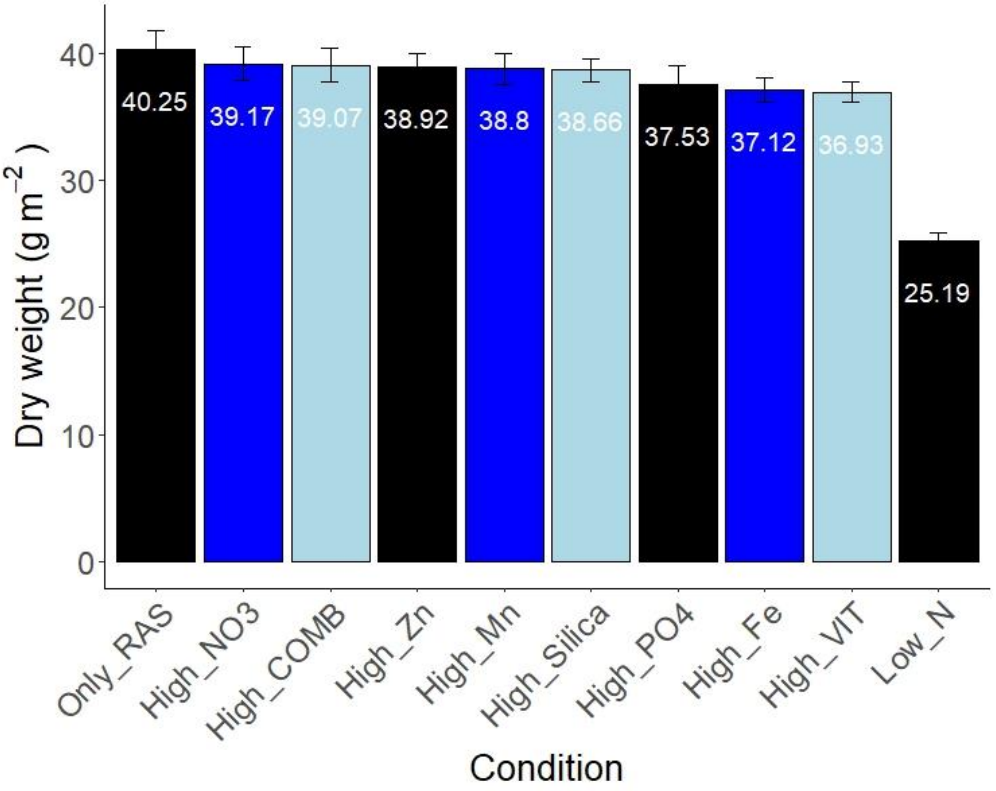

Figure 18: A stick and bar plot showing the effect of different nutrient additions on the total amount of dried biomass (g m^{-2}) at the end of the experimental period (T48). For each condition: Only_RAS, High_NO3, High_COMB, High_Zn, High_Mn, High_Silica, High_PO4, High_Fe, High_VIT, and Low_N, the standard errors were indicated as error bars. The abbreviation "COMB" indicated a combination of nutrients: Fe, Zn, Mn, Cu and Co. The abbreviation "VIT" indicated a combination of vitamin B12 and B1. The condition "Only_RAS" indicated that the samples contained only RAS water. The prefaces "High" and "Low" indicated whether the condition contained a high or low nutrient load in addition to the element(s) tested.

3.3.3 Microbial community analysis

A. Microscope pictures

Microscope pictures from the first part of the experiment (*Figure 19*) revealed that both treatment and control contained diatom microalgae species. In the second part of the experiment, the microscope pictures (*Appendix D*, *Figure D. 6* and *Figure D. 7*) indicated that the species diversity had increased. The two diatom species seemed to be dominating; however, circular green algae and sigmoidal microalgae species were also observed.

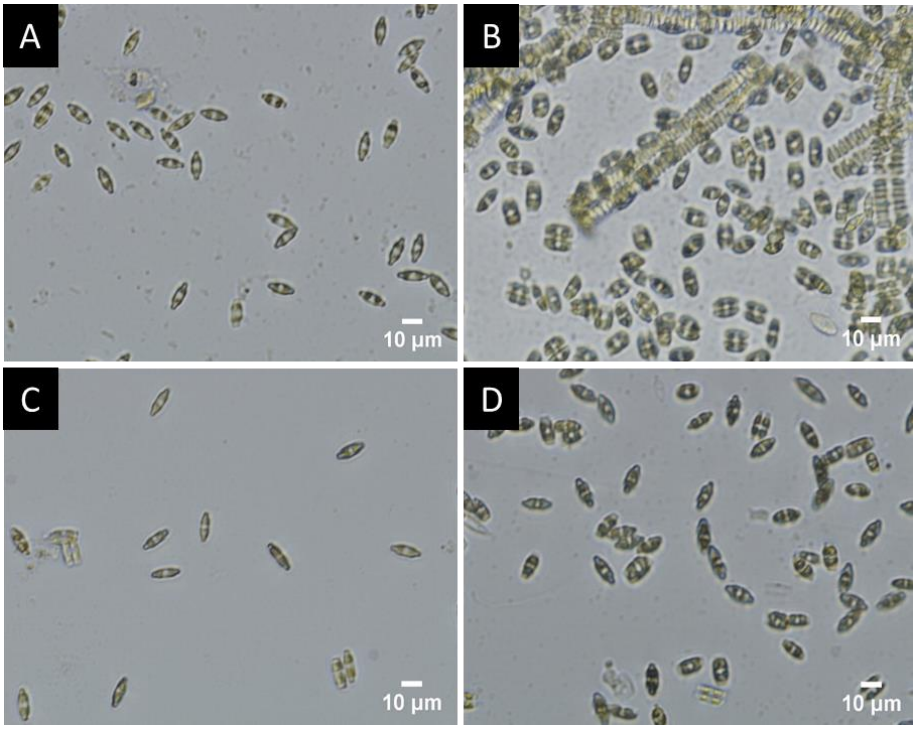

Figure 19: Microscope pictures (A, B, C, and D) taken in an inverse microscope at 200x magnification. At the top, from left to right, pictures (A and B) from the treatment: High nutrient load, at the start (T2)- and end (T18) of the experiment, respectively. At the bottom, from left to right, pictures (C and D) from the control: Low nutrient load, at the start (T4) and end (T18) of the experiment, respectively. Diatoms were dominating for both treatment and control.

B. Prokaryote part of the community

The genetic analysis showed that the most abundant prokaryote contributors (*Appendix H*, *Table H. 1*) of the microbial community coming from the different treatments, as well as from the start water, were mainly species coming from the taxonomic Class *Alphaproteobacteria*. However, other abundant species were of the taxonomic Class *Actinomycetia*, *Phycisphaerae*, *Flavobacteriia*, and *Gammaproteobacteria*. Abundant species were from the Genus *Sulfitobacter, SM1A02*, *Kordia, Hyphomonas, Maribacter, Rheinheimer,* and *Flavobacterium.*

No significant difference was found between conditions. The composition differences (Bray-Curtis distances) of ASVs for the different conditions are presented in a PCoA plot (*Appendix H, Figure H. 11).* The relative abundance of prokaryote species for the different conditions are presented in a bar chart (*Appendix H, Figure H. 12*).

C. Eukaryote part of the community

The most abundant eukaryote species (*Figure 20* and *Appendix H*, *Figure H. 14*) of the microbial communities were diatoms (*Bacillariophyceae*). The most abundant eukaryote species were similar between conditions; however, the species abundancy varied between them. All conditions were highly dominated by Phaeodactylum (*Phaeodactylum tricornutum CCAP 1055/1*): High_Comb (relative abundance = 74%), High_NO3 (relative abundance = 40%), High_Silica (relative abundance = 60%), and High_Vit (relative abundance = 81%). The second most abundant diatom was Nitzschia (*Nitzschia sp. ChengR-2013*); however, the relative abundancy was low (<10%) compared to *P. tricornutum*. This was underlined by the investigation of the diatom community (*Figure 21*).

Other abundant eukaryote species were fungi (*Mortierellomycotina incertae sedis*), microalgae parasites (*Aphelidium desmodesmi*), and protists (*Thraustochytrium aureum* and *Thraustochytriidae sp*). All conditions, except the conditions testing a combination of nutrients (High_COMB), were abundant in the protist (*Aplanochytrium kerguelense*). Additionally, the condition testing addition of nitrate were abundant in the protist (*Labyrinthula sp.*) (relative abundance = 30%).

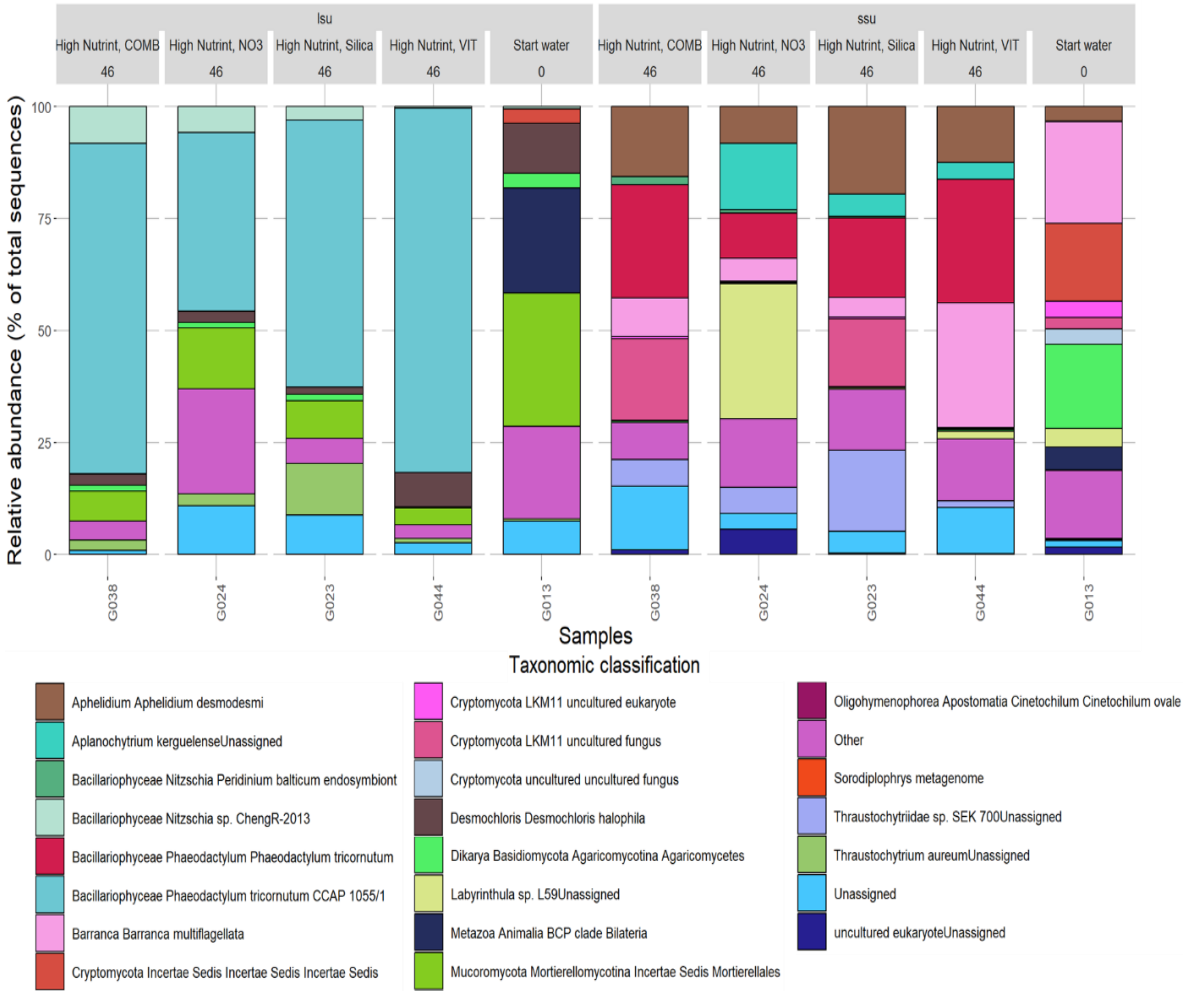

Figure 20: The relative abundance (%of total sequences) of eukaryote species in the community of the experiment testing addition of nutrients. The different conditions (High_COMB, High_NO3, High_Silica, High_VIT, as well as the start water) are shown. The abbreviation "COMB" indicates a combination of nutrients: Fe, Zn, Mn, Cu and Co. The abbreviation "VIT" indicates a combination of vitamin B12- and B1. The timepoint for when the samples were collected (0 or 46) are shown. The taxonomic classification is presented on the bottom, with respective color coding.

The start water was dominated by other eukaryote species rather than diatoms (relative abundance < 1%). The start water was abundant in Metazoa (Unassigned), fungi (*Mortierellomycotina incertae sedis*), and microalgae multiflagellata (*Barranca multiflagellata*).

There was a significant difference between High_PO4 compared to High_COMB (p = 0.04), High_NO3 (p = 0.02), and High_Conw (p = 0.02). Similarly, there was a significant difference between High_Fe compared to High_Comb (p = 0.04), and for High_NO3 (p = 0.03), compared to High_Zn and High_Comb (p = 0.04). The composition differences (Bray-Curtis distances) of ASVs for the different conditions are presented in a PCoA plot (*Figure H. 13)*.

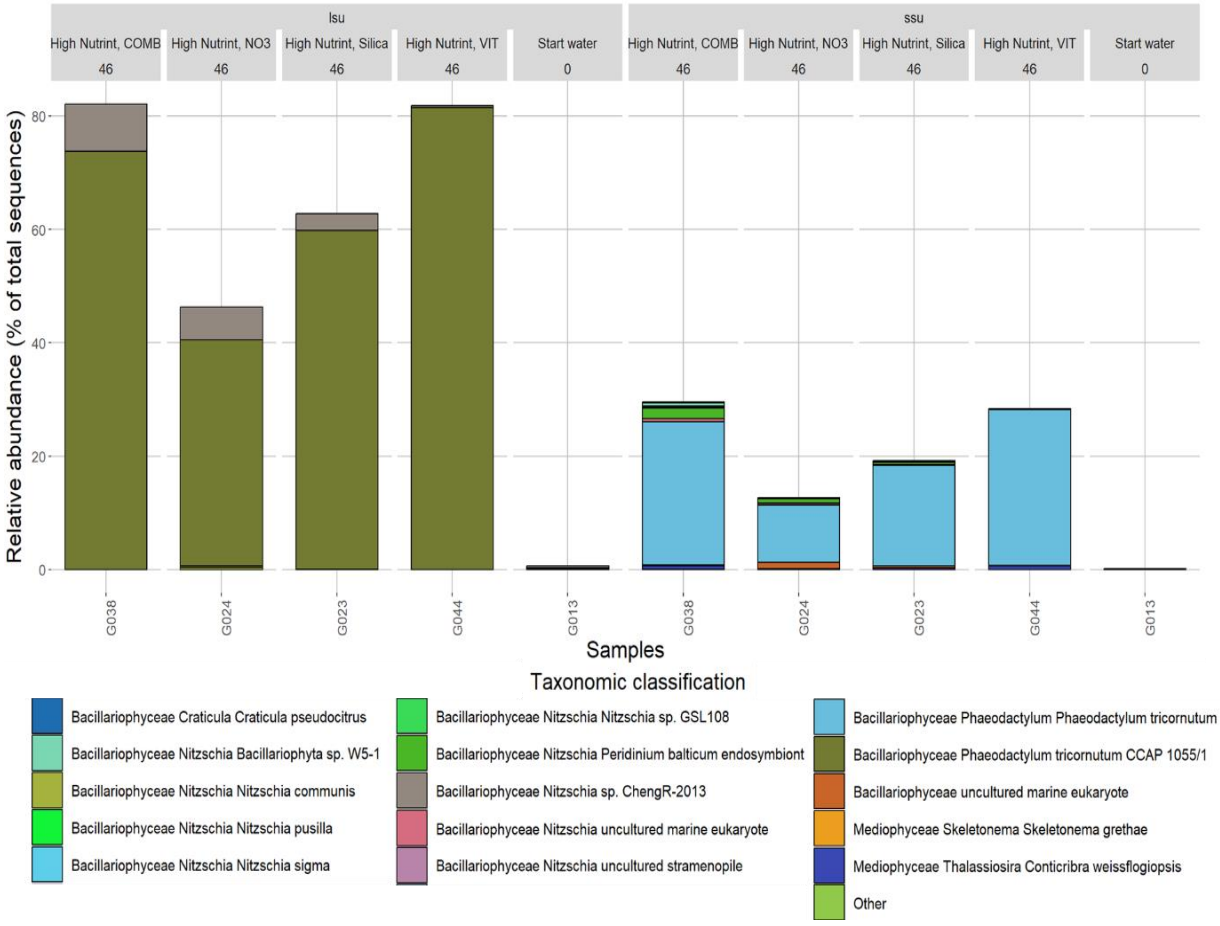

Figure 21: The relative abundance (%of total sequences) of diatom microalgae species in the eukaryote community of the experiment testing addition of nutrients. The different conditions (High_COMB, High_NO3, High_Silica, High_VIT, as well as the start water are shown. The abbreviation "COMB" indicates a combination of nutrients: Fe, Zn, Mn, Cu and Co. The abbreviation "VIT" indicates a combination of vitamin B12- and B1. The timepoint for when the samples were collected (0 or 46) are shown. The taxonomic classification is presented on the bottom, with respective color coding.

3.4 Effect of harvesting rates

3.4.1 Nutrient content of the RAS water

The analyzed concentration of dissolved inorganic N and P in the batch of RAS water are presented in *Table 13*. The salinity was 12.9 PPT.

Table 13: The water parameters of the batch of RAS water coming from Hardingsmolt AS.

Water parameter	**mg L^{-1}**
Nitrite ($N\text{-}NO_2^-$)	0.1 ± 0.008
Nitrate ($N\text{-}NO_3^-$)	8.5 ± 1.8
Phosphate ($P\text{-}PO_4^{3-}$)	1.2 ± 0.2

3.4.2 Biomass, productivity, thickness, and growth rate

During the experimental period of 36 days (T0-T36), the average biomass yield (g m^{-2}) obtained from each harvest for each condition (n=4): Harvest every 4th, 8th, and 12th day (*Figure 22*), showed that the biofilm production was stable during the experimental period. Kruskal-Wallis test reviled that there was a significant difference in biomass yield (g m^{-2}) between the conditions tested ($p = 0.002$). Pairwise Wilcoxon test found a significant difference between the two conditions: Every 4th day compared to every 8th day ($p = 0.008$), and every 4th day compared to every 12th day ($p = 0.014$).

The average of the harvested biomass (g m^{-2}) during the experimental period (*Figure 23*) showed that the 12th day condition produced more biomass compared to the other two conditions. This was also reflected by looking at the productivity (*Table 14*), showing that the 12th day condition obtained the highest productivity. Based on the average of the first harvest for each condition, referred to as the 12-day continues system (*Figure 22*), the maximum productivity and the growth rate were calculated (*Table 15*). Compared to the productivity of the 12th day condition, the productivity of the 12-day continuous system suggested that the productivity of the 12th day condition could be improved.

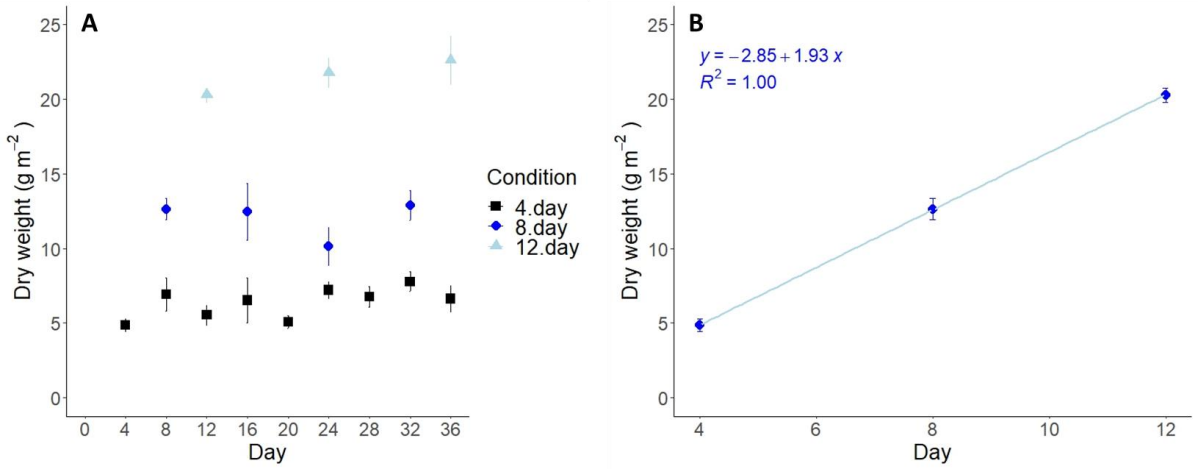

Figure 22: The average increase in dried biomass (g m^{-2}) for the different harvest conditions tested (n=4): Every 4th day, every 8th day, and every 12th day (A), with respective standard errors. The average increase in biomass (g m^{-2}) from day 0 – 12 (B), referred to as the 12-days continuous system. The points (Day: 4, 8, 12) were values of the average dry weight coming from the four reactors from each condition at the first day of harvest for each condition.

Table 14: The calculated productivity and thickness for the three harvesting conditions tested: Every 4th day, every 8th day, and every 12th day, with respective standard error.

Condition	Productivity ($g\ m^{-2}\ day^{-1}$)	Thickness of biofilm (µm)
4. day	1.59 ± 0.23	130 ± 12
8. day	1.50 ± 0.14	170 ± 27
12. day	1.80 ± 0.08	280 ± 9.5

Table 15: The estimated values of the 12-day continues system, being the average of the first harvest for each of the three conditions. The table shows the calculated maximum productivity and growth rate, with respective standard errors. The significance of the calculated values were annotated as p-values (***p < 0.001, **p < 0.01, *p < 0.05, p > 0.049).

Measurement / Condition	Maximum productivity ($g\ m^{-2}\ day^{-1}$)	Growth rate (Day^{-1})
4., 8., 12. day	1.93 ± 0.01**	0.18 ± 0.04

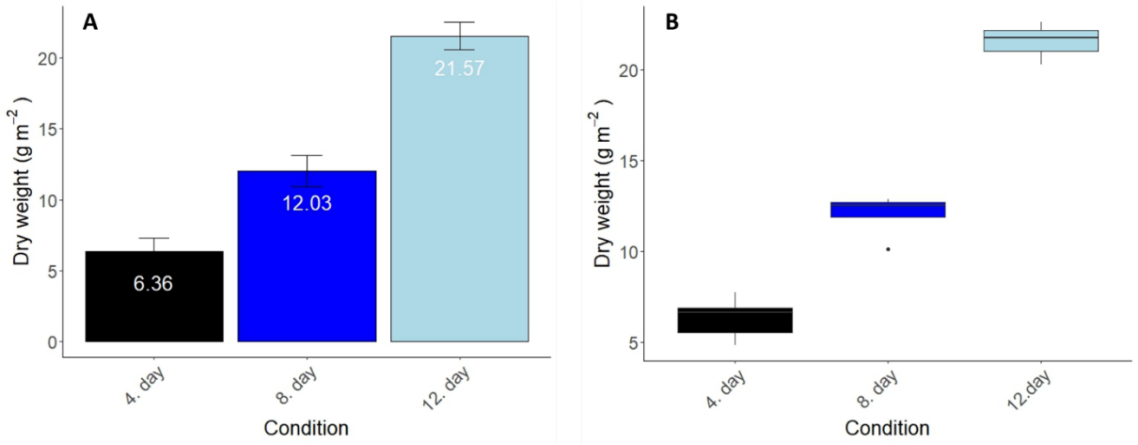

Figure 23: A stick- and bar plot (A), showing the effect of harvest rate on the average amount of dried biomass ($g\ m^{-2}$) obtained for each condition: Every 4th day, every 8th day, and every 12th day. The box plot (B) shows the distribution of datapoints during the experimental period.

3.4.3 The pH during the experimental period

During the experimental period, the pH of the photoautotrophic reactors was measured. The average pH for each condition (*Figure 24*), shows that the pH increased from ~7 to 9-10 in the acclimation and initiation period, and was stable between 9 - 10.5 for all conditions during the experimental period (T0-T36). The pH of the input water was ~7.

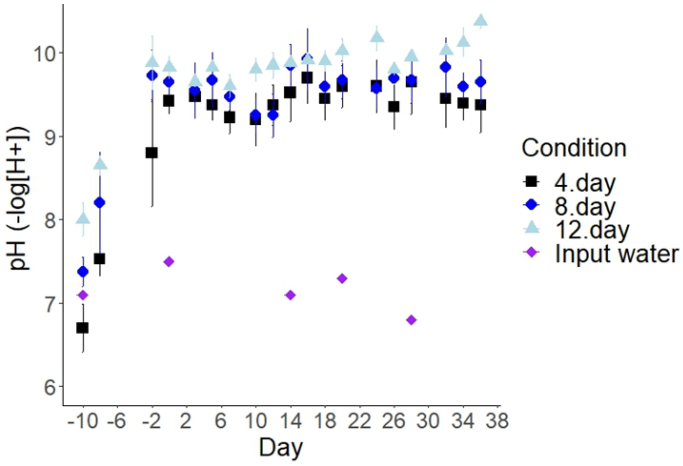

Figure 24: A scatterplot showing the average pH for the three harvest conditions tested: Every 4th day, every 8th day, and every 12th day, during the experimental period. The pH measurements of the input water (Input water) are also shown. The plot includes measurements from the initiation and acclimation period (T-10_T-1).

3.4.4 Microbial community analysis

A. Microscope pictures

Microscope pictures from the initiation and acclimation period (*Figure 25*), shows that the species diversity was rich. Among others, two types of diatoms were observed, as well as some ciliates (*Tintinnid sp*.). This was confirmed by microalgae expert- and CEO of the DareWin project at Inria, Hubert Bonnefond (Bonnefond, 2022). Microscope pictures (*Appendix D*, *Figure D. 8)* from the end of the experimental period suggested that the diversity was decreased. Diatoms were still observed; however, other species, such as fungi looked more prominent in the community.

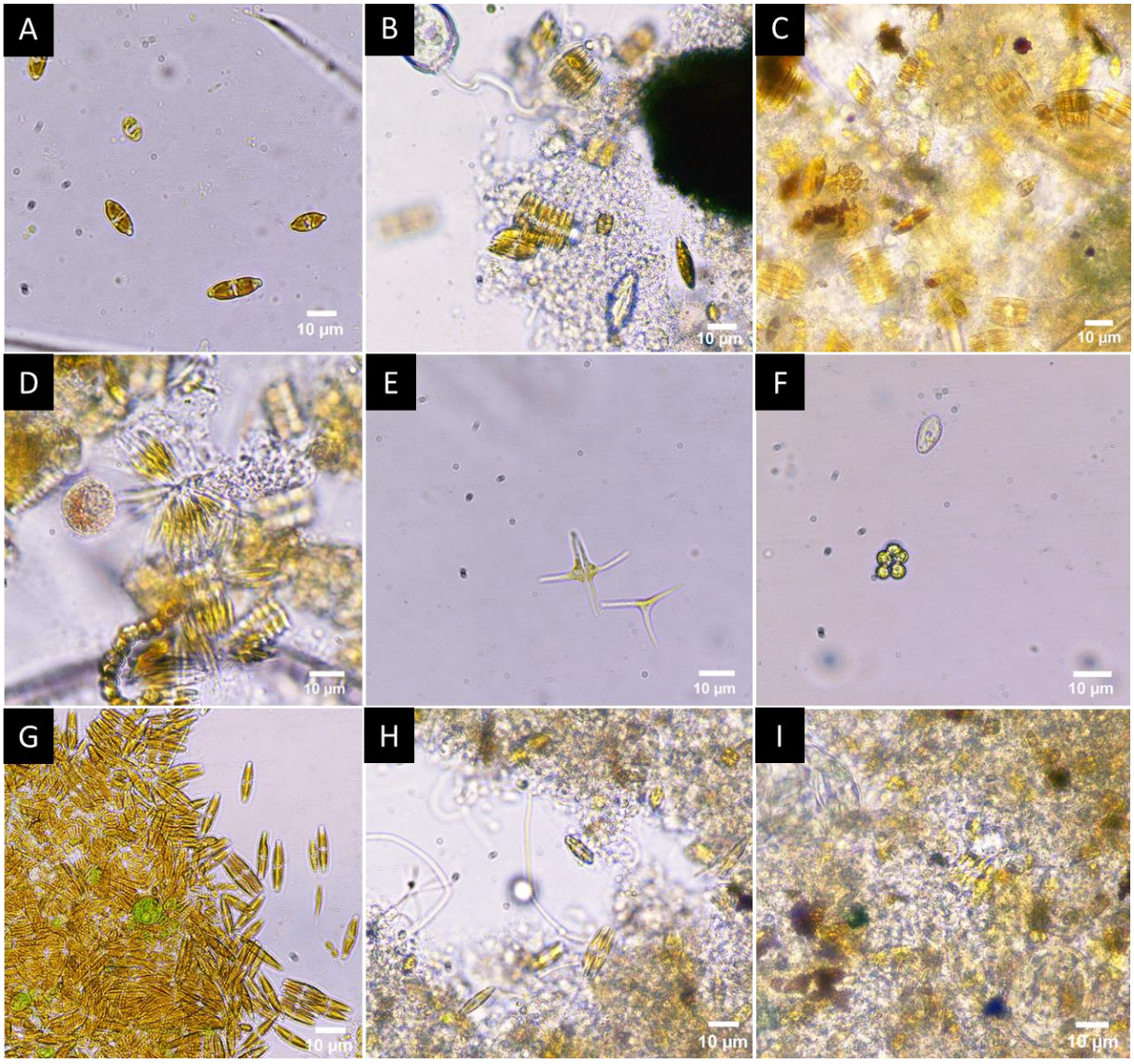

Figure 25: Microscope pictures (A-I) of the community coming from the three conditions: Harvest every 4. day (A-C), harvest every 8. day (D-F) and harvest every 12. day (G-I), taken in an inverse microscope. The pictures were from the initiation- and acclimation period before the harvest regimes were initiated. The pictures were mainly taken with a magnification of 400x, except couple of pictures that were taken on 600x (D and E). The microscope pictures showed diatom microalgae species *(A and G)*, as well as some green algae (F and G), and ciliates (F), among others the *Tintinnid sp.* (B).

B. Prokaryote part of the community

Table 16: The Taxa (Class/Order/Family/Genus) of the three most abundant prokaryote species for the conditions tested, as well as for the start water. The table shows only defined species. These samples were analyzed with the DNBSEQ technology. If (“), the taxa are the same as the one above.

Condition	Taxa (Class/Order/Family/Genus)	Abundance (%)
Every 4th day	*Alphaproteobacteria/Rhodobacterales/Rhodobacteraceae/Unassigned*	49.3
	Alphaproteobacteria/Rhizobiales/Beijerinckiaceae/Methylobacterium-Methylorubrum	47.5
	Alphaproteobacteria/Rhodobacterales/Rhodobacteraceae/Unassigned	46.3
Every 8th day	*Alphaproteobacteria/Rhodobacterales/Rhodobacteraceae/Unassigned*	75.0
	“	72.6
	“	68.5
Every 12th day	*Alphaproteobacteria/Rhodobacterales/Rhodobacteraceae/Unassigned*	75.7
	“	69.3
	“	65.2
Start water	Flavobacteriia/Flavobacteriales/Flavobacteriaceae/Flavobacterium	10.6
	*Alphaproteobacteria/*Rhodobacterales/Rhodobacteraceae/Pseudorhodobacter	9.1
	“	8.9

The genetic analysis showed that the most abundant prokaryote contributors (*Table 16*) of the microbial communities, as well as from the start water, were mainly species of the taxonomic Class *Alphaproteobacteria*. Species from the Class *Flavobacteriia* were abundant in the start water. *Methylorubrum*, *Flavobacterium*, and *Pseudorhodobacter* were abundant Genus. There was a significant difference in distance between the conditions ($p = 0.001$-0.04), except for the 8th day condition compared to the 12th day condition ($p = 0.99$). Composition differences (Bray-Curtis distances) of ASVs for the different conditions are presented in a PCoA plot (*Appendix H, Figure H. 15*). The relative abundance of prokaryote species for the different conditions are presented in a bar chart (*Appendix H, Figure H. 16).*

C. Eukaryote part of the community

The most abundant eukaryote species (*Figure 26* and *Appendix H*, *Figure H. 18*) in the conditions testing a harvest frequency of every 4th-, 8th-, and 12th day were similar between conditions. The results revealed that the species composition of the T0 samples (first harvest after initiation and acclimation period) were like the composition later in the experiment, indicating a consistent community despite harvesting.

The taxonomic classification showed that the eukaryote communities were highly dominated by the diatom Phaeodactylum (*Phaeodactylum tricornutum CCAP 1055/1*) during the whole experimental period (T0-T32/36). The diatom was already abundant in the T0 samples (relative abundance = 87%). The investigation of the diatom community (*Figure 27*) underlined these findings.

The conditions were also abundant in microalgae endoparasites (*Aphelidium desmodesmi*) (relative abundance > 25%), and fungi (*Mortierellomycotina Incertae Sedis*) (relative abundance < 5%). The microalgae multiflagellata (*Barranca multiflagellata*) was abundant in the T0 sample and in the first harvest (T4) of the condition having a harvest frequency of every 4th day.

There was no significant difference between the conditions. The composition differences (Bray-Curtis distances) of the ASVs for the different conditions are presented in a PCoA plot (*Appendix H, Figure H. 17*). The distances were significantly ($p < 0.05$) different between the conditions, except for the condition testing a harvest frequency of every 4th day compared to every 12th day ($p = 0.1$).

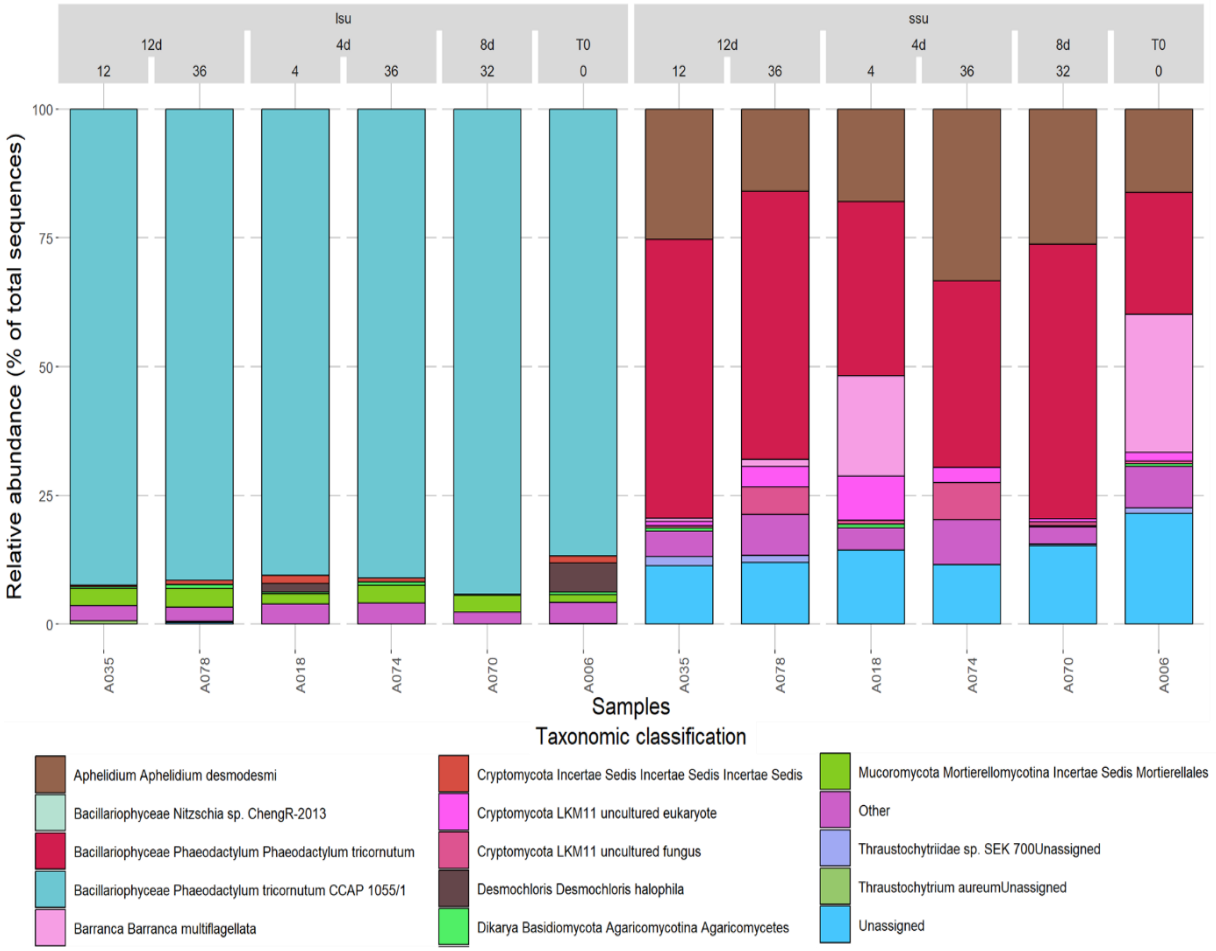

Figure 26: The relative abundance (%of total sequences) of eukaryote species in the community of the experiment testing harvest rate. The sequences were obtained by ONT sequencing. The treatments: Harvest every 4th-, 8th-, and 12th day, as well as the start water are shown. The timepoint for when the samples were collected (0, 4, 32, and 36) are shown. The taxonomic classification is presented on the bottom, with respective color coding.

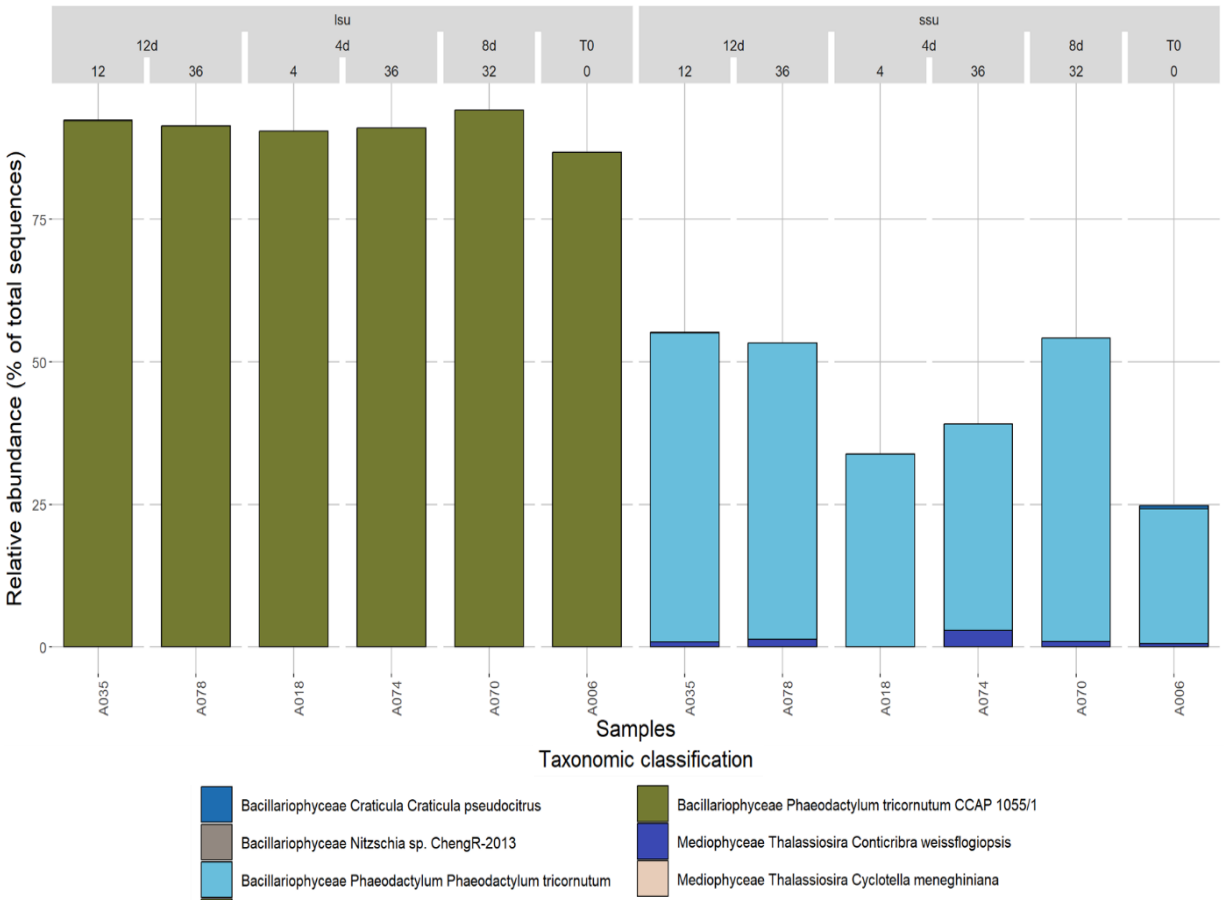

Figure 27: The relative abundance (%of total sequences) of diatom microalgae species in the eukaryote community of the experiment testing harvest rate. The sequences were obtained by ONT sequencing. The treatments: Harvest every 4th-, 8th-, and 12th day, as well as the start water are shown. The timepoint for when the samples were collected (0, 4, 32, and 36) are shown. The taxonomic classification is presented on the bottom, with respective color coding.

3.5 The pilot reactor at Hardingsmolt AS

3.5.1 Demonstration of biomass production

The Horizontal pilot reactor had on average a higher biomass yield compared to the vertical pilot reactor (*Table 17*); however, Kruskal-Wallis test could not find a significant difference in biomass yield between the two reactor systems (p = 0.093).

Table 17: Calculated biomass yield (g m^{-2}), with respective standard error, for the horizontal and vertical pilot reactor during the last three days of operation.

Pilot reactor	Average biomass yield (g m^{-2})	Productivity (g m^{-2} day^{-1})
Horizontal	24.3 ± 13.2	8.1 ± 4.4
Vertical	13.8 ± 7.9	4.6 ± 2.6

3.5.2 Microbial community analysis

A. Microscope pictures

Microscope pictures (*Figure 28*) were obtained at the end of the operational period. The microscope pictures suggested that the species composition was different between the two pilot reactors. Diatoms were observed in the horizontal pilot reactor (*Figure 28, A and B*); however, the species diversity seemed to be large. For the vertical system (*Figure 28, C and D)*, the microscope pictures implied that other microalgae species were dominating.

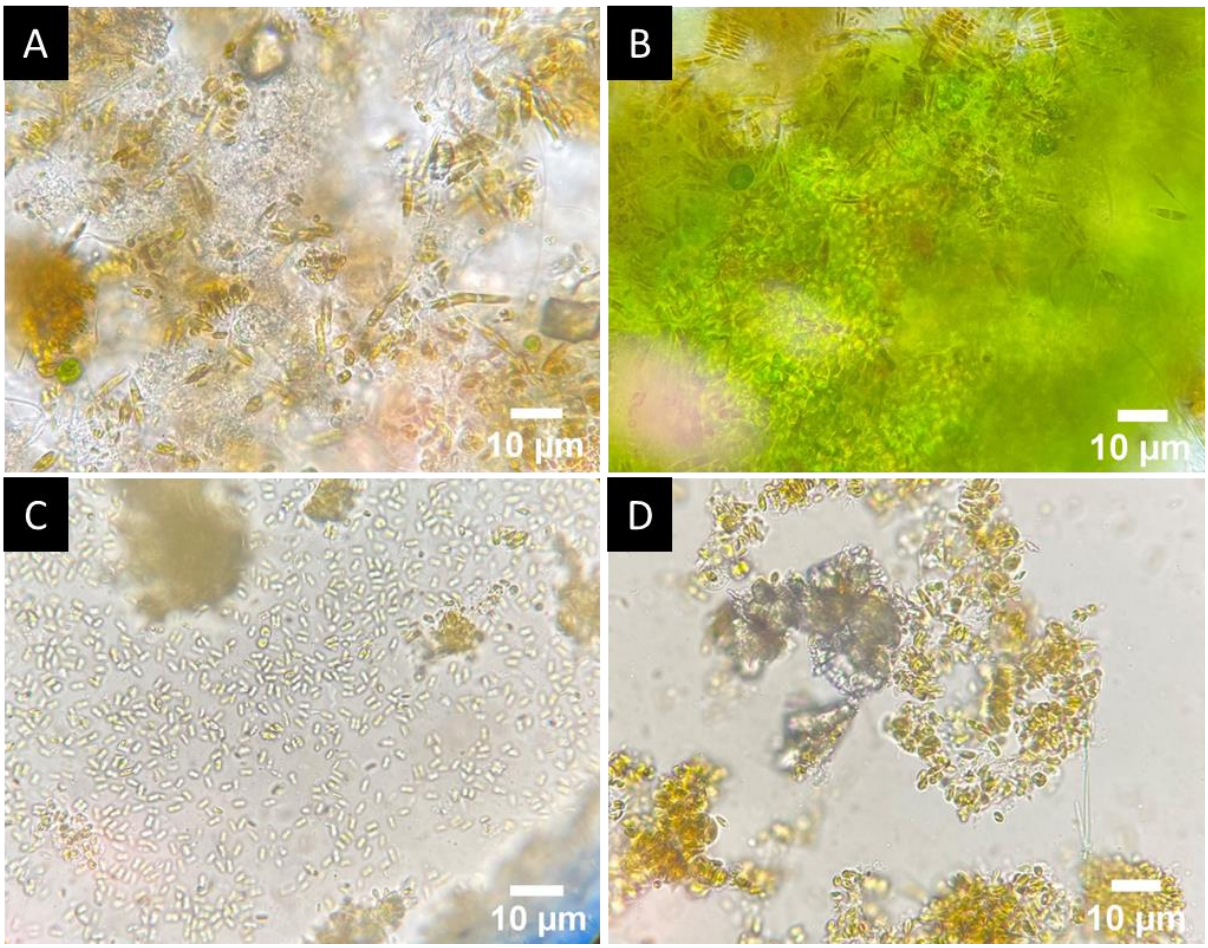

Figure 28: Microscope pictures (A-D) of the community coming from the pilot reactors with horizontal growth plates (A and B) and vertical growth pates (C and D), respectively. The microscope pictures were taken in a light microscope at 400x magnification at the end of the operational period, approximately 3 months after initiation.

B. Prokaryote part of the community

The genetic analysis showed that the most abundant prokaryote contributors (*Table 18*) of the vertical and the horizontal pilot reactors, as well as the nitrifying biofilter, were mainly dominated by species coming from the taxonomic Class *Alphaproteobacteria*. Other dominating taxa were from the Class *Flavobacteriia*. *Pseudorhodobacter*, *Kordia,* and Yoonia-*Loktanella* were abundant Genus.

Table 18: Taxa (Class/Order/Family/Genus) of the three most abundant prokaryote species for the horizontal- and vertical pilot reactor, as well as from the nitrifying biofilter.

Condition	Taxa (Class/Order/Family/Genus)	Abundance (%)
Horizontal	*Alphaproteobacteria/Rhodobacterales/Rhodobacteraceae/ Pseudorhodobacter*	16.0
	"	14.5
	"	13.4
Vertical	*Flavobacteriia/Flavobacteriales/Flavobacteriaceae/Kordia*	44.5
	Alphaproteobacteria/Rhodobacterales/Rhodobacteraceae/Yoonia-Loktanella	42.6
	Alphaproteobacteria/Rhodobacterales/Rhodobacteraceae/Unassigned	39.3
Biofilter	*Alphaproteobacteria/Rhodobacterales/Rhodobacteraceae/Unassigned*	11.5
	"	9.6
	Alphaproteobacteria/Rhodobacterales/Rhodobacteraceae/Pseudorhodobacter	8.9

The vertical pilot reactor was significantly different from the horizontal pilot reactor ($p = 0.00001$ and $p = 0.0004$) and the biofilter ($p = 0.00001$ and $p = 0.001$), for the Chao1- and the Shannon diversity index, respectively. The composition differences (Bray-Curtis distances) of ASVs for the different conditions are presented in a PCoA plot (*Appendix H, Figure H. 19)*. There was a significant difference in distance for the vertical pilot reactor compared to the horizontal pilot reactor ($p = 0.003$) and the nitrifying biofilter ($p = 0.03$). The relative abundance of prokaryote species for the different conditions are presented in a bar chart (*Appendix H, Figure H. 20).*

C. Eukaryote part of the community

The most abundant eukaryote species (*Figure 29* and *Appendix H, Figure H. 22*) in the microbial communities were similar between the two pilot reactors. However, the species abundancy varied between them. The results revealed that the vertical pilot reactor contained almost exclusively the diatom microalgae Phaeodactylum (*Phaeodactylum tricornutum CCAP 1055/1*) (relative abundance = 91%). The horizontal pilot reactor was also abundant in Phaeodactylum (*Phaeodactylum tricornutum CCAP 1055/1*) (relative abundance = 35%); however, metazoans and fungi were also abundant. The investigation of the diatom community (*Figure 30*) underlined these findings.

In addition, the taxonomic classification revealed that the two pilotreactors contained fungi (*Agaricomycetes sp.*) and microalgae parasites (*Aphelidium desmodesmi*). The vertical pilot reactor also contained protists (*Labyrinthula sp.*). The horizontal pilot reactor, as well as the nitrifying biofilter, were abundant in Metazoans (Unassigned) and two types of fungi: *Mortierellomycotina incertae sedis* (relative abundance = 9% and 23%, respectively) and Agaricomycetes *sp.* No diatoms were found in the nitrifying biofilter.

The results showed that there was a significant difference between the vertical and the horizontal pilot reactor ($p = 0.02$). The composition differences (Bray-Curtis distances) of ASVs for the vertical- and the horizontal pilot reactor, as well as for the nitrifying biofilter are presented in a PCoA plot (*Figure H. 21)*. The differences in distances were found to be significant between the vertical pilot reactor compared to the biofilter ($p = 0.03$) and the horizontal pilot reactor ($p = 0.004$).

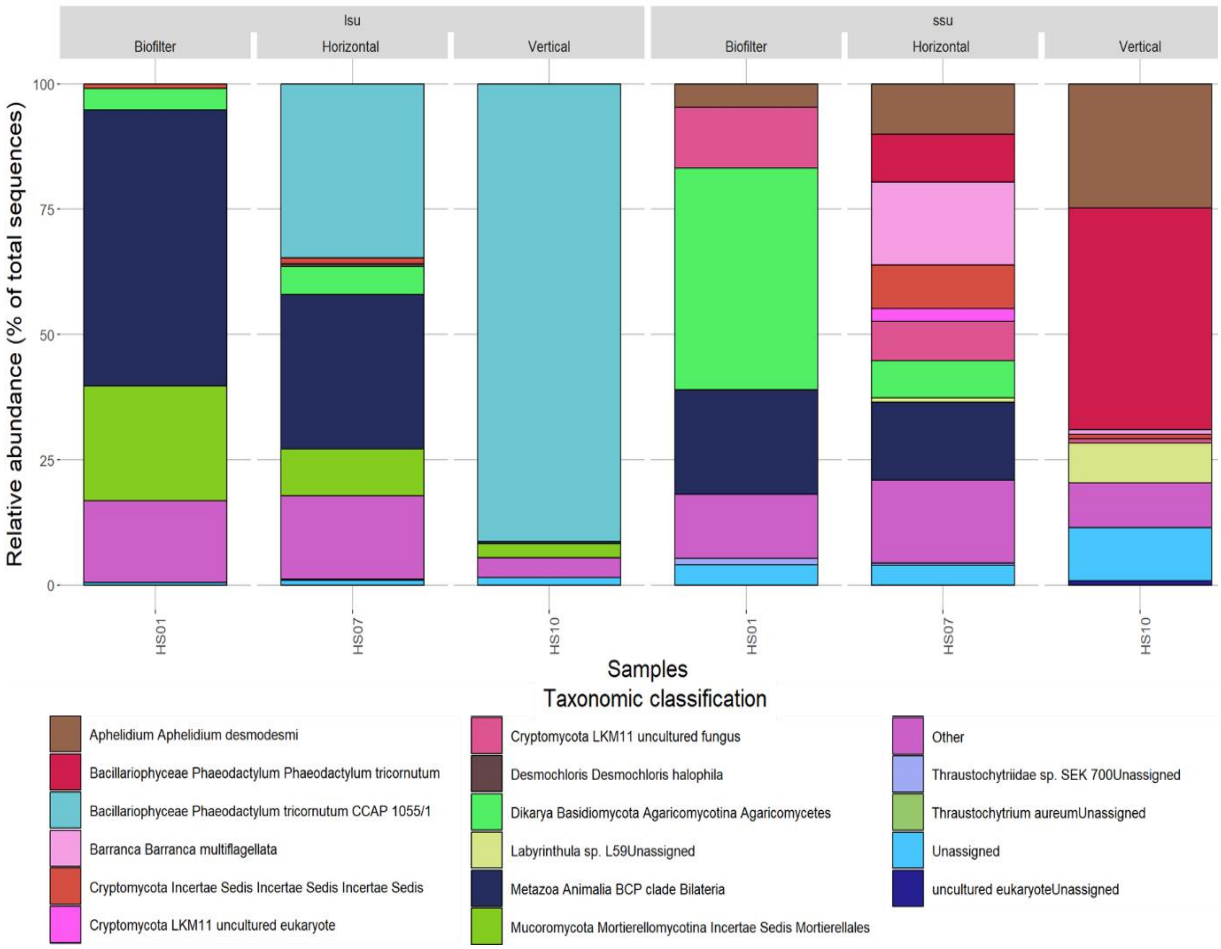

Figure 29: The relative abundance (%of total sequences) of eukaryote species in the community of the two pilot reactors at Hardingsmolt, as well as for the nitrifying biofilter. The sequences were obtained by ONT sequencing. The taxonomic classification is presented on the bottom, with respective color coding.

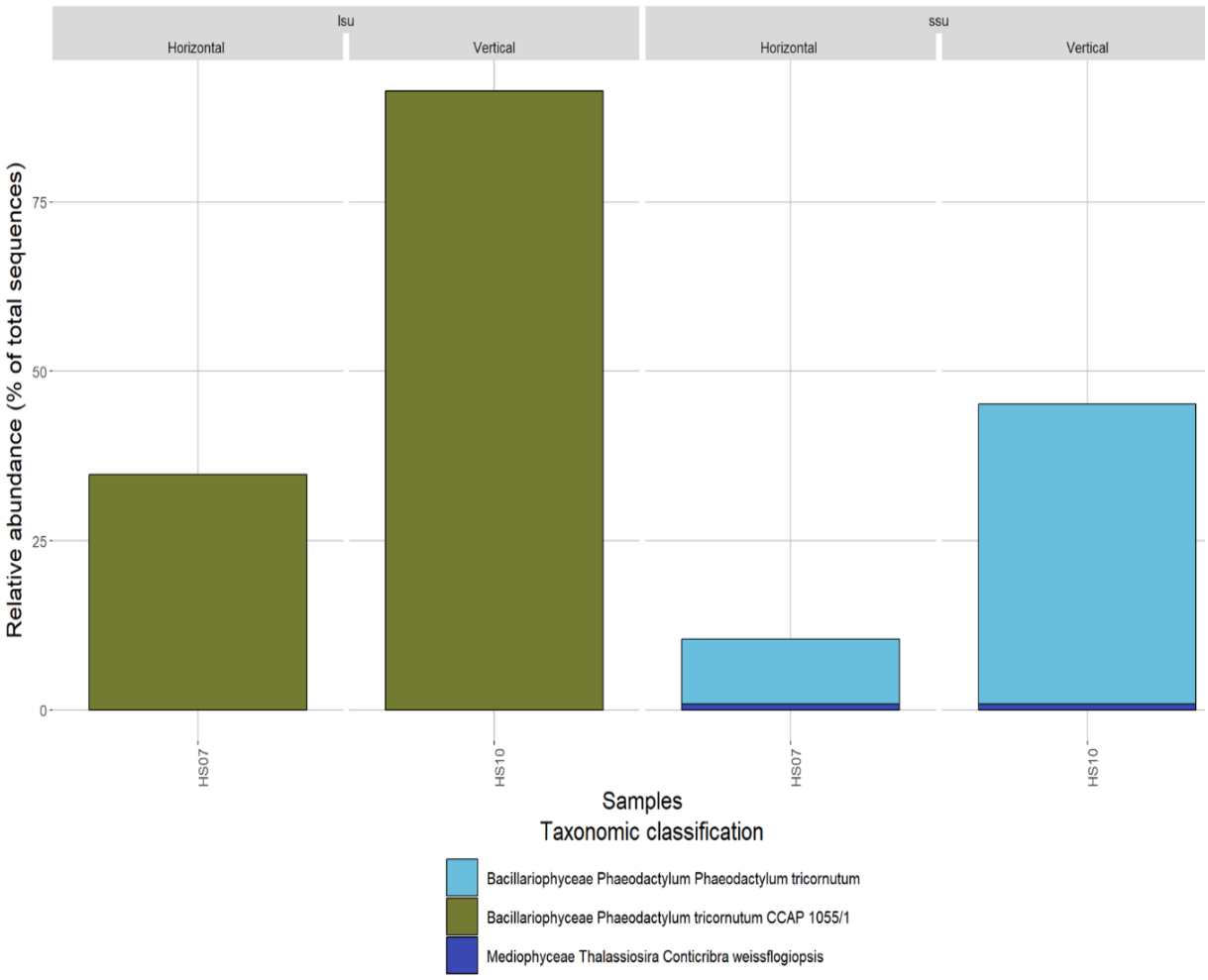

Figure 30: The relative abundance (%of total sequences) of diatom microalgae species in the eukaryote community of the two pilot reactors at Hardingsmolt, as well as for the nitrifying biofilter. The sequences were obtained by ONT sequencing. The taxonomic classification is presented on the bottom, with respective color coding.

4. Discussion

4.1 Production of biofilm containing microalgae

Light is the fundamental source of energy that drives the life-sustaining process of photosynthesis. In the first experiment of this master's, three different light intensities were tested to investigate the microbial growth, especially the microalgal growth, which was expected to be in a planktonic form. As the cultivation medium had a balanced N:P ratio (*Table 6*) (Mohsenpour et al., 2021), it was hypothesized that it would be observed growth of microalgae in both conditions where light was added (high and medium), and that no photoautotrophs would be observed in the condition where light was absent. It was thought that heterotrophs would thrive in all conditions.

Even though (Hill et al., 2009) and (Liu et al., 2013) described light saturation at 100 and 150 µmol photon $m^{-2}\,s^{-1}$, (Hill and Fanta, 2008) considered growth below 88 µmol photon $m^{-2}\,s^{-1}$ as light limited. It was therefore decided that the medium light condition should be close to the values described by Hill and Liu, resulting in a light intensity of 160 µE $m^{-2}\,s^{-}$. As microalgal productivity can increase with increasing light intensities (Liu et al., 2012, Juneja et al., 2013), and the lipid content has been reported to increase when light intensities increases (Ruane et al., 2010, Liu et al., 2013), it was decided that the high light condition should be 240 µE $m^{-2}\,s^{-1}$.

The results demonstrated that microalgae were able to grow in the conditions where light was added; however, no growth was observed in the condition where light was absent, neither photoautotrophs nor heterotrophs. The results showed that the microbial growth was benthic, producing a biofilm on the bottom of the cell cultivation flasks. As the growth was benthic, a spectrophotometer was not a valid tool to monitor the microbial growth. However, visual observations suggested that there was more microbial biomass when the light intensity was high. As a result, the subsequent experiments were conducted with a high light intensity (202 – 333 µE $m^{-2}\,s^{-1}$).

Microscope pictures revealed that the benthic community consisted of diatom microalgae species. As diatoms lack organic cell walls, and rather live in open houses of opaline silica (Eilertsen et al., 2022), a genuine question arose whether the concentration of silica in the RAS water coming from Hardingsmolt AS was sufficient for cultivation of benthic diatoms. The second experiment was therefore a natural continuation of the investigation of the RAS water, testing if the addition of silica influenced the growth and species composition of the biofilm. As silica is an obligate requirements for most diatoms (Kumar Singh et al., 2022), it was hypothesized that there would be an increased growth of benthic diatoms when silica was added to the cultivation medium.

The results showed that the addition of silica had a significant ($p = 0.00035$) effect on the biomass yield (g m^{-2}) (*Figure 12*). After 8 days, the treatment had obtained a much higher biomass yield (29.4 g m^{-2}) compared to the control (27.8 g m^{-2}). Both the maximum productivity and the growth rate (*Table 9*) were found to be significantly higher when silica was added, reflecting the importance of silica on benthic growth of diatoms. Similar findings has been reported (Kumar Singh et al., 2022), showing that the growth rate of *Thalassiosira sp.*, *Skeletonema sp*., and *Chaetoceros sp.* was highest when a concentration of 30 mg L^{-1} Si was used. Even though the addition of silica resulted in an increased growth of diatom microalgae, the calculated productivity and the maximum productivity were low compared to the literature (Liu et al., 2020, Zhuang et al., 2018). The low growth values could be due to the experimental setup, using small cell cultivation flasks as the cultivation units, as well as using a relatively low cultivation temperature (Brindhadevi et al., 2021). In either way, the low growth-values suggested that a deeper investigation of microalgae

cultivation on RAS water was necessary to obtain high productivity and growth rate, which in return also would increase the cleaning properties of the biofilm (Liu et al., 2020).

During the experimental period, a plateau was reached after ~6 days; however, the treatment obtained a higher biomass yield during this period compared to the control. The RAS water had an unbalanced N:P ratio of 6:1, suggesting that the treatment could have been limited by the available amount of N (Larsdotter, 2006). As a result, Conway medium was added to the cell cultivation flasks on day 15 to overcome these issues. After Conway medium was added, the microbial selection pressure changed, altering the community from a benthic community of oval diatoms to a planktonic community of pennate microalgae species (*Figure 13* and *Figure 14*).

In the experiment testing addition of silica, the amount of nitrogen in the batch of RAS water was low. It was later learned that the batch of RAS water was collected during a period when the fish was not feed at the RAS facility, meaning that fish and microbial metabolism was low. Occasionally in RAS, especially before fish are vaccinated or transported, they are not feed (often 2-4 days). This is natural parts of the production cycle at a RAS facility. Because of this, it was desirable to investigate the effects of the nutrient load on the microbial growth, wanting to understand how much biofilm could be produced (g m^{-2}) during the different operational periods in the production cycle at the RAS facility.

As a result, the third experiment was conducted in two parts, where the first part tested high and low nutrient load, whereas the second part tested addition of certain micronutrients. As the treatment contained ~10 times more nutrients compared to the control, it was hypothesized that the treatment would obtain a higher biomass yield and productivity compared to the control. Regarding the addition of micronutrients, it was thought that if any of the tested nutrients were scarce in the cultivation medium, the condition testing that particular nutrient would obtain a higher biomass yield compared to the other treatments.

The results showed that the nutrient load had a significant ($p = 0.004$) effect on the biomass yield (*Figure 17*). During the experimental period (T0-T18), the treatment obtained a higher biomass yield (32.5 g m^{-2}) compared to the control (28.9 g m^{-2}). The control reached a plateau after approximately 8 days, whereas the treatment continued to increase in biomass throughout the experimental period. The productivity and the maximum productivity (*Table 12*) were found to be significantly higher for the treatment compared to the control; however, like in the experiment testing addition of silica, the calculated productivities were low compared to the literature (Liu et al., 2020, Zhuang et al., 2018). The results reflected the importance of having a high nutrient load in the cultivation medium, to obtain a higher productivity and biomass yield. Similar findings was found by (Liu et al., 2020) and (Yun et al., 2015).

As seen from the scatterplot (*Figure 17)*, the treatment encountered two plateaus during the experimental period. One plateau was reached early in the experiment (T4-T8), and one was reached at the end (T12-T18). The first plateau could be due to preferential uptake of ammonia before nitrate (Wilkie and Mulbry, 2002). If both ammonium and nitrate are available in the cultivation medium, microalgae consume ammonium before they consume nitrate (Syrett, 1981). Since the concentration of ammonium in the RAS water was low (*Appendix B, Table B. 2*), the ammonium was probably depleted fast. However, as diatoms can assimilate- and save nutrients in their vacuoles, they can divide 2-3 times even after nutrients in their surroundings are exhausted. This could explain the modest increase in growth observed during the first plateau, before microalgae growth continued on nitrate (Kumar Singh et al., 2022).

Concerning the addition of micronutrients, the results (*Figure 18*) showed that all treatments obtained a higher biomass yield (36.93 – 40.25 g m^{-2}) compared to the control (25.19 g m^{-2}). However, no significant difference was found between any of the treatments when compared to each other (p = 0.3-1). Similar conclusions were retrieved from (Bastos et al., 2022), who found no significant difference between conditions when phosphate, iron, or micronutrients were tested on microalgae growth.

Perhaps, the RAS water was low in several micronutrients, and in that way created a colimitation for the benthic microalgae. (Olguín, 2012) suggested that nutrient additions may be required to optimize the molar stoichiometry of C:N:P when algal biofilms are utilized for effluent polishing. In this experiment, the batch of RAS water (*Table 11*) had a balanced N:P ratio of 16:1; however, the amount of C was unknown. Perhaps was the concentration of DIC in the RAS water low, which created an unbalanced C:N:P ratio (Redfield, 1963). The pH of the system could be measured to give an indication of the bioavailable part of DIC for microalgae. As microalgae normally consume only carbon dioxide and bicarbonate, a high pH would indicate that there could be a carbon limitation in the system.

The fourth and final experiment tested different harvesting rates, to determine what harvest frequency gave the highest productivity and biomass yield. The aim of the experiment was to investigate how often the biofilm could be harvested and still be able to regenerate. The hypothesis was that the harvest every 4^{th} day would be a too frequent harvest frequency, and in that way make the biofilm unable to regenerate between harvests (Gross et al., 2013). Similarly, it was thought that the condition testing a harvest frequency of every 12^{th} day would have a too seldom harvest frequency, and in that way produce a too thick biofilm which would limit the microbial growth (Kesaano and Sims, 2014). Because of these assumptions, it was thought that the condition having a harvest frequency of every 8^{th} day would obtain the highest biomass yield during the experimental period. This was inspired by (Zhuang et al., 2018, Gross et al., 2013), who found that high productivity could not be obtained in either too thin or too thick biofilm, due to the difficult mass- and light transfer- or the "lag phase" growth, respectively.

During the experiment, an equilibrium was obtained for each condition (*Figure 22*), indicating that the biofilm systems were able to regenerate between each harvest. Because of this, it was observed a stable biomass yield during the entire experimental period for all conditions. The stability of the biofilm, even though the systems were exposed to high mechanical stress upon harvest, suggested that the cultivation systems were robust. The biomass yield was almost doubled when the harvest frequency was lowered from four days to eight days and increased 3.4 times when the harvest frequency was lowered to twelve days. The results showed that a harvest frequency of every 12^{th} day was the best. This condition produced on average more biomass (21.57 g m^{-2}) (*Figure 23*), as well as had a higher productivity compared to the other two conditions (*Table 14*). In comparison to the literature, the calculated productivities were comparable to other studies (Liu et al., 2020, Zhuang et al., 2018); however, they were on the lower limits. This could be due to the change in experimental design, performing the experiment with flow through system rather than in batch.

The productivity of the harvest every 12^{th} day condition was less compared to the maximum productivity (1.93 ± 0.01) of the system. This could be due to mechanical stress inflicted upon the biofilm upon harvest, or it could be due to the high pH of the system. Even though the entire reactor volume was changed 2.8 times a day (3.5 L day^{-1}), it seemed like the added nutrients were metabolized by the biofilm faster than new water could supply them. The average pH for the three conditions during the experimental period (*Figure 24*), was high (~9.3-10.5) during most of the experimental period. Even though it

is not unusual to encounter pH as high as 11 in intensive cultivation of microalgae (Brewer and Goldman, 1976, Moheimani and Borowitzka, 2006, Moheimani et al., 2011), the high pH implies that there could be a carbon limitation in the system. An increased pH tends to create a carbon limitation for algal biofilms, by producing a significant increase in carbonate, compared to carbon dioxide and bicarbonate (Kesaano and Sims, 2014). As carbonate is not an available source of carbon for most microalgae (Larsdotter, 2006), the elevated pH might have created a limitation. Not only is a moderate pH important for bioavailability of DIC, but also for metabolic activities (Thornton, 2009, Kumar Singh et al., 2022). The optimal pH for microalgae is species dependent; however, previous studies showed that maximum growth for the species studied (diatoms), where found within the pH range of 5.5 – 8 (Kumar Singh et al., 2022, Taraldsvik and Myklestad, 2000). In real-life RAS, the amount of water that can pass though the photoautotrophic biofilter can be substantially increased, which could possibly eliminate these problems.

At the RAS facility Hardingsmolt AS, two attached photobioreactors for cultivation of microbial biofilm containing microalgae were tested as pilot scale reactors. The aim was to demonstrate at site, that it was possible to cultivate a photoautotrophic biofilm from the RAS water in a vertical and horizontal pilot reactor, and to investigate the species composition of the biofilm. It was hypothesized that the horizontal pilot reactor would obtain more biomass compared to the vertical one. Even though the RAS water was collected just after the mechanical filtration (grid size = 10-500 µm), it was thought that small particles would sediment onto the growth plates of the horizontal system. In contrast, the vertical pilot reactor contained vertically placed growth plates, and had additional water filtration (0.46- and 0.22 µm). It was therefore thought that the vertical pilot reactor would contain less particles, and therefore also less biomass.

Visual inspections, as well as dry weight measurements (*Table 17*) revealed that the horizontal pilot reactor obtained a higher biomass yield and productivity compared to the vertical one. Still, large standard errors were associated with the measured values, probably originating from the thick biofilm harvested the first day. Compared to the experiment testing harvest rates, the pilot reactors produced more biomass and had a higher productivity, even after the standard error was subtracted from the measured value. As the pilot reactors had plenty of water compared to the lab-scale experiment, the problems related to pH was probably not encountered, which might have been why a higher biomass yield and productivity was observed. However, the pH was not measured in the pilot reactors, so these assumptions are only speculations. Similarly, the harvesting regimes were not similar, which must be considered. In comparison to the literature, the two pilot reactors were able to obtain comparable productivities (Liu et al., 2020, Zhuang et al., 2018).

4.2 Genetic community analysis of the biomass

4.2.1 Prokaryote

The genetic analysis showed that the communities of the different experiments contained a diversity of prokaryote microorganisms. The most abundant prokaryote taxa varied (*Table 7*, *Table 10, Table H. 1, Table 16, and Table 18*); however, *Alphaproteobacteria* was the most abundant Class in all the experiments, including the pilot reactors at Hardingsmolt AS. *Alphaproteobacteria* are heterotrophic bacteria, and the Class contains a broad range of species. In the experiments, Genus such as *Pseudorhodobacter, Yoonia-Loktanella, Hyphomonas, Sulfitobacter, Marivita, and Methylobacterium-Methylorubrum* were abundant. The genus *Pseudorhodobacter* have previously been associated with contaminated environments, where they were thought to contribute to nitrite reduction (Chen et al., 2022) and/or denitrification (Maier et al., 2022). Other interesting Genus from

the Class were from the Family *Rhodobacteraceae*, which are often found in marine environments where they mainly are composed of aerobic photo- and chemoheterotrophic species. These species are often involved in biogeochemical cycling of sulphur and carbon (Pujalte et al., 2014). This aligns with the characteristics found for the Genus discovered. *Yoonia-Loktanella* and *Sulfitobacter* were abundant, which are involved in demethylation of dimethylsulfoniopropionate (DMSP) (Piontek et al., 2022). DMSP is an organic osmolyte produced by phytoplankton (Hacquard, 2017). As the communities contained phytoplankton (*Eukaryote*), a symbiotic relationship probably excited, where the produced DMSP possibly served as a reduced carbon and sulphur source for heterotrophic bacteria (Bullock et al., 2017).

Generally, the Class *Alphaproteobacteria*, *Gammaproteobacteria*, and *Flavobacteriia* were abundant in the microbial communities. The fact that *Alphaproteobacteria* and *Gammaproteobacteria* were the most dominating Classes of bacteria aligns with the theory, which emphasizes that RAS communities often are dominated by *Alphaproteobacteria* and *Gammaproteobacteria* (Blancheton et al., 2013, Tal et al., 2003, Wietz et al., 2009). *Gammaproteobacteria* contains a broad range of heterotrophic bacteria, by which abundant Genus in the experiments were *Rheinheimera, Shewanella, Glaciecola, and Alcanivorax*. The Genus *Rheinheimera* are capable of ammonia removal (Yan et al., 2023), which implies that there might exist a synergistic relationship between microalgae and bacteria in the photoautotrophic biofilm for cleaning of N and P from the RAS water.

In the experiment testing light intensities, the condition testing medium light were abundant in the Genus *Pseudomonas*. *Pseudomonades* are often associated with heterotrophic denitrification (*Table 1*), which can indicate that the microbial biofilm removed some of the nitrate-N through denitrification. Different strains of *Pseudomonas and Flavobacteriia* have been found to dominate the microbiota of gut and intestine in juvenile farmed Atlantic salmon (Navarrete et al., 2009, Ringø et al., 1995, Hovda et al., 2007). *Flavobacteria* play a key role in establishment of marine biofilms (Pollet et al., 2018); however, it must be kept in mind that some strains are associated with disease in Atlantic salmon (Birkbeck and Ringø, 2005); among others cold water disease (Bernardet and Bowman, 2006, Barnes and Brown, 2011). However, most species of *Pseudomonas* and *Flavobacteria* are not obligate pathogens, but rather opportunistic bacteria (Bruno and Ellis, 1996), which underline the importance of good management at the RAS facility to avoid stressed and injured fish.

In the experiment testing harvest rates, the results implied that the species communities changed as a function of time rather than the harvest frequencies (*Appendix H, Figure H. 15*). In the beginning, the samples (initiation and acclimation period (T0)) were clustered together with the first harvest of every 4th day condition (T4). Similarly, the first harvest for the other two conditions (T8 and T12) were clustered together. At the end of the experimental period, all samples were clustered together (T32 and T36). The relative abundance of prokaryote species (*Appendix H, Figure H. 16*) showed that the diversity was reduced during the experimental period, illustrated by the change in taxa and relative abundance from the first harvest for each condition to the last harvest for each condition.

In the pilot demonstration at Hardingsmolt AS, the results showed that the vertical pilot reactor was more diverse, compared to the horizontal pilot reactor and the biofilter. The horizontal pilot reactor and the biofilter were clustered together (*Figure H. 19*), demonstrating that these contained similar prokaryote species. This was also illustrated by the relative abundance of prokaryote species (*Appendix H, Figure H. 20*). The horizontal reactor and the biofilter were abundant in the bacterial Genus *Polaribacter*, *Pseudorhodobacter*, as well as species from the Family *Rhodobacteraceae*. In contrast, the vertical pilot reactor had a high relative abundance of species coming from the Family

Rhodobacteraceae, as well as Genus such as *Yoonia-Loktanella, Maribacter*, and *Novosphingobium*.

Neither of the experiments, nor the pilot reactors, were abundant in species typically linked to nitrification, e.g., *Nitrospira sp.*, *Nitrobacter sp.*, or *Nitrosomonas sp.* It was surprising that neither of these were represented in the investigation; however, as heterotrophic bacteria typically sustain 98% of the species population of nitrifying biofilters (Aalto et al., 2022, Hüpeden et al., 2020), they probably did not end up as the most abundant taxa in the analysis.

4.2.2 Eukaryote

In the different experiments, as well as in the two pilot reactors at Hardingsmolt AS, microscope pictures (*Figure 9*, *Figure 13, Figure 14*, *Figure 19, Figure D. 6, Figure D. 7, Figure 25, Figure D. 8, and Figure 28*) showed that two types of diatoms were dominating in the communities. This was confirmed by microalgae expert- and CEO of the DareWin project at Inria, Hubert Bonnefond (Bonnefond, 2022).

Genetic analysis revealed that the eukaryote part of the community contained diatom microalgae species (*Bacillariophyceae*) (*Figure H. 6, Figure H. 10, Figure H. 14, Figure H. 18, and Figure H. 22*). The analysis also showed that other eukaryote species were abundant in the conditions, as well as the start water and the nitrifying biofilter (*Figure 10*, *Figure 15*, *Figure 20*, *Figure 26*, and *Figure 29*). In all four experiments, as well as in the pilot reactors, different types of fungi (*Mortierellomycotina incertae sedis*, *Cryptomycota incertae sedis, Agaricomycetes sp,* and *Cryptomycota LKM11*), protists (*Aplanochytrium kerguelense*, *Thraustochytrium aureum, Thraustochytriidae sp., and Labyrinthula sp.*), choanoflagellates (*Craspedida codonosigidae*), microalgae parasites (*Aphelidium desmodesmi*), ciliates (*Cinetochilum ovale*), metazoans (Unassigned), and microalgae multiflagellata (*Barranca multiflagellata*) were abundant.

In marine environments, diatom microalgae species are the most successful and productive photoautotrophs in the communities. Diatoms are responsible for approximately 40% of the primary production in the oceans, constituting 20% of the carbon fixation on the planet (Bowler et al., 2010). As diatoms are known to produce PUFAs, especially omega-3 fatty acids (Eilertsen et al., 2022), a high relative abundance of diatoms in the biomass could highlight the potential as an ingredient in fish feed. The genetic analysis showed that the two most abundant diatom microalgae species were Phaeodactylum (*Phaeodactylum tricornutum CCAP 1055/1*) and Nitzschia (*Nitzschia sp. ChengR-2013*). Nitzschia was more abundant (relative abundance = 62%, and 75%, for high and medium light, respectively) in the experiment testing addition of light, whereas *P. tricornutum* was the most abundant species in all the other experiments: Testing addition of silica (relative abundance = 82%), testing addition of nutrients (High_Vit: Relative abundance = 81%), testing harvest frequency (all conditions: Relative abundance > 90%), and the vertical pilot reactor (relative abundance = 91%).

Nitzschia has been found to be the most frequent phytoplankton, as well as the most thoroughly studied diatom associated with agricultural runoffs (Singh et al., 2023). Nitzschia is a promising candidate for production of EPA (Ma et al., 2023, Mao et al., 2020). When Nitzschia was cultivated with fertilizer, the lipid content was found to constitute 15% of the dried biomass (Singh et al., 2023). Similarly, the total lipid content of the dried biomass ranged from 5-15% when Nitzschia were grown under different silica concentrations. The study also found that the amount of EPA in the biomass ranged from ~1 to ~3% (Mao et al., 2020). These findings illustrate the potential of *Nitzschia sp*. to

boost the lipid content of the produced biomass, potentially increasing the amount of valuable fatty acids in the biomass.

P. tricornutum is often found in marine ecosystems (Butler et al., 2020). *P. tricornutum* produce lipids, among others, both EPA and DHA (Butler et al., 2020, Cui et al., 2019). A study conducted in the western part of Norway, found that the EPA content of cultured *P. tricornutum* in a flat plate cultivation system constituted 3-4% of the dried biomass (Steinrücken et al., 2018). (Wang et al., 2019a) found that a high lipid productivity (54.76 mg L^{-1} day^{-1}) could be achieved when a mixture of municipal wastewater and seawater was used as the cultivation medium. *P. tricornutum* can thrive in low-light conditions, as well as being tolerant to high pH. In a RAS facility, the light availability is often low. *P. tricornutum* has previously shown to be a robust candidate for microalgae mass-production, where it often dominated and outcompeted other microalgae species (Remmers et al., 2017, Spilling et al., 2013). This could be why *P. tricornutum* were dominating in these experiments too. In biofilm cultivation of *P. tricornutum*, green extraction processes such as microwave-assisted and pressurized liquid extraction already exists, allowing sustainable and cost-efficient biorefinery methods (Butler et al., 2020).

One curiosity of *P. tricornutum* is its great adaptability concerning pleiomorphism, where four different morphotypes are known: Crusiform, triradiate, oval, and fusiform (Steinrücken et al., 2018, Martino et al., 2007, Ovide et al., 2018). In the experiment testing addition of silica, an observation was described after Conway medium was added, where the community changed from oval diatoms to fusiform species (*Figure 13* and *Figure 14*). Based on the genetic analysis, the microscope observations could be explained by a change from oval to fusiform morphotype for *P. tricornutum*. All known diatom microalgae species, except for *P. tricornutum,* has shown obligate requirements for dissolved silica to grow (Kumar Singh et al., 2022). Perhaps is the fusiform morphotype dominating in silica depleted environments.

The species composition of the eukaryote part of the communities contained valuable diatoms. Both *Nitzschia sp.* and *P. tricornutum* produce valuable fatty acids: EPA and DHA, which highlights the potential of the harvested biomass as an ingredient in fish feed.

4.2.3 Comparison between DNBSEQ and Oxford nanopore sequencing

DNBSEQ sequencing allow high throughput and accuracy sequencing with relatively low cost (Jeon et al., 2021). DNBSEQ is restricted to a read length of approximately 150-300 base pairs (Jeon et al., 2021, Kumar et al., 2019), which makes DNBSEQ a good tool for amplicon sequencing where high accuracy and coverage are required. Because of the high accuracy (~99.5%), DNBSEQ produces reads with high quality (Jeon et al., 2021). However, if the region examined has a high degree of similarity between more species, it can be difficult to separate species from each other in a microbial community analysis (Santos et al., 2020).

In contrast, ONT can generate long reads, tens of kilobases in length (Santos et al., 2020). Even though ONT can generate long reads, it is also more prone to error (~5%). However, in taxonomic investigation of microbial communities, the long reads of ONT are advantageous over DNBSEQ. This is because the long reads allow discrimination between different species in a much broader range, giving higher resolution and depth of the investigation. While DNBSEQ must discriminate species based on a small fragment of the ribosomal DNA, for instance the V7 of the eukaryote 18S rRNA gene, ONT can differentiate species based on large fragments (e.g., the whole ribosomal 18S rDNA gene (V1-V9)), and in that way allow for increased taxonomic and phylogenetic resolution. In contrast to

DNBSEQ, which often fails to discriminate species beyond genus level (Feng et al., 2015), ONT can. For such purposes, the increased error rate of ONT is considered a fair trade for the capability of high-level species differentiation- and classification.

In this thesis, the eukaryote community of the biofilm was investigated with both DNBSEQ and ONT. The prokaryote part of the community was investigated through the V3-V4 variable region in DNBSEQ only. As microalgae were the most interesting microorganisms of this project, it was important to discriminate the eukaryote part on a deep taxonomic level. The eukaryote contributors of the biofilm were identified through V7 in DNBSEQ, and the whole 18S rRNA operon (V1-V9) in Oxford nanopore sequencing. As seen from the investigation, DNBSEQ sequencing were not able to discriminate eukaryote microalgae beyond the taxonomic resolution of Class (*Figure H. 6, Figure H. 10, Figure H. 14, Figure H. 18, and Figure H. 22*). The analysis showed that the community contained diatoms (*Bacillariophyceae*); however, the examined region (V7) could not be used to discriminate what diatoms were present in the community. In contrast, the data obtained by ONT sequencing was used to increase the taxonomic resolution. ONT allowed species differentiation down to Genus level (*Figure 10*, *Figure 15*, *Figure 20*, *Figure 26*, and *Figure 29*). This illustrates how ONT contributed with high taxonomic resolution compared to DNBSEQ sequencing, increasing the depth of the taxonomic investigation.

Even though the 16- and 18S rRNA marker genes are considered gold standard for taxonomic classification, the sequencing efficiency can be impacted by several factors that can result in false species abundancy, as well as remain species as undetected. This can for instance be related to which region of the rRNA gene that is sequenced, the sequencing technology itself, and the bioinformatic workflow(s) used to distinguish between species (Winand et al., 2019). For instance, samples of microbial communities can be difficult to interpret correctly, due to variation in 16- and 18S rRNA gene copy number (Winand et al., 2019). For instance, *Mycoplasma pneumoniae* has only one copy of the 16S rRNA gene, whereas *Escherichia coli* have more than 7, and *Bacillus subtilis* can have up to 15 (Bercovier et al., 1986, Ellwood and Nomura, 1980, Rainey et al., 1996). This can potentially lead to false representation of the community, resulting in species with low copy number to remain undetected, or to seem less abundant in the microbial community (Winand et al., 2019).

4.3 Correlation between %area and dry weight

A correlation was made between average %area and dry weight (g m^{-2}) to be able to extrapolate values obtained in the inverse microscope (average %area) into dry weight (g m^{-2}). As seen from the scatterplot (*Figure 8*), the datapoints did not occupy the full length of the two axes. Instead, datapoints were mostly gathered within the range of 30 to 70 %area, and mostly between 32 and 42 g m^{-2} for the x and y axis, respectively. Two datapoints were located below 20 %area, having corresponding g m^{-2} values between 20-25. These two datapoints had a big effect on the best fitted line of the plot. The correlation was good to extrapolate values found within the range; however, when samples from the lower- and higher limits were extrapolated, the accuracy was not that good. This could be illustrated by the best fitted line ($y = 0.219x + 26.417$) of the scatterplot, showing that a sample with an average %area of zero, meaning that there were no particles observed on the surface of the cell cultivation flasks, would still obtain a biomass yield of 26.417 g m^{-2} after the extrapolation, which obviously is wrong.

Even though the extrapolation had its weaknesses, it is emphasized that the extrapolated values were not intended to tell the true biomass yield of the experiments, but rather as an indication of the growth potential of the different systems. Because both treatment and

control were extrapolated with the same correlation coefficient, the difference in growth potential between the two conditions would still be valid. This must be kept in mind. In addition, the P-value of the correlation was highly significant ($p = 0.000023$), indicating that the correlation could be used- and trusted. The R^2 of the correlation was 53%, indicating that the relationship between the two units was moderate to strong.

4.4 Photoautotrophic biofilter in real life RAS

There has been an increased awareness related to the release of nutritious effluents from RAS facilities, highlighted by the negative effects associated with eutrophication and deterioration of recipient water bodies (Chowdhury et al., 2013). In the future, the production of aquatic species on land will probably have to be more environmentally sustainable and cost-effective. This is recognized by the implementation of the EU Water Framework Directive (Directive 2000/60/EC), emphasizing the need for effluent polishing to reduce the footprint on the environment. According to (Suhr et al., 2013), RAS facilities in Denmark must regulate the amount of N, P, and organic matter that can be released into the recipient water bodies. This is regulated by a licensed maximum, describing the allowed nutrient waste output. In time, nutrient polishing of the effluent waste stream from RAS facilities might be implemented in Norway as well. If this happens, one solution could be the implementation of a photoautotrophic biofilter for microalgae production. In contrast to the options existing today, which could be a combination of denitrification and phosphorus recovery, the photoautotrophic biofilter has the ability of nutrient recovery.

In this master's thesis, it was demonstrated that it was possible to cultivate a benthic biofilm from the RAS water. However, low productivity was associated with the lab scale experiments. It was thought that there was a lack of some nutrients, possibly an insufficient amount of DIC in the RAS water. As diffusion of CO_2 from air into water is slow (Unver and Himmelblau, 1964), it was suggested that CO_2 could be added to the photoautotrophic biofilter to increase the amount of bioavailable DIC for the microalgae, and in that way possibly increase the productivity as well. However, in a RAS, these problems are likely not to be observed due to the large water to bioreactor ratio. An advantage with the high CO_2 consumption associated with the photoautotrophic bioreactor is the possibility of decreasing the degasser, which could have beneficial effects in respect to cost and construction of the RAS facility.

A photoautotrophic biofilter can be operated in several ways in RAS, for instance with a high or low HRT. When the HRT is kept low, more RAS water is introduced to the biofilter per time unit. An increased water flow will only allow the autotrophic biofilter to remove a fraction of the total nutrient content of the RAS water. What HRT should be applied depends on the aim of the cleaning at the facility. If the aim is to keep the level of nitrate below a certain treshhold, it is sufficient to only remove a fraction of the nutrients. If the aim is to implement the photoautotrophic biofilter for nutrient polishing of the effluent waste stream, the HRT should be kept high to allow through removal of C, N, and P from the RAS water. This increases the cleaning properties, and in that way decreases the negative effects of the effluent waste stream on the recipient water bodies. However, when the HRT is kept high, problems like those seen in the lab might be encountered in the RAS facility too. This could possibly be mitigated by altering the chemistry of the RAS water prior to the photoautotrophic biofilter. Nutrient additions might be needed to optimize the molar stoichiometry of C, N, and P, as well as the concentration of silica.

4.5 Future work

Lab-scale experiments, as well as the pilot demonstration at Hardingsmolt AS gave information on the microbial productivity. Compared to the literature, most of the calculated productivities were low (Boelee et al., 2014, Brennan and Owende, 2010, Liu et al., 2013, Liu et al., 2020, Zhuang et al., 2018). (Boelee et al., 2014), found that in an outdoor pilot scale phototrophic biofilm reactor for effluent polishing, the biomass yield remained relatively constant around 7 g m^{-2} day^{-1} when the harvest frequency ranged from 2 to 7 days. The productivities in the experiment testing harvest frequencies were comparable to the literature; however, it was in the lower limits. On the other hand, the pilot reactors showed results relatable to (Boelee et al., 2014).

The low productivity encountered in the experiments underlined the potential of improving microalgae cultivation on RAS water. To be able to increase the productivity, the water chemistry, the growth conditions, as well as the cultivation technology need to be improved. An increased productivity will increase the biomass yield, which again will increase the profitability of the production. In addition, as the photoautotrophic reactors are improved and optimized, the cleaning properties are increased, resulting in more efficient nutrient recovery. This can potentially reduce the size of the photoautotrophic biofilter, which again can reduce cost and footprint associated with constructions. To be able to improve the bioreactors, these questions need to be addressed:

- Should test if the overall productivity is increased when silica is added, together with pH control and/or the addition of CO_2.
- The cleaning properties (N and P) of the microbial community must be investigated (Kesaano and Sims, 2014).
- The water chemistry of the RAS water must be analyzed, especially the content of micro- and macro nutrients, to better be able to modify the RAS water.
- Different light intensities- and light waves should be tested to investigate what is optimal for growth (Kesaano and Sims, 2014).
- The biochemical composition of the produced biomass must be investigated to identify the amount of protein and fat, especially the amount of EPA and DHA.
- A large-scale pilot reactor should be operated to produce more biomass, which can be tested as an ingredient in Atlantic salmon fish feed.
- There is a need to calculate a budget, to estimate costs related to construction and operation of the photoautotrophic biofilter, as well as what can be expected as a market price for the produced biomass (Kesaano and Sims, 2014).

5. Conclusion

Four lab scale experiments, as well as two pilot demonstrations at the RAS facility Hardingsmolt AS showed that it was possible to cultivate a microbial biofilm containing microalgae with RAS water as cultivation medium. The productivity and the biomass yield for the different cultivation systems were defined by the dry weight of the samples. The investigation showed that addition of light and silica, as well as a high nutrient load of the RAS water, had a strong effect on the biomass yield and productivity of the cultivation system. Similarly, a harvest frequency of every 12^{th} day showed a positive effect on the developing biofilm, giving the highest productivity and biomass yield of the conditions tested. It is emphasized that the results presented in this master's thesis can be used to increase the overall productivity, cleaning capacity, and biomass yield of a photoautotrophic biofilter in an operational RAS.

The calculated productivities of the lab scale experiments suggested that the cultivation conditions could be optimized. It was thought that the RAS water had a low concentration of dissolved inorganic carbon, which possibly limited the microalgae growth. Carbon dioxide can be added to the photoautotrophic biofilter to mitigate the limitation, and in that way increase the productivity, cleaning properties, and the sustainability of the reactor.

The prokaryote and eukaryote parts of the microbial communities of the microbial biofilms were investigated by 16- and 18S rRNA amplicon sequencing, respectively. The prokaryote part of the community was investigated through V3-V4 in DNBSEQ sequencing, whereas the eukaryote part of the biofilm was investigated by both DNBSEQ sequencing (V7) and Oxford nanopore sequencing (whole 18S rRNA operon (V1-V9). The characterization of the prokaryote part of the community showed that similar prokaryote species were abundant in all five experiments, mainly coming from the bacterial Class *Alphaproteobacteria*. Other abundant taxa were from the Class *Gammaproteobacteria* and *Flavobactriia*. The characterization of the eukaryote part showed that the communities contained a diversity of eukaryote organisms; however, that the microalgae communities were highly dominated by diatom microalgae species. *Nitzschia sp.* was dominating in the experiment testing addition of light, whereas *P. tricornutum* was the most abundant species in all the other experiments.

Both *Nitzschia sp.* and *P. tricornutum* are species known to produce valuable fatty acids: EPA and DHA, which highlights the potential of the mixed community biomass as a sustainable ingredient in fish feed.

6. References

ADAMS, M. A., BUCHMANN, N., SPRENT, J., BUCKLEY, T. N. & TURNBULL, T. L. 2018. Crops, Nitrogen, Water: Are Legumes Friend, Foe, or Misunderstood Ally? *Trends in Plant Science,* 23**,** 539-550.

AGILENT TECHNOLOGIES 2015. Agilent Genomic DNA ScreenTape Quick Guide for TapeStation Systems. *In:* © AGILENT TECHNOLOGIES, I.-., 2015 (ed.). Agilent Technologies.

AGOVINO, M., CASACCIA, M., CIOMMI, M., FERRARA, M. & MARCHESANO, K. 2019. Agriculture, climate change and sustainability: The case of EU-28. *Ecological Indicators,* 105**,** 525-543.

AHMED, N. & TURCHINI, G. M. 2021. Recirculating aquaculture systems (RAS): Environmental solution and climate change adaptation. *Journal of Cleaner Production,* 297**,** 126604.

ANDERSEN, R. A. 2005. *Algal Culturing Techniques,* Elsevier Inc, Elsevier Inc.

ANSORGE, W. J. 2009. Next-generation DNA sequencing techniques. *New biotechnology,* 25**,** 195-203.

ATLAS, W. 2020. *Largest Soybean-Producing Countries*. World Atlas. Available: https://www.worldatlas.com/articles/largest-soybean-producing-countries.html.

ATTRAMADAL, K. J. K., SALVESEN, I., XUE, R., ØIE, G., STØRSETH, T. R., VADSTEIN, O. & OLSEN, Y. 2012. Recirculation as a possible microbial control strategy in the production of marine larvae. *Aquacultural Engineering,* 46**,** 27-39.

BARBA, M., CZOSNEK, H. & HADIDI, A. 2014. Historical perspective, development and applications of next-generation sequencing in plant virology. *Viruses,* 6**,** 106-36.

BARNES, M. E. & BROWN, M. L. 2011. A review of *Flavobacterium psychrophilum* biology, clinical signs, and bacterial cold water disease prevention and treatment. *Open Fish Science Journal,* 4**,** 40.

BASTOS, C. R. V., MAIA, I. B., PEREIRA, H., NAVALHO, J. & VARELA, J. C. S. 2022. Optimisation of Biomass Production and Nutritional Value of Two Marine Diatoms (*Bacillariophyceae*), *Skeletonema costatum* and *Chaetoceros calcitrans*. *Biology,* 11**,** 594.

BERCOVIER, H., KAFRI, O. & SELA, S. 1986. *Mycobacteria* possess a surprisingly small number of ribosomal RNA genes in relation to the size of their genome. *Biochemical and biophysical research communications,* 136**,** 1136-1141.

BERDY, B., SPOERING, A. L., LING, L. L. & EPSTEIN, S. S. 2017. In situ cultivation of previously uncultivable microorganisms using the ichip. *Nature protocols,* 12**,** 2232-2242.

BERNARDET, J.-F. & BOWMAN, J. P. 2006. The genus *flavobacterium*. *The prokaryotes,* 7**,** 481-531.

BIRKBECK, T. H. & RINGØ, E. 2005. Chapter 10 Pathogenesis and the gastrointestinal tract of growing fish. *In:* HOLZAPFEL, W. H., NAUGHTON, P. J., PIERZYNOWSKI, S. G., ZABIELSKI, R. & SALEK, E. (eds.) *Biology of Growing Animals.* Elsevier.

BLANCHETON, J. P., ATTRAMADAL, K. J. K., MICHAUD, L., D'ORBCASTEL, E. R. & VADSTEIN, O. 2013. Insight into bacterial population in aquaculture systems and its implication. *Aquacultural Engineering,* 53**,** 30-39.

BLANCO, A. & BLANCO, G. 2017. Chapter 3 - Proteins. *In:* BLANCO, A. & BLANCO, G. (eds.) *Medical Biochemistry.* Academic Press.

BOELEE, N., JANSSEN, M., TEMMINK, H., SHRESTHA, R., BUISMAN, C. & WIJFFELS, R. 2014. Nutrient removal and biomass production in an outdoor pilot-scale phototrophic biofilm reactor for effluent polishing. *Applied biochemistry and biotechnology,* 172**,** 405-422.

BOLLMANN, A., FRENCH, E. & LAANBROEK, H. J. 2011. Chapter three - Isolation, Cultivation, and Characterization of Ammonia-Oxidizing Bacteria and Archaea Adapted to Low Ammonium Concentrations. *In:* KLOTZ, M. G. (ed.) *Methods in Enzymology.* Academic Press.

BOLYEN, E., RIDEOUT, J. R., DILLON, M. R., BOKULICH, N. A., ABNET, C. C., AL-GHALITH, G. A., ALEXANDER, H., ALM, E. J., ARUMUGAM, M., ASNICAR, F., BAI, Y., BISANZ, J. E., BITTINGER, K., BREJNROD, A., BRISLAWN, C. J., BROWN, C. T., CALLAHAN, B. J., CARABALLO-RODRÍGUEZ, A. M., CHASE, J., COPE, E. K., DA SILVA, R., DIENER, C., DORRESTEIN, P. C., DOUGLAS, G. M., DURALL, D. M., DUVALLET, C., EDWARDSON, C. F., ERNST, M., ESTAKI, M., FOUQUIER, J., GAUGLITZ, J. M., GIBBONS, S. M., GIBSON, D. L., GONZALEZ, A., GORLICK, K., GUO, J., HILLMANN, B., HOLMES, S., HOLSTE, H., HUTTENHOWER, C., HUTTLEY, G. A., JANSSEN, S., JARMUSCH, A. K., JIANG, L., KAEHLER, B. D., KANG, K. B., KEEFE, C. R., KEIM, P., KELLEY, S. T., KNIGHTS, D., KOESTER, I., KOSCIOLEK, T., KREPS, J., LANGILLE, M. G. I., LEE, J., LEY, R., LIU, Y. X., LOFTFIELD, E., LOZUPONE, C., MAHER, M., MAROTZ, C., MARTIN, B. D., MCDONALD, D., MCIVER, L. J., MELNIK, A. V., METCALF, J. L., MORGAN, S. C., MORTON, J. T., NAIMEY, A. T., NAVAS-MOLINA, J. A., NOTHIAS, L. F., ORCHANIAN, S. B., PEARSON, T., PEOPLES, S. L., PETRAS, D., PREUSS, M. L., PRUESSE, E., RASMUSSEN, L. B., RIVERS, A., ROBESON, M. S., 2ND, ROSENTHAL, P., SEGATA, N., SHAFFER, M., SHIFFER, A., SINHA, R., SONG, S. J., SPEAR, J. R., SWAFFORD, A. D., THOMPSON, L. R., TORRES, P. J., TRINH, P., TRIPATHI, A., TURNBAUGH, P. J., UL-HASAN, S., VAN DER HOOFT, J. J. J., VARGAS, F., VÁZQUEZ-BAEZA, Y., VOGTMANN, E., VON HIPPEL, M., WALTERS, W., et al. 2019. Reproducible, interactive, scalable and extensible microbiome data science using QIIME 2. *Nat Biotechnol,* 37**,** 852-857.

BONNEFOND, H. 2022. Classification of diatoms by microalgae expert- and CEO of the DareWin project at Inria. *In:* IVERSEN, J. E. (ed.).

BOWLER, C., VARDI, A. & ALLEN, A. E. 2010. Oceanographic and biogeochemical insights from diatom genomes. *Annual review of marine science,* 2**,** 333-365.

BRAY, J. R. & CURTIS, J. T. 1957. An ordination of the upland forest communities of southern Wisconsin. *Ecological monographs,* 27**,** 326-349.

BRENNAN, L. & OWENDE, P. 2010. Biofuels from microalgae—A review of technologies for production, processing, and extractions of biofuels and co-products. *Renewable and Sustainable Energy Reviews,* 14**,** 557-577.

BREWER, P. G. & GOLDMAN, J. C. 1976. Alkalinity changes generated by phytoplankton growth 1. *Limnology and Oceanography,* 21**,** 108-117.

BRINDHADEVI, K., MATHIMANI, T., RENE, E. R., SHANMUGAM, S., CHI, N. T. L. & PUGAZHENDHI, A. 2021. Impact of cultivation conditions on the biomass and lipid in microalgae with an emphasis on biodiesel. *Fuel,* 284**,** 119058.

BRUNO, D. E. & ELLIS, A. E. 1996. Chapter 13 - Salmonid Disease Management. *In:* PENNELL, W. & BARTON, B. A. (eds.) *Developments in Aquaculture and Fisheries Science.* Elsevier.

BUGTEN, A. V., ATTRAMADAL, K. J. K., FOSSMARK, R. O., ROSTEN, T. W., VADSTEIN, O. & BAKKE, I. 2022. Changes in rearing water microbiomes in RAS induced by membrane filtration alters the hindgut microbiomes of Atlantic salmon (*Salmo salar*) parr. *Aquaculture,* 548**,** 737661.

BULLOCK, H. A., LUO, H. & WHITMAN, W. B. 2017. Evolution of Dimethylsulfoniopropionate Metabolism in Marine Phytoplankton and Bacteria. *Frontiers in Microbiology,* 8.

BUTLER, T., KAPOORE, R. V. & VAIDYANATHAN, S. 2020. *Phaeodactylum tricornutum*: A Diatom Cell Factory. *Trends in Biotechnology,* 38**,** 606-622.

CADILLO-BENALCAZAR, J. J., GIAMPIETRO, M., BUKKENS, S. G. F. & STRAND, R. 2020. Multi-scale integrated evaluation of the sustainability of large-scale use of alternative feeds in salmon aquaculture. *Journal of Cleaner Production,* 248**,** 119210.

CALLAHAN, B. J., MCMURDIE, P. J., ROSEN, M. J., HAN, A. W., JOHNSON, A. J. & HOLMES, S. P. 2016. DADA2: High-resolution sample inference from Illumina amplicon data. *Nat Methods,* 13**,** 581-3.

CHAO, A. 1984. Nonparametric estimation of the number of classes in a population. *Scandinavian Journal of statistics***,** 265-270.

CHEN, Z., ZHONG, X., ZHENG, M., LIU, W. S., FEI, Y., DING, K., LI, Y., LIU, Y., CHAO, Y. & TANG, Y. T. 2022. Indicator species drive the key ecological functions of

microbiota in a river impacted by acid mine drainage generated by rare earth elements mining in South China. *Environmental Microbiology,* 24**,** 919-937.

CHERKASOV, N., IBHADON, A. O. & FITZPATRICK, P. 2015. A review of the existing and alternative methods for greener nitrogen fixation. *Chemical Engineering and Processing: Process Intensification,* 90**,** 24-33.

CHOWDHURY, M. K., SIDDIQUI, S., HUA, K. & BUREAU, D. P. 2013. Bioenergetics-based factorial model to determine feed requirement and waste output of tilapia produced under commercial conditions. *Aquaculture,* 410**,** 138-147.

CHRISTENSON, L. & SIMS, R. 2011. Production and harvesting of microalgae for wastewater treatment, biofuels, and bioproducts. *Biotechnology Advances,* 29**,** 686-702.

CUI, Y., THOMAS-HALL, S. R. & SCHENK, P. M. 2019. *Phaeodactylum tricornutum* microalgae as a rich source of omega-3 oil: Progress in lipid induction techniques towards industry adoption. *Food Chemistry,* 297**,** 124937.

D. P. CLARK, N. J. P., M. R. MCGEHEE 2019. *Molecular Biology,* Elsevier Science & technology books, Academic press.

DA COSTA, T. H. M. & ITO, M. K. 2003. PHOSPHOLIPIDS | Physiology. *In:* CABALLERO, B. (ed.) *Encyclopedia of Food Sciences and Nutrition (Second Edition).* Oxford: Academic Press.

DAHLE, S. W., ATTRAMADAL, K. J. K., VADSTEIN, O., HESTDAHL, H. I. & BAKKE, I. 2022. Microbial community dynamics in a commercial RAS for production of Atlantic salmon fry (*Salmo salar*). *Aquaculture,* 546**,** 737382.

DAVIDSON, J., GOOD, C., WILLIAMS, C. & SUMMERFELT, S. T. 2017. Evaluating the chronic effects of nitrate on the health and performance of post-smolt Atlantic salmon (*Salmo salar*) in freshwater recirculation aquaculture systems. *Aquacultural Engineering,* 79**,** 1-8.

DEHLER, C. E., SECOMBES, C. J. & MARTIN, S. A. M. 2017. Environmental and physiological factors shape the gut microbiota of Atlantic salmon parr (*Salmo salar L.*). *Aquaculture,* 467**,** 149-157.

DENG, M., LI, L., DAI, Z., SENBATI, Y., SONG, K. & HE, X. 2020. Aerobic denitrification affects gaseous nitrogen loss in biofloc-based recirculating aquaculture system. *Aquaculture,* 529**,** 735686.

DOE, U. 2002. Energy and environmental profile of the US mining industry. *US Department of Energy Office of energy efficiency and renewable energy. Energiebilanz der Nuklearindustrie*.

EILERTSEN, H. C., ERIKSEN, G. K., BERGUM, J.-S., STRØMHOLT, J., ELVEVOLL, E., EILERTSEN, K.-E., HEIMSTAD, E. S., GIÆVER, I. H., ISRAELSEN, L., SVENNING, J. B., DALHEIM, L., OSVIK, R., HANSEN, E., INGEBRIGTSEN, R. A., ASPEN, T. & WINTERVOLL, G.-H. 2022. Mass Cultivation of Microalgae: I. Experiences with Vertical Column Airlift Photobioreactors, Diatoms and CO2 Sequestration. *Applied Sciences,* 12**,** 3082.

ELLWOOD, M. & NOMURA, M. 1980. Deletion of a ribosomal ribonucleic acid operon in *Escherichia coli. Journal of Bacteriology,* 143**,** 1077-1080.

ELVY, J. E., SYMONDS, J. E., HILTON, Z., WALKER, S. P., TREMBLAY, L. A., CASANOVAS, P. & HERBERT, N. A. 2022. The relationship of feed intake, growth, nutrient retention, and oxygen consumption to feed conversion ratio of farmed saltwater Chinook salmon (*Oncorhynchus tshawytscha*). *Aquaculture,* 554**,** 738184.

ERISMAN, J. W., GALLOWAY, J., SEITZINGER, S., BLEEKER, A. & BUTTERBACH-BAHL, K. 2011. Reactive nitrogen in the environment and its effect on climate change. *Current Opinion in Environmental Sustainability,* 3**,** 281-290.

FENG, Y., ZHANG, Y., YING, C., WANG, D. & DU, C. 2015. Nanopore-based fourth-generation DNA sequencing technology. *Genomics, proteomics & bioinformatics,* 13**,** 4-16.

FJELLHEIM. A.J., H.-E. O. K., ATTRAMADAL. K., VADSTEIN. O., 2016. *Resirkulering av vann i settefiskproduksjon*, NIVA.

FOSSMARK, R. O., ATTRAMADAL, K. J. K., NORDØY, K., ØSTERHUS, S. W. & VADSTEIN, O. 2021. A comparison of two seawater adaptation strategies for Atlantic salmon

post-smolt (*Salmo salar*) grown in recirculating aquaculture systems (RAS): Nitrification, water and gut microbiota, and performance of fish. *Aquaculture,* 532**,** 735973.

FREITAG, A. R., THAYER, L. R., LEONETTI, C., STAPLETON, H. M. & HAMLIN, H. J. 2015. Effects of elevated nitrate on endocrine function in Atlantic salmon, *Salmo salar*. *Aquaculture,* 436**,** 8-12.

FROEHLICH, H. E., RUNGE, C. A., GENTRY, R. R., GAINES, S. D. & HALPERN, B. S. 2018. Comparative terrestrial feed and land use of an aquaculture-dominant world. *Proceedings of the National Academy of Sciences,* 115**,** 5295-5300.

FUKS, G., ELGART, M., AMIR, A., ZEISEL, A., TURNBAUGH, P. J., SOEN, Y. & SHENTAL, N. 2018. Combining 16S rRNA gene variable regions enables high-resolution microbial community profiling. *Microbiome,* 6**,** 17.

GAO, Y., GUO, L., SHAO, M., HU, F., WANG, G., ZHAO, Y., GAO, M., JIN, C. & SHE, Z. 2020. Denitrification performance evaluation and kinetics analysis with mariculture solid wastes (MSW) derived carbon source in marine recirculating aquaculture systems (RAS). *Bioresource Technology,* 313**,** 123649.

GONG, Y., BANDARA, T., HUNTLEY, M., JOHNSON, Z. I., DIAS, J., DAHLE, D., SØRENSEN, M. & KIRON, V. 2019. Microalgae *Scenedesmus sp.* as a potential ingredient in low fishmeal diets for Atlantic salmon (*Salmo salar L.*). *Aquaculture,* 501**,** 455-464.

GROSS, M., HENRY, W., MICHAEL, C. & WEN, Z. 2013. Development of a rotating algal biofilm growth system for attached microalgae growth with in situ biomass harvest. *Bioresource technology,* 150**,** 195-201.

GUZZON, A., BOHN, A., DIOCIAIUTI, M. & ALBERTANO, P. 2008. Cultured phototrophic biofilms for phosphorus removal in wastewater treatment. *Water Research,* 42**,** 4357-4367.

HACQUARD, S. 2017. Commentary: Microbial Small Talk: Volatiles in Fungal-Bacterial Interactions. *Front Microbiol,* 8**,** 1.

HADZIAVDIC, K., LEKANG, K., LANZEN, A., JONASSEN, I., THOMPSON, E. M. & TROEDSSON, C. 2014. Characterization of the 18S rRNA gene for designing universal eukaryote specific primers. *PloS one,* 9**,** e87624.

HAHN, M. W., KOLL, U. & SCHMIDT, J. 2019. Isolation and cultivation of bacteria. *The structure and function of aquatic microbial communities.* Springer.

HAIDARI, A. H., WITKAMP, G. J. & HEIJMAN, S. G. J. 2022. High silica concentration in RO concentrate. *Water Resources and Industry,* 27**,** 100171.

HE, H., ZHEN, Y., MI, T., FU, L. & YU, Z. 2018. Ammonia-Oxidizing Archaea and Bacteria Differentially Contribute to Ammonia Oxidation in Sediments from Adjacent Waters of Rushan Bay, China. *Frontiers in Microbiology,* 9.

HILL, W., FANTA, S. & ROBERTS, B. 2009. Quantifying phosphorus and light effects in stream algae. *Limnology and Oceanography - LIMNOL OCEANOGR,* 54**,** 368-380.

HILL, W. R. & FANTA, S. E. 2008. Phosphorus and light colimit periphyton growth at subsaturating irradiances. *Freshwater Biology,* 53**,** 215-225.

HONG, M. E., YU, B. S., PATEL, A. K., CHOI, H. I., SONG, S., SUNG, Y. J., CHANG, W. S. & SIM, S. J. 2019. Enhanced biomass and lipid production of *Neochloris oleoabundans* under high light conditions by anisotropic nature of light-splitting CaCO3 crystal. *Bioresource Technology,* 287**,** 121483.

HOVDA, M. B., LUNESTAD, B. T., FONTANILLAS, R. & ROSNES, J. T. 2007. Molecular characterisation of the intestinal microbiota of farmed Atlantic salmon (*Salmo salar L.*). *Aquaculture,* 272**,** 581-588.

HÜPEDEN, J., WEMHEUER, B., INDENBIRKEN, D., SCHULZ, C. & SPIECK, E. 2020. Taxonomic and functional profiling of nitrifying biofilms in freshwater, brackish and marine RAS biofilters. *Aquacultural Engineering,* 90**,** 102094.

JEON, S. A., PARK, J. L., PARK, S.-J., KIM, J. H., GOH, S.-H., HAN, J.-Y. & KIM, S.-Y. 2021. Comparison between MGI and Illumina sequencing platforms for whole genome sequencing. *Genes & Genomics,* 43**,** 713-724.

JUNEJA, A., CEBALLOS, R. M. & MURTHY, G. S. 2013. Effects of environmental factors and nutrient availability on the biochemical composition of algae for biofuels production: a review. *Energies,* 6**,** 4607-4638.

KARST, S. M., DUEHOLM, M. S., MCILROY, S. J., KIRKEGAARD, R. H., NIELSEN, P. H. & ALBERTSEN, M. 2018. Retrieval of a million high-quality, full-length microbial 16S and 18S rRNA gene sequences without primer bias. *Nature Biotechnology,* 36**,** 190-195.

KATOH, K., ASIMENOS, G. & TOH, H. 2009. Multiple alignment of DNA sequences with MAFFT. *Methods Mol Biol,* 537**,** 39-64.

KESAANO, M. & SIMS, R. C. 2014. Algal biofilm based technology for wastewater treatment. *Algal Research,* 5**,** 231-240.

KOLAREVIC, J., TAKLE, H., FELIP, O., YTTEBORG, E., SELSET, R., GOOD, C. M., BAEVERFJORD, G., ÅSGÅRD, T. & TERJESEN, B. F. 2012. Molecular and physiological responses to long-term sublethal ammonia exposure in Atlantic salmon (*Salmo salar*). *Aquatic Toxicology,* 124-125**,** 48-57.

KONONOVA, S. V., ZINCHENKO, D. V., MURANOVA, T. A., BELOVA, N. A. & MIROSHNIKOV, A. I. 2019. Intestinal microbiota of salmonids and its changes upon introduction of soy proteins to fish feed. *Aquaculture International,* 27**,** 475-496.

KROGDAHL, Å., KORTNER, T. M., JARAMILLO-TORRES, A., GAMIL, A. A. A., CHIKWATI, E., LI, Y., SCHMIDT, M., HERMAN, E., HYMOWITZ, T., TEIMOURI, S. & STOREBAKKEN, T. 2020. Removal of three proteinaceous antinutrients from soybean does not mitigate soybean-induced enteritis in Atlantic salmon (*Salmo salar, L*). *Aquaculture,* 514**,** 734495.

KRZANOWSKI, W. J. & KRZANOWSKI, W. 2000. *Principles of multivariate analysis*, Oxford University Press.

KRZEMIŃSKA, I., PAWLIK-SKOWROŃSKA, B., TRZCIŃSKA, M. & TYS, J. 2014. Influence of photoperiods on the growth rate and biomass productivity of green microalgae. *Bioprocess Biosyst Eng,* 37**,** 735-41.

KUMAR, K. R., COWLEY, M. J. & DAVIS, R. L. Next-generation sequencing and emerging technologies. Seminars in thrombosis and hemostasis, 2019. Thieme Medical Publishers, 661-673.

KUMAR SINGH, P., BHATTACHARJYA, R., KIRAN MARELLA, T., SAXENA, A., MISHRA, B., SAVIO, S., CONGESTRI, R., SINDHU, R., BINOD, P. & TIWARI, A. 2022. Production of lipids and proteins from marine diatoms under changing pH and silica. *Bioresource Technology,* 362**,** 127766.

KUMAR, V. J. R., JOSEPH, V., VIJAI, R., PHILIP, R. & SINGH, I. S. B. 2011. Nitrification in a packed bed bioreactor integrated into a marine recirculating maturation system under different substrate concentrations and flow rates. *Journal of Chemical Technology & Biotechnology,* 86**,** 790-797.

LANGILLE, M. G., ZANEVELD, J., CAPORASO, J. G., MCDONALD, D., KNIGHTS, D., REYES, J. A., CLEMENTE, J. C., BURKEPILE, D. E., VEGA THURBER, R. L. & KNIGHT, R. 2013. Predictive functional profiling of microbial communities using 16S rRNA marker gene sequences. *Nature biotechnology,* 31**,** 814-821.

LARSDOTTER, K. 2006. Wastewater treatment with microalgae-a literature review. *Vatten,* 62**,** 31.

LEBEDEVA, E., ALAWI, M., MAIXNER, F., JOZSA, P.-G., DAIMS, H. & SPIECK, E. 2008. Physiological and phylogenetic characterization of a novel lithoautotrophic nitrite-oxidizing bacterium,'*Candidatus Nitrospira bockiana*'. *International journal of systematic and evolutionary microbiology,* 58**,** 242-250.

LEKANG, O. I. 2020. *Aquaculture Engineering,* Wiley Blackwell, John Wiley & Sons Ltd.

LI, H. 2021. New strategies to improve minimap2 alignment accuracy. *Bioinformatics,* 37**,** 4572-4574.

LIU, J., PEMBERTON, B., LEWIS, J., SCALES, P. J. & MARTIN, G. J. O. 2020. Wastewater treatment using filamentous algae – A review. *Bioresource Technology,* 298**,** 122556.

LIU, J., YUAN, C., HU, G. & LI, F. 2012. Effects of light intensity on the growth and lipid accumulation of microalga *Scenedesmus sp.* 11-1 under nitrogen limitation. *Applied biochemistry and biotechnology,* 166**,** 2127-2137.

LIU, T., WANG, J., HU, Q., CHENG, P., JI, B., LIU, J., CHEN, Y., ZHANG, W., CHEN, X., CHEN, L., GAO, L., JI, C. & WANG, H. 2013. Attached cultivation technology of

microalgae for efficient biomass feedstock production. *Bioresource Technology,* 127**,** 216-222.

LOVE, D. C., FRY, J. P., CABELLO, F., GOOD, C. M. & LUNESTAD, B. T. 2020. Veterinary drug use in United States net pen Salmon aquaculture: Implications for drug use policy. *Aquaculture,* 518**,** 734820.

LOZUPONE, C. & KNIGHT, R. 2005. UniFrac: a New Phylogenetic Method for Comparing Microbial Communities. *Applied and Environmental Microbiology,* 71**,** 8228-8235.

LUNDBERG, D. S., YOURSTONE, S., MIECZKOWSKI, P., JONES, C. D. & DANGL, J. L. 2013. Practical innovations for high-throughput amplicon sequencing. *Nature Methods,* 10**,** 999-1002.

M. T. MADIGAN, K. S. B., D. H. BUCKLEY, W. M. SATTLEY, D. A. STAHL 2019. *Brock Biology of Microorganisms*, Pearson Education.

MA, R., YOU, Y., LIU, X., HO, S.-H., XIE, Y. & CHEN, J. 2023. Highly efficient co-production of fucoxanthin and eicosapentaenoic acid by heterotrophic cultivation of a newly isolated microalga *Nitzschia sp.* FZU62. *Algal Research,* 71**,** 103046.

MAIER, S., KRATZ, A., WEBER, J., PRASS, M., LIU, F., CLARK, A., ABED, R., SU, H., CHENG, Y. & EICKHORST, T. 2022. Water-driven microbial nitrogen transformations in biological soil crusts causing atmospheric nitrous acid and nitric oxide emissions. *The ISME Journal,* 16**,** 1012-1024.

MAO, X., CHEN, S. H. Y., LU, X., YU, J. & LIU, B. 2020. High silicate concentration facilitates fucoxanthin and eicosapentaenoic acid (EPA) production under heterotrophic condition in the marine diatom *Nitzschia laevis. Algal Research,* 52**,** 102086.

MARDIS, E. R. 2008. Next-generation DNA sequencing methods. *Annual review of genomics and human genetics,* 9**,** 387-402.

MARTINO, A. D., MEICHENIN, A., SHI, J., PAN, K. & BOWLER, C. 2007. Genetic and phenotypic characterization of *Phaeodactylum tricornutum* (*Bacillariophyceae*) accessions 1. *Journal of Phycology,* 43**,** 992-1009.

MARTINS, C. I. M., EDING, E. H., VERDEGEM, M. C. J., HEINSBROEK, L. T. N., SCHNEIDER, O., BLANCHETON, J. P., D'ORBCASTEL, E. R. & VERRETH, J. A. J. 2010. New developments in recirculating aquaculture systems in Europe: A perspective on environmental sustainability. *Aquacultural Engineering,* 43**,** 83-93.

MOHEIMANI, N. R. 2013. Inorganic carbon and pH effect on growth and lipid productivity of *Tetraselmis suecica* and *Chlorella sp* (*Chlorophyta*) grown outdoors in bag photobioreactors. *Journal of Applied Phycology,* 25**,** 387-398.

MOHEIMANI, N. R. & BOROWITZKA, M. A. 2006. The long-term culture of the coccolithophore *Pleurochrysis carterae* (*Haptophyta*) in outdoor raceway ponds. *Journal of Applied Phycology,* 18**,** 703-712.

MOHEIMANI, N. R., ISDEPSKY, A., LISEC, J., RAES, E. & BOROWITZKA, M. A. 2011. Coccolithophorid algae culture in closed photobioreactors. *Biotechnology and bioengineering,* 108**,** 2078-2087.

MOHSENPOUR, S. F., HENNIGE, S., WILLOUGHBY, N., ADELOYE, A. & GUTIERREZ, T. 2021. Integrating micro-algae into wastewater treatment: A review. *Science of The Total Environment,* 752**,** 142168.

MOWI, A. 2019. Salmon farming industry handbook. Mowi Bergen, Norway.

NAVARRETE, P., ESPEJO, R. T. & ROMERO, J. 2009. Molecular Analysis of Microbiota Along the Digestive Tract of Juvenile Atlantic Salmon (*Salmo salar L.*). *Microbial Ecology,* 57**,** 550-561.

OLGUÍN, E. J. 2012. Dual purpose microalgae–bacteria-based systems that treat wastewater and produce biodiesel and chemical products within a Biorefinery. *Biotechnology advances,* 30**,** 1031-1046.

ORIJ, R., BRUL, S. & SMITS, G. J. 2011. Intracellular pH is a tightly controlled signal in yeast. *Biochimica et Biophysica Acta (BBA) - General Subjects,* 1810**,** 933-944.

OVIDE, C., KIEFER-MEYER, M.-C., BÉRARD, C., VERGNE, N., LECROQ, T., PLASSON, C., BUREL, C., BERNARD, S., DRIOUICH, A. & LEROUGE, P. 2018. Comparative in depth RNA sequencing of *P. tricornutum*'s morphotypes reveals specific features of the oval morphotype. *Scientific reports,* 8**,** 14340.

OXFORD NANOPORE TECHNOLOGIES 2019. PCR Barcoding Kit protocol. PBK_9073_V1_REVH_14AUG2019 ed. Oxford Nanopore Technologies.

OZKAN, A., KINNEY, K., KATZ, L. & BERBEROGLU, H. 2012. Reduction of water and energy requirement of algae cultivation using an algae biofilm photobioreactor. *Bioresource Technology,* 114**,** 542-548.

PATEL, A. K., ALBARICO, F. P. J. B., PERUMAL, P. K., VADRALE, A. P., NIAN, C. T., CHAU, H. T. B., ANWAR, C., WANI, H. M. U. D., PAL, A., SAINI, R., HA, L. H., SENTHILKUMAR, B., TSANG, Y.-S., CHEN, C.-W., DONG, C.-D. & SINGHANIA, R. R. 2022. Algae as an emerging source of bioactive pigments. *Bioresource Technology,* 351**,** 126910.

PATEL, A. K., CHOI, Y. Y. & SIM, S. J. 2020. Emerging prospects of mixotrophic microalgae: Way forward to sustainable bioprocess for environmental remediation and cost-effective biofuels. *Bioresource Technology,* 300**,** 122741.

PATEL, A. K., SINGHANIA, R. R., DONG, C.-D., OBULISAMI, P. K. & SIM, S. J. 2021a. Mixotrophic biorefinery: A promising algal platform for sustainable biofuels and high value coproducts. *Renewable and Sustainable Energy Reviews,* 152**,** 111669.

PATEL, A. K., SINGHANIA, R. R., SIM, S. J. & DONG, C. D. 2021b. Recent advancements in mixotrophic bioprocessing for production of high value microalgal products. *Bioresource Technology,* 320**,** 124421.

PETERS, C. J., PICARDY, J. A., DARROUZET-NARDI, A. & GRIFFIN, T. S. 2014. Feed conversions, ration compositions, and land use efficiencies of major livestock products in U.S. agricultural systems. *Agricultural Systems,* 130**,** 35-43.

PHAM, V. H. & KIM, J. 2012. Cultivation of unculturable soil bacteria. *Trends in biotechnology,* 30**,** 475-484.

PIONTEK, J., MEESKE, C., HASSENRÜCK, C., ENGEL, A. & JÜRGENS, K. 2022. Organic matter availability drives the spatial variation in the community composition and activity of Antarctic marine bacterioplankton. *Environmental Microbiology,* 24**,** 4030-4048.

POLLET, T., BERDJEB, L., GARNIER, C., DURRIEU, G., LE POUPON, C., MISSON, B. & BRIAND, J.-F. 2018. Prokaryotic community successions and interactions in marine biofilms: the key role of *Flavobacteriia*. *FEMS Microbiology Ecology,* 94.

PRICE, M. N., DEHAL, P. S. & ARKIN, A. P. 2009. FastTree: computing large minimum evolution trees with profiles instead of a distance matrix. *Molecular biology and evolution,* 26**,** 1641-1650.

PUJALTE, M. J., LUCENA, T., RUVIRA, M. A., ARAHAL, D. R. & MACIÁN, M. C. 2014. The Family Rhodobacteraceae. *In:* ROSENBERG, E., DELONG, E. F., LORY, S., STACKEBRANDT, E. & THOMPSON, F. (eds.) *The Prokaryotes: Alphaproteobacteria and Betaproteobacteria.* Berlin, Heidelberg: Springer Berlin Heidelberg.

QI, W., SKOV, P. V., DE JESUS GREGERSEN, K. J. & PEDERSEN, L.-F. 2022. Estimation of nitrifying and heterotrophic bacterial activity in biofilm formed on RAS biofilter carriers by respirometry. *Aquaculture,* 561**,** 738730.

RAINEY, F. A., WARD-RAINEY, N. L., JANSSEN, P. H., HIPPE, H. & STACKEBRANDT, E. 1996. *Clostridium paradoxum DSM 7308T* contains multiple 16S rRNA genes with heterogeneous intervening sequences. *Microbiology,* 142**,** 2087-2095.

REDFIELD A. C., K. B. H., RICHARDS F. A. 1963. The influence of organisms on the composition of sea water. . *The sea,* Vol. 2**,** 26-77.

REIS-FILHO, J. S. 2009. Next-generation sequencing. *Breast Cancer Research,* 11**,** S12.

REMMERS, I. M., MARTENS, D. E., WIJFFELS, R. H. & LAMERS, P. P. 2017. Dynamics of triacylglycerol and EPA production in *Phaeodactylum tricornutum* under nitrogen starvation at different light intensities. *PloS one,* 12**,** e0175630.

RINGØ, E., STRØM, E. & TABACHEK, J. A. 1995. Intestinal microflora of salmonids: a review. *Aquaculture Research,* 26**,** 773-789.

RUANE, J., SONNINO, A. & AGOSTINI, A. 2010. Bioenergy and the potential contribution of agricultural biotechnologies in developing countries. *Biomass and Bioenergy,* 34**,** 1427-1439.

SANGER, F., NICKLEN, S. & COULSON, A. R. 1977. DNA sequencing with chain-terminating inhibitors. *Proceedings of the National Academy of Sciences,* 74**,** 5463-5467.

SANTOS, A., VAN AERLE, R., BARRIENTOS, L. & MARTINEZ-URTAZA, J. 2020. Computational methods for 16S metabarcoding studies using Nanopore sequencing data. *Computational and Structural Biotechnology Journal,* 18**,** 296-305.

SCHREIER, H. J., MIRZOYAN, N. & SAITO, K. 2010. Microbial diversity of biological filters in recirculating aquaculture systems. *Current Opinion in Biotechnology,* 21**,** 318-325.

SCHUSTER, S. C. 2008. Next-generation sequencing transforms today's biology. *Nature Methods,* 5**,** 16-18.

SHANNON, C. E. 1948. A mathematical theory of communication. *The Bell system technical journal,* 27**,** 379-423.

SILVA, C. A. & LIMA, M. 2018. Soy Moratorium in Mato Grosso: Deforestation undermines the agreement. *Land Use Policy,* 71**,** 540-542.

SINGH, P. K., SAXENA, A., TYAGI, R., SINDHU, R., BINOD, P. & TIWARI, A. 2023. Biomass valorization of agriculture wastewater grown freshwater diatom *Nitzschia sp*. for metabolites, antibacterial activity, and biofertilizer. *Bioresource Technology,* 377**,** 128976.

SPILLING, K., BRYNJÓLFSDÓTTIR, Á., ENSS, D., RISCHER, H. & SVAVARSSON, H. G. 2013. The effect of high pH on structural lipids in diatoms. *Journal of applied phycology,* 25**,** 1435-1439.

SPRAGUE, M., DICK, J. R. & TOCHER, D. R. 2016. Impact of sustainable feeds on omega-3 long-chain fatty acid levels in farmed Atlantic salmon (*Salmo salar*), 2006–2015. *Scientific Reports,* 6**,** 21892.

STATISTISK SENTRALBYRÅ, S. 2020. *Akvakultur*. Statistisk sentalbyrå: Statistics Norway. Available: https://www.ssb.no/fiskeoppdrett.

STEINRÜCKEN, P., PRESTEGARD, S. K., DE VREE, J. H., STORESUND, J. E., PREE, B., MJØS, S. A. & ERGA, S. R. 2018. Comparing EPA production and fatty acid profiles of three *Phaeodactylum tricornutum* strains under western Norwegian climate conditions. *Algal research,* 30**,** 11-22.

STIPS, A., BOLDING, K., MACÍAS, D., BRUGGEMAN, J. & EAYRS, C. 2016. *Scoping report on the potential impact of on-board desulphurisation on the water quality in SOx Emission Control*.

SUHR, K. I., PEDERSEN, P. B. & ARVIN, E. 2013. End-of-pipe denitrification using RAS effluent waste streams: Effect of C/N-ratio and hydraulic retention time. *Aquacultural Engineering,* 53**,** 57-64.

SYRETT, P. 1981. Nitrogen metabolism of microalgae. *Can. Bull. Fish. Aquat. Sci.,* 210**,** 182-210.

SØRENSEN, M., BERGE, G. M., REITAN, K. I. & RUYTER, B. 2016. Microalga *Phaeodactylum tricornutum* in feed for Atlantic salmon (*Salmo salar*) —Effect on nutrient digestibility, growth and utilization of feed. *Aquaculture,* 460**,** 116-123.

TAL, Y., WATTS, J. E. M., SCHREIER, S. B., SOWERS, K. R. & SCHREIER, H. J. 2003. Characterization of the microbial community and nitrogen transformation processes associated with moving bed bioreactors in a closed recirculated mariculture system. *Aquaculture,* 215**,** 187-202.

TARALDSVIK, M. & MYKLESTAD, S. M. 2000. The effect of pH on growth rate, biochemical composition and extracellular carbohydrate production of the marine diatom *Skeletonema costatum. European Journal of Phycology,* 35**,** 189-194.

TEAM, R. C. 2022. *R: A language and environment for statistical computing.* R Foundation for Statistical Computing, Vienna, Austria. Available: https://www.R-project.org/.

TERMOFISHER SCIENTIFIC. 2020. Qubit 1X dsDNA HS Assey Kits. *In:* INC, T. F. S. (ed.) *Invitrogen User Guide.* ThermoFisher Scientific

THORNTON, D. C. 2009. Effect of low pH on carbohydrate production by a marine planktonic diatom (*Chaetoceros muelleri*). *International Journal of Ecology,* 2009.

TURLEY, C., NIGHTINGALE, P., RILEY, N., WIDDICOMBE, S., JOINT, I., GALLIENNE, C., LOWE, D., GOLDSON, L. & BEAUMONT, N. 2004. Literature Review: environmental

impacts of a gradual or catastrophic release of CO2 into the marine environment following carbon dioxide capture. *Report to the UK Department for Environment*.
UNITED NATIONS, 2015. 2050. *Sustainable development goals*.
UNITED NATIONS, 2022a. *Goal 2: Zero hunger. The United Nations, environment programe: United Nations.* https://www.un.org/sustainabledevelopment/hunger/.
UNITED NATIONS, 2022b. *GOAL 12: Sustainable consumption and production.* The United Nations, environment programme: United Nations. https://www.unep.org/explore-topics/sustainable-development-goals/why-do-sustainable-development-goals-matter/goal-12.
UNVER, A. & HIMMELBLAU, D. 1964. Diffusion Coefficients of CO_2, C_2H_4, C_3H_6 and C_4H_8 in Water from 6° to 65° C. *Journal of Chemical & Engineering Data,* 9**,** 428-431.
VAN DIJK, E. L., AUGER, H., JASZCZYSZYN, Y. & THERMES, C. 2014. Ten years of next-generation sequencing technology. *Trends in Genetics,* 30**,** 418-426.
VAN HOOF, L., FABI, G., JOHANSEN, V., STEENBERGEN, J., IRIGOIEN, X., SMITH, S., LISBJERG, D. & KRAUS, G. 2019. Food from the ocean; towards a research agenda for sustainable use of our oceans' natural resources. *Marine Policy,* 105**,** 44-51.
VAN RIJN, J., TAL, Y. & SCHREIER, H. J. 2006. Denitrification in recirculating systems: Theory and applications. *Aquacultural Engineering,* 34**,** 364-376.
VON AHNEN, M., DALSGAARD, J. & PEDERSEN, P. B. 2021. Effect of different C/N ratios and hydraulic retention times on denitrification in saline, recirculating aquaculture system effluents. *Aquacultural Engineering,* 94**,** 102170.
WADE, W. 2002. Unculturable bacteria—the uncharacterized organisms that cause oral infections. *Journal of the Royal Society of Medicine,* 95**,** 81-83.
WAHIDIN, S., IDRIS, A. & SHALEH, S. R. M. 2013. The influence of light intensity and photoperiod on the growth and lipid content of microalgae *Nannochloropsis sp*. *Bioresource Technology,* 129**,** 7-11.
WANG, X.-W., HUANG, L., JI, P.-Y., CHEN, C.-P., LI, X.-S., GAO, Y.-H. & LIANG, J.-R. 2019a. Using a mixture of wastewater and seawater as the growth medium for wastewater treatment and lipid production by the marine diatom *Phaeodactylum tricornutum*. *Bioresource Technology,* 289**,** 121681.
WANG, Y. & QIAN, P.-Y. 2013. Conserved Regions in 16S Ribosome RNA Sequences and Primer Design for Studies of Environmental Microbes. *In:* NELSON, K. E. (ed.) *Encyclopedia of Metagenomics.* New York, NY: Springer New York.
WANG, Y., YING, H., YIN, Y., ZHENG, H. & CUI, Z. 2019b. Estimating soil nitrate leaching of nitrogen fertilizer from global meta-analysis. *Science of The Total Environment,* 657**,** 96-102.
WENTZEL, M. C., EKAMA, G. A. & LOEWENTHAL, R. E. 2003. 9 - Fundamentals of biological behaviour and wastewater strength tests. *In:* MARA, D. & HORAN, N. (eds.) *Handbook of Water and Wastewater Microbiology.* London: Academic Press.
WICKHAM, H. 2016. *ggplot2: Elegant Graphics for Data Analysis*, Springer-Verlag New York.
WIETZ, M., HALL, M. R. & HØJ, L. 2009. Effects of seawater ozonation on biofilm development in aquaculture tanks. *Systematic and Applied Microbiology,* 32**,** 266-277.
WILKIE, A. C. & MULBRY, W. W. 2002. Recovery of dairy manure nutrients by benthic freshwater algae. *Bioresource technology,* 84**,** 81-91.
WINAND, R., BOGAERTS, B., HOFFMAN, S., LEFEVRE, L., DELVOYE, M., VAN BRAEKEL, J., FU, Q., ROOSENS, N. H., DE KEERSMAECKER, S. C. & VANNESTE, K. 2019. Targeting the 16s rRNA gene for bacterial identification in complex mixed samples: Comparative evaluation of second (illumina) and third (oxford nanopore technologies) generation sequencing technologies. *International journal of molecular sciences,* 21**,** 298.
YAN, X., HE, L., ZHANG, W., CHEN, W., WU, J., YANG, N., CAI, X., LI, L., YAN, L. & RAO, P. 2023. Efficient ammonia-nitrogen removal and recovery from wastewater via the continuous flat-sheet gas-permeable membranes reactor pretreatment. *Journal of Water Process Engineering,* 52**,** 103571.

YILMAZ, P., PARFREY, L. W., YARZA, P., GERKEN, J., PRUESSE, E., QUAST, C., SCHWEER, T., PEPLIES, J., LUDWIG, W. & GLÖCKNER, F. O. 2013. The SILVA and "All-species Living Tree Project (LTP)" taxonomic frameworks. *Nucleic Acids Research,* 42**,** D643-D648.

YOGEV, U., SOWERS, K. R., MOZES, N. & GROSS, A. 2017. Nitrogen and carbon balance in a novel near-zero water exchange saline recirculating aquaculture system. *Aquaculture,* 467**,** 118-126.

YOGEV, U., VOGLER, M., NIR, O., LONDONG, J. & GROSS, A. 2020. Phosphorous recovery from a novel recirculating aquaculture system followed by its sustainable reuse as a fertilizer. *Science of The Total Environment,* 722**,** 137949.

YTRESTØYL, T., AAS, T. S. & ÅSGÅRD, T. 2015. Utilisation of feed resources in production of Atlantic salmon (*Salmo salar*) in Norway. *Aquaculture,* 448**,** 365-374.

YUAN, Z., JIANG, S., SHENG, H., LIU, X., HUA, H., LIU, X. & ZHANG, Y. 2018. Human Perturbation of the Global Phosphorus Cycle: Changes and Consequences. *Environmental Science & Technology,* 52**,** 2438-2450.

YUN, J.-H., SMITH, V. H. & PATE, R. C. 2015. Managing nutrients and system operations for biofuel production from freshwater macroalgae. *Algal Research,* 11**,** 13-21.

ZHANG, X., LU, M., IDRUS, M. A. M., CROMBIE, C. & JEGATHEESAN, V. 2019. Performance of precipitation and electrocoagulation as pretreatment of silica removal in brackish water and seawater. *Process Safety and Environmental Protection,* 126**,** 18-24.

ZHUANG, L.-L., YU, D., ZHANG, J., LIU, F.-F., WU, Y.-H., ZHANG, T.-Y., DAO, G.-H. & HU, H.-Y. 2018. The characteristics and influencing factors of the attached microalgae cultivation: A review. *Renewable and Sustainable Energy Reviews,* 94**,** 1110-1119.

AALTO, S. L., LETELIER-GORDO, C. O., PEDERSEN, L.-F. & PEDERSEN, P. B. 2022. Effect of biocarrier material on nitrification performance during start-up in freshwater RAS. *Aquacultural Engineering,* 99**,** 102292.

AAS, T. S., YTRESTØYL, T. & ÅSGÅRD, T. 2019. Utilization of feed resources in the production of Atlantic salmon (*Salmo salar*) in Norway: An update for 2016. *Aquaculture Reports,* 15**,** 100216.

Appendix A – Prokaryote microorganisms that dominate in RAS

Table A. 1: The different microbial processes taking place in marine RAS biofilters, the respective reaction-equation, and microbes responsible. The table is modified from (Schreier et al., 2010, Blancheton et al., 2013, Tal et al., 2003, Wietz et al., 2009).

Process	Reaction equation	Microorganisms responsible
Nitrification		*-Nitrosomonas sp.* *-Nitrosomonas cryotolerans*
Ammonium oxidation (AO)	$NH_4^+ + 1.5O_2$ $\rightarrow NO_2^- + 2H^+ + H_2O$	*-Nitrosomonas europaea* *-Nitrosomonas cinnybus/nitrosa* *-Nitrosococcus mobilis*
Nitrite oxidation (NO)	$NO_2^- + H_2O$ $\rightarrow NO_3^- + 2H^+ + 2e^-$	*-Nitrospira marina* *-Nitrospira moscoviensis*
Heterotrophic respiration	CH2O + O2 -> CO2 + H2O	*- Alphaproteobacteria* *- Gammaproteobacteria*
Denitrification		*-Thiomicrosporia denitrificans*
Autotrophic (sulfide-dependent)	$S^{2-} + 1.6NO_3^- + 1.6H^+$ $\rightarrow SO_4^{2-} + 0.8N_2(g) + 0.8H_2O$	*-Thiothrix disciformisa* *-Rhodobacter litoralisa* *-Hydrogenophaga sp.* *-Pseudomonas fluorescens*
Heterotrophic	$5CH_3COO^- + 8NO_3^- + 3H^+$ $\rightarrow 10HCO_3^- + 4N_2(g) + 4H_2O$	*-Pseudomonas stutzeri* *-Pseudomonas sp.* *-Paracoccus denitrificans*
Dissimilatory nitrate reduction to ammonia (DNRA)	$NO_3^- + 2H^+ + 4H_2 \rightarrow NH_4^+ + 3H_2O$	*-Proteobacteria sp.* *-Firmicutes sp.*
Anaerobic ammonium oxidation (Anammox)	NH4+ + NO2− → N2(g) + 2H2O	*-Planctomycetes spp.* *-Brocadia sp*
Sulfate reduction	$O_4^{2-} + CH_3COO^- + 3H^+$ $\rightarrow HS^- + 2HCO_3^- + 3H^+$	*-Desulfovibrio sp.* *-Dethiosulfovibrio sp.* *-Fusibacter sp.* *-Bacteroides sp.*
Sulfide oxidation	$HS^- + 2O_2 \rightarrow SO_4^{2-} + H^+$	*-Thiomicrospira sp.*
Methanogenesis	$4H_2 + H^+ + HCO_3^-$ $\rightarrow CH_4(g) + 3H_2O$	*-Methanogenic Archaea*

Appendix B – Production data from the RAS facility Hardingsmolt AS, at the days the batches of RAS water was collected

Table B. 1: Parameters of the batch of RAS water coming from Hardingsmolt AS, used in the experiment testing light intensity.

Water parameter	Value
Fish density (kg m^{-3})	52,43
Amount (Nr. of fish)	268 694
Average weight (kg)	0,331
Amount of feed fed (kg)	780,52
Temperature (°C)	10,8
Salinity (ppt)	12,8
Carbon dioxide saturation (mg L^{-1})	10
Total ammonia nitrogen (mg L^{-1})	0,33
Nitrite concentration (mg L^{-1})	0,6
Nitrate concentration mg L^{-1})	56,0
Alkalinity (mg L^{-1})	270
pH before rearing tanks	7,9
pH after rearing tanks	7,6
Makeup water (m^3 h^{-1})	15

In the experiment testing addition of silica, the fish was not feed due to transportation of the fish. Because of this, the staff at the RAS facility Hardingsmolt AS did not measure water parameters during this period. As a result of this, there were no available data from the batch of RAS water used in the experiment testing addition of silica.

Table B. 2: Parameters of the batch of RAS water coming from Hardingsmolt AS, used in the experiment testing addition of nutrients.

Water parameter	Value
Fish density (kg m^{-3})	35,2
Amount (Nr. of fish)	89454
Average weight (kg)	0,667
Amount of feed fed (kg)	1020,00
Temperature (°C)	11,6
Salinity (ppt)	11,2
Carbon dioxide saturation (mg L^{-1})	12
Total ammonia nitrogen (mg L^{-1})	0,6
Nitrite concentration (mg L^{-1})	0,06
Nitrate concentration (mg L^{-1})	56
Alkalinity (mg L^{-1})	105
pH before rearing tanks	7,3
pH after rearing tanks	6,9
Makeup water (m^3 h^{-1})	20

Table B. 3: Parameters of the batch of RAS water coming from Hardingsmolt AS, used in the experiment testing harvest rate.

Water parameter	**Value**
Fish density (kg m^{-3})	34,17
Amount (Nr. of fish)	286 357
Average weight (kg)	0,202
Amount of feed fed (kg)	1260
Temperature (°C)	11,8
Salinity (ppt)	12,9
Carbon dioxide saturation (mg L^{-1})	13
Total ammonia nitrogen (mg L^{-1})	0,57
Nitrite concentration (mg L^{-1})	0,15
Nitrate concentration (mg L^{-1})	15,6
Alkalinity (mg L^{-1})	139
pH before rearing tanks	7,5
pH after rearing tanks	6,9
Makeup water (m^3 h^{-1})	25

Appendix C – The experimental setup of the two parts comprising the experiment testing addition of nutrients (Part 1: Testing nutrient load and Part 2: testing addition of micronutrients)

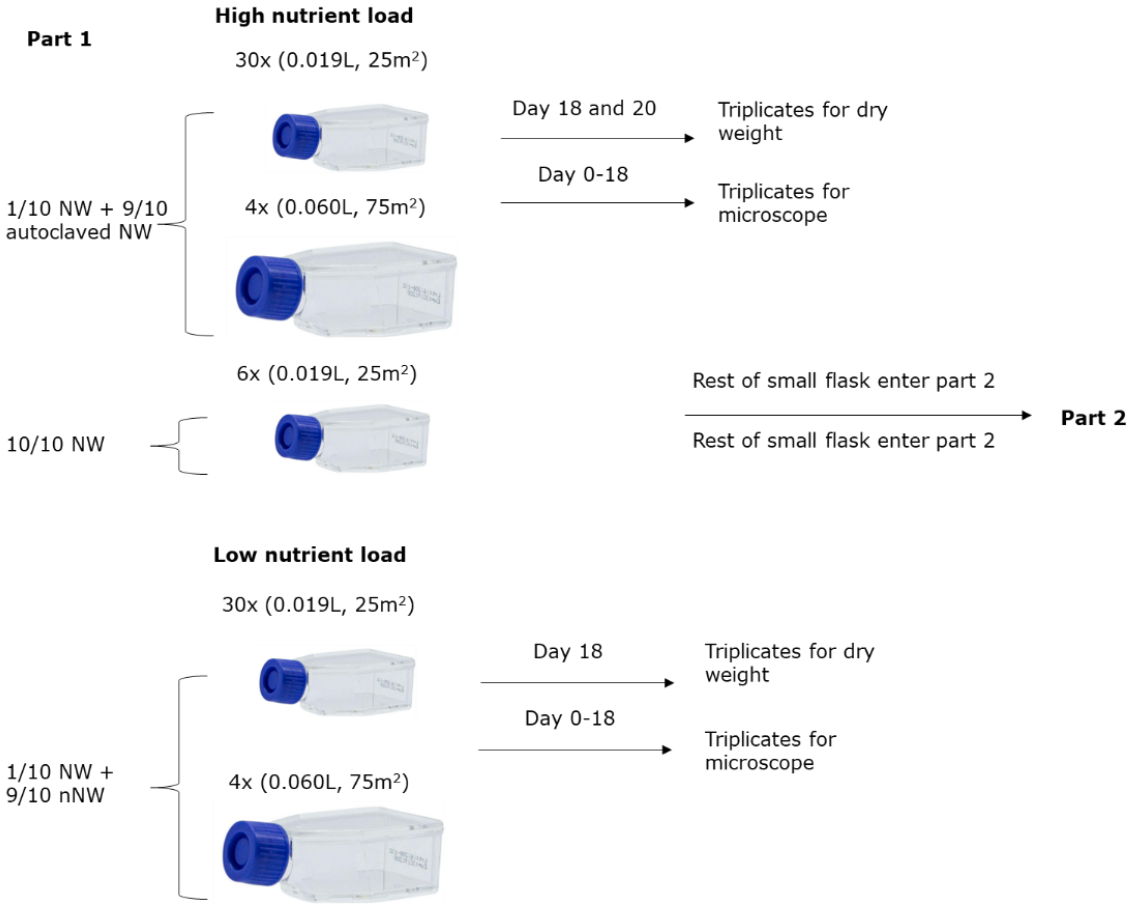

Figure C. 1: The experimental setup of the first part (testing nutrient load) of the experiment testing addition of nutrients. The illustration shows the treatment: High nutrient load, and the control: Low nutrient load, as well as the respective amount- and size of cell cultivation flasks. The illustration shows what day the different flasks were harvested for the different analysis, and what flasks were included in the subsequent Part 2 of the experiment. The abbreviations NW and nNW are short for nutritious water and non-nutritious water, respectively.

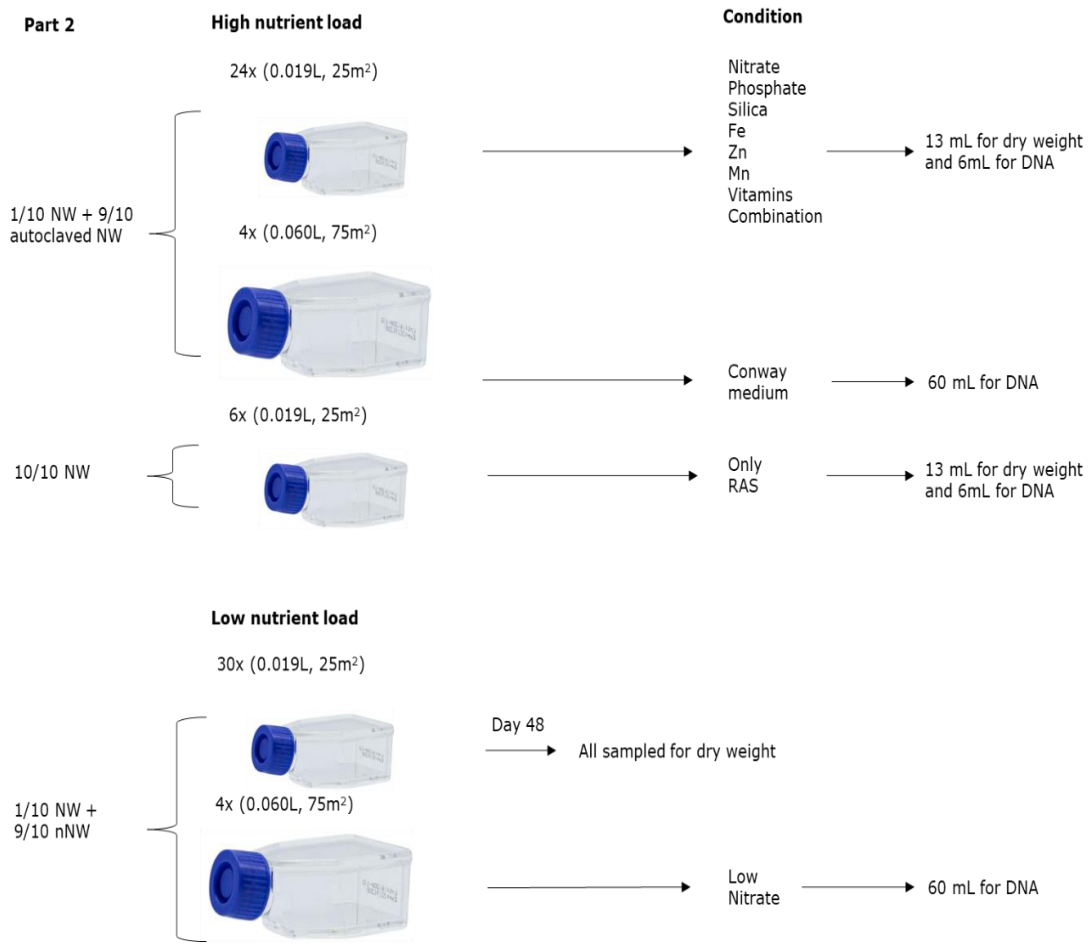

Figure C. 2: The experimental setup of the second part (testing addition of micronutrients) of the experiment testing addition of nutrients. The illustration shows flasks used to create the different conditions (Nitrate, Phosphate, Silica, Iron (Fe), Sink (Zn), Manganese (Mn), Combination, Vitamins, Conway medium, and only RAS water) and the control (Low nutrient load). In addition, the respective amount- and size of cell cultivation flasks are illustrated. The illustration also shows when the different flasks were harvested for the different analysis. The abbreviations NW and nNW are short for nutritious water and non-nutritious water, respectively.

Table C. 1: The different treatments tested in the second part of the experiment testing addition of nutrients. The table shows what elements were added in the different treatments, and the respective concentration, size of the cell cultivation flasks, and number of replicas.

Treatment	Elements added	Concentration (g L^{-1})	Type of flask	Number of replicas
Nitrate	$NaNO_3$	100.18	0.019 L, 0.0025 m^2	3
Phosphate	NaH_2PO_4	17.41	0.019 L, 0.0025 m^2	3
Only RAS	RAS	10/10 RAS water	0.019 L, 0.0025 m^2	6
Low nutrient load	Diluted RAS	1/10 of RAS water	0.019 L, 0.0025 m^2	30
			0.060 L, 0.0075 m^2	4
Silica	(*Table 3*)	(*Table 3*)	0.019 L, 0.0025 m^2	3
		)		
Iron	$FeCl_3 - 6H_2O$	1.3	0.019 L, 0.0025 m^2	3
Zink	$ZnSO_4 - 7H_2O$	1.06	0.019 L, 0.0025 m^2	3
Manganese	$MnCl_2 - 4H_2O$	0.36	0.019 L, 0.0025 m^2	3
Vitamins			0.019 L, 0.0025 m^2	3
Vit. B12	Cyanocobalamin	0.005		
Vit. B1	Thiamin HCl (vit. B1)	0.106		
Conway medium	(*Table 3*)	(*Table 3*)	0.060 L, 0.0075 m^2	4
Combined elements			0.019 L, 0.0025 m^2	3
Copper	$CuSO_4 - 5H_2O$	0.48		
Cobalt	$CoCl_2 - 6H_2O$	0.48		
Iron	$FeCl_3 - 6H_2O$	1.3		
Zink	$ZnSO_4 - 7H_2O$	1.06		

Appendix D – Photos from the experiments, and of the experimental setups for the different experiments

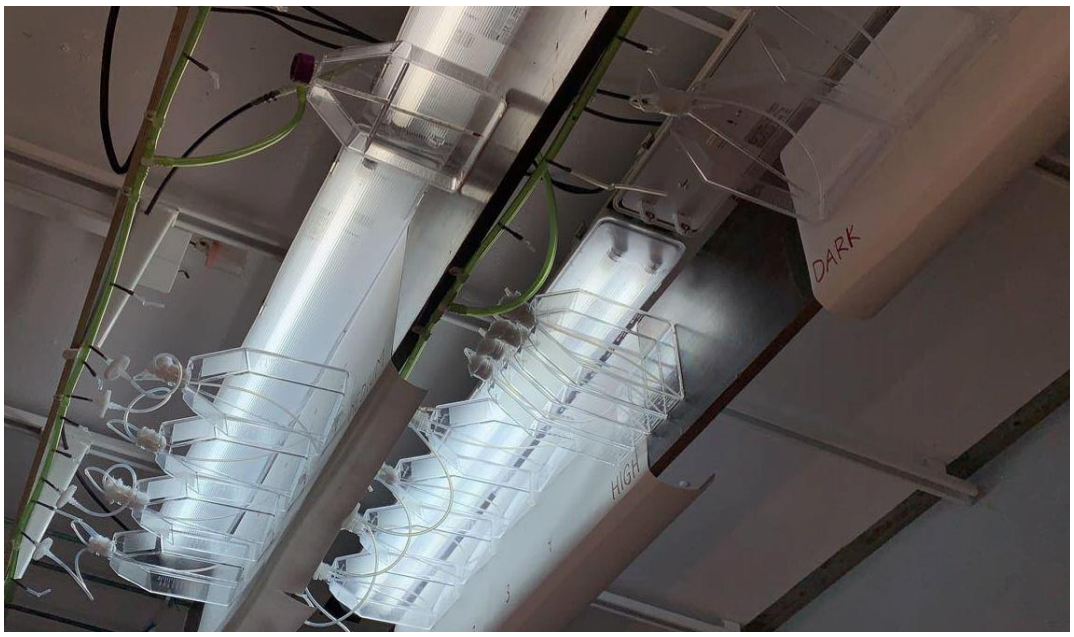

Figure D. 1: A photo of the experimental setup for the experiment testing light intensities. The photo shows the different conditions tested (High: 240 µE m^{-2} s^{-1} (down left), Medium: 160 µE m^{-2} s^{-1} (up left), and no: <20 µE m^{-2} s^{-1}, light). The picture was taken before cultivation water was added to the flasks. The flasks of the condition with no light were covered with aluminum foil after water was introduced (not shown). The four flasks in the middle of the picture (between the conditions High- and No light) were not used during the experiment. The flask at the top right contained water and a thermometer and was used to track the temperature of the cultivation medium inside the flask.

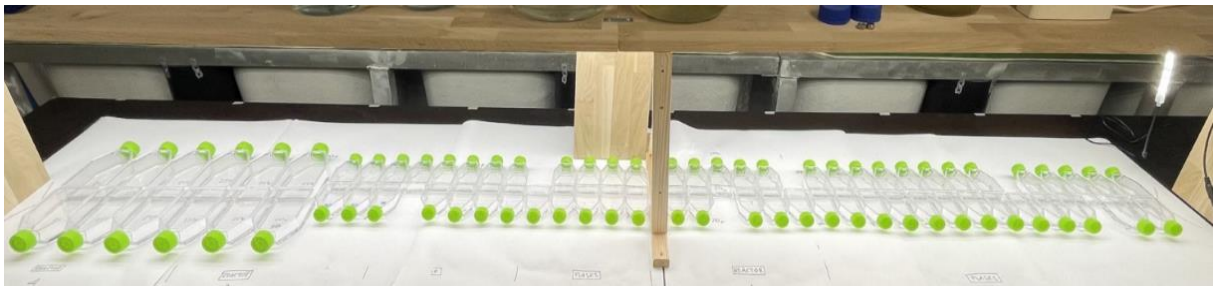

Figure D. 2: A photo showing the experimental setup of the experiment testing addition of Silica. The photo shows the cell cultivation flasks, laying horizontally on a white cower board below the light source. The three empty spots illustrate how the cell cultivation flasks were picked for investigation in the inverse microscope.

Figure D. 3: A photo showing the experimental setup of the experiment testing addition of nutrients. The photo shows the cell cultivation flasks, laying horizontally on a white cower board below the light source. The picture also illustrate how cell cultivation flasks were transported to the inverse microscope for investigation.

Figure D. 4: A photo showing the experimental setup of the experiment testing harvest rate. At the top, reactor 1-6, with respective water supply beneath the light bench. The peristaltic pumps are placed above the light bench. At the bottom, reactor 7-12, with the same setup as for reactor 1-6. The water cans (50L) were covered in black plastic bags (seen beneath the reactors) to ensure no photoautotrophic growth in the cans.

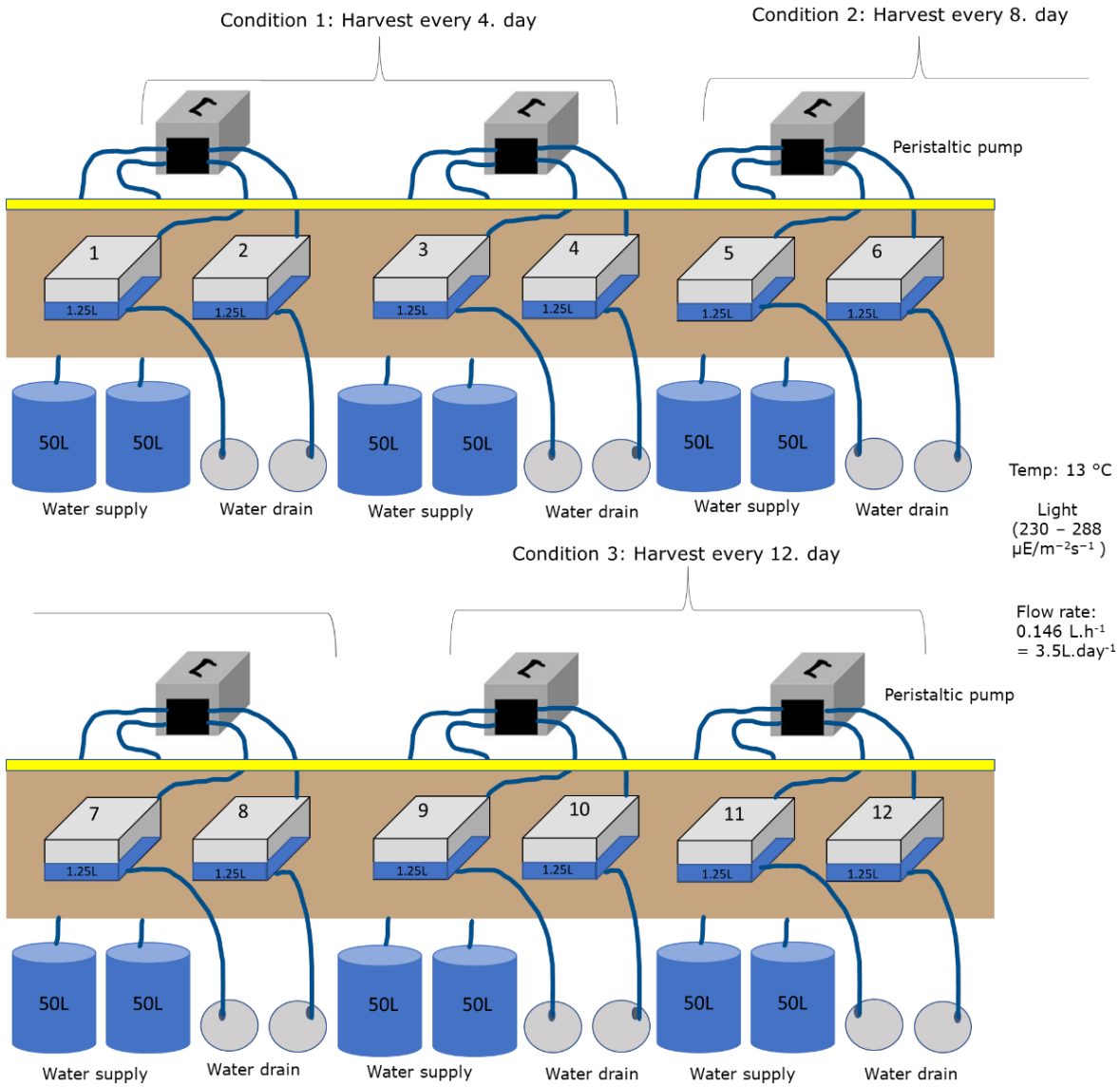

Figure D. 5: The experimental setup of the experiment testing harvest rate, showing the three growth conditions: Harvest every 4th day, harvest every 8th day, and harvest every 12th day. The water supply is illustrated as blue cylinders containing 50L of RAS water. The reactors (1-12) are illustrated as gray boxes containing RAS water (blue). From each the blue cylinders (new RAS water), a blue straw is drawn, connecting the water supply to the respective reactor through a peristaltic pump (grey and black cube). The reactors are placed on a growth bench (brown), with the light source above (yellow).

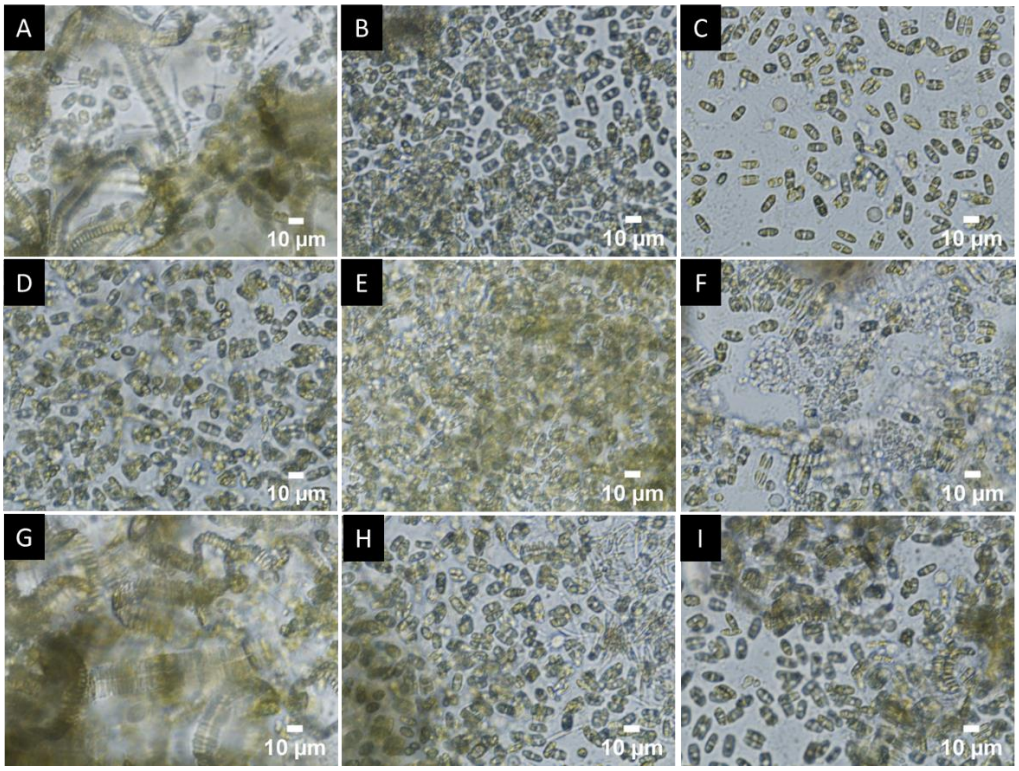

Figure D. 6: Microscope pictures (A-I) taken in an inverse microscope at 200x magnification, for the experiment testing addition of nutrients. The microscope pictures were taken at the end (T46) of the experimental period. The photos are from the conditions: High_Mn (A and B), High_Silica (C and D), High_Zn (E and F), High_NO3 (G and H), and High_Comb (I).

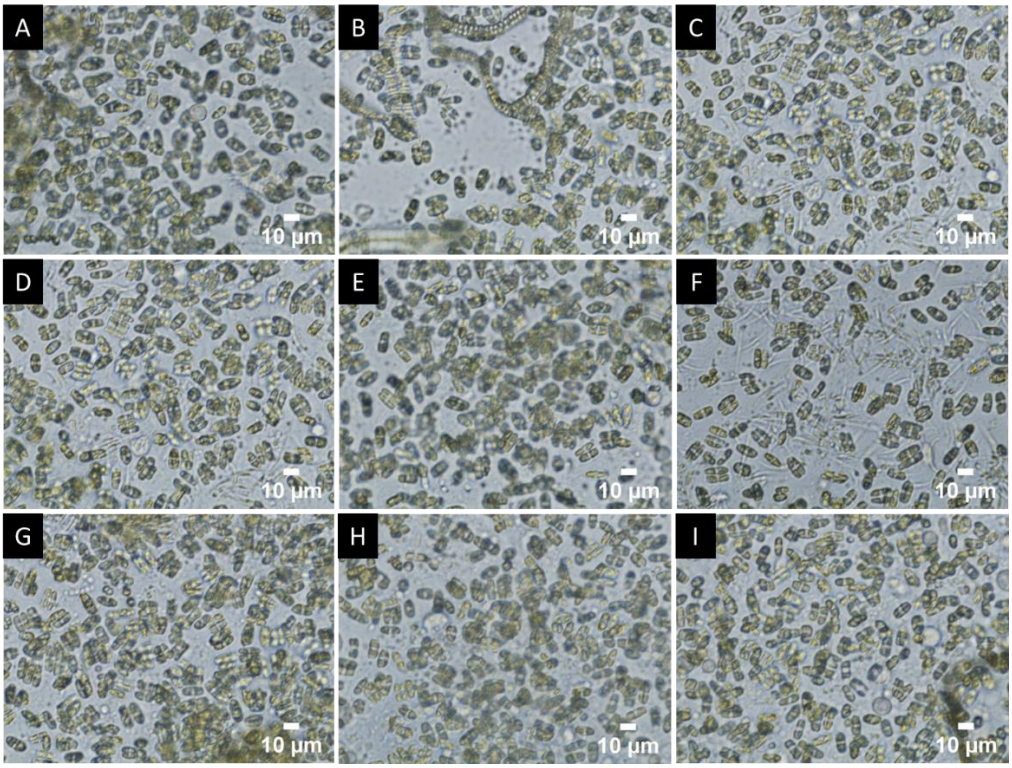

Figure D. 7: Microscope pictures (A-I) taken in an inverse microscope at 200x magnification, from the experiment testing addition of nutrients. The microscope pictures were taken at the end (T46) of the experimental period. The photos are from the conditions: High_COMB (A), High_VIT (B and C), High_Fe (D and E), High_PO4 (F and G), and High_conw (H and I).

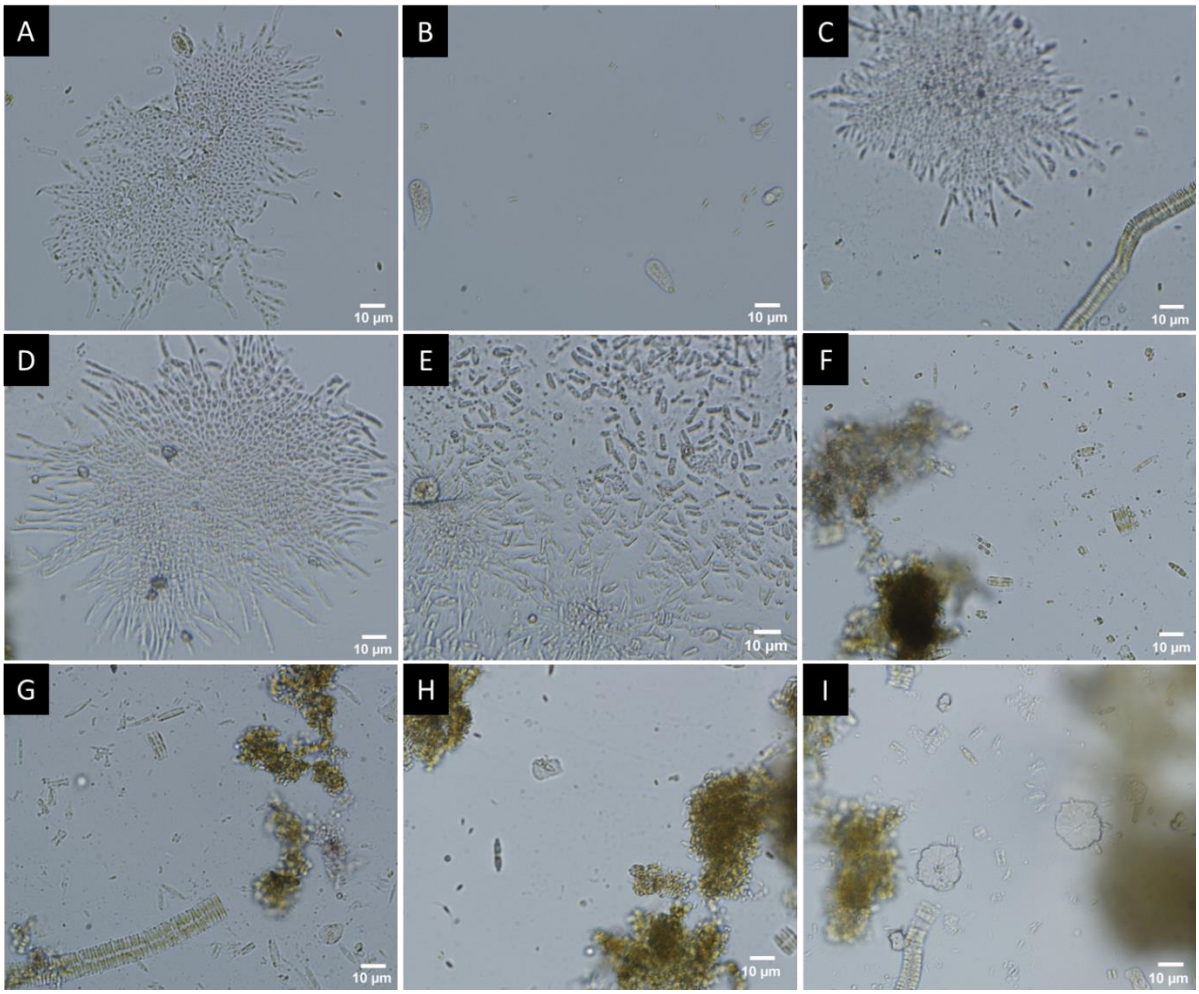

Figure D. 8: Microscope pictures (A-I) of the community coming from the three conditions: Harvest every 4. day (A-B), harvest every 8. day (C-E) and harvest every 12. day (F-I), taken in an inverse microscope. The pictures were taken at the end of the experimental period (T24), with 400x magnification. The microscope pictures showed the diatom microalgae species encountered before (C and G), as well as some fungi (A, C, and D). In addition, a lot of gray structures were observed (E).

Appendix E – Macros used for photo analysis in ImageJ

Macro E. 1: The Macro uses to analyze the pictures taken on inverse microscope with 10x on the ocular (100x magnification). The macro was obtained by Hubert Bonefond (Bonnefond, 2022).

```
//https://imagej.nih.gov/ij/docs/menus/analyze.html

//https://imagej.nih.gov/ij/docs/menus/process.html#find


PictureDirectory = "C:\\Users\\johan\\Desktop\\Masteroppgave\\Eksp
1.1\\Eksp 1.1 - Cultivation flask
(starvation)\\20220325_ImageJ\\Silica\\"; //lieu d'enregistrement des
images.

liste = getFileList(PictureDirectory);

setBatchMode(false); //travailler sans affichage = true

for (i=0; i<(liste.length); i++){

      if (endsWith(liste[i], ".jpg")){

            NamePicture= liste[i];

            NamePictureAdress = PictureDirectory + liste[i] ; //ouverture
des images

            open (NamePictureAdress); //ouverture des images

            setOption("BlackBackground", false);

            run("8-bit");

            run("Sharpen");

            run("Find Edges");

            run("Convert to Mask");

            setAutoThreshold("Default");

            run("Close-");

            run("Analyze Particles...", "size=5-Infinity show=Masks clear
include summarize"); //valeur initiale size = 3000}}
```

Macro E. 2: The Macro uses to analyze the pictures taken on inverse microscope with 20x on the ocular (200x magnification). The macro was obtained by Hubert Bonefond (Bonnefond, 2022).

```
//https://imagej.nih.gov/ij/docs/menus/analyze.html
//https://imagej.nih.gov/ij/docs/menus/process.html#find

PictureDirectory = "C:\\Users\\johan\\Desktop\\Masteroppgave\\Eksp 1.2 -
Cultivation flask\\Analyze\\"; //lieu d'enregistrement des images.
liste = getFileList(PictureDirectory);
setBatchMode(false); //travailler sans affichage = true
for (i=0; i<(liste.length); i++){
      if (endsWith(liste[i], ".jpg")){
            NamePicture= liste[i];
            NamePictureAdress = PictureDirectory + liste[i] ; //ouverture
des images
            open (NamePictureAdress); //ouverture des images
            setOption("BlackBackground", false);
            run("8-bit");
            run("Sharpen");
            run("Find Edges");
            run("Convert to Mask");
            setAutoThreshold("Default");
            run("Close-");
            run("Analyze Particles...", "size=5-Infinity show=Masks clear
include summarize"); //valeur initiale size = 3000}}
```

Appendix F – The raw data generated on microbial growth and water analysis from the four different experiments, with average and standard errors included.

The raw data used for the different experiments: Testing addition of silica (sheet 1), testing addition of nutrients (sheet 2), testing harvest rate (sheet 3), the pilot reactors at Hardingsmolt AS (sheet 4), and the water analysis (sheet 5) are presented in the google document provided in the link below:

https://docs.google.com/spreadsheets/d/159QgPCPXFro54x9JK2_N9EOYy8Ld2jvLnhtPvI59-lQ/edit?usp=sharing

For each experiment, the raw data contains the raw data to the left, followed by two tables calculating the average and the standard error for each experimental day. To the right, the final table that is used in RStudio to generate the plots are shown.

Appendix G – The data obtained by tapestation electrophoresis, with respective calculations

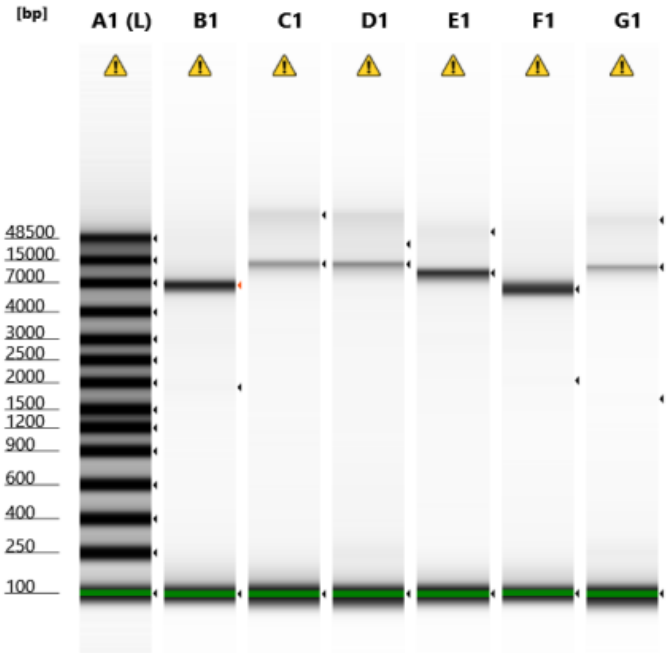

Figure 31: The figure shows the electrophoresis of the ladder (A1), and the samples tested (B1-G2). The figure shows that all samples have a clear bond between 6000-13000bp.

B1: W004

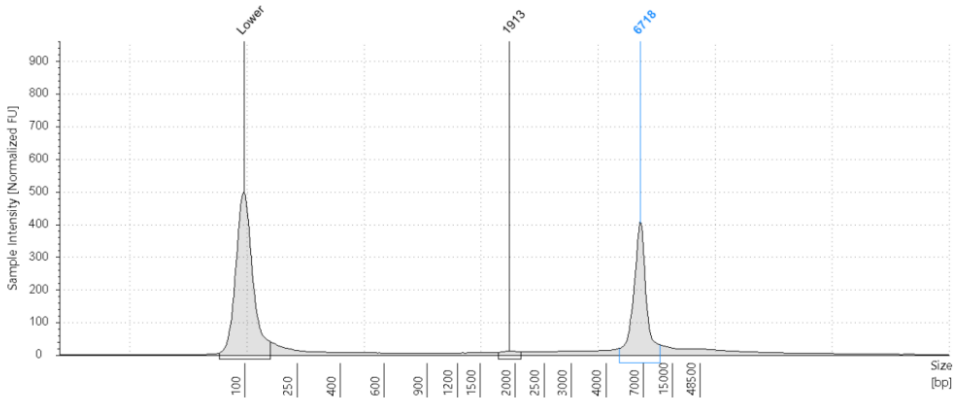

Sample Table

Well	DIN	Conc. [ng/µl]	Sample Description	Alert	Observations
B1	6.5	9.66	W004	⚠	Caution! Expired ScreenTape device; Sample concentration outside recommended range

Peak Table

Size [bp]	Calibrated Conc. [ng/µl]	Assigned Conc. [ng/µl]	% Integrated Area	From [bp]	To [bp]	Peak Comment	Observations
100	8.50	8.50	-	64	158		Lower Marker
1913	0.196	-	3.56	1751	2099		
6718	5.01	-	90.94	4891	10847		
-	-	-	-	-	-		Sample Well

Figure G. 1: The electrophoresis of the sample (W004) located in well B1. At the top, the peaks of the electrophoresis are shown. In this figure, three peaks are indicated. The first is around 100bp (Lower) and is probably primer dimers and small DNA contaminations. The second is at 1913bp, and probably is a contamination or a fragment of the 18S rDNA operon. The last peak is located at 6718bp

and is the amplified region of the eukaryote 18S rDNA operon. Below is the sample table, showing the respective well of the sample, the DNA Integrity Number (DIN), the total DNA concentration of the sample, and the sample description. At the bottom, the specific peak table for the sample is presented. For this table, the different peaks (Size[bp]) and the respective calibrated concentrations (Calibrated Conc. [ng μL^{-1}]) are the values of interest.

C1: W022

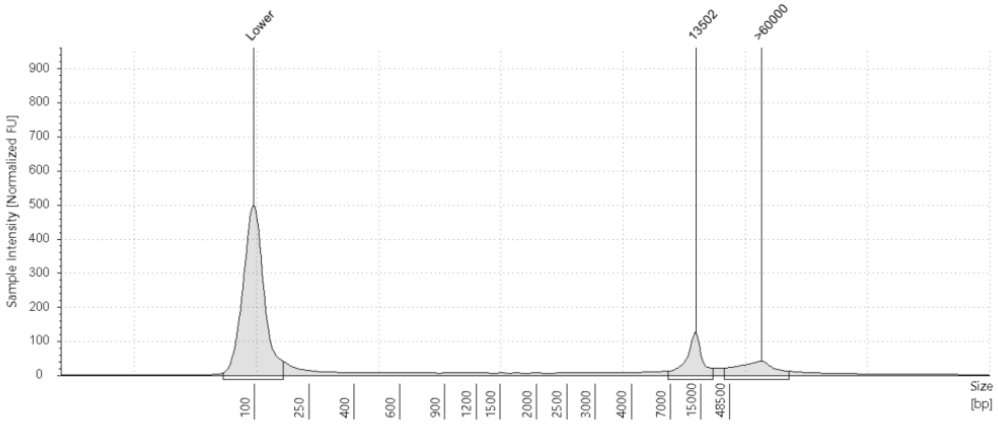

Sample Table

Well	DIN	Conc. [ng/µl]	Sample Description	Alert	Observations
C1	7.1	5.44	W022	⚠	Caution! Expired ScreenTape device; Sample concentration outside recommended range

Peak Table

Size [bp]	Calibrated Conc. [ng/µl]	Assigned Conc. [ng/µl]	% Integrated Area	From [bp]	To [bp]	Peak Comment	Observations
100	8.50	8.50	-	60	165		Lower Marker
13502	1.50	-	48.89	6844	20938		
>60000	1.20	-	39.32	29641	>60000		
-	-	-	-	-	-		Sample Well

Figure G. 2: The electrophoresis of the sample (W022) located in well C1. At the top, the peaks of the electrophoresis are shown. In this figure, three peaks are indicated. The first is around 100bp (Lower) and is probably primer dimers and small DNA contaminations. The second is at 113502bp and is the amplified region of the eukaryote 18S rDNA operon. The third peak is >60 000bp and is probably an aggregation of more DNA molecules. Below is the sample table, showing the respective well of the sample, the DNA Integrity Number (DIN), the total DNA concentration of the sample, and the sample description. At the bottom, the specific peak table for the sample is presented. For this table, the different peaks (Size[bp]) and the respective calibrated concentrations (Calibrated Conc. [ng μL^{-1}]) are the values of interest.

D1: W024

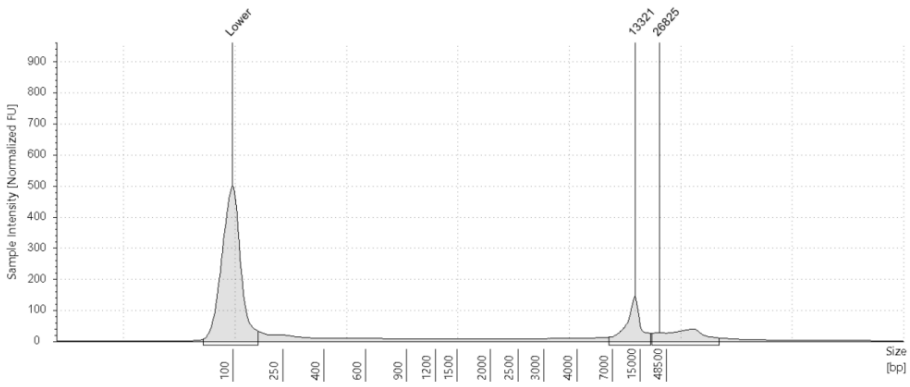

Sample Table

Well	DIN	Conc. [ng/µl]	Sample Description	Alert	Observations
D1	6.7	6.14	W024	⚠	Caution! Expired ScreenTape device; Sample concentration outside recommended range

Peak Table

Size [bp]	Calibrated Conc. [ng/µl]	Assigned Conc. [ng/µl]	% Integrated Area	From [bp]	To [bp]	Peak Comment	Observations
100	8.50	8.50	-	58	160		Lower Marker
13321	1.70	-	50.53	6659	20239		
26825	1.39	-	41.56	21326	>60000		
-	-	-	-	-	-		Sample Well

Figure G. 3: The electrophoresis of the sample (W024) located in well D1. At the top, the peaks of the electrophoresis are shown. In this figure, three peaks are indicated. The first is around 100bp (Lower) and is probably primer dimers and small DNA contaminations. The second is at 13 321bp and is the amplified region of the eukaryote 18S rDNA operon. The third peak is 26 825bp and is probably an aggregation of more DNA molecules. Below is the sample table, showing the respective well of the sample, the DNA Integrity Number (DIN), the total DNA concentration of the sample, and the sample description. At the bottom, the specific peak table for the sample is presented. For this table, the different peaks (Size[bp]) and the respective calibrated concentrations (Calibrated Conc. [ng μL^{-1}]) are the values of interest.

E1: W030

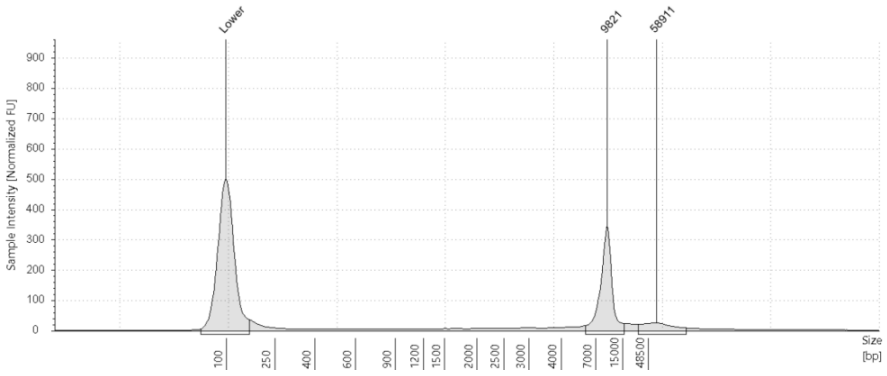

Sample Table

Well	DIN	Conc. [ng/µl]	Sample Description	Alert	Observations
E1	7.2	7.67	W030	⚠	Caution! Expired ScreenTape device; Sample concentration outside recommended range

Peak Table

Size [bp]	Calibrated Conc. [ng/µl]	Assigned Conc. [ng/µl]	% Integrated Area	From [bp]	To [bp]	Peak Comment	Observations
100	8.50	8.50	-	62	156		Lower Marker
9821	3.87	-	78.89	5980	15605		
58911	0.786	-	16.01	23586	>60000		
-	-	-	-	-	-		Sample Well

Figure G. 4: The electrophoresis of the sample (W030) located in well D1. At the top, the peaks of the electrophoresis are shown. In this figure, three peaks are indicated. The first is around 100bp

(Lower) and is probably primer dimers and small DNA contaminations. The second is at 9821bp and is the amplified region of the eukaryote 18S rDNA operon. The third peak is 58911bp and is probably an aggregation of more DNA molecules. Below is the sample table, showing the respective well of the sample, the DNA Integrity Number (DIN), the total DNA concentration of the sample, and the sample description. At the bottom, the specific peak table for the sample is presented. For this table, the different peaks (Size[bp]) and the respective calibrated concentrations (Calibrated Conc. [ng μL^{-1}]) are the values of interest.

F1: G002

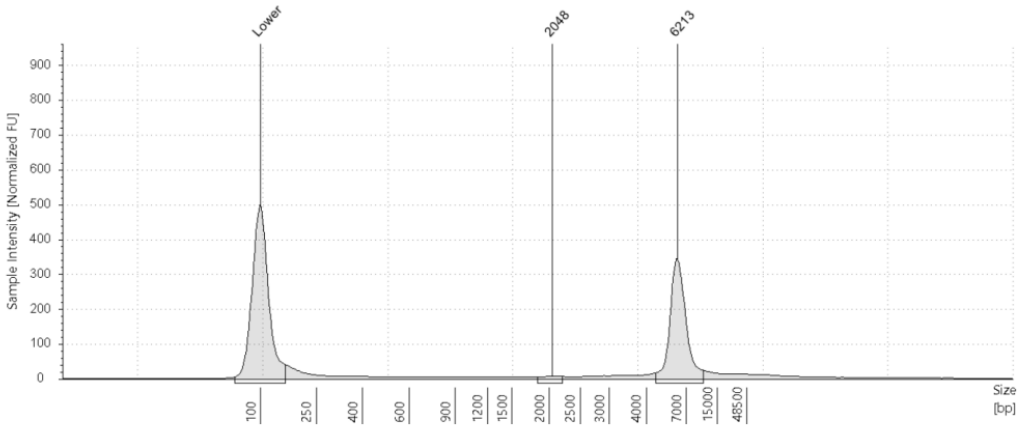

Sample Table

Well	DIN	Conc. [ng/µl]	Sample Description	Alert	Observations
F1	6.5	9.75	G002	⚠	Caution! Expired ScreenTape device; Sample concentration outside recommended range

Peak Table

Size [bp]	Calibrated Conc. [ng/µl]	Assigned Conc. [ng/µl]	%Integrated Area	From [bp]	To [bp]	Peak Comment	Observations
100	8.50	8.50	-	65	151		Lower Marker
2048	0.144	-	2.45	1833	2207		
6213	5.60	-	95.05	4591	10724		
-	-	-	-	-	-		Sample Well

Figure G. 5: The electrophoresis of the sample (G002) located in well F1. At the top, the peaks of the electrophoresis are shown. In this figure, three peaks are indicated. The first is around 100bp (Lower) and is probably primer dimers and small DNA contaminations. The second is at 2048bp, and probably is a contamination or a fragment of the 18S rDNA operon. The last peak is located at 6213bp and is the amplified region of the eukaryote 18S rDNA operon. Below is the sample table, showing the respective well of the sample, the DNA Integrity Number (DIN), the total DNA concentration of the sample, and the sample description. At the bottom, the specific peak table for the sample is presented. For this table, the different peaks (Size[bp]) and the respective calibrated concentrations (Calibrated Conc. [ng μL^{-1}]) are the values of interest.

G1: G008

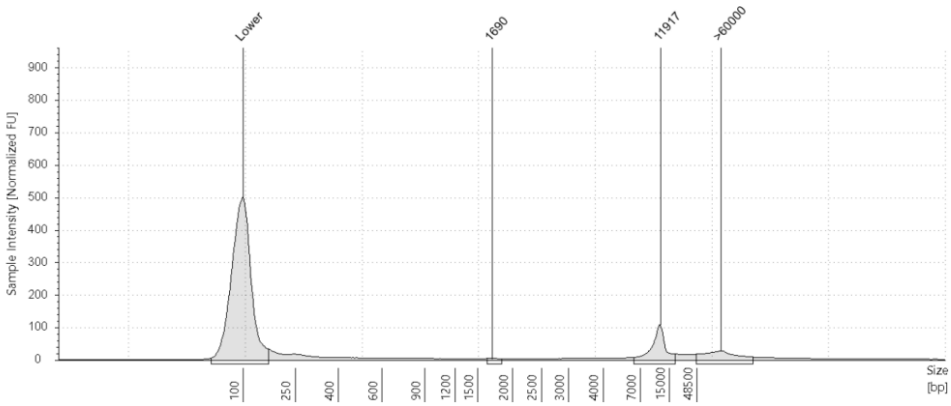

Sample Table

Well	DIN	Conc. [ng/µl]	Sample Description	Alert	Observations
G1	7.2	4.45	G008	⚠	Caution! Expired ScreenTape device; Sample concentration outside functional range for DIN and the assay

Peak Table

Size [bp]	Calibrated Conc. [ng/µl]	Assigned Conc. [ng/µl]	% Integrated Area	From [bp]	To [bp]	Peak Comment	Observations
100	8.50	8.50	-	57	157		Lower Marker
1690	0.0450	-	2.06	1622	1834		
11917	1.17	-	53.79	6359	17602		
>60000	0.774	-	35.52	40405	>60000		
-	-	-	-	-	-		Sample Well

Figure G. 6: The electrophoresis of the sample (A008) located in well G1. At the top, the peaks of the electrophoresis are shown. In this figure, four peaks are indicated. The first is around 100bp (Lower) and is probably primer dimers and small DNA contaminations. The second is at 1690bp, and probably is a contamination or a fragment of the 18S rDNA operon. The third peak is located at 11 917bp and is the amplified region of the eukaryote 18S rDNA operon. The fourth peak is at >60 000 and is probably an aggregate of more DNA molecules. Below is the sample table, showing the respective well of the sample, the DNA Integrity Number (DIN), the total DNA concentration of the sample, and the sample description. At the bottom, the specific peak table for the sample is presented. For this table, the different peaks (Size[bp]) and the respective calibrated concentrations (Calibrated Conc. [ng μL^{-1}]) are the values of interest.

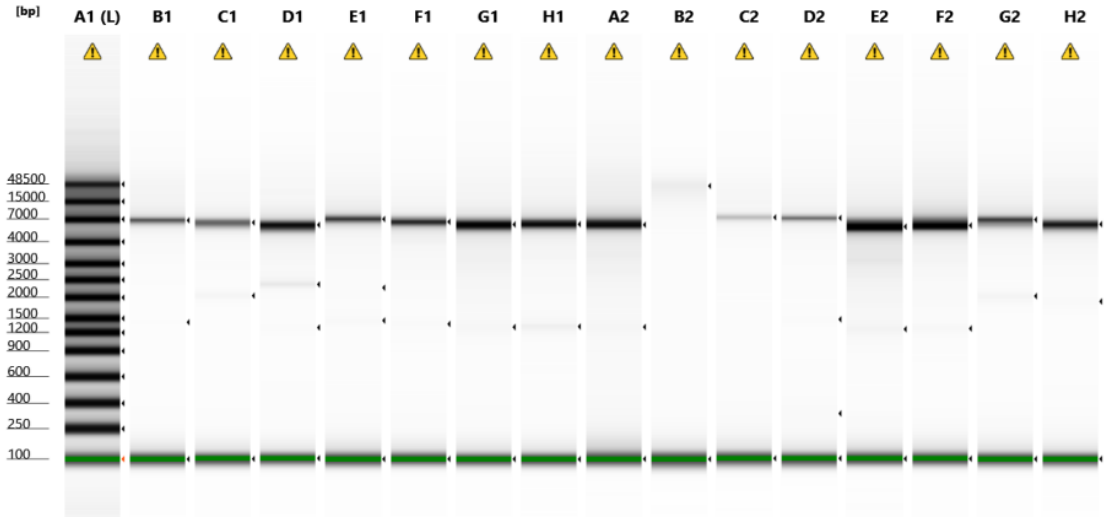

Figure G. 7: The electrophoresis of the ladder (A1), and the samples tested (B1-H2. The figure shows that all samples, except B2, have a clear bond around ~7000bp.

B1: G011

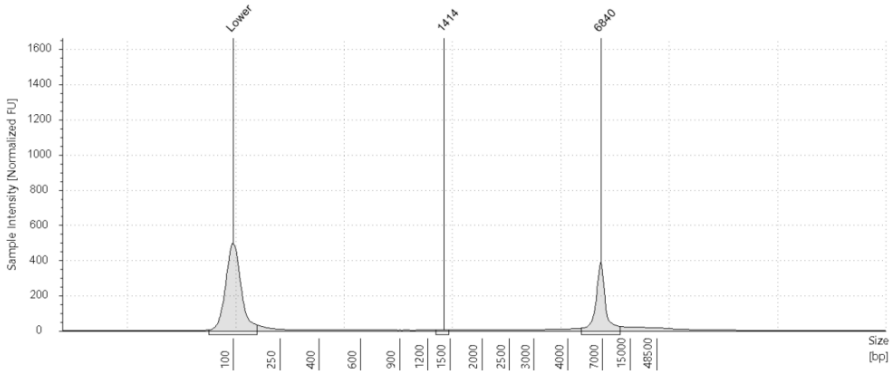

Sample Table

Well	DIN	Conc. [ng/µl]	Sample Description	Alert	Observations
B1	6.8	7.23	G011	⚠	Caution! Expired ScreenTape device; Sample concentration outside recommended range

Peak Table

Size [bp]	Calibrated Conc. [ng/µl]	Assigned Conc. [ng/µl]	% Integrated Area	From [bp]	To [bp]	Peak Comment	Observations
100	8.50	8.50	-	62	161		Lower Marker
1414	0.0563	-	1.35	1299	1483		
6840	4.02	-	96.53	4995	11567		
-	-	-	-	-	-		Sample Well

Figure G. 8: The electrophoresis of the sample (G011) located in well B1. At the top, the peaks of the electrophoresis are shown. In this figure, three peaks are indicated. The first is around 100bp (Lower) and is probably primer dimers and small DNA contaminations. The second is at 1414bp, and probably is a contamination or a fragment of the 18S rDNA operon. The last peak is located at 6840bp and is the amplified region of the eukaryote 18S rDNA operon. Below is the sample table, showing the respective well of the sample, the DNA Integrity Number (DIN), the total DNA concentration of the sample, and the sample description. At the bottom, the specific peak table for the sample is presented. For this table, the different peaks (Size[bp]) and the respective calibrated concentrations (Calibrated Conc. [ng μL^{-1}]) are the values of interest.

C1: G013

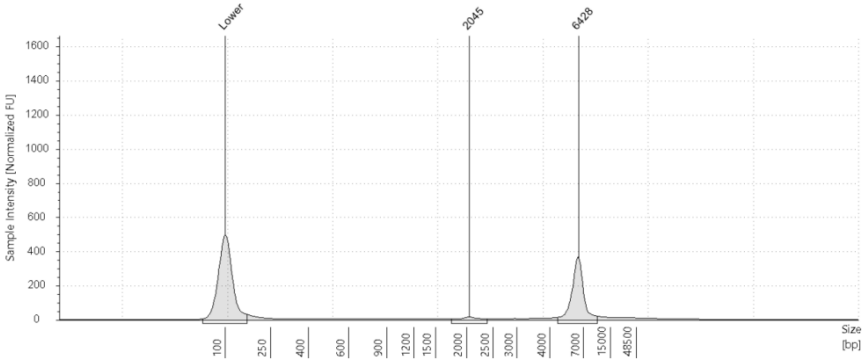

Sample Table

Well	DIN	Conc. [ng/µl]	Sample Description	Alert	Observations
C1	6.6	8.31	G013	⚠	Caution! Expired ScreenTape device; Sample concentration outside recommended range

Peak Table

Size [bp]	Calibrated Conc. [ng/µl]	Assigned Conc. [ng/µl]	% Integrated Area	From [bp]	To [bp]	Peak Comment	Observations
100	8.50	8.50	-	63	155		Lower Marker
2045	0.335	-	6.22	1734	2379		
6428	5.03	-	93.27	4552	10403		
-	-	-	-	-	-		Sample Well

Figure G. 9: The electrophoresis of the sample (G013) located in well C1. At the top, the peaks of the electrophoresis are shown. In this figure, three peaks are indicated. The first is around 100bp

(Lower) and is probably primer dimers and small DNA contaminations. The second is at 2045bp, and probably is a contamination or a fragment of the 18S rDNA operon. The last peak is located at 6428bp and is the amplified region of the eukaryote 18S rDNA operon. Below is the sample table, showing the respective well of the sample, the DNA Integrity Number (DIN), the total DNA concentration of the sample, and the sample description. At the bottom, the specific peak table for the sample is presented. For this table, the different peaks (Size[bp]) and the respective calibrated concentrations (Calibrated Conc. [ng μL^{-1}]) are the values of interest.

D1: G023

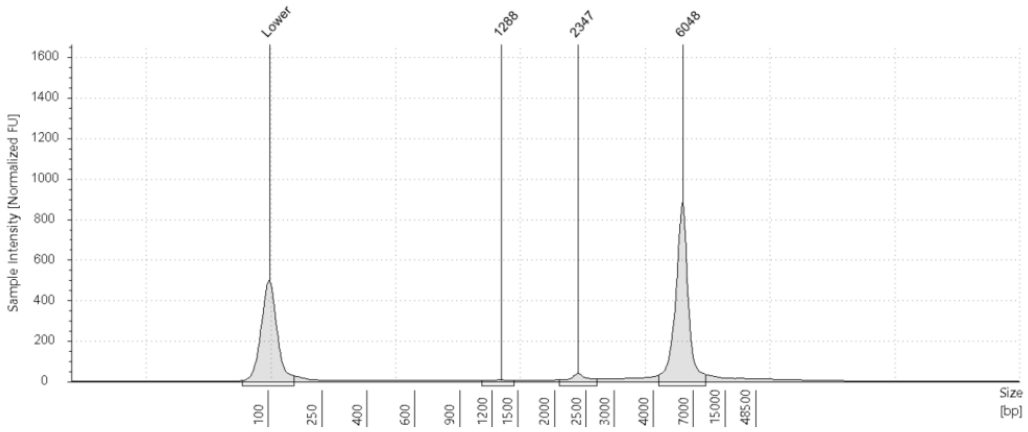

Sample Table

Well	DIN	Conc. [ng/µl]	Sample Description	Alert	Observations
D1	6.5	16.4	G023	⚠	Caution! Expired ScreenTape device

Peak Table

Size [bp]	Calibrated Conc. [ng/µl]	Assigned Conc. [ng/µl]	% Integrated Area	From [bp]	To [bp]	Peak Comment	Observations
100	8.50	8.50	-	63	153		Lower Marker
1288	0.170	-	1.34	1085	1445		
2347	0.648	-	5.09	2061	2674		
6048	11.9	-	93.23	4272	9404		
-	-	-	-	-	-		Sample Well

Figure G. 10: the electrophoresis of the sample (G023) located in well D1. At the top, the peaks of the electrophoresis are shown. In this figure, four peaks are indicated. The first is around 100bp (Lower) and is probably primer dimers and small DNA contaminations. The second and third is at 1288bp and 2347bp and are probably contaminations or fragments of the 18S rDNA operon. The last peak is located at 6048bp and is the amplified region of the eukaryote 18S rDNA operon. Below is the sample table, showing the respective well of the sample, the DNA Integrity Number (DIN), the total DNA concentration of the sample, and the sample description. At the bottom, the specific peak table for the sample is presented. For this table, the different peaks (Size[bp]) and the respective calibrated concentrations (Calibrated Conc. [ng μL^{-1}]) are the values of interest.

E1: G024

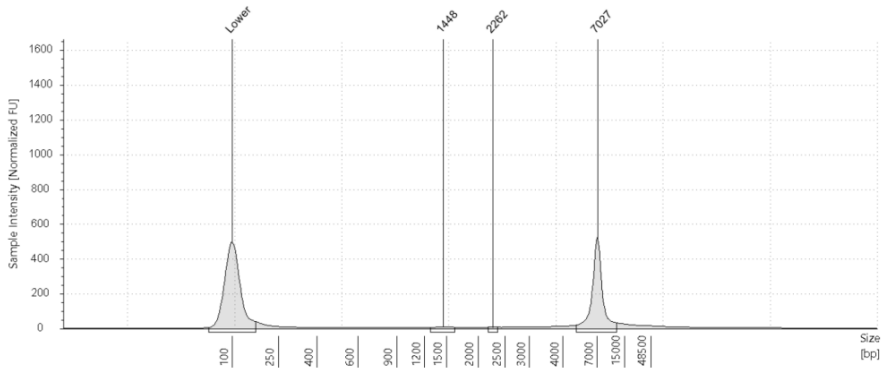

Sample Table

Well	DIN	Conc. [ng/µl]	Sample Description	Alert	Observations
E1	6.6	9.56	G024	⚠	Caution! Expired ScreenTape device; Sample concentration outside recommended range

Peak Table

Size [bp]	Calibrated Conc. [ng/µl]	Assigned Conc. [ng/µl]	%Integrated Area	From [bp]	To [bp]	Peak Comment	Observations
100	8.50	8.50	-	63	160		Lower Marker
1448	0.184	-	3.12	1271	1619		
2262	0.0679	-	1.15	2179	2348		
7027	5.55	-	93.96	4991	12015		
-	-	-	-	-	-		Sample Well

Figure G. 11: The electrophoresis of the sample (G024) located in well E1. At the top, the peaks of the electrophoresis are shown. In this figure, four peaks are indicated. The first is around 100bp (Lower) and is probably primer dimers and small DNA contaminations. The second and third is at 1448bp and 2262bp and are probably contaminations or fragments of the 18S rDNA operon. The last peak is located at 7027bp and is the amplified region of the eukaryote 18S rDNA operon. Below is the sample table, showing the respective well of the sample, the DNA Integrity Number (DIN), the total DNA concentration of the sample, and the sample description. At the bottom, the specific peak table for the sample is presented. For this table, the different peaks (Size[bp]) and the respective calibrated concentrations (Calibrated Conc. [ng μL^{-1}]) are the values of interest.

F1: G038

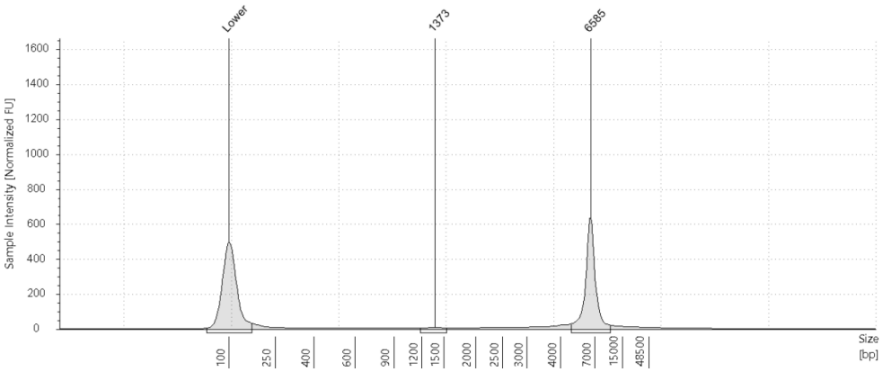

Sample Table

Well	DIN	Conc. [ng/µl]	Sample Description	Alert	Observations
F1	6.5	11.1	G038	⚠	Caution! Expired ScreenTape device

Peak Table

Size [bp]	Calibrated Conc. [ng/µl]	Assigned Conc. [ng/µl]	%Integrated Area	From [bp]	To [bp]	Peak Comment	Observations
100	8.50	8.50	-	64	157		Lower Marker
1373	0.194	-	2.56	1183	1544		
6585	7.32	-	96.83	4759	10753		
-	-	-	-	-	-		Sample Well

Figure G. 12: The electrophoresis of the sample (G038) located in well F1. At the top, the peaks of the electrophoresis are shown. In this figure, three peaks are indicated. The first is around 100bp (Lower) and is probably primer dimers and small DNA contaminations. The second is at 1373bp, and

probably is a contamination or a fragment of the 18S rDNA operon. The last peak is located at 6079bp and is the amplified region of the eukaryote 18S rDNA operon. Below is the sample table, showing the respective well of the sample, the DNA Integrity Number (DIN), the total DNA concentration of the sample, and the sample description. At the bottom, the specific peak table for the sample is presented. For this table, the different peaks (Size[bp]) and the respective calibrated concentrations (Calibrated Conc. [ng μL^{-1}]) are the values of interest.

G1: G044

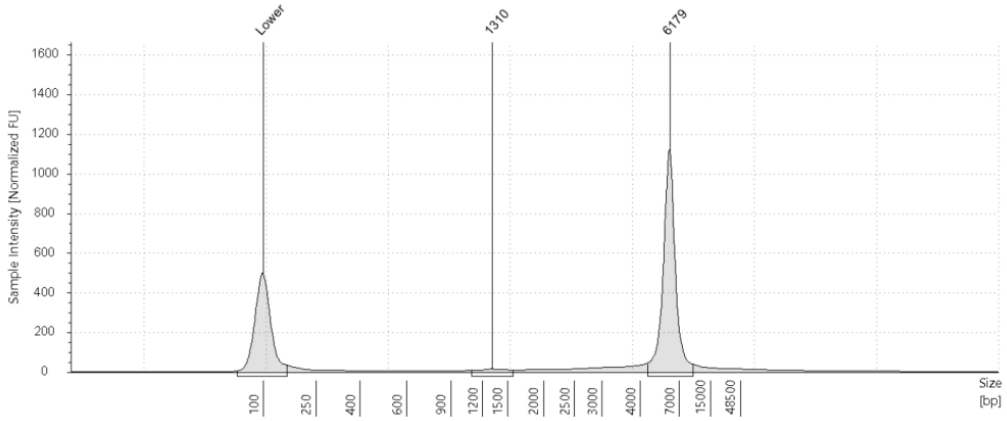

Sample Table

Well	DIN	Conc. [ng/µl]	Sample Description	Alert	Observations
G1	6.4	20.7	G044	⚠	Caution! Expired ScreenTape device

Peak Table

Size [bp]	Calibrated Conc. [ng/µl]	Assigned Conc. [ng/µl]	% Integrated Area	From [bp]	To [bp]	Peak Comment	Observations
100	8.50	8.50	-	64	152		Lower Marker
1310	0.424	-	2.81	1086	1570		
6179	14.6	-	96.61	4460	9906		
-	-	-	-	-	-		Sample Well

Figure G. 13: The electrophoresis of the sample (G044) located in well G1. At the top, the peaks of the electrophoresis are shown. In this figure, three peaks are indicated. The first is around 100bp (Lower) and is probably primer dimers and small DNA contaminations. The second is at 1310bp, and probably is a contamination or a fragment of the 18S rDNA operon. The last peak is located at 6179bp and is the amplified region of the eukaryote 18S rDNA operon. Below is the sample table, showing the respective well of the sample, the DNA Integrity Number (DIN), the total DNA concentration of the sample, and the sample description. At the bottom, the specific peak table for the sample is presented. For this table, the different peaks (Size[bp]) and the respective calibrated concentrations (Calibrated Conc. [ng μL^{-1}]) are the values of interest.

H1: A006

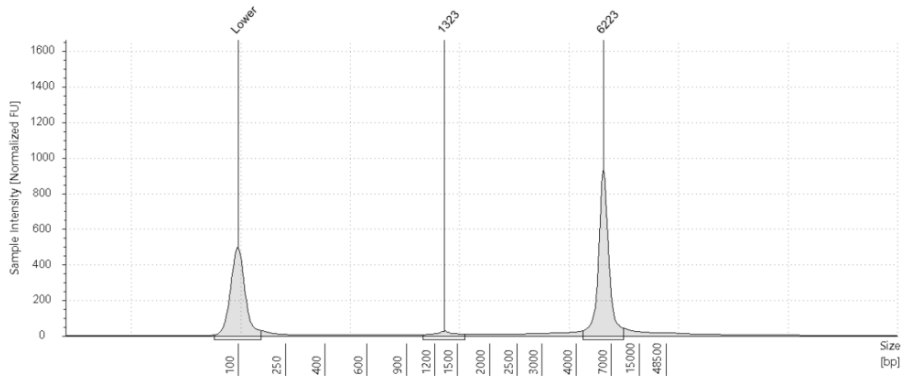

Sample Table

Well	DIN	Conc. [ng/µl]	Sample Description	Alert	Observations
H1	6.5	16.6	A006	⚠	Caution! Expired ScreenTape device

Peak Table

Size [bp]	Calibrated Conc. [ng/µl]	Assigned Conc. [ng/µl]	%Integrated Area	From [bp]	To [bp]	Peak Comment	Observations
100	8.50	8.50	-	63	155		Lower Marker
1323	0.568	-	4.71	1064	1615		
6223	11.4	-	94.45	4471	9850		
-	-	-	-	-	-		Sample Well

Figure G. 14: The electrophoresis of the sample (A006) located in well H1. At the top, the peaks of the electrophoresis are shown. In this figure, three peaks are indicated. The first is around 100bp (Lower) and is probably primer dimers and small DNA contaminations. The second is at 1323bp, and probably is a contamination or a fragment of the 18S rDNA operon. The last peak is located at 6223bp and is the amplified region of the eukaryote 18S rDNA operon. Below is the sample table, showing the respective well of the sample, the DNA Integrity Number (DIN), the total DNA concentration of the sample, and the sample description. At the bottom, the specific peak table for the sample is presented. For this table, the different peaks (Size[bp]) and the respective calibrated concentrations (Calibrated Conc. [ng μL^{-1}]) are the values of interest.

A2: A018

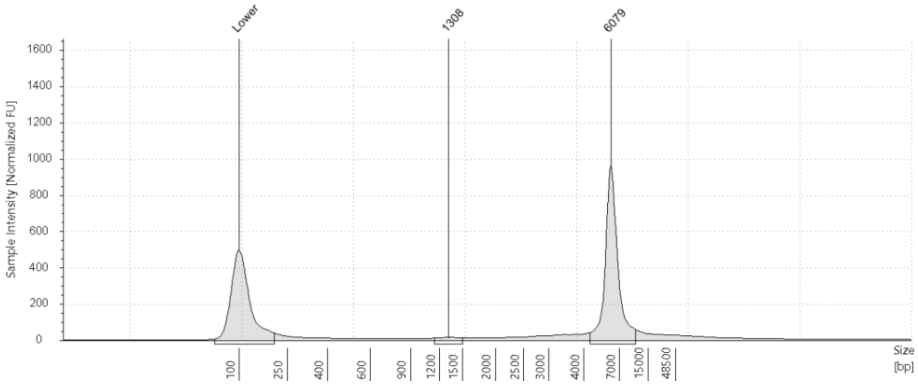

Sample Table

Well	DIN	Conc. [ng/µl]	Sample Description	Alert	Observations
A2	6.4	17.9	A018	⚠	Caution! Expired ScreenTape device

Peak Table

Size [bp]	Calibrated Conc. [ng/µl]	Assigned Conc. [ng/µl]	%Integrated Area	From [bp]	To [bp]	Peak Comment	Observations
100	8.50	8.50	-	63	195		Lower Marker
1308	0.315	-	2.77	1137	1503		
6079	10.9	-	95.92	4395	10631		
-	-	-	-	-	-		Sample Well

Figure G. 15: The electrophoresis of the sample (A018) located in well A2. At the top, the peaks of the electrophoresis are shown. In this figure, three peaks are indicated. The first is around 100bp (Lower) and is probably primer dimers and small DNA contaminations. The second is at 1308bp, and

probably is a contamination or a fragment of the 18S rDNA operon. The last peak is located at 6079bp and is the amplified region of the eukaryote 18S rDNA operon. Below is the sample table, showing the respective well of the sample, the DNA Integrity Number (DIN), the total DNA concentration of the sample, and the sample description. At the bottom, the specific peak table for the sample is presented. For this table, the different peaks (Size[bp]) and the respective calibrated concentrations (Calibrated Conc. [ng μL^{-1}]) are the values of interest.

B2: A026

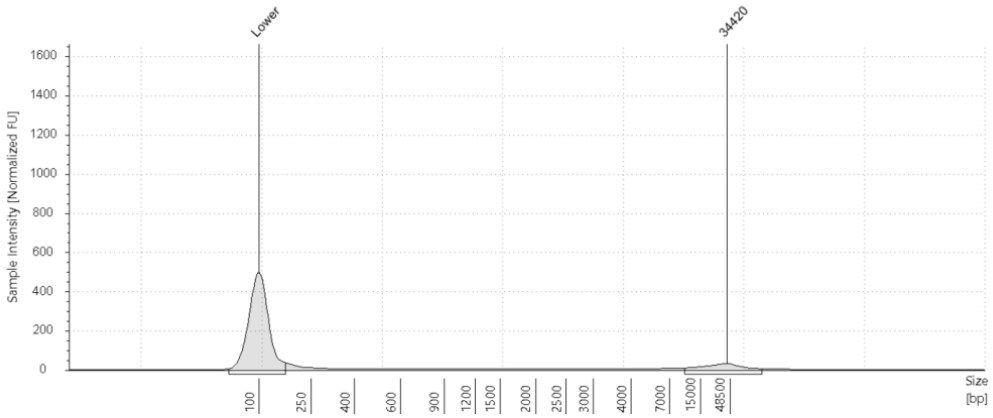

Sample Table

Well	DIN	Conc. [ng/µl]	Sample Description	Alert	Observations
B2	6.8	3.27	A026	⚠	Caution! Expired ScreenTape device; Sample concentration outside functional range for DIN and the assay

Peak Table

Size [bp]	Calibrated Conc. [ng/µl]	Assigned Conc. [ng/µl]	% Integrated Area	From [bp]	To [bp]	Peak Comment	Observations
100	8.50	8.50	-	59	161		Lower Marker
34420	1.05	-	89.79	10166	>60000		
-	-	-	-	-	-		Sample Well

Figure G. 16: The electrophoresis of the sample (A026) located in well B2. At the top, the peaks of the electrophoresis are shown. In this figure, two peaks are indicated. The first is around 100bp (Lower) and is probably primer dimers and small DNA contaminations. The second is at 34420bp and might be the amplified region of the eukaryote 18S rDNA operon, where DNA molecules have attached to other, thereby creating this long reads. Below is the sample table, showing the respective well of the sample, the DNA Integrity Number (DIN), the total DNA concentration of the sample, and the sample description. At the bottom, the specific peak table for the sample is presented. For this table, the different peaks (Size[bp]) and the respective calibrated concentrations (Calibrated Conc. [ng μL^{-1}]) are the values of interest.

C2: A035

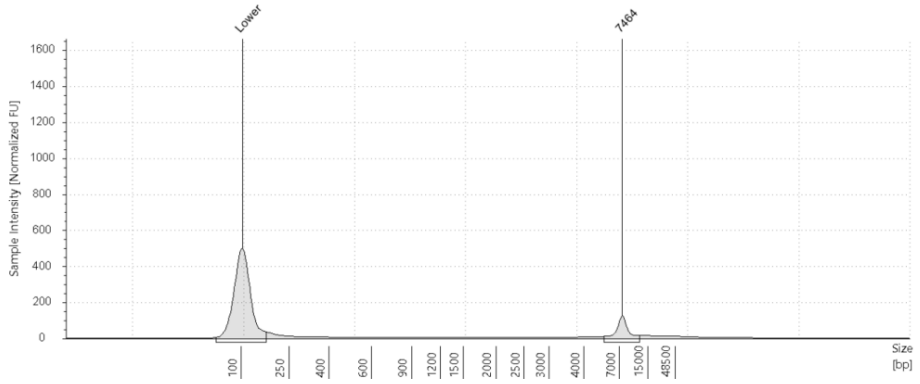

Sample Table

Well	DIN	Conc. [ng/µl]	Sample Description	Alert	Observations
C2	6.4	4.65	A035	⚠	Caution! Expired ScreenTape device; Sample concentration outside functional range for DIN and the assay

Peak Table

Size [bp]	Calibrated Conc. [ng/µl]	Assigned Conc. [ng/µl]	% Integrated Area	From [bp]	To [bp]	Peak Comment	Observations
100	8.50	8.50	-	61	158		Lower Marker
7464	1.36	-	96.69	5455	11921		
-	-	-	-	-	-		Sample Well

Figure G. 17: The electrophoresis of the sample (A035) located in well C2. At the top, the peaks of the electrophoresis are shown. In this figure, two peaks are indicated. The first is around 100bp (Lower) and is probably primer dimers and small DNA contaminations. The second is at 7464bp and is the amplified region of the eukaryote 18S rDNA operon. Below is the sample table, showing the respective well of the sample, the DNA Integrity Number (DIN), the total DNA concentration of the sample, and the sample description. At the bottom, the specific peak table for the sample is presented. For this table, the different peaks (Size[bp]) and the respective calibrated concentrations (Calibrated Conc. [ng μL^{-1}]) are the values of interest.

D2: A070

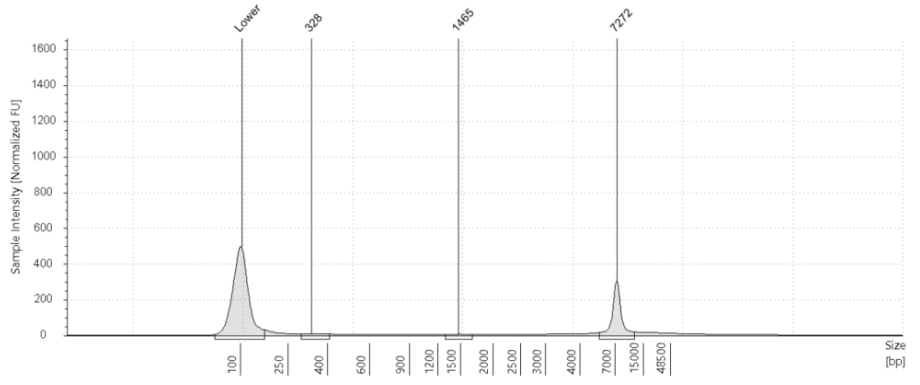

Sample Table

Well	DIN	Conc. [ng/µl]	Sample Description	Alert	Observations
D2	6.5	6.48	A070	⚠	Caution! Expired ScreenTape device; Sample concentration outside recommended range

Peak Table

Size [bp]	Calibrated Conc. [ng/µl]	Assigned Conc. [ng/µl]	% Integrated Area	From [bp]	To [bp]	Peak Comment	Observations
100	8.50	8.50	-	60	156		Lower Marker
328	0.239	-	7.18	290	404		
1465	0.148	-	4.43	1283	1653		
7272	2.90	-	86.95	5374	11615		
-	-	-	-	-	-		Sample Well

Figure G. 18: The electrophoresis of the sample (A070) located in well D2. At the top, the peaks of the electrophoresis are shown. In this figure, four peaks are indicated. The first is around 100bp

(Lower) and is probably primer dimers and small DNA contaminations. The second and third is at 328 and 1465, respectively, and are probably due to contamination or fragments of the 18S rDNA operon. The last peak is located at 7272bp and is the amplified region of the eukaryote 18S rDNA operon. Below is the sample table, showing the respective well of the sample, the DNA Integrity Number (DIN), the total DNA concentration of the sample, and the sample description. At the bottom, the specific peak table for the sample is presented. For this table, the different peaks (Size[bp]) and the respective calibrated concentrations (Calibrated Conc. [ng μL^{-1}]) are the values of interest.

E2: A074

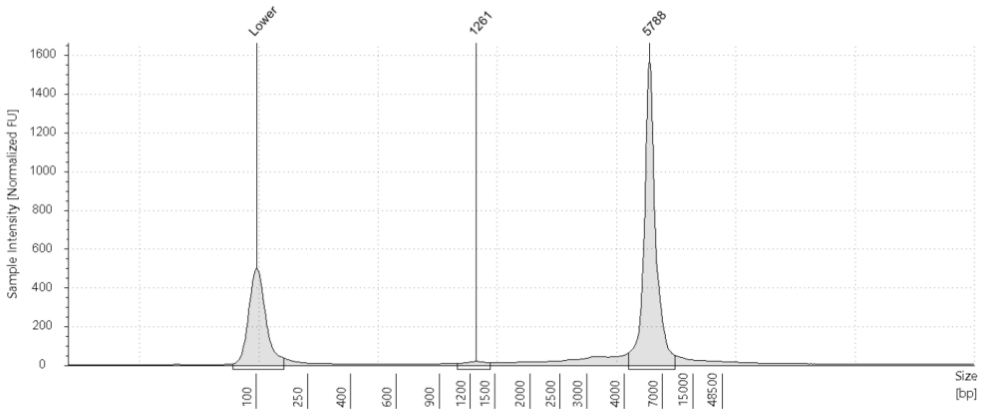

Sample Table

Well	DIN	Conc. [ng/µl]	Sample Description	Alert	Observations
E2	6.4	25.0	A074	⚠	Caution! Expired ScreenTape device

Peak Table

Size [bp]	Calibrated Conc. [ng/µl]	Assigned Conc. [ng/µl]	% Integrated Area	From [bp]	To [bp]	Peak Comment	Observations
100	8.50	8.50	-	65	162		Lower Marker
1261	0.400	-	2.16	1059	1435		
5788	17.8	-	96.39	4258	9471		
-	-	-	-	-	-		Sample Well

Figure G. 19: The electrophoresis of the sample (A074) located in well E2. At the top, the peaks of the electrophoresis are shown. In this figure, three peaks are indicated. The first is around 100bp (Lower) and is probably primer dimers and small DNA contaminations. The second is at 1261bp, and probably is a contamination or a fragment of the 18S rDNA operon. The last peak is located at 5788bp and is the amplified region of the eukaryote 18S rDNA operon. Below is the sample table, showing the respective well of the sample, the DNA Integrity Number (DIN), the total DNA concentration of the sample, and the sample description. At the bottom, the specific peak table for the sample is presented. For this table, the different peaks (Size[bp]) and the respective calibrated concentrations (Calibrated Conc. [ng μL^{-1}]) are the values of interest.

F2: A078

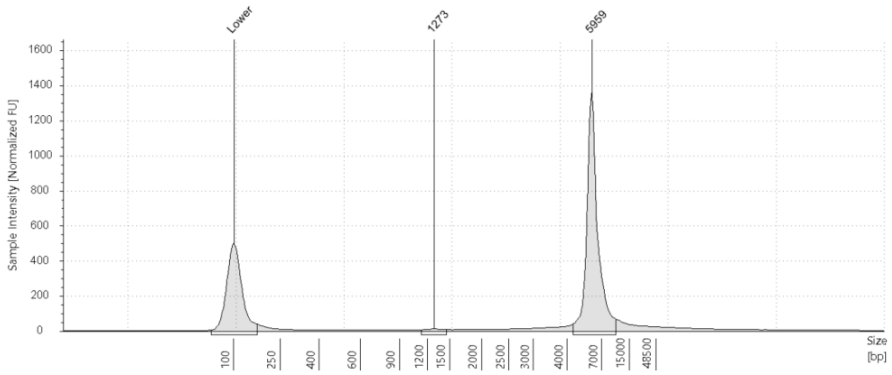

Sample Table

Well	DIN	Conc. [ng/µl]	Sample Description	Alert	Observations
F2	6.6	22.3	A078	⚠	Caution! Expired ScreenTape device

Peak Table

Size [bp]	Calibrated Conc. [ng/µl]	Assigned Conc. [ng/µl]	% Integrated Area	From [bp]	To [bp]	Peak Comment	Observations
100	8.50	8.50	-	64	159		Lower Marker
1273	0.209	-	1.23	1119	1449		
5959	16.5	-	97.08	4384	10215		
-	-	-	-	-	-		Sample Well

Figure G. 20: The electrophoresis of the sample (A078) located in well F2. At the top, the peaks of the electrophoresis are shown. In this figure, three peaks are indicated. The first is around 100bp (Lower) and is probably primer dimers and small DNA contaminations. The second is at 1273bp, and probably is a contamination or a fragment of the 18S rDNA operon. The last peak is located at 5959bp and is the amplified region of the eukaryote 18S rDNA operon. Below is the sample table, showing the respective well of the sample, the DNA Integrity Number (DIN), the total DNA concentration of the sample, and the sample description. At the bottom, the specific peak table for the sample is presented. For this table, the different peaks (Size[bp]) and the respective calibrated concentrations (Calibrated Conc. [ng μL^{-1}]) are the values of interest.

G2: HS01

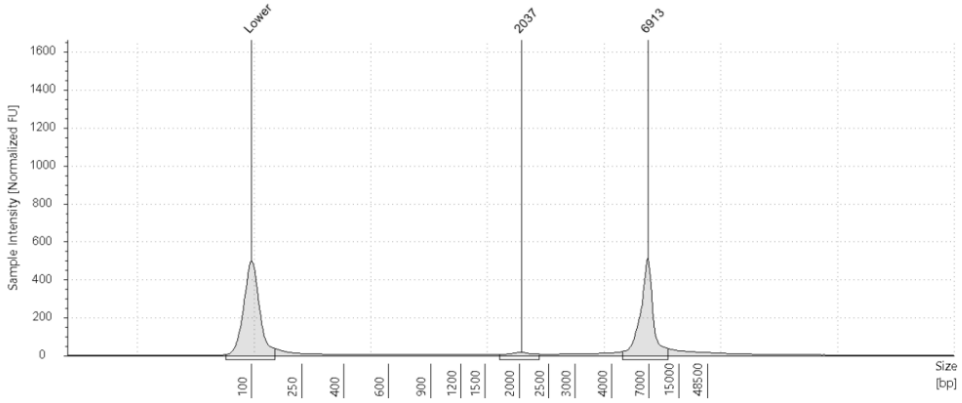

Sample Table

Well	DIN	Conc. [ng/µl]	Sample Description	Alert	Observations
G2	6.6	10.8	HS01	⚠	Caution! Expired ScreenTape device

Peak Table

Size [bp]	Calibrated Conc. [ng/µl]	Assigned Conc. [ng/µl]	% Integrated Area	From [bp]	To [bp]	Peak Comment	Observations
100	8.50	8.50	-	63	154		Lower Marker
2037	0.375	-	5.18	1702	2330		
6913	6.81	-	94.06	4704	11416		
-	-	-	-	-	-		Sample Well

Figure G. 21: The electrophoresis of the sample (HS01) located in well G2. At the top, the peaks of the electrophoresis are shown. In this figure, three peaks are indicated. The first is around 100bp

(Lower) and is probably primer dimers and small DNA contaminations. The second is at 2037bp, and probably is a contamination or a fragment of the 18S rDNA operon. The last peak is located at 6913bp and is the amplified region of the eukaryote 18S rDNA operon. Below is the sample table, showing the respective well of the sample, the DNA Integrity Number (DIN), the total DNA concentration of the sample, and the sample description. At the bottom, the specific peak table for the sample is presented. For this table, the different peaks (Size[bp]) and the respective calibrated concentrations (Calibrated Conc. [ng μL^{-1}]) are the values of interest.

H2: HS07

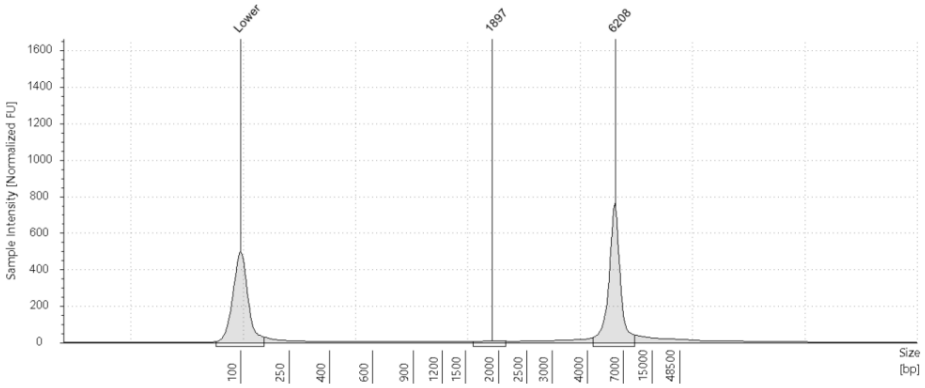

Sample Table

Well	DIN	Conc. [ng/µl]	Sample Description	Alert	Observations
H2	6.6	14.2	HS07	⚠	Caution! Expired ScreenTape device

Peak Table

Size [bp]	Calibrated Conc. [ng/µl]	Assigned Conc. [ng/µl]	% Integrated Area	From [bp]	To [bp]	Peak Comment	Observations
100	8.50	8.50	-	63	154		Lower Marker
1897	0.225	-	2.25	1609	2116		
6208	9.70	-	97.18	4356	9468		
-	-	-	-	-	-		Sample Well

Figure G. 22: The electrophoresis of the sample (HS07) located in well H2. At the top, the peaks of the electrophoresis are shown. In this figure, three peaks are indicated. The first is around 100bp (Lower) and is probably primer dimers and small DNA contaminations. The second is at 1897bp, and probably is a contamination or a fragment of the 18S rDNA operon. The last peak is located at 6208bp and is the amplified region of the eukaryote 18S rDNA operon. Below is the sample table, showing the respective well of the sample, the DNA Integrity Number (DIN), the total DNA concentration of the sample, and the sample description. At the bottom, the specific peak table for the sample is presented. For this table, the different peaks (Size[bp]) and the respective calibrated concentrations (Calibrated Conc. [ng μL^{-1}]) are the values of interest.

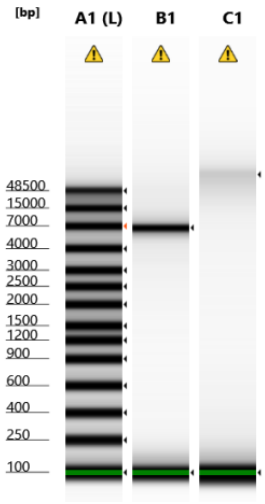

Figure G. 23: The electrophoresis of the ladder (A1), a sample (B1) and a negative control (C1). For the sample, the figure clearly shows one thick bond at ~7000 bp.

B1: HS10

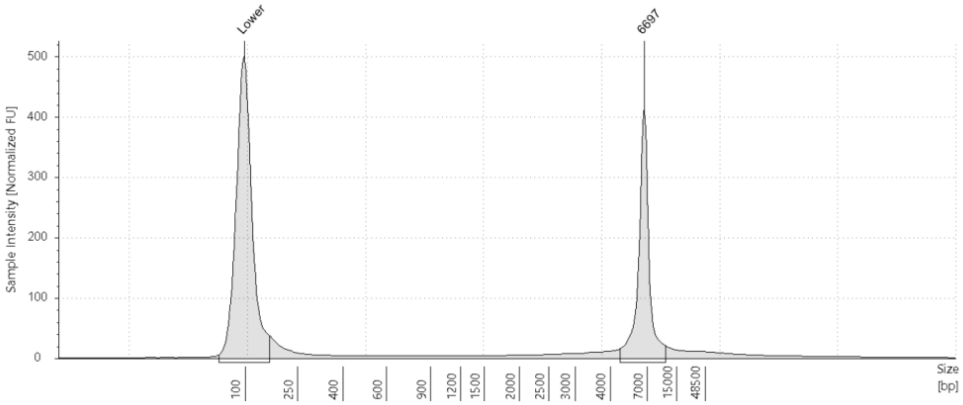

Sample Table

Well	DIN	Conc. [ng/µl]	Sample Description	Alert	Observations
B1	6.6	7.88	HS10	⚠	Caution! Expired ScreenTape device; Sample concentration outside recommended range

Peak Table

Size [bp]	Calibrated Conc. [ng/µl]	Assigned Conc. [ng/µl]	% Integrated Area	From [bp]	To [bp]	Peak Comment	Observations
100	8.50	8.50	-	64	153		Lower Marker
6697	4.51	-	98.91	4622	11100		
-	-	-	-	-	-		Sample Well

Figure G. 24: The electrophoresis of the sample (HS10) located in well B1. At the top, the peaks of the electrophoresis are shown. In this figure, two peaks are indicated. The first is around 100bp (Lower) and is probably primer dimers and small DNA contaminations. The second peak is located at 6697bp and is the amplified region of the eukaryote 18S rDNA operon. Below is the sample table, showing the respective well of the sample, the DNA Integrity Number (DIN), the total DNA concentration of the sample, and the sample description. At the bottom, the specific peak table for the sample is presented. For this table, the different peaks (Size[bp]) and the respective calibrated concentrations (Calibrated Conc. [ng μL^{-1}]) are the values of interest.

Table G. 1: The data obtained for each of the samples sequenced by Oxford nanopore sequencing. From left to right, the table show the sample name of the specific samples, the concentration of DNA obtained from Tapestation electrophoresis, the amount of sample in the tube containing the DNA, the corresponding total concentration of DNA (ng) in the tube, the size (bp) of the amplicon obtained from the PCR, the moles (fmol) of DNA in the tube containing DNA, the dilution (amount of sample and amount of Tris-HCl), and how much volume (uL) for each sample has to go into the reaction to get a total volume of 10uL in the sequencing.

Sample name	Cons. (ng μL^{-1}) of DNA	Amount of sample in the tube (uL)	Cons. (ng) in the tube	Nr. of bases (bp) in the amplicon	Fmoles of DNA	Dillution to get to ~same fmol (sample)	Dillution to get to ~same fmol (water)	In reaction to get to final volume of 10uL	Sequence run
W004	5,0	8,0	40,1	6718	9,7	1,45	8,55	1,67	1
W022	1,5	8,0	12,0	13502	1,4	None	None	1,67	1
W024	1,7	8,0	13,6	13321	1,7	None	None	1,67	1
W030	3,9	8,0	31,0	9821	5,1	2,74	7,26	1,67	1
G002	5,6	8,0	44,8	6213	11,7	1,20	8,80	1,67	1
G008	1,2	8,0	9,4	11917	1,3	None	None	1,67	1
G011	4,02	9,0	36,2	6840	8,6	None	None	1,67	2
G013	5,0	9,0	45,3	6428	11,4	1,49	8,51	1,67	2
G023	11,9	9,0	107,1	6048	28,7	0,59	9,41	1,67	2
G024	5,6	9,0	50,0	7027	11,5	1,48	8,52	1,67	2
G038	7,3	9,0	65,9	6585	16,2	1,05	8,95	1,67	2
G044	14,6	9,0	131,4	6179	34,4	0,49	9,51	1,67	2
A006	11,4	9,0	102,6	6223	26,7	0,22	9,78	1,11	3
A018	10,9	9,0	98,1	6079	26,1	0,23	9,77	1,11	3
A035	1,4	9,0	12,2	7464	2,7	None	None	1,11	3
A070	2,9	9,0	26,1	7272	5,8	1,03	8,97	1,11	3
A074	17,8	9,0	160,2	5788	44,8	0,13	9,87	1,11	3
A078	16,5	9,0	148,5	5959	40,3	0,15	9,85	1,11	3
HS01	6,8	9,0	61,3	6913	14,3	0,42	9,58	1,11	3
HS07	9,7	9,0	87,3	6208	22,8	0,26	9,74	1,11	3
HS10	4,51	9,0	40,6	6697	9,8	0,61	9,39	1,11	3

Appendix H – Bioinformatic workflow, diversity plots (PCoA plots and Bar-charts), and analysis for the prokaryote and eukaryote part of the microbial communities for the different experiments.

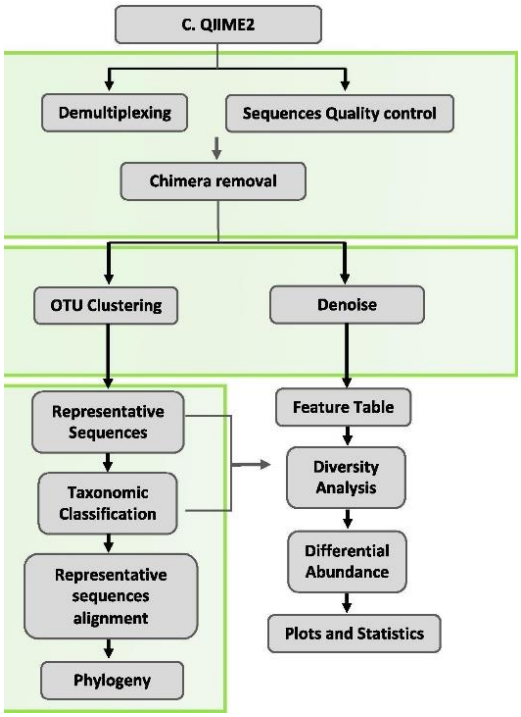

Figure H. 1: The bioinformatic workflow executed in Qiime2 (green background), as well as the last steps (Feature Table, Diversity Analysis, Differential abundance, Plots and Statistics) executed in RStudio (white background). The illustration is collected from (Santos et al., 2020).

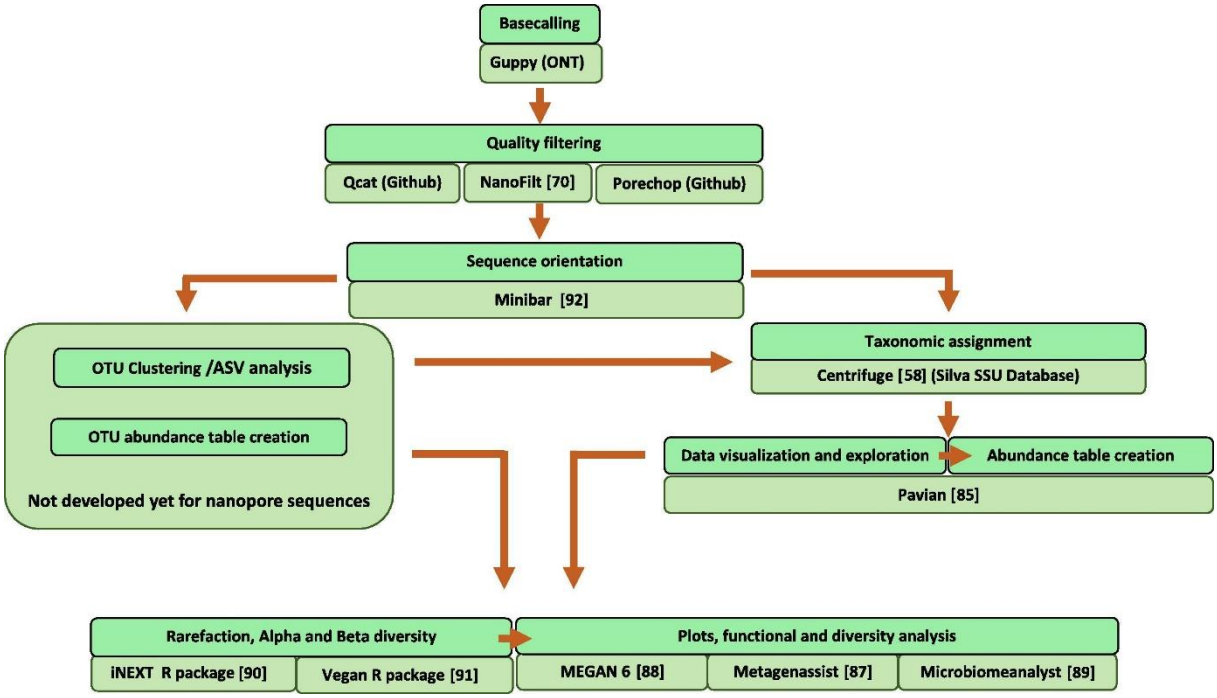

Figure H. 2: The bioinformatic workflow, collected from (Santos et al., 2020). The figure shows the actuall bioinformatic steps (green), and the respective software that can be used to solve these steps (olive green). The figure includes the steps executed at BGI Genomics, before the sequence

reads were made available for this master's thesis (Basecalling and Quality filtering). After that, the subsequent steps are shown from sequence orientation, ASV clustering- and analysis, taxonomic assignments, Data visualization and exploration, creation of an abundance table, rarefaction plotting, alpha and beta diversity, and the final diversity analysis plotting.

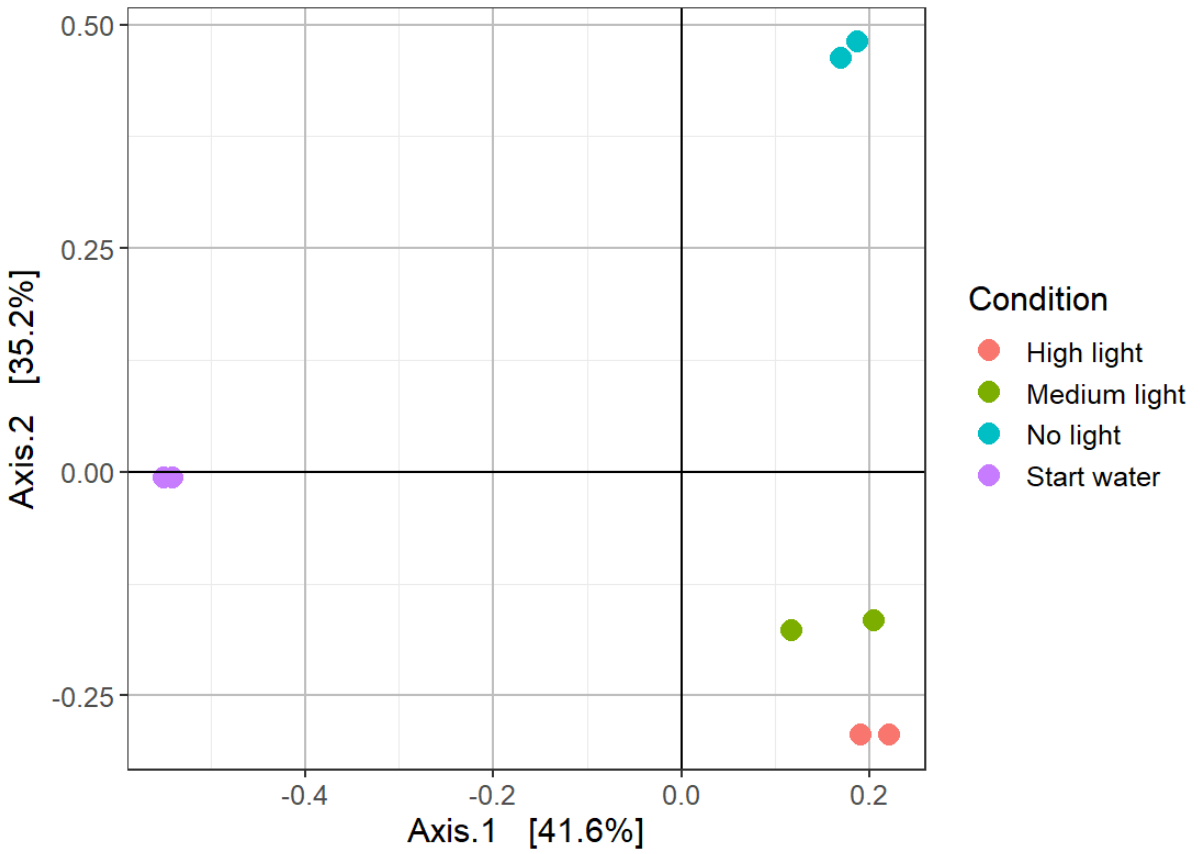

Figure H. 3: A PCoA plot showing the composition differences (Bray-Curtis distances) of ASVs for the prokaryote contributors of the communities coming from the different conditions, as well as from the start water, for the experiment testing light intensities. The Pairwise Adonis test showed that the findings were not significant ($p = 0.33$).

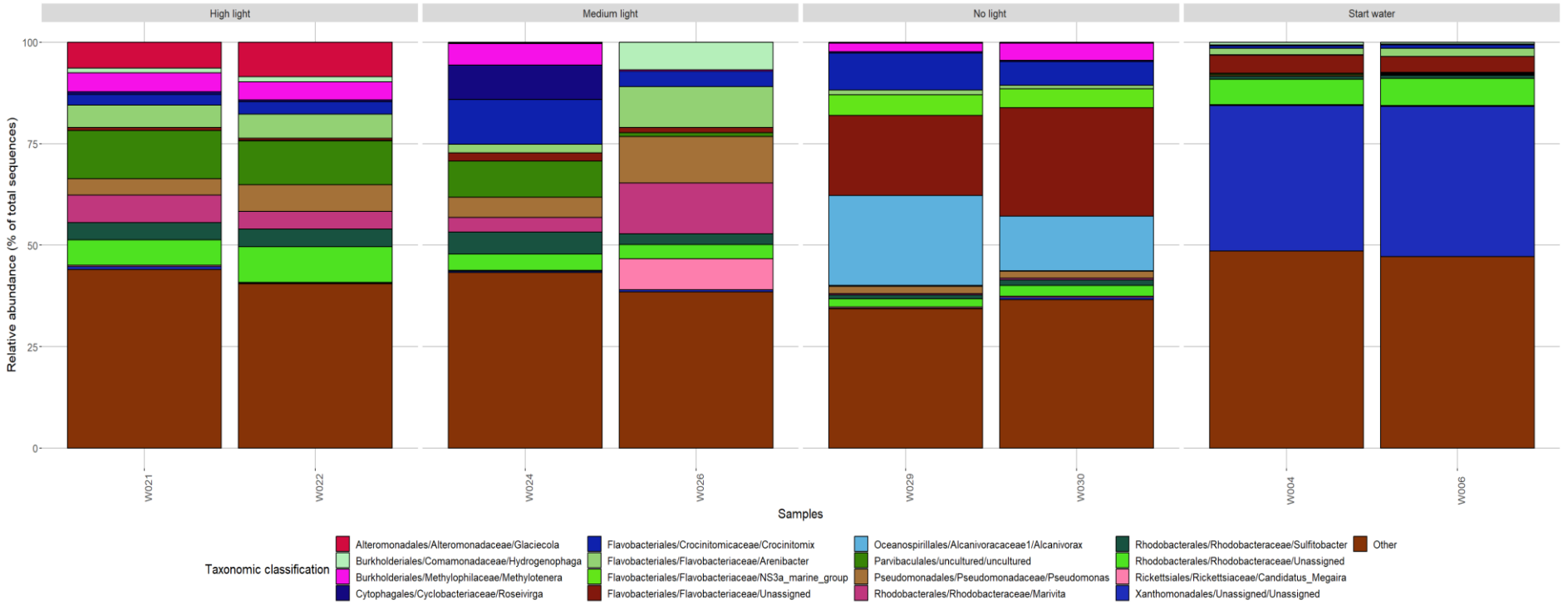

Figure H. 4: Taxonomic classification, with relative abundance of species, for the prokaryote part of the community for the different conditions tested (High, medium, and no light), as well as for the start water, for the experiment testing light intensities. The respective sample names are indicated below each bar, as well as the color coding for the different taxa.

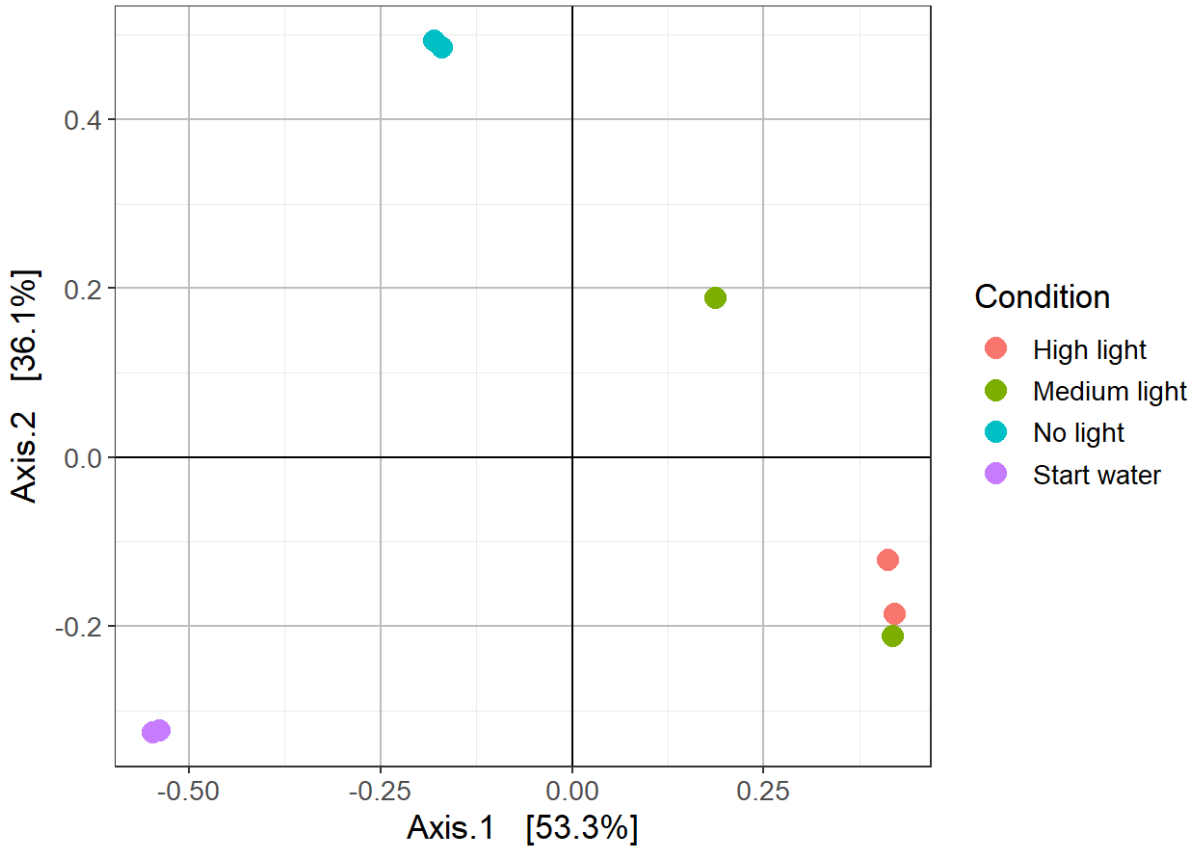

Figure H. 5: A PCoA plot showing the composition differences (Bray-Curtis distances) of ASVs for the eukaryote part of the communities coming from the different conditions, as well as from the start water, in the experiment testing light intensities. The Pairwise Adonis test showed that the results were not significant ($p > 0.3$). The PCoA plot was generated based on sequences from DNBSEQ.

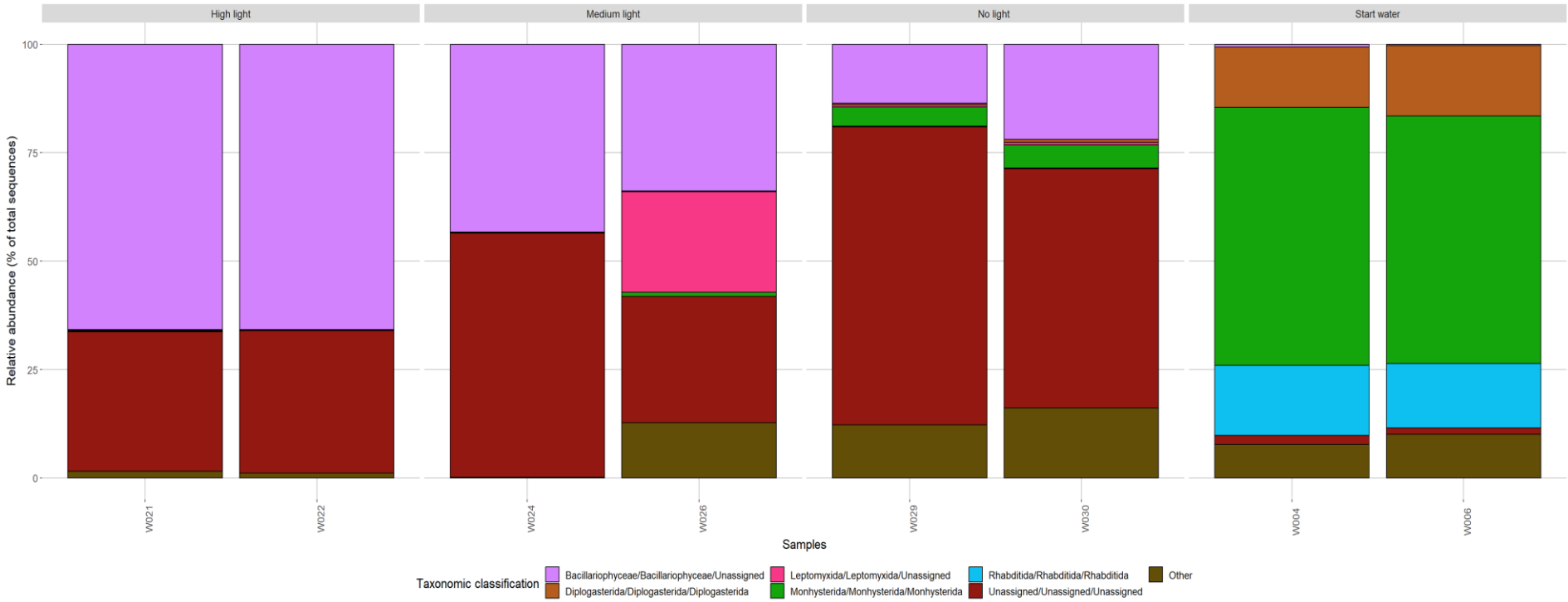

Figure H. 6: Taxonomic classification, with relative abundance of species, for the eukaryote part of the community in the experiment testing light intensities. The respective sample names are indicated below each bar, as well as the color coding for the different taxa. The bar chart was generated based on sequences from DNBSEQ sequencing.

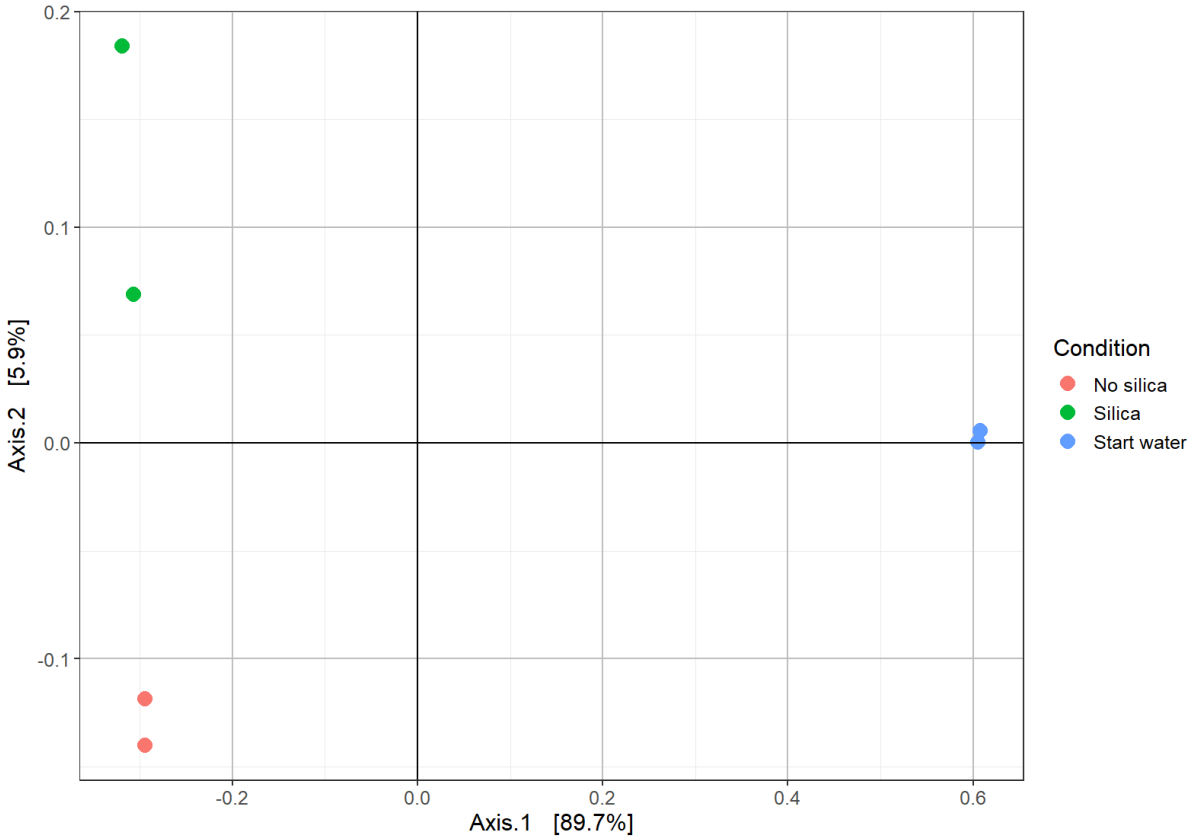

Figure H. 7: A PCoA plot showing the composition differences (Bray-Curtis distances) of ASVs for the prokaryote contributors of the communities coming from the treatment (addition of silica), the control (No addition of silica), as well as from the start water, for the experiment testing addition of silica. The. The Pairwise Adonis test showed that the findings were not significant (p = 0.33).

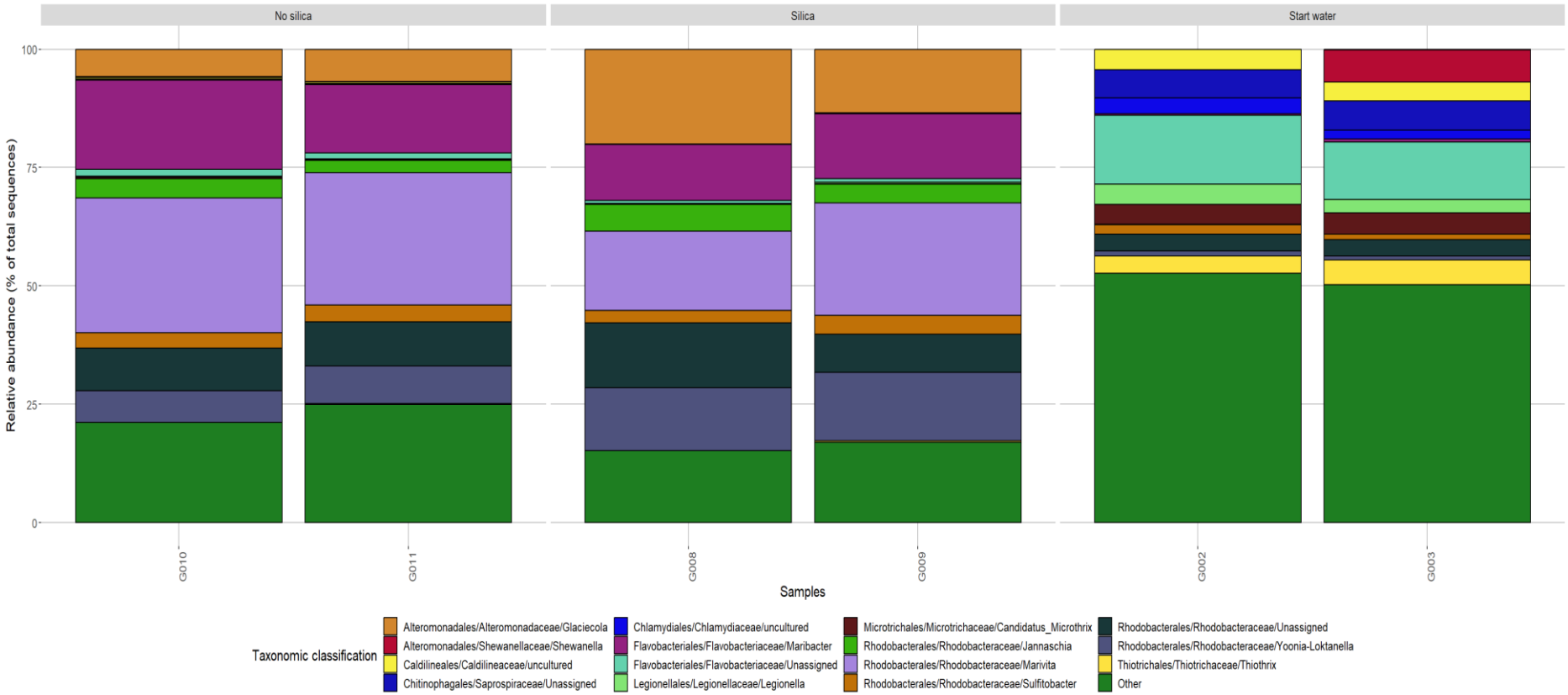

Figure H. 8: Taxonomic classification, with relative abundance of species, for the prokaryote part of the community of the treatment (addition of silica), the control (no addition of silica), as well as for the start water, for the experiment testing addition of silica. The respective sample names are indicated below each bar, as well as the color coding for the different taxa.

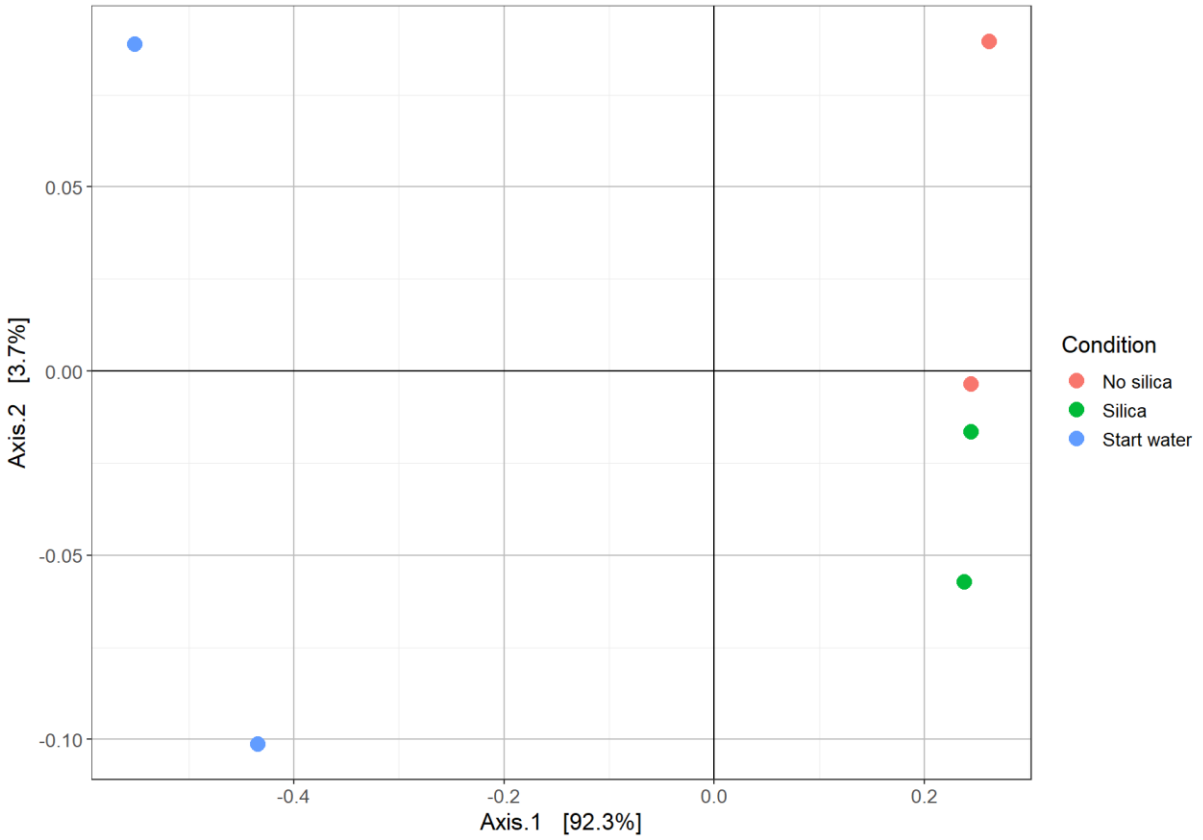

Figure H. 9: A PCoA plot showing the composition differences (Bray-Curtis distances) of ASVs for the eukaryote part of the communities coming from the different conditions, as well as from the start water, in the experiment testing addition of silica. The Pairwise Adonis test showed that the results were not significant (p = 0.33). The PCoA plot was generated based on sequences from DNBSEQ.

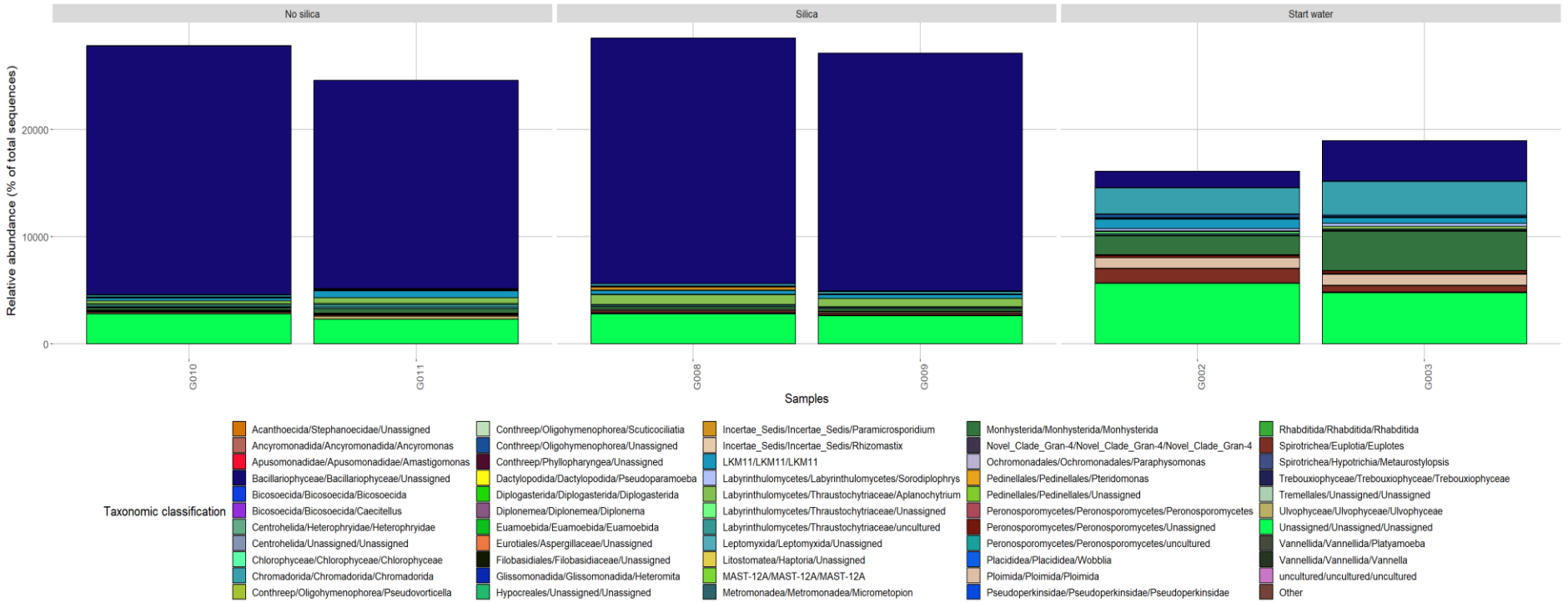

Figure H. 10: Taxonomic classification, with relative abundance of species, for the eukaryote part of the community in the experiment testing addition of silica. The respective sample names are indicated below each bar, as well as the color coding for the different taxa. The bar chart was generated based on sequences from DNBSEQ sequencing.

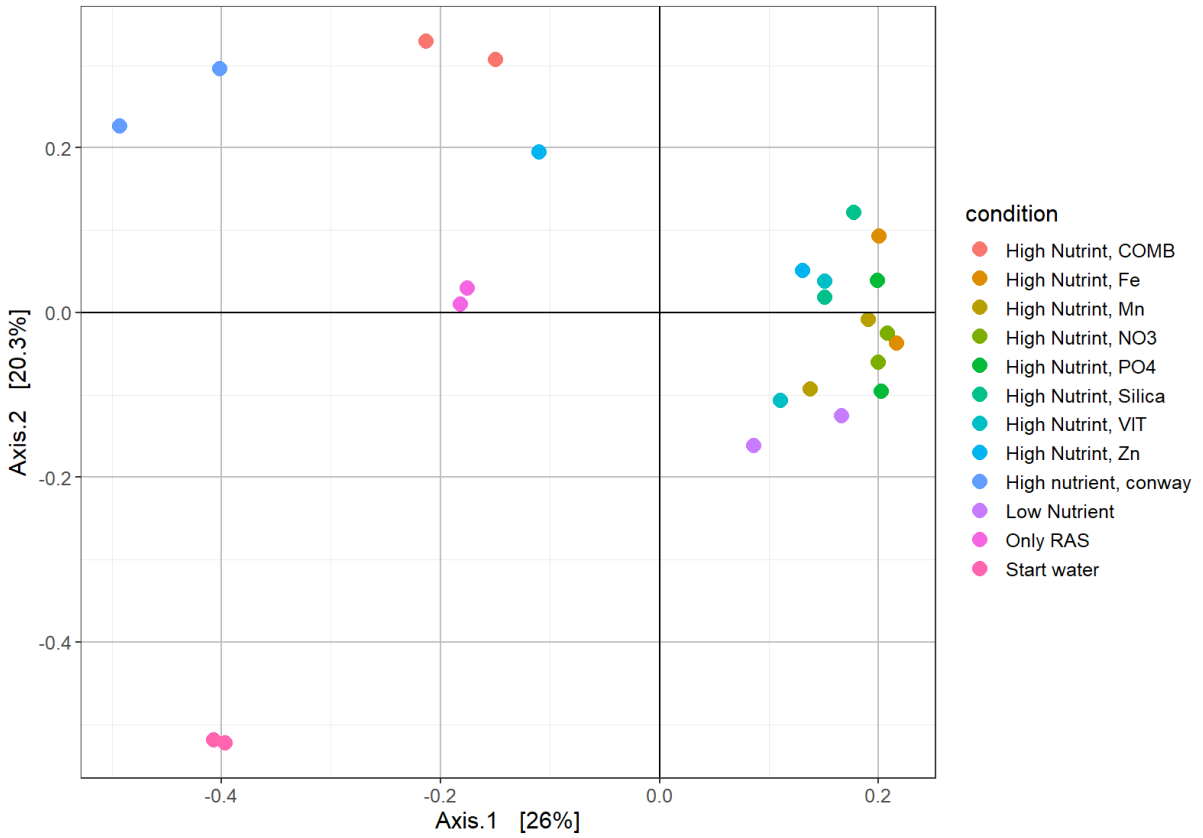

Figure H. 11: A PCoA plot showing the composition differences (Bray-Curtis distances) of ASVs for the prokaryote contributors of the communities coming from the different treatments of the second part of the experiment testing addition of nutrients, as well as from the start water. The Pairwise Adonis test showed that the findings were not significant (p = 0.33-1.0).

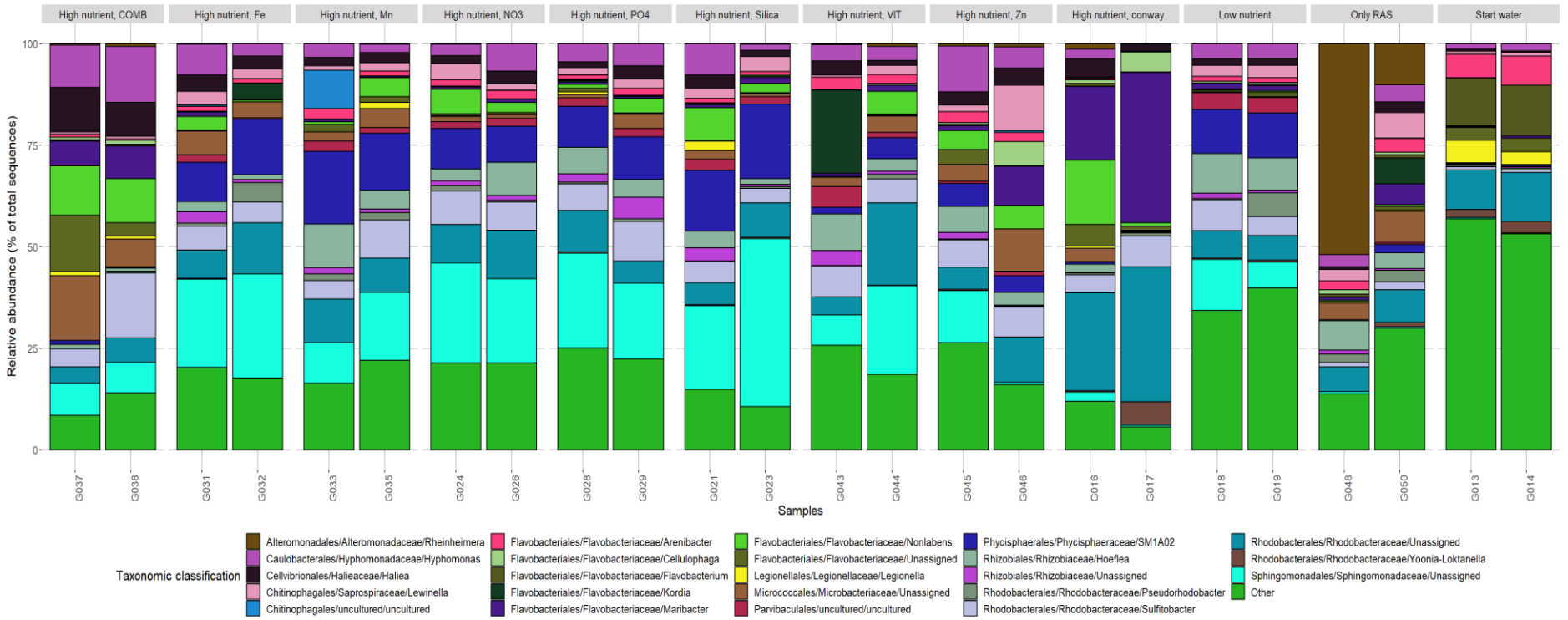

Figure H. 12: Taxonomic classification, with relative abundance of species, for the prokaryote part of the community for the different treatments of the second part of the experiment testing addition of nutrients, as well as for the start water. The respective sample names are indicated below each bar, as well as the color coding for the different taxa.

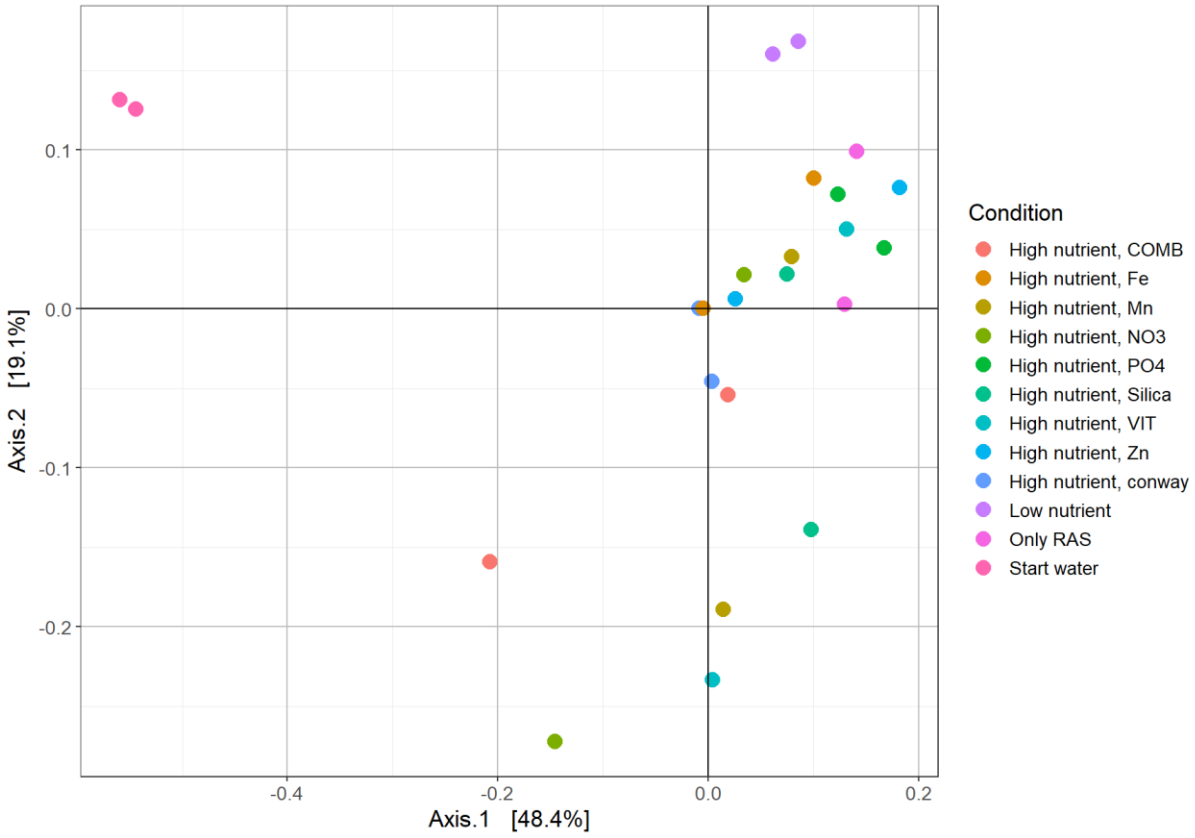

Figure H. 13: A PCoA plot showing the composition differences (Bray-Curtis distances) of ASVs for the eukaryote part of the communities coming from the different conditions, as well as from the start water, in the experiment testing addition of nutrients. The Pairwise Adonis test showed that the results were not significant ($p > 0.33$). The PCoA plot was generated based on sequences from DNBSEQ.

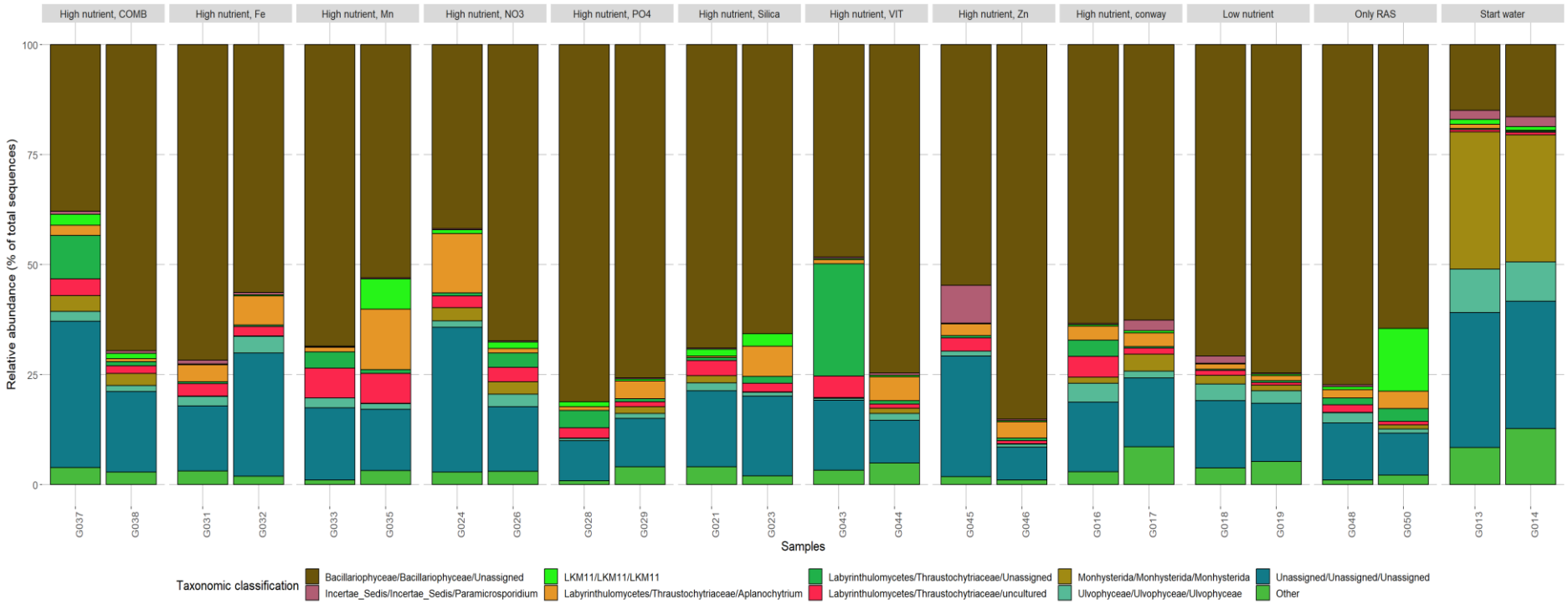

Figure H. 14: Taxonomic classification, with relative abundance of species, for the eukaryote part of the community in the experiment testing addition of nutrients. The respective sample names are indicated below each bar, as well as the color coding for the different taxa. The bar chart was generated based on sequences from DNBSEQ sequencing.

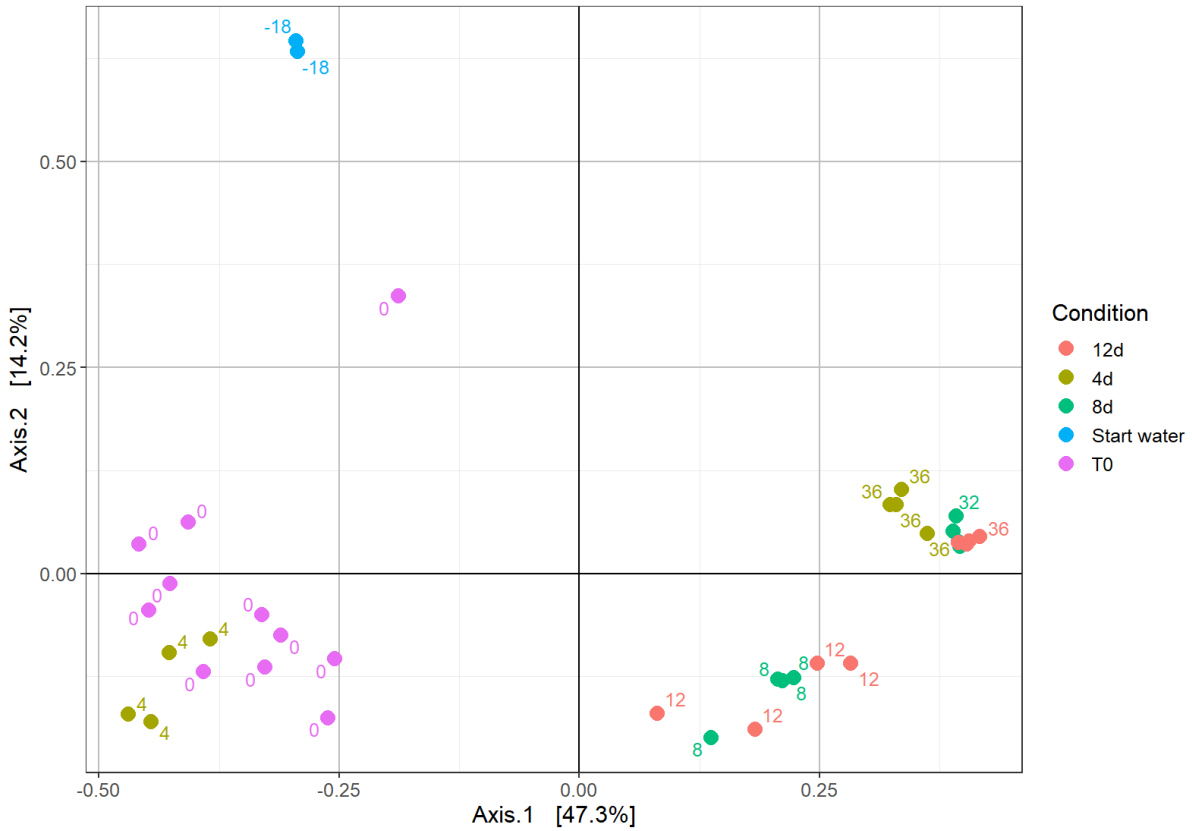

Figure H. 15: A PCoA plot showing the composition differences (Bray-Curtis distances) of ASVs for the prokaryote contributors of the communities coming from the different conditions tested in the experiment testing harvest rate, as well as from the start water. The numbers indicate what day in the experimental period the samples were obtained. The Pairwise Adonis test showed that the findings were significant (p = 0.001-0.04), except for the condition Harvest every 8. day compared to Harvest every 12. day (p = 0.99).

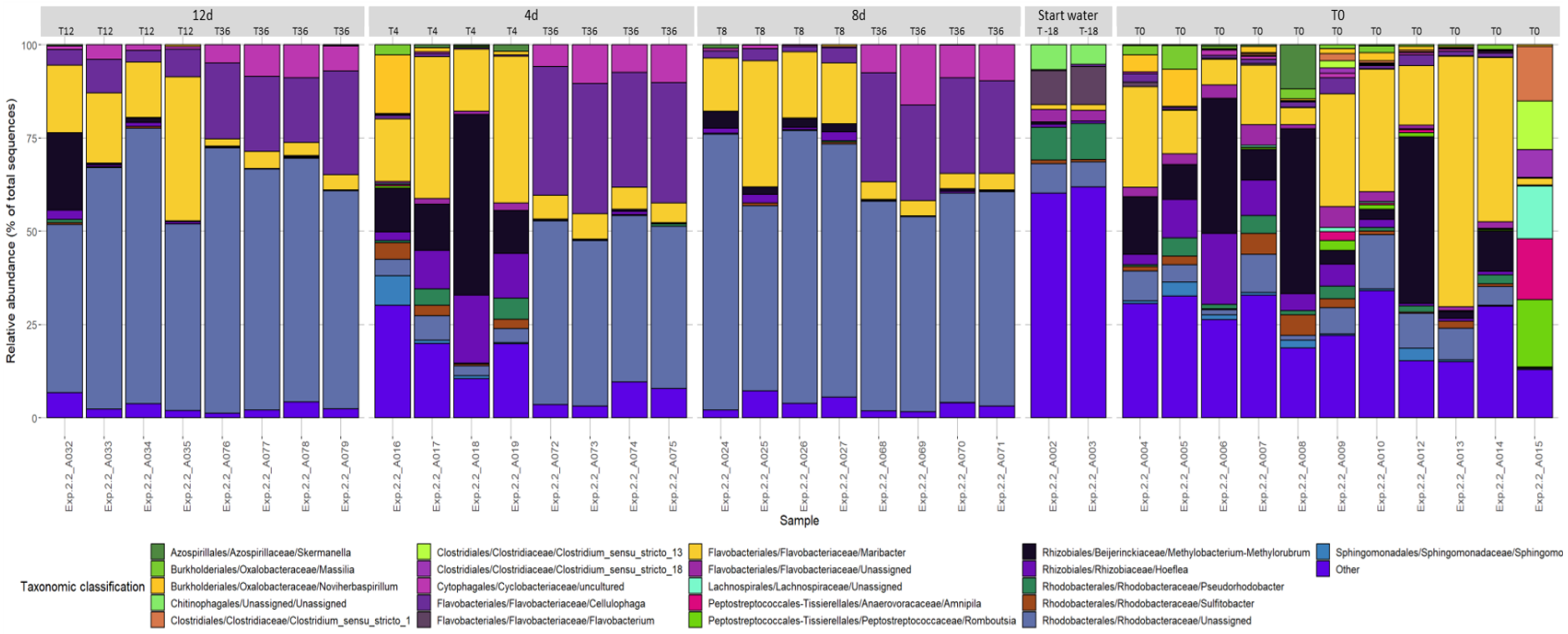

Figure H. 16: Taxonomic classification, with relative abundance of species, for the prokaryote part of the community for the different treatments coming from the experiment testing harvest rate, as well as for the start water and the T0 samples. The respective sample names are indicated below each bar, as well as the color coding for the different taxa. The respective conditions are indicated above each group of bars, with respective time of harvest (T) for the particular sample.

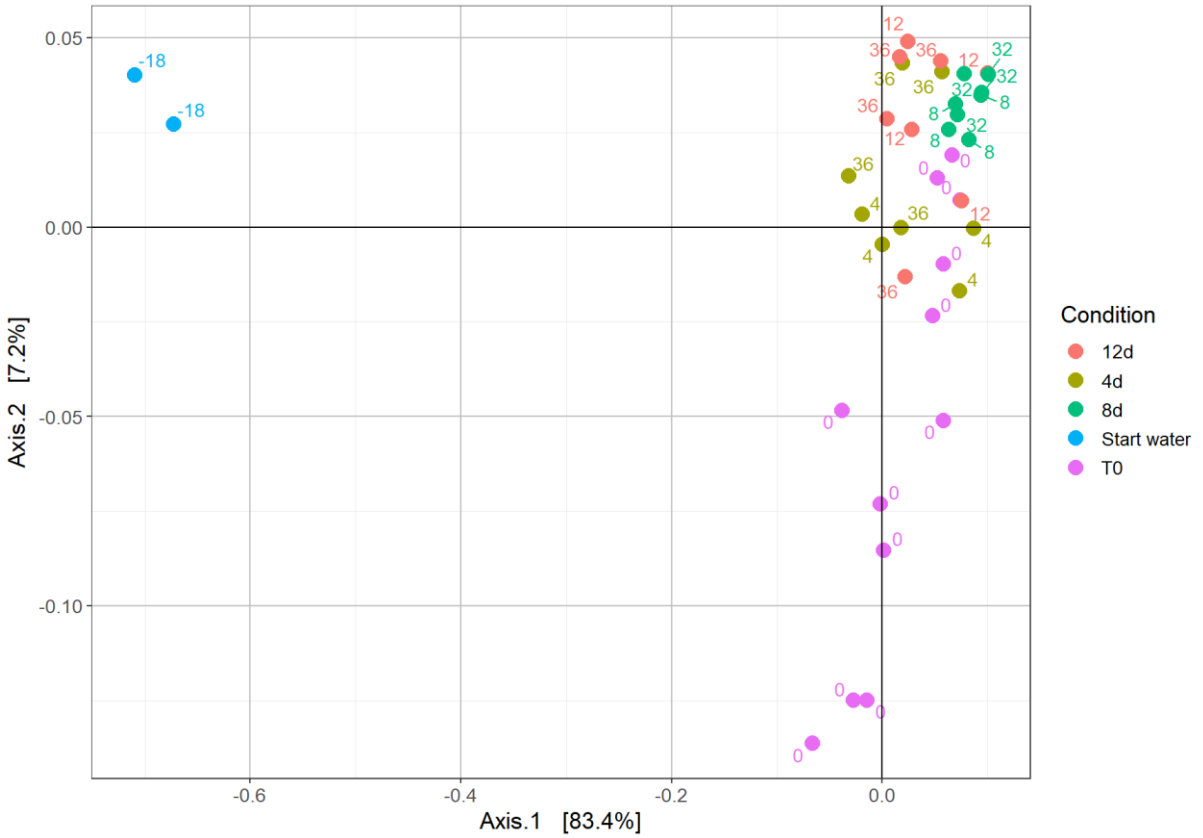

Figure H. 17: A PCoA plot showing the composition differences (Bray-Curtis distances) of ASVs for the eukaryote part of the communities coming from the different conditions, as well as from the start water and the T0 samples, in the experiment testing harvest frequencies. The Pairwise Adonis test showed that the results were significant ($p < 0.05$), except for the condition testing a harvest frequency of every 4. day compared to every 12. day ($p = 0.1$). The PCoA plot was generated based on sequences from DNBSEQ.

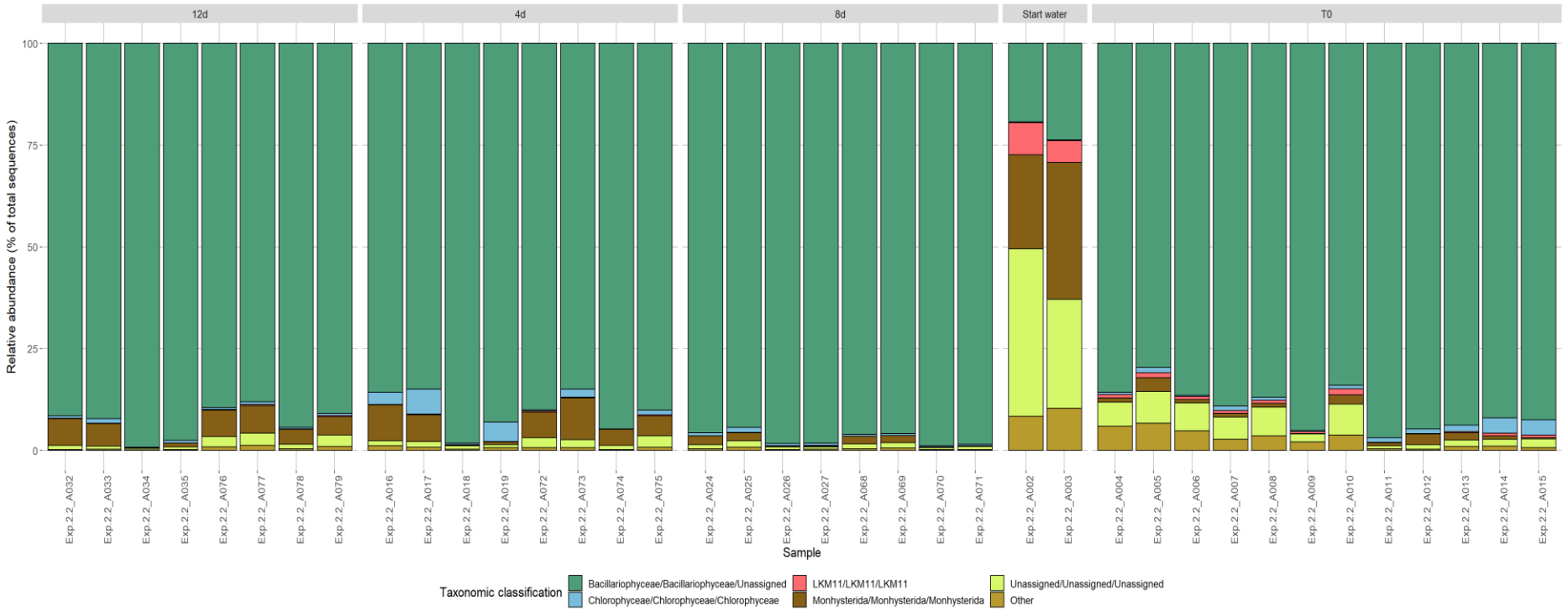

Figure H. 18: Taxonomic classification, with relative abundance of species, for the eukaryote part of the community for the different treatments coming from the experiment testing harvest rate, as well as for the start water and the T0 samples. The respective sample names are indicated below each bar, as well as the color coding for the different taxa. The respective conditions are indicated above each group of bars, with respective time of harvest (T) for the particular sample. The bar chart was generated based on sequences from DNBSEQ sequencing.

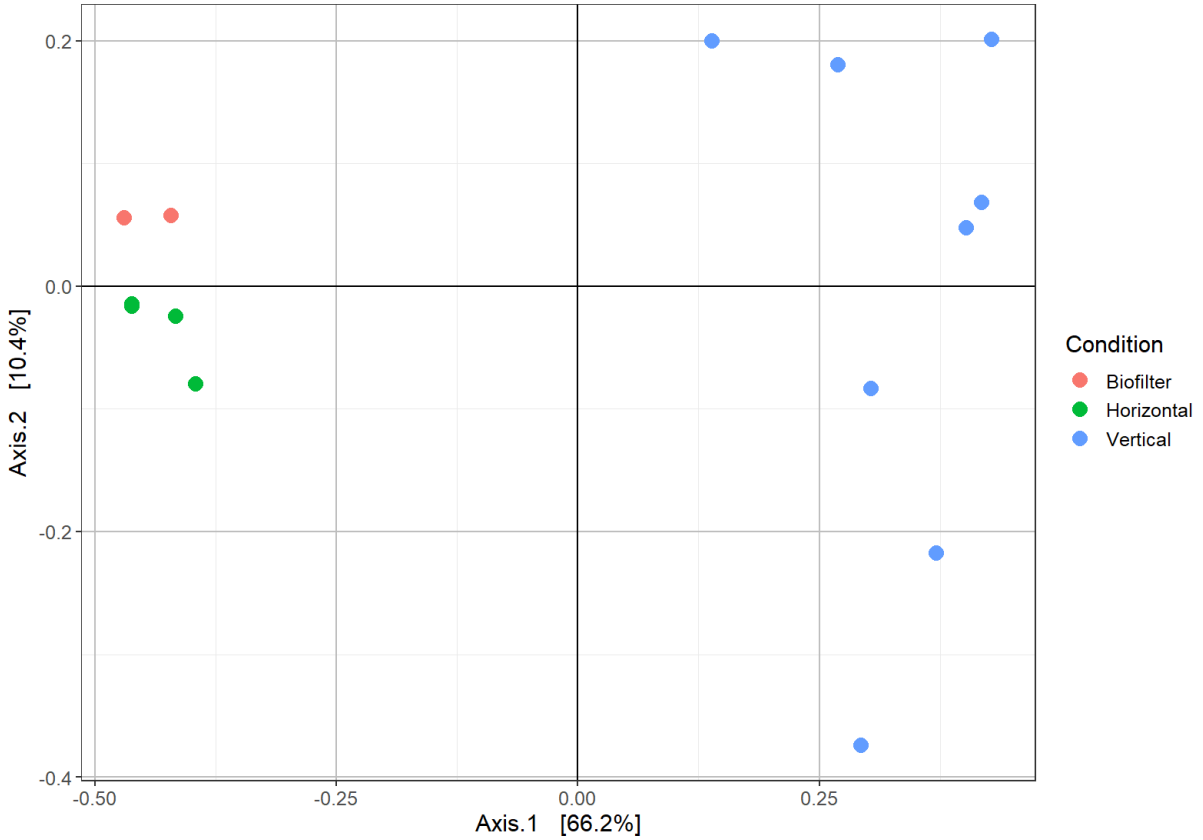

Figure H. 19: A PCoA plot showing the composition differences (Bray-Curtis distances) of ASVs for the prokaryote contributors of the communities coming from the different conditions tested (Horizontal and vertical pilot reactors) in the experiment testing the pilot reactors at the RAS facility Hardingsmolt AS, as well as from the nitrifying biofilter. The Pairwise Adonis test showed that there was a significant difference between the vertical pilot reactor compared to the horizontal one ($p = 0.003$), and the nitrifying biofilter ($p = 0.03$); however, no significant difference was found between the horizontal pilot reactor and the biofilter ($p = 0.07$).

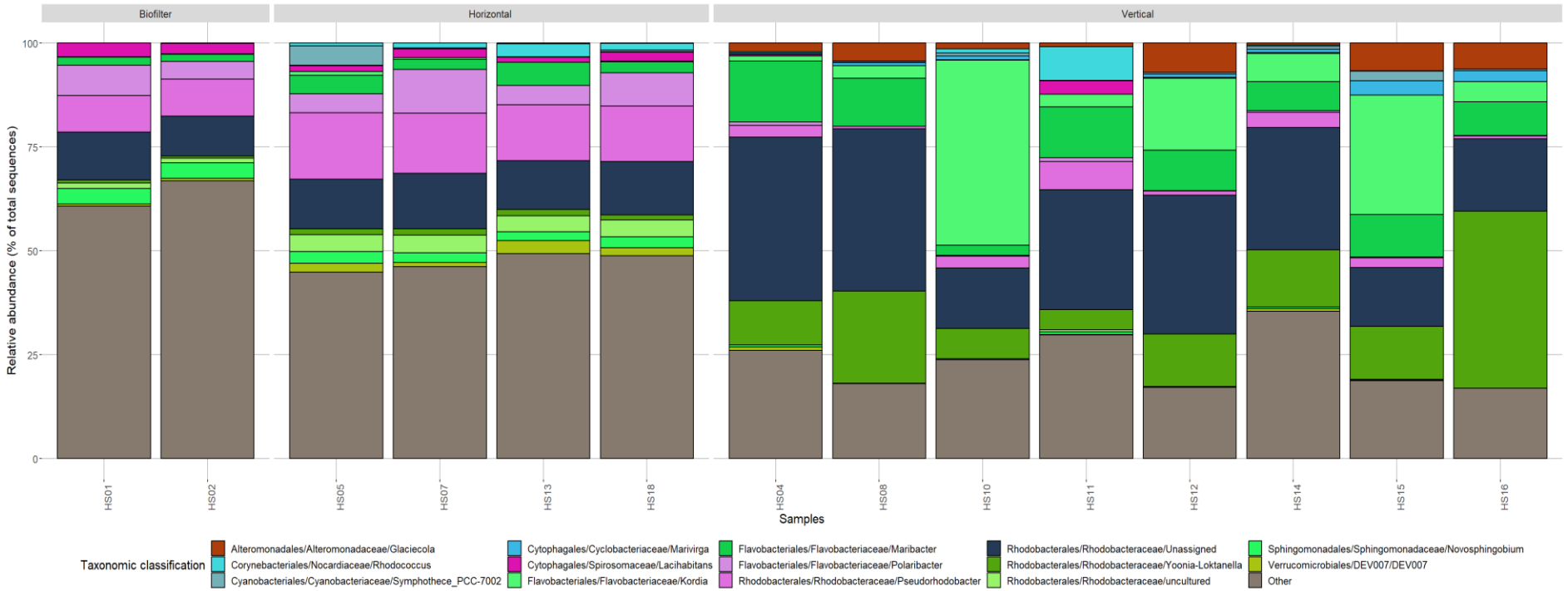

Figure H. 20: Taxonomic classification, with relative abundance of species, for the prokaryote part of the community for the different treatments (Horizontal and Vertical growth plates) coming from the experiment testing the pilot reactors at the RAS facility Hardingsmolt AS, as well as from the nitrifying biofilter. The respective sample names are indicated below each bar, as well as the color coding for the different taxa.

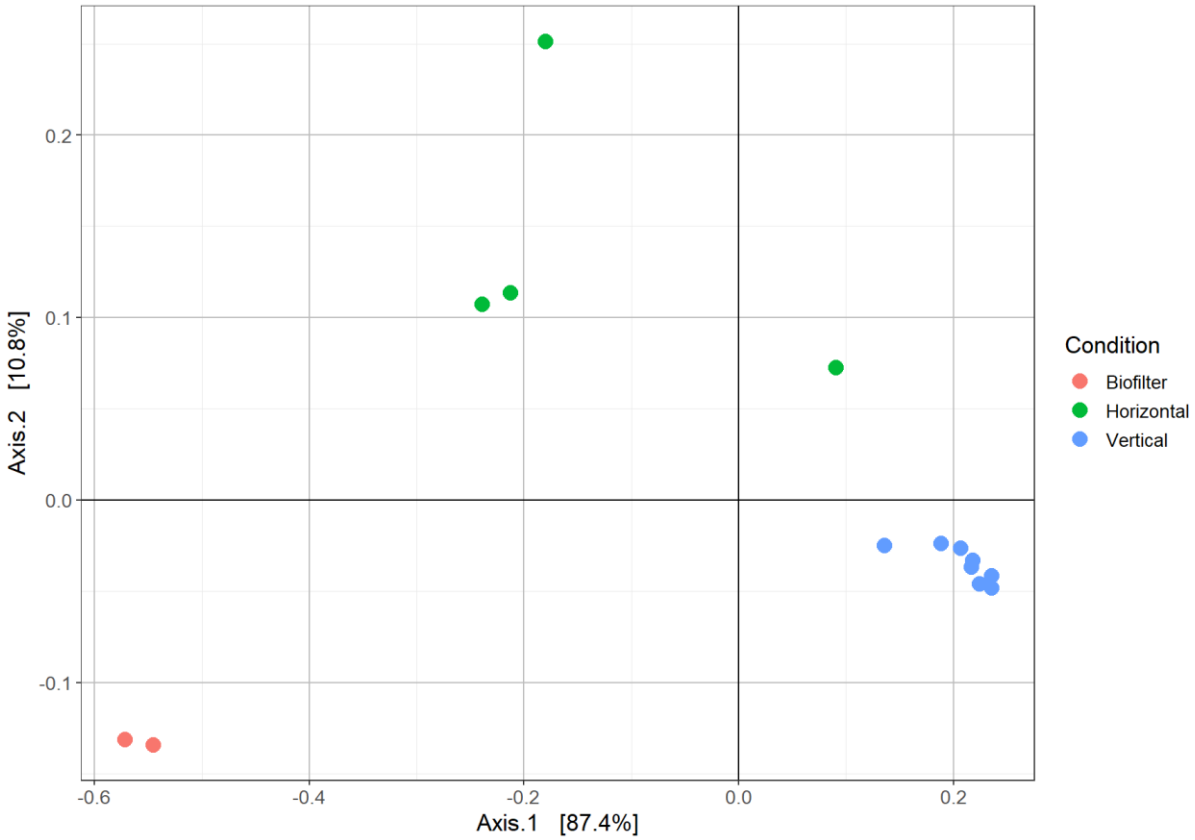

Figure H. 21: A PCoA plot showing the composition differences (Bray-Curtis distances) of ASVs for the eukaryote part of the communities coming from the different conditions, as well as from the biofilter, in the experiment testing the pilot reactors at Hardingsmolt AS. The Pairwise Adonis test showed that it was a significant difference for the vertical pilot reactor compared to the nitrifying biofilter ($p = 0.03$) and the horizontal pilot reactor ($p = 0.004$); however, that there was not a significant difference between the horizontal pilot reactor and the biofilter ($p = 0.07$). PCoA plot was generated based on sequences from DNBSEQ.

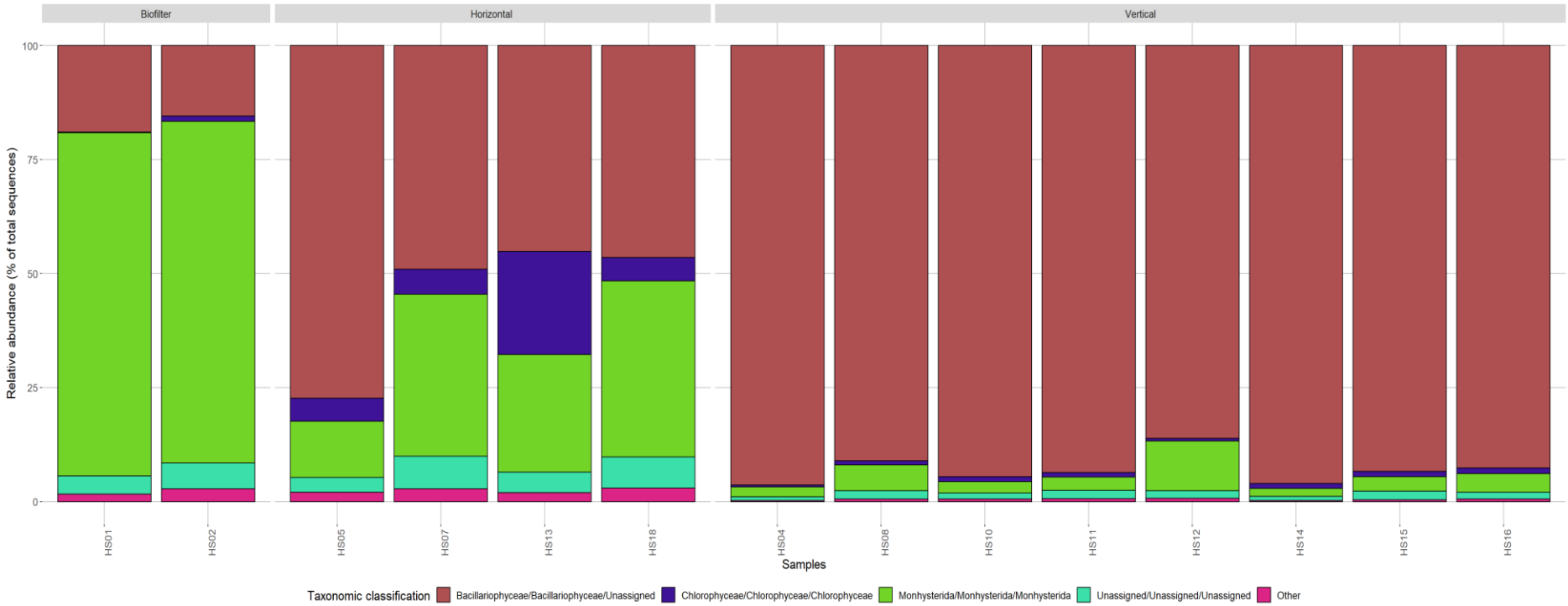

Figure H. 22: Taxonomic classification, with relative abundance of species, for the eukaryote part of the community for the vertical- and the horizontal pilot reactor, as well as for the nitrifying biofilter, in the experiment testing the pilot reactors at Hardningsmolt AS. The respective sample names are indicated below each bar, as well as the color coding for the different taxa. The respective conditions are indicated above each group of bars. The bar chart was generated based on sequences from DNBSEQ sequencing.

Table H. 1: Taxa (Class/Order/Family/Genus) of the two most abundant prokaryote species for the treatments: High_COMB, High_Fe, High_Mn, High_NO3, High_PO4, High_Silica, High_VIT, High_Zn, High_Conway, and Only_RAS, the control: Low_Nutrient, as well as for the start water, in the experiment testing addition of nutrients. The abbreviation "COMB" indicates a combination of nutrients: Fe, Zn, Mn, Cu and Co. The abbreviation "VIT" indicates a combination of vitamin B12- and B1. The condition "Only_RAS" indicate that the samples contained only RAS water. The prefaces "High" and "Low" indicate whether the condition had high or low nutrient load in addition to the element(s) tested. These samples were analyzed with the DNBSEQ technology. If ("), the taxa are the same as the one above.

Condition	Taxa (Class/Order/Family/Genus)	Abundance (%)
High_COMB	*Actinomycetia/Micrococcales/Microbacteriaceae/Unassigned*	16.0
	Alphaproteobacteria/Rhodobacterales/Rhodobacteraceae/Sulfitobacter	16.0
High_fe	*Alphaproteobacteria/Sphingomonadales/Sphingomonadaceae/Unassigned*	25.6
	"	21.8
High_Mn	*Phycisphaerae/Phycisphaerales/Phycisphaeraceae/SM1A02*	17.9
	Alphaproteobacteria/Sphingomonadales/Sphingomonadaceae/Unassigned	16.8
High_NO3	*Alphaproteobacteria/Sphingomonadales/Sphingomonadaceae/Unassigned*	24.6
	"	20.7
High_PO4	*Alphaproteobacteria/Sphingomonadales/Sphingomonadaceae/Unassigned*	23.4
	"	18.7
High_Silica	*Alphaproteobacteria/Sphingomonadales/Sphingomonadaceae/Unassigned*	41.3
	"	20.6
High_Vit	*Alphaproteobacteria/Sphingomonadales/Sphingomonadaceae/Unassigned*	21.9
	Flavobacteriia/Flavobacteriales/Flavobacteriaceae/Kordia	20.5
High_Zn	*Alphaproteobacteria/Sphingomonadales/Sphingomonadaceae/Unassigned*	12.8
	Alphaproteobacteria/Caulobacterales/Hyphomonadaceae/Hyphomonas	11.3
High_Conway	*Flavobacteriia/Flavobacteriales/Flavobacteriaceae/Maribacter*	37.1
	Alphaproteobacteria/Rhodobacterales/Rhodobacteraceae/Unassigned	33.2
Low_N	*Alphaproteobacteria/Sphingomonadales/Sphingomonadaceae/Unassigned*	12.6
	Phycisphaerae/Phycisphaerales/Phycisphaeraceae/SM1A02	11.1
Only_RAS	*Gammaproteobacteria/Alteromonadales/Alteromonadaceae/Rheinheimera*	51.9
	"	10.1
Start water	*Flavobacteriia/ Flavobacteriales/Flavobacteriaceae/Flavobacterium*	12.5
	Alphaproteobacteria/Rhodobacterales/Rhodobacteraceae/Unassigned	12.0

Appendix I – List of chemicals used during the master's thesis

Table I. 1: List of chemicals used during the master's thesis.

Name of chemical	Formula/ description	Producer
Liquid nitrogen	N^2 (aq)	Linde Gas AS (Leirdal, Norway)
ZymoBIOMICS™ DNA Miniprep Kit	Kit	Zymo Research (California, USA)
Hydrochloric acid fuming [370.5M]	HCl	Supelco® (Darmstadt, Germany)
Qubit™ 1X dsDNA HS Assey kit	Kit	Thermo Fisher Scientific (Massachusetts, USA)
High sensitivity D1000 Reagents	Kit	Agilent Technologies (California, USA)
LongAmp Hot Start Taq 2X Master mix, (NEB, M0533S)	Reagent	New England Biolabs$_{inc}$ (Ipswich, Massachusetts, USA)
Primer (21R_28S)	Reagent	Eurofins Genomics (Ebersberg, Germany)
Primer (3NDF_18S)	Reagent	Eurofins Genomics (Ebersberg, Germany)
Ethanol [96%]	H_3CCH_2OH	VWR Chemicals (Fontenay-sous-Bois, France)
Sodium chloride	NaCl - HCl	Sigma Aldrich (Darmstadt, Germany).
Trizma ® Hydrochloride (TRIS HCl)	$C_4H_{11}NO_3$	Sigma Aldrich (Darmstadt, Germany).
Nuclease free water, cat #AM9937	H_2O (aq)	Thermo Fisher Scientific (Massachusetts, USA)
Agencourt AMPure XP beads, cat # A63881	Reagent	Beckman coulter™ (Brea, California, USA)
NEBNext ultra II End repair/dA-tailing Module, E7546	Kit	New England Biolabs$_{inc}$ (Ipswich, Massachusetts, USA)
NEB Blunt/TA Ligase Master Mix, cat #M0367	Reagent	New England Biolabs$_{inc}$ (Ipswich, Massachusetts, USA)
PCR barcoding kit (SQK-PBK004)	Kit	Oxford Nanopore (Oxford, UK)
Flow cell priming kit (EXP-FLP002)	Kit	Oxford Nanopore (Oxford, UK)
Flow cell wash kit (EXP-RAP001)	Kit	Oxford Nanopore (Oxford, UK)

Appendix J – Workflow of the protocols concerning DNA extraction, End-Prep, PCR adapters ligation- and amplification, Rapid adapter ligation, and Priming- and loading the SpotOn flow cell

ZymoBIOMICS™ DNA Miniprep Kit

DNA for microbiome or metagenome analyses

Highlights

- **Validated Unbiased for Microbiome Measurements:** Unbiased cellular lysis validated using the ZymoBIOMICS Microbial Community Standard.
- **Inhibitor-Free DNA from Any Sample:** Isolate ultra-pure DNA ready for any downstream application.
- **Certified Low Bioburden:** Boost your detection limit for low abundance microbes.
- **Simple Workflow:** Simply bead-beat sample, purify via spin-column, and filter to remove PCR inhibitors. No precipitation or lengthy incubations!

Protocol

1. Add sample to a **ZR BashingBead™ Lysis Tubes (0.1 & 0.5 mm)**. Add 750 µl **ZymoBIOMICS™ Lysis Solution** to the tube and cap tightly.

   ***Note**: For samples stored and lysed in **DNA/RNA Shield™ Lysis Tubes**, do not add ZymoBIOMICS™ Lysis Solution and proceed to Step 2.*

Sample Type	Maximum Input
Feces	200 mg
Soil	250 mg
Liquid Samples[1] and Swab Collections[2]	250 µl
Cells (isotonic buffer, *e.g.* PBS)	50-100 mg (wet weight) (10^9 bacterial and 10^8 yeast cells)
Samples in DNA/RNA Shield™[3]	≤ 1 ml

2. Secure in a bead beater fitted with a 2 ml tube holder assembly and process using optimized beat beating conditions (speed and time) for your device (see Appendix D)[4].

***Optional Stopping Point:** Following Step 2 is the best stopping point if breaking up the work is needed. Samples can be stored post-lysis for several hours at room temperature, or frozen at – 80 °C for long term storage.*

3. Centrifuge the **ZR BashingBead™ Lysis Tubes (0.1 & 0.5 mm)** in a microcentrifuge at ≥ 10,000 x *g* for 1 minute.

4. Transfer up to 400 µl supernatant to the **Zymo-Spin™ III-F Filter** in a **Collection Tube** and centrifuge at 8,000 x *g* for 1 minute. Discard the Zymo-Spin™ III-F Filter.

5. Add 1,200 µl of **ZymoBIOMICS™ DNA Binding Buffer** to the filtrate in the Collection Tube from Step 4. Mix well.

6. Transfer 800 µl of the mixture from Step 5 to a **Zymo-Spin™ IICR Column** in a Collection Tube and centrifuge at 10,000 x *g* for 1 minute.

7. Discard the flow through from the Collection Tube and repeat Step 6.

8. Add 400 µl **ZymoBIOMICS™ DNA Wash Buffer 1** to the Zymo-Spin™ IICR Column in a new Collection Tube and centrifuge at 10,000 x *g* for 1 minute. Discard the flow-through.

9. Add 700 µl **ZymoBIOMICS™ DNA Wash Buffer 2** to the Zymo-Spin™ IICR Column in a Collection Tube and centrifuge at 10,000 x *g* for 1 minute. Discard the flow-through.

10. Add 200 µl **ZymoBIOMICS™ DNA Wash Buffer 2** to the Zymo-Spin™ IICR Column in a Collection Tube and centrifuge at 10,000 x *g* for 1 minute.

11. Transfer the Zymo-Spin™ IICR Column to a clean 1.5 ml microcentrifuge tube and add 100 µl (50 µl minimum) **ZymoBIOMICS™ DNase/RNase Free Water** directly to the column matrix and incubate for 1 minute. Centrifuge at 10,000 x *g* for 1 minute to elute the DNA[5, 6].

12. Place a **Zymo-Spin™ III-HRC Filter** in a new Collection Tube and add 600 µl **ZymoBIOMICS™ HRC Prep Solution**. Centrifuge at 8,000 x *g* for 3 minutes.

13. Transfer the eluted DNA (Step 11) to a prepared Zymo-Spin™ III-HRC Filter in a clean 1.5 ml microcentrifuge tube and centrifuge at exactly 16,000 x *g* for 3 minutes.

    The filtered DNA is now suitable for PCR and other downstream applications.

End-prep

~50 minutes

Materials	• 100 ng fragmented DNA in 50 µl
Consumables	• NEBNext Ultra II End repair/dA-tailing Module (NEB, E7546) • Freshly prepared 70% ethanol in nuclease-free water • 0.2 ml thin-walled PCR tubes • 1.5 ml Eppendorf DNA LoBind tubes • Nuclease-free water (e.g. ThermoFisher, cat # AM9937) • Agencourt AMPure XP beads (Beckman Coulter™, cat # A63881)
Equipment	• Thermal cycler • Magnetic separator, suitable for 1.5 ml Eppendorf tubes • Hula mixer (gentle rotator mixer) • Vortex mixer • Ice bucket with ice
Optional Equipment	• Qubit fluorometer (or equivalent for QC check)

1 Prepare the NEBNext Ultra II End Repair/dA-Tailing Module reagents according to the manufacturer's instructions, and place on ice.

For optimal performance, NEB recommend the following:

1. Thaw all reagents on ice.
2. Flick and/or invert reagent tube to ensure they are well mixed.
3. Always spin down tubes before opening for the first time each day.
4. The Ultra II End prep buffer and FFPE DNA Repair buffer may have a little precipitate. Allow the mixture to come to room temperature and pipette the buffer up and down several times to break up the precipitate, followed by vortexing the tube for several seconds to ensure the reagent is thoroughly mixed.
5. The FFPE DNA repair buffer may have a yellow tinge and is fine to use if yellow.

2 Mix the following reagents in a 0.2 ml thin-walled PCR tube:

Reagent	Volume
100 ng fragmented DNA	50 µl
Ultra II End-prep reaction buffer	7 µl
Ultra II End-prep enzyme mix	3 µl
Total	**60 µl**

3 Mix well by gently pipetting the entire volume within the tube up and down 10 times.

4 Using a thermal cycler, incubate at 20°C for 5 minutes and 65°C for 5 minutes.

5 Resuspend the AMPure XP beads by vortexing.

6 Transfer the sample to a clean 1.5 ml Eppendorf DNA LoBind tube.

7 Add 60 µl of resuspended AMPure XP beads to the end-prep reaction and mix by pipetting.

8 Incubate on a Hula mixer (rotator mixer) for 5 minutes at room temperature.

9 Prepare 500 µl of fresh 70% ethanol in nuclease-free water.

10 Spin down the sample and pellet on a magnet. Keep the tube on the magnet, and pipette off the supernatant.

11 Keep the tube on the magnet and wash the beads with 200 µl of freshly prepared 70% ethanol without disturbing the pellet. Remove the ethanol using a pipette and discard.

12 **Repeat the previous step.**

13 **Spin down and place the tube back on the magnet. Pipette off any residual 70% ethanol. Briefly allow to dry.**

14 **Remove the tube from the magnetic rack and resuspend pellet in 16 µl nuclease-free water. Incubate for 2 minutes at room temperature.**

15 **Pellet the beads on a magnet until the eluate is clear and colourless.**

16 **Remove and retain 16 µl of eluate into a clean 1.5 ml Eppendorf DNA LoBind tube.**

17 **Quantify 1 µl of end-prepped DNA using a Qubit fluorometer.**

PCR adapters ligation and amplification

~135 minutes

Materials	• Barcode Adapter (BCA) • Barcode Primers (BP 01-12, at 10 µM)
Consumables	• NEB Blunt/TA Ligase Master Mix (NEB, cat # M0367) • Agencourt AMPure XP beads (Beckman Coulter™, cat # A63881) • Freshly prepared 70% ethanol in nuclease-free water • Nuclease-free water (e.g. ThermoFisher, cat # AM9937) • 1.5 ml Eppendorf DNA LoBind tubes • LongAmp Hot Start Taq 2X Master Mix (NEB, M0533S) • 10 mM Tris-HCl pH 8.0 with 50 mM NaCl • (optional) Exonuclease I (NEB, M0293)
Equipment	• Hula mixer (gentle rotator mixer) • Magnetic separator, suitable for 1.5 ml Eppendorf tubes • Thermal cycler
Optional Equipment	• Qubit fluorometer (or equivalent for QC check)

1 **Thaw the Blunt/TA Ligase Master Mix, spin down and mix by pipetting the entire volume within the tube up and down 10 times. Check for any precipitate (if any is visible, continue to mix) and place on ice.**

2 **Thaw the Barcode Adapter (BCA), spin down and mix by pipetting the entire volume within the tube up and down 10 times. Place on ice.**

3 **Add the reagents in the order given below, mixing by flicking the tube between each sequential addition:**

Reagent	Volume
End-prepped DNA	15 µl
Barcode Adapters (BCA)	10 µl
Blunt/TA Ligase Master Mix	25 µl
Total	**50 µl**

4 **Mix well by gently pipetting the entire volume within the tube up and down 10 times.**

5 **Incubate the reaction for 10 minutes at room temperature.**

6 **Resuspend the AMPure XP beads by vortexing.**

7 **Add 20 µl of resuspended AMPure XP beads to the reaction and mix by pipetting.**

8 **Incubate on a Hula mixer (rotator mixer) for 5 minutes at room temperature.**

9 **Prepare 500 µl of fresh 70% ethanol in nuclease-free water.**

10 **Spin down the sample and pellet on a magnet. Keep the tube on the magnet, and pipette off the supernatant.**

11 **Keep the tube on the magnet and wash the beads with 200 µl of freshly prepared 70% ethanol without disturbing the pellet. Remove the ethanol using a pipette and discard.**

12 **Repeat the previous step.**

13 **Spin down and place the tube back on the magnet. Pipette off any residual ethanol. Allow to dry for ~30 seconds, but do not dry the pellet to the point of cracking.**

14 **Remove the tube from the magnetic rack and resuspend pellet in 21 µl nuclease-free water. Incubate for 2 minutes at room temperature.**

15 **Pellet the beads on a magnet until the eluate is clear and colourless.**

16 Remove and retain 21 µl of eluate into a clean 1.5 ml Eppendorf DNA LoBind tube.

- Remove and retain the eluate which contains the DNA library in a clean 1.5 ml Eppendorf DNA LoBind tube
- Dispose of the pelleted beads

17 Quantify 1 µl of adapted DNA using a Qubit fluorometer.

18 Calculate how much DNA to take forward into the PCR step for a final DNA concentration of 0.2 ng/µl in a 50 µl reaction.

19 Thaw the LongAmp® Hot Start Taq 2X Master Mix at room temperature, spin down and mix by pipetting the entire volume within the tube up and down 10 times. Place on ice.

20 Thaw the required Barcode Primers (BP01-12) at room temperature, spin down and mix by pipetting the entire volume within the tube up and down 10 times. Place on ice.

21 Set up the adapted DNA PCR as follows:

Reagent	Volume	Final concentration in 50 µl
Adapter ligated DNA, diluted	x µl	0.2 ng/µl
Nuclease-free water	24-x µl	
Barcode Primers (BP 01-12, at 10 µM)	1 µl	
LongAmp® Hot Start Taq 2x Master Mix	25 µl	
Total	**50 µl**	

If the amount of input material is altered, the number of PCR cycles may need to be adjusted to produce the same yield.

22 Mix well by gently pipetting the entire volume within the tube up and down 10 times.

23 Amplify using the following cycling conditions:

Cycle step	Temperature	Time	No. of cycles
Initial denaturation	95 °C	3 mins	1
Denaturation	95 °C	15 secs	14 (b)
Annealing	56 °C (a)	15 secs (a)	14 (b)
Extension	65 °C (c)	50 secs/kb	14 (b)
Final extension	65 °C	6 mins	1
Hold	4 °C	∞	

a. This is specific to the Oxford Nanopore Whole Genome Primer and should be maintained

b. Adjust accordingly if input quantities are altered

c. This temperature is determined by the type of polymerase that is being used (given here for LongAmp Taq polymerase)

Optional Action
(optional) Add 1 µl of ExoI, mix gently by flicking the tube, spin down briefly and incubate at 37° C for 10 min.

Carrying out this step may give a ~20% improvement in sequencing throughput.

24 Resuspend the AMPure XP beads by vortexing.

25 Add 30 µl of resuspended AMPure XP beads to the reaction and mix by pipetting.

26 Incubate on a Hula mixer (rotator mixer) for 5 minutes at room temperature.

27 Prepare 500 µl of fresh 70% ethanol in nuclease-free water.

28 Spin down the sample and pellet on a magnet. Keep the tube on the magnet, and pipette off the supernatant.

29 Keep the tube on the magnet and wash the beads with 200 µl of freshly prepared 70% ethanol without disturbing the pellet. Remove the ethanol using a pipette and discard.

30 Repeat the previous step.

31 Spin down and place the tube back on the magnet. Pipette off any residual ethanol. Allow to dry for ~30 seconds, but do not dry the pellet to the point of cracking.

32 Remove the tube from the magnetic rack and resuspend pellet in 10 µl of 10 mM Tris.HCl pH 8.0 with 50 mM NaCl. Incubate for 2 minutes at room temperature.

33 Pellet the beads on a magnet until the eluate is clear and colourless.

34 Remove and retain 10 µl of eluate into a clean 1.5 ml Eppendorf DNA LoBind tube.

- Dispose of the pelleted beads

35 Quantify 1 µl of adapted DNA using a Qubit fluorometer.

Gel analysis of amplified and ligated DNA

Sometimes a high-molecular weight product is visible in the wells of the gel when the PCR products are run, instead of the expected smear. These libraries are typically associated with poor sequencing performance. We have found that repeating the PCR with fewer cycles can remedy this.

36 Pool all barcoded libraries in the desired ratios to a total of 50-100 fmoles in 10 µl of 10 mM Tris-HCl pH 8.0 with 50 mM NaCl.

Rapid adapter ligation

~5 minutes

Materials	• Rapid Adapter (RAP)
Equipment	• Microfuge

1 Add 1 µl RAP to the 10 µl amplified DNA library.

2 Mix gently by flicking the tube, and spin down.

3 Incubate the reaction for 5 minutes at room temperature.

END OF STEP

The prepared library is used for loading into the flow cell. Store the library on ice until ready to load.

Priming and loading the SpotON flow cell

~10 minutes

Materials	• Flow Cell Priming Kit (EXP-FLP002)

	• Sequencing Buffer (SQB) • Loading Beads (LB)
Consumables	• 1.5 ml Eppendorf DNA LoBind tubes • Nuclease-free water (e.g. ThermoFisher, cat # AM9937)
Equipment	• MinION Mk1B or Mk1C • SpotON Flow Cell • P1000 pipette and tips • P100 pipette and tips • P20 pipette and tips • P10 pipette and tips

IMPORTANT

Please note that the Sequencing Tether (SQT) tube will NOT be used in this protocol.

1 **Thaw the Sequencing Buffer (SQB), Loading Beads (LB), Flush Tether (FLT) and one tube of Flush Buffer (FB) at room temperature before mixing the reagents by vortexing, and spin down at room temperature.**

2 **To prepare the flow cell priming mix, add 30 µl of thawed and mixed Flush Tether (FLT) directly to the tube of thawed and mixed Flush Buffer (FB), and mix by vortexing at room temperature.**

3 **Open the MinION device lid and slide the flow cell under the clip.**

Press down firmly on the flow cell to ensure correct thermal and electrical

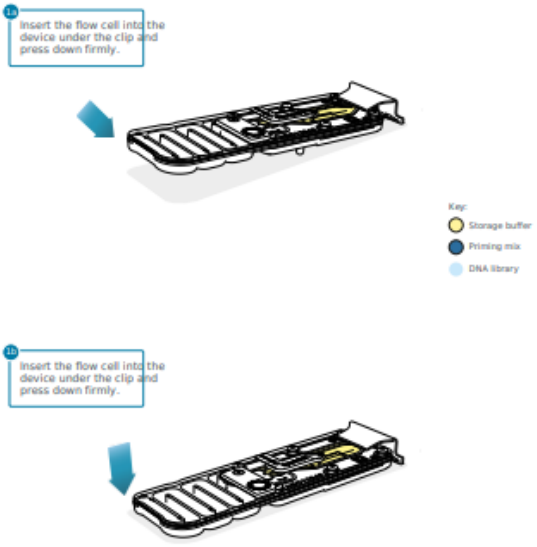

Optional Action
Complete a flow cell check to assess the number of pores available before loading the library.

This step can be omitted if the flow cell has been checked previously.

See the flow cell check instructions in the MinKNOW protocol for more information.

4 **Slide the priming port cover clockwise to open the priming port.**

IMPORTANT

Take care when drawing back buffer from the flow cell. Do not remove more than 20-30 µl, and make sure that the array of pores are covered by buffer at all times. Introducing air bubbles into the array can irreversibly damage pores.

5 After opening the priming port, check for a small air bubble under the cover. Draw back a small volume to remove any bubbles:

1. Set a P1000 pipette to 200 µl
2. Insert the tip into the priming port
3. Turn the wheel until the dial shows 220-230 ul, to draw back 20-30 ul, or until you can see a small volume of buffer entering the pipette tip
   Note: Visually check that there is continuous buffer from the priming port across the sensor array.

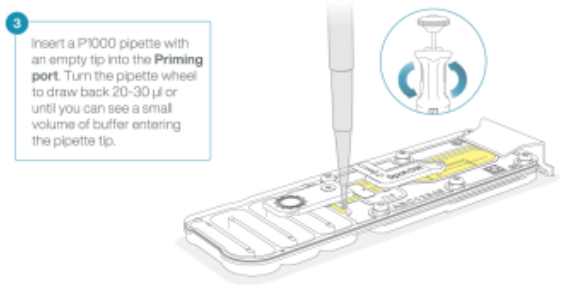

6 **Load 800 µl of the priming mix into the flow cell via the priming port, avoiding the introduction of air bubbles. Wait for 5 minutes. During this time, prepare the library for loading by following the steps below.**

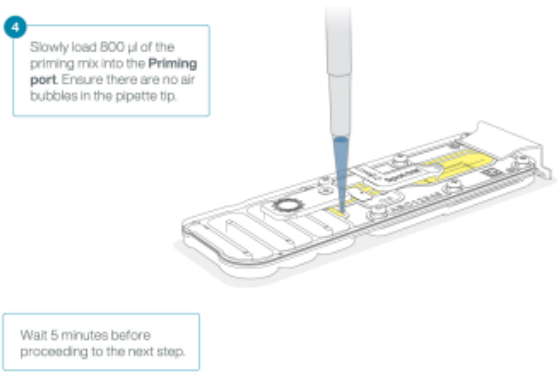

7 **Thoroughly mix the contents of the Loading Beads (LB) tubes by vortexing.**

> IMPORTANT
>
> **The Loading Beads (LB) tube contains a suspension of beads. These beads settle very quickly. It is vital that they are mixed immediately before use.**

8 **In a new tube, prepare the library for loading as follows:**

Reagent	Volume per flow cell
Sequencing Buffer (SQB)	34 µl
Loading Beads (LB), mixed immediately before use	25.5 µl
Nuclease-free water	4.5 µl
DNA library	11 µl
Total	**75 µl**

Note: Load the library onto the flow cell immediately after adding the Sequencing Buffer (SQB) and Loading Beads (LB) because the fuel in the buffer will start to be consumed by the adapter.

9 Complete the flow cell priming:

1. Gently lift the SpotON sample port cover to make the SpotON sample port accessible.
2. Load **200 µl** of the priming mix into the flow cell priming port (**not** the SpotON sample port), avoiding the introduction of air bubbles.

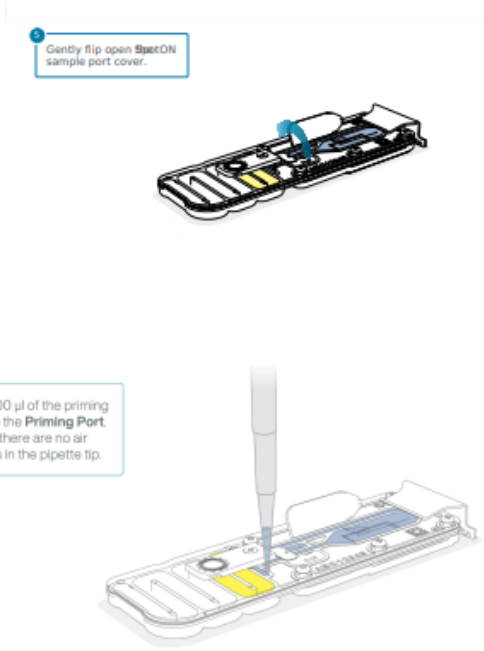

10 Mix the prepared library gently by pipetting up and down just prior to loading.

11 Add 75 µl of the prepared library to the flow cell via the SpotON sample port in a dropwise fashion. Ensure each drop flows into the port before adding the next.

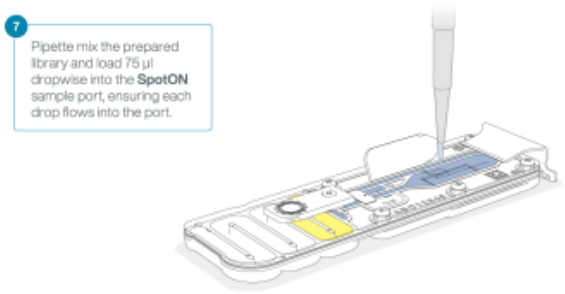

12 Gently replace the SpotON sample port cover, making sure the bung enters the SpotON port, close the priming port and replace the MinION device lid.

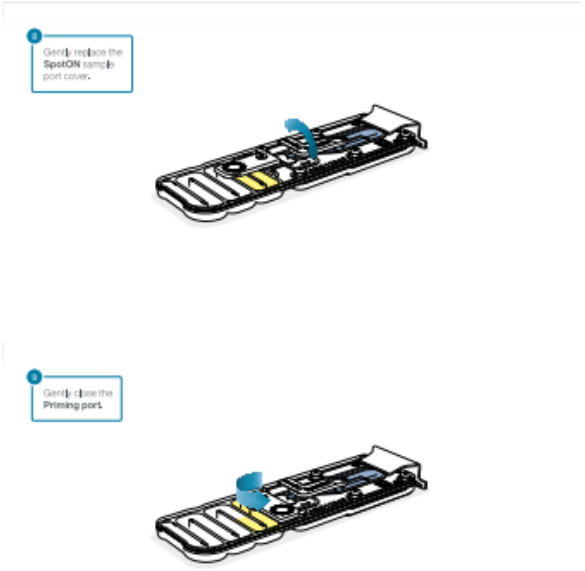

Appendix K – The workflow of the job assisted by BGI for DNBSEQ of the 16S rDNA sequencing (library preparation, sequencing, and sequence modifications)

华大基因
BGI

Project brief

Content

1 Project information

Basic information is shown in the table below:

Table1 Project information

Project_Info	Desc
Project_Code	F23A430000266_BAChbjuM
Region	16S-V3-V4
Tagnumber	20000
AnnoDB	RDP
Sample_Size	90

2 Introduction of experiment workflow

30ng qualified DNA template and the 16S rRNA fusion primers are added for Polymerase chain reaction (PCR). All PCR products are purified by Agencourt AMPure XP beads, dissolved in Elution Buffer and eventually labeled to finish library construction. Library size and concentration are detected by Agilent 2100 Bioanalyzer. Qualified libraries are sequenced with DNB platform according to their insert size.

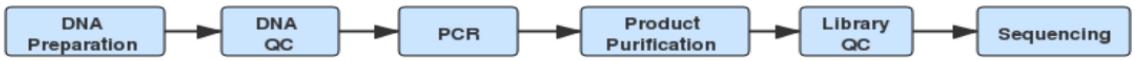

Figure1 experiment workflow.

3 Bioinformatics analysis workflow

Raw data are filtered to obtain the high-quality clean data, after which clean reads that can overlap with each other are merged to tags.

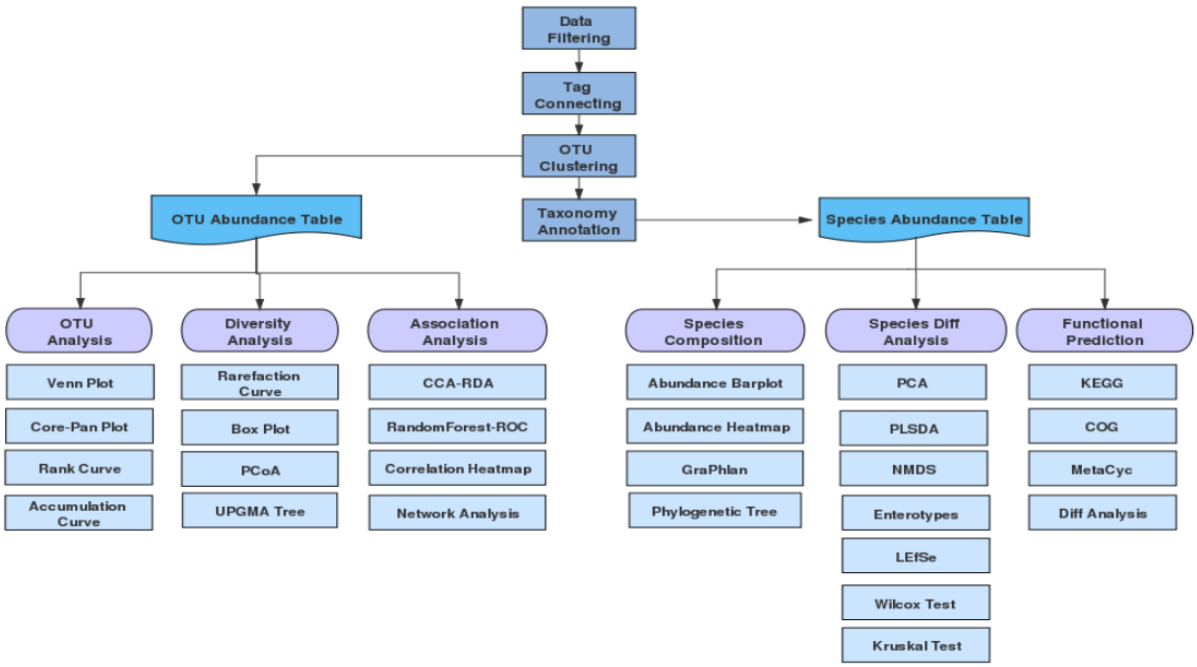

Figure2 Bioinformatics analysis workflow.

4 Data Filtering

Raw data are filtered to generate high quality clean reads as follows::

1) Truncate primmer and adapter contamination with cutadapt v2.6;

2) Truncate reads whose average phred quality values are lower than 20 over a 30 bp sliding window then remove reads whose length are %75 of their original lengths after truncation;

3)Remove reads with ambiguous base;

4)Remove low-complexity reads (default:reads with 10 consecutive same base).

Table2 Statistic of data filter

#OldSampleName	Sample Number	ReadsLength(bp)	RawData(Mbp)	PloyBase(%)	LowQuality(%)	CleanData(Mbp)	DataUtilizationRatio(%)	RawReads	Clean Reads	RemovePrimerReads
WL001	852230300383	300:300	17.16	0.000	0.013	17.14	99.89	31041*2	30913*2	30913*2
WL002	852230300384	300:300	17.16	0.003	0.005	17.14	99.93	31082*2	30958*2	30958*2
WL003	852230300384	300:300	17.16	0.000	0.006	17.14	99.90	31129*2	31026*2	31026*2
WL004	852230300384	300:300	17.16	0.000	0.013	17.14	99.88	31269*2	31139*2	31139*2
WL005	852230300384	300:300	17.16	0.003	0.005	17.14	99.91	31295*2	31191*2	31191*2
WL006	852230300384	300:300	17.16	0.000	0.006	17.14	99.92	30965*2	30805*2	30805*2
WL007	852230300384	300:300	17.15	0.000	0.003	17.14	99.94	31047*2	30905*2	30905*2
WL008	852230300385	300:300	17.16	0.002	0.014	17.14	99.90	31098*2	30961*2	30961*2
WL009	852230300385	300:300	17.15	0.000	0.003	17.14	99.93	31136*2	31016*2	31016*2
WL010	852230300385	300:300	17.15	0.000	0.005	17.14	99.93	31220*2	31070*2	31070*2
WL011	852230300385	300:300	17.16	0.003	0.008	17.14	99.92	31307*2	31181*2	31181*2
WL012	852230300385	300:300	17.16	0.000	0.008	17.14	99.92	31356*2	31236*2	31236*2
WL013	852230300385	300:300	17.16	0.000	0.005	17.14	99.92	31009*2	30852*2	30852*2
WL014	852230300385	300:300	17.15	0.000	0.002	17.14	99.93	31064*2	30903*2	30903*2
WL015	852230300385	300:300	17.16	0.000	0.011	17.14	99.88	31094*2	30973*2	30973*2
WL016	852230300385	300:300	17.17	0.000	0.014	17.14	99.87	31147*2	31030*2	31030*2
WL017	852230300385	300:300	17.16	0.000	0.010	17.14	99.91	31175*2	31068*2	31068*2
WL018	852230300386	300:300	17.16	0.000	0.019	17.14	99.89	31233*2	31132*2	31132*2
WL019	852230300386	300:300	17.16	0.000	0.006	17.14	99.91	31350*2	31242*2	31242*2
WL020	852230300386	300:300	17.16	0.002	0.011	17.14	99.89	31396*2	31299*2	31299*2
WL021	852230300386	300:300	17.16	0.000	0.014	17.14	99.89	31061*2	30910*2	30910*2
WL022	852230300386	300:300	17.16	0.000	0.011	17.14	99.90	31094*2	30963*2	30963*2
WL023	852230300386	300:300	17.16	0.000	0.006	17.14	99.92	31159*2	31023*2	31023*2
WL024	852230300386	300:300	17.16	0.002	0.008	17.14	99.90	31203*2	31078*2	31078*2
WL025	852230300386	300:300	17.16	0.002	0.002	17.14	99.93	31227*2	31122*2	31122*2
WL026	852230300386	300:300	17.16	0.000	0.010	17.14	99.92	31293*2	31186*2	31186*2
WL027	852230300386	300:300	17.16	0.000	0.010	17.14	99.92	31435*2	31292*2	31292*2
WL028	852230300387	300:300	17.16	0.002	0.019	17.14	99.89	31472*2	31355*2	31355*2
WL029	852230300387	300:300	17.16	0.002	0.011	17.14	99.91	31131*2	30961*2	30961*2
WL030	852230300387	300:300	17.16	0.002	0.010	17.14	99.91	31167*2	31019*2	31019*2
WL031	852230300387	300:300	17.16	0.000	0.010	17.14	99.92	31198*2	31066*2	31066*2
WL032	852230300387	300:300	17.16	0.000	0.011	17.14	99.90	31247*2	31127*2	31127*2
WL033	852230300387	300:300	17.16	0.000	0.011	17.14	99.92	31303*2	31175*2	31175*2
WL034	852230300387	300:300	17.16	0.000	0.014	17.14	99.91	31472*2	31346*2	31346*2
WL035	852230300387	300:300	17.16	0.000	0.010	17.14	99.93	31514*2	31394*2	31394*2
WL036	852230300387	300:300	17.16	0.000	0.011	17.14	99.92	31165*2	31011*2	31011*2
WL037	852230300387	300:300	17.15	0.002	0.006	17.14	99.94	31207*2	31065*2	31065*2
WL038	852230300388	300:300	17.15	0.000	0.003	17.14	99.93	30819*2	30695*2	30695*2
WL039	852230300388	300:300	17.16	0.000	0.005	17.14	99.93	30888*2	30749*2	30749*2
WL040	852230300388	300:300	17.16	0.002	0.011	17.14	99.93	30932*2	30794*2	30794*2
WL041	852230300388	300:300	17.16	0.000	0.013	17.14	99.91	30982*2	30857*2	30857*2
WL042	852230300388	300:300	17.16	0.002	0.003	17.14	99.93	31084*2	30967*2	30967*2
WL043	852230300388	300:300	17.16	0.000	0.006	17.14	99.93	31132*2	31019*2	31019*2
WL044	852230300388	300:300	17.15	0.000	0.002	17.14	99.94	30778*2	30638*2	30638*2
WL045	852230300388	300:300	17.15	0.000	0.003	17.14	99.94	30837*2	30687*2	30687*2
WL046	852230300388	300:300	17.16	0.000	0.008	17.14	99.92	30850*2	30743*2	30743*2
WL047	852230300388	300:300	17.16	0.000	0.008	17.14	99.90	30905*2	30807*2	30807*2
WL048	852230300389	300:300	17.16	0.000	0.005	17.14	99.92	30946*2	30852*2	30852*2
WL049	852230300389	300:300	17.16	0.000	0.002	17.14	99.92	30997*2	30912*2	30912*2
WL050	852230300389	300:300	17.16	0.000	0.005	17.14	99.92	31131*2	31022*2	31022*2
WL051	852230300389	300:300	17.16	0.000	0.006	17.14	99.93	31170*2	31074*2	31074*2
WL052	852230300389	300:300	17.16	0.002	0.007	17.14	99.92	30855*2	30692*2	30692*2
WL053	852230300389	300:300	17.16	0.000	0.007	17.14	99.92	30864*2	30742*2	30742*2
WL054	852230300389	300:300	17.15	0.000	0.003	17.14	99.93	30899*2	30795*2	30795*2
WL055	852230300389	300:300	17.16	0.000	0.006	17.14	99.91	30964*2	30857*2	30857*2
WL056	852230300389	300:300	17.16	0.000	0.003	17.14	99.93	31001*2	30904*2	30904*2
WL057	852230300389	300:300	17.16	0.000	0.006	17.14	99.91	31059*2	30964*2	30964*2
WL058	852230300390	300:300	17.16	0.000	0.010	17.14	99.92	31173*2	31072*2	31072*2
WL059	852230300390	300:300	17.16	0.000	0.005	17.14	99.91	31221*2	31129*2	31129*2
WL060	852230300390	300:300	17.16	0.000	0.008	17.14	99.92	30877*2	30744*2	30744*2
WL061	852230300390	300:300	17.15	0.000	0.002	17.14	99.93	30901*2	30797*2	30797*2
WL062	852230300390	300:300	17.16	0.000	0.008	17.14	99.91	30960*2	30853*2	30853*2
WL063	852230300390	300:300	17.17	0.003	0.018	17.14	99.87	31035*2	30914*2	30914*2
WL064	852230300390	300:300	17.16	0.000	0.010	17.14	99.91	31066*2	30959*2	30959*2
WL065	852230300390	300:300	17.16	0.002	0.010	17.14	99.90	31157*2	31019*2	31019*2
WL066	852230300390	300:300	17.16	0.000	0.011	17.14	99.91	31254*2	31128*2	31128*2
WL067	852230300390	300:300	17.16	0.002	0.006	17.14	99.91	31287*2	31182*2	31182*2
WL068	852230300391	300:300	17.16	0.000	0.003	17.14	99.92	30947*2	30798*2	30798*2
WL069	852230300391	300:300	17.16	0.003	0.003	17.14	99.91	31026*2	30851*2	30851*2
WL070	852230300391	300:300	17.16	0.000	0.008	17.14	99.91	31058*2	30906*2	30906*2
WL071	852230300391	300:300	17.16	0.002	0.010	17.14	99.89	31112*2	30967*2	30967*2
WL072	852230300391	300:300	17.16	0.000	0.006	17.14	99.92	31147*2	31011*2	31011*2
WL073	852230300391	300:300	17.16	0.000	0.008	17.14	99.91	31222*2	31072*2	31072*2
WL074	852230300391	300:300	17.16	0.000	0.010	17.14	99.91	31324*2	31184*2	31184*2
WL075	852230300391	300:300	17.16	0.002	0.006	17.14	99.91	31378*2	31239*2	31239*2
WL076	852230300391	300:300	17.16	0.002	0.010	17.14	99.91	31027*2	30850*2	30850*2
WL077	852230300391	300:300	17.16	0.002	0.005	17.14	99.92	31079*2	30904*2	30904*2
WL078	852230300392	300:300	17.15	0.002	0.003	17.14	99.93	31092*2	30959*2	30959*2
WL079	852230300392	300:300	17.16	0.000	0.006	17.14	99.90	31137*2	31018*2	31018*2
WL080	852230300392	300:300	17.16	0.005	0.010	17.14	99.90	31185*2	31065*2	31065*2
WL081	852230300392	300:300	17.16	0.002	0.008	17.14	99.91	31251*2	31127*2	31127*2
WL082	852230300392	300:300	17.16	0.000	0.008	17.14	99.92	31335*2	31237*2	31237*2
WL083	852230300392	300:300	17.16	0.000	0.010	17.14	99.90	31406*2	31296*2	31296*2
WL084	852230300392	300:300	17.16	0.000	0.008	17.14	99.91	31074*2	30907*2	30907*2
WL085	852230300392	300:300	17.16	0.003	0.006	17.14	99.91	31095*2	30958*2	30958*2
WL086	852230300392	300:300	17.16	0.000	0.003	17.14	99.93	31192*2	31072*2	31072*2
WL087	852230300392	300:300	17.16	0.000	0.011	17.14	99.92	31240*2	31123*2	31123*2
WL088	852230300393	300:300	17.16	0.005	0.008	17.14	99.91	31300*2	31181*2	31181*2
WL089	852230300393	300:300	17.16	0.000	0.011	17.14	99.92	31427*2	31292*2	31292*2
WL090	852230300393	300:300	17.16	0.002	0.011	17.14	99.91	31469*2	31350*2	31350*2

First Column: Sample ID; Second Column: Reads length; Third Column: Raw data size; Fourth column: N%; Fifth column : PolyN%; Sixth column : Low quality%; Seventh column:Cleandata Size; Eighth column:cleandata/rawdata; Ninth column: Rawdata num;Tenth column:Cleandata num;Eleventh column:Reads contain primer number;Twelfth column: Reads usage% .

5 Tags connection

If paired-end reads overlap with each other, then a consensus sequence will be generated by FLASH (Fast Length Adjustment of Short reads, v1.2.11). Details are given as follows:

1) Minimum overlapping length: 15 bp;

2) Mismatching ratio of overlapped region: <= 0.1.

Table3 Statistic of tags

#OldSampleName	SampleNumber	TotalPairsReadNumber	ConnectTagNumber	ConnectRatio(%)	AverageLengthAndSD
WL001	852230300383	30913	30822	99.71	421/10
WL002	852230300384	30958	30841	99.62	421/10
WL003	852230300384	31026	30899	99.59	411/9
WL004	852230300384	31139	31046	99.70	413/10
WL005	852230300384	31191	31084	99.66	414/10
WL006	852230300384	30805	30693	99.64	417/11
WL007	852230300384	30905	30821	99.73	420/10
WL008	852230300385	30961	30852	99.65	419/10
WL009	852230300385	31016	30882	99.57	416/10
WL010	852230300385	31070	30939	99.58	416/10
WL011	852230300385	31181	31106	99.76	408/5
WL012	852230300385	31236	31159	99.75	408/6
WL013	852230300385	30852	30751	99.67	407/5
WL014	852230300385	30903	30832	99.77	407/4
WL015	852230300385	30973	30876	99.69	417/10
WL016	852230300385	31030	30877	99.51	417/10
WL017	852230300385	31068	30951	99.62	411/8
WL018	852230300386	31132	31007	99.60	410/7
WL019	852230300386	31242	31173	99.78	408/6
WL020	852230300386	31299	31197	99.67	408/6

WL021	852230300386 3	30910	30817	99.70	408/7
WL022	852230300386 4	30963	30900	99.80	407/5
WL023	852230300386 5	31023	30938	99.73	409/8
WL024	852230300386 6	31078	30981	99.69	408/6
WL025	852230300386 7	31122	31029	99.70	407/6
WL026	852230300386 8	31186	31085	99.68	407/6
WL027	852230300386 9	31292	31202	99.71	408/7
WL028	852230300387 0	31355	31256	99.68	408/7
WL029	852230300387 1	30961	30875	99.72	408/7
WL030	852230300387 2	31019	30950	99.78	408/8
WL031	852230300387 3	31066	30947	99.62	411/8
WL032	852230300387 4	31127	31021	99.66	410/7
WL033	852230300387 5	31175	31072	99.67	410/8
WL034	852230300387 6	31346	31267	99.75	408/6
WL035	852230300387 7	31394	31287	99.66	408/7
WL036	852230300387 8	31011	30893	99.62	408/6
WL037	852230300387 9	31065	30958	99.66	411/8
WL038	852230300388 0	30695	30602	99.70	411/8
WL039	852230300388 1	30749	30637	99.64	415/10
WL040	852230300388 2	30794	30695	99.68	416/10
WL041	852230300388 3	30857	30761	99.69	408/5
WL042	852230300388 4	30967	30904	99.80	408/6
WL043	852230300388 5	31019	30940	99.75	408/6
WL044	852230300388 6	30638	30574	99.79	408/5
WL045	852230300388 7	30687	30633	99.82	407/5
WL046	852230300388 8	30743	30679	99.79	407/3
WL047	852230300388 9	30807	30732	99.76	409/6
WL048	852230300389 0	30852	30759	99.70	407/3
WL049	852230300389 1	30912	30825	99.72	407/3
WL050	852230300389 2	31022	30939	99.73	409/6
WL051	852230300389 3	31074	30972	99.67	410/7
WL052	852230300389 4	30692	30608	99.73	405/5
WL053	852230300389 5	30742	30673	99.78	408/5
WL054	852230300389 6	30795	30718	99.75	409/6
WL055	852230300389 7	30857	30757	99.68	407/5
WL056	852230300389 8	30904	30801	99.67	409/6
WL057	852230300389 9	30964	30870	99.70	407/3
WL058	852230300390 0	31072	30987	99.73	407/4
WL059	852230300390 1	31129	31034	99.69	407/3
WL060	852230300390 2	30744	30672	99.77	407/2
WL061	852230300390 3	30797	30740	99.81	407/2
WL062	852230300390 4	30853	30772	99.74	407/3
WL063	852230300390 5	30914	30845	99.78	407/4
WL064	852230300390 6	30959	30863	99.69	408/4
WL065	852230300390 7	31019	30901	99.62	410/7
WL066	852230300390 8	31128	31047	99.74	410/7
WL067	852230300390 9	31182	31094	99.72	408/5
WL068	852230300391 0	30798	30715	99.73	408/5
WL069	852230300391 1	30851	30739	99.64	411/8
WL070	852230300391 2	30906	30785	99.61	412/9
WL071	852230300391 3	30967	30864	99.67	411/8
WL072	852230300391 4	31011	30896	99.63	411/8
WL073	852230300391 5	31072	30937	99.57	410/9
WL074	852230300391 6	31184	31086	99.69	410/8
WL075	852230300391 7	31239	31139	99.68	409/7
WL076	852230300391 8	30850	30725	99.59	411/8
WL077	852230300391 9	30904	30828	99.75	413/10
WL078	852230300392 0	30959	30850	99.65	413/10
WL079	852230300392 1	31018	30926	99.70	407/5
WL080	852230300392 2	31065	30962	99.67	409/8
WL081	852230300392 3	31127	30995	99.58	412/9
WL082	852230300392 4	31237	31159	99.75	407/4
WL083	852230300392 5	31296	31210	99.73	409/7
WL084	852230300392 6	30907	30805	99.67	408/6
WL085	852230300392 7	30958	30895	99.80	408/5
WL086	852230300392 8	31072	30978	99.70	410/9
WL087	852230300392 9	31123	31038	99.73	407/5
WL088	852230300393 0	31181	31088	99.70	409/7
WL089	852230300393 1	31292	31193	99.68	407/5
WL090	852230300393 2	31350	31245	99.67	411/9

First Column: Sample ID; Second Column: Cleandata number;Third Column:Tag number;Fourth column: Tag connect rate.

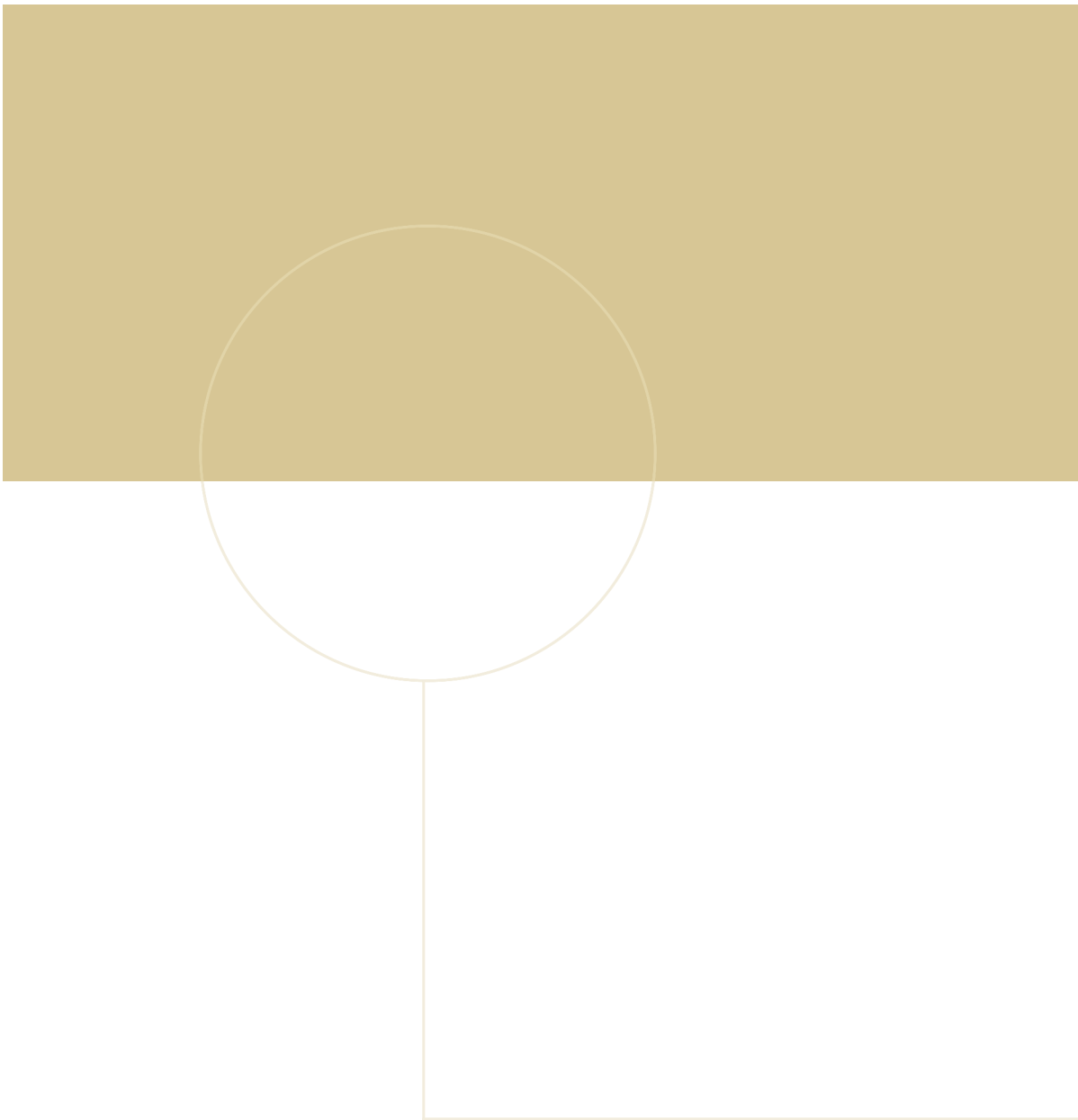

NTNU

Norwegian University of
Science and Technology